INDIAN INSTITUTE OF TECHNOLOGY GUWAHATI

Synthesis and Modification of Aniline-Formaldehyde Condensate and Chitosan Schiff Base Polymers for Application in Cr(VI) and Hg(II) Binding

by

Tanmay Dutta

March 2022

Synthesis and Modification of Aniline-Formaldehyde Condensate and Chitosan Schiff Base Polymers for Application in Cr(VI) and Hg(II) Binding

A Dissertation *Submitted*
in Partial Fulfilment of the Requirements
for the Degree of
Doctor of Philosophy

by
Tanmay Dutta

to the
Centre for the Environment
Indian Institute of Technology Guwahati
March 2022

For my family

भारतीय प्रौद्योगिकी संस्थान गुवाहाटी
पर्यावरण केंद्र
गुवाहाटी-७८१०३९, असम, भारत

INDIAN INSTITUTE OF TECHNOLOGY GUWAHATI
CENTRE FOR THE ENVIRONMENT
GUWAHATI-781039, ASSAM, INDIA

Declaration

I hereby declare that the matter embodied in this thesis, "*Synthesis and Modification of Aniline-Formaldehyde Condensate and Chitosan Schiff Base Polymers for Application in Cr(VI) and Hg(II) Binding*" is the result of investigations carried out by me in the Centre for the Environment, Indian Institute of Technology Guwahati, India under the supervision of Prof. Manabendra Ray, Professor, Department of Chemistry, Indian Institute of Technology Guwahati, India.

In keeping with the general practice of reporting scientific observations, due acknowledgment has been made wherever the work described is based on the findings of other investigators.

March 2022

IIT Guwahati

T. Dutta.

[Tanmay Dutta]

भारतीय प्रौद्योगिकी संस्थान गुवाहाटी
पर्यावरण केंद्र
गुवाहाटी-७८१०३९, असम, भारत

Indian Institute of Technology Guwahati
Centre for the Environment
Guwahati-781039, Assam, India

Certificate

This is to certify that Mr. Tanmay Dutta has been working under my supervision since July 2010. I am forwarding his thesis, entitled, "*Synthesis and Modification of Aniline-Formaldehyde Condensate and Chitosan Schiff Base Polymers for Application in Cr(VI) and Hg(II) Binding*" being submitted for the degree of Doctorate of Philosophy of this Institute. I certify that he has fulfilled all the requirements according to the rules of this Institute and that the investigations embodied in this thesis have not been submitted elsewhere for a degree.

March 2022
IIT Guwahati

[Prof. Manabendra Ray]
Professor, Department of Chemistry
Indian Institute of Technology Guwahati
Guwahati-781039, Assam, India

Acknowledgment

Firstly, I would like to acknowledge my indebtedness and extend my sincere appreciation to my supervisor, Prof. Manabendra Ray, Department of Chemistry, IIT Guwahati, for giving me the opportunity to pursue research in such a distinctive field. It would never have been possible for me to complete my research without his friendly guidance and expert advice. I am thankful to him for giving me intellectual freedom in my projects, engaging me in new research ideas, and demanding excellence of work in all my ventures.

I would also wish to express my gratitude to my committee members, Prof. G. Das, Prof. C.K. Jana, Prof. S. Chakraborty, and Prof. Sreedeep S. for their valuable suggestions throughout every stage of the work, which has contributed remarkably to get a better shape of the dissertation.

Some of the experimental data in this thesis were carried out with the help and suggestions from Dr. U. Manna, Department of Chemistry, Prof. S. Chakraborty, Department of Civil Engineering, Dr. Praisy Terangpi, Centre for the Environment, IIT Guwahati. My sincere thanks to them.

I am grateful to all non-teaching staffs of the Centre for the Environment and Department of Chemistry for their technical support.

I would like to thank the Central Instruments Facility, Department of Chemistry and Centre for the Environment, Indian Institute of Technology Guwahati for providing an excellent working atmosphere and the instrumentation support; Ministry of Human Resource Development (MHRD), Govt. of India for the financial support.

I take this opportunity to express my profound gratitude and deep regards to my teachers from school, college and university. The blessing, help, constant encouragements

and guidance given by them time to time shall carry me a long way in the journey of life on which I am about to embark.

Sincere gratitude goes to Dr. Pinaki Bandyopadhyay, University of North Bengal, for his valuable suggestions and motivation during M.Sc. times to pursue research.

I am thankful to my friend, Ananya, thank you for your continued support over the years, Soutick, Debojit, Sayantan, Nirmalya; lab colleagues, Sounak, Jinat, Chan, Somnath, hostel mates, Jinesh, Manish, my therapist who have offered warm friendship, insightful advice and support which directly or indirectly helped me in both academic and nonacademic affairs.

Nobody has been more valuable to me in the quest of this research work than my family members. I would like to thank my parents and brother, whose love and guidance are with me in whatever I pursue.

March 2022
Indian Institute of Technology Guwahati

Tanmay Dutta

Synopsis

This thesis represents our effort in using principles of coordination chemistry to address problems related to heavy metal removal from wastewater. In the present research, emphasis was given to understanding amine polymers and increasing their adsorption capacities by modifying their current forms or introducing new functional groups to the monomeric units to increase site accessibility for better metal adsorption.

The thesis has been divided into five chapters. A chapter-wise summary of the work is given below.

Chapter 1.

This chapter contains an up-to-date brief literature review on the toxicity of various heavy metals, different methods, materials used for the heavy metal removal, and the underlying chemistry.

Chapter 2.

This dissertation chapter explores the synthesis, characterization, and application of aniline formaldehyde condensate (AFC) polymers. AFC is a polymer with an amine functional group. It can exist in either an acid salt or free amine form. AFC Polymers in salt form, Poly-1s, and Poly-2s, were synthesized by switching the ratio between isopropanol to an aqueous solution in the reaction medium from 3:1 to 1:3. Another Poly-3s was prepared in a reduced volume using an intermediate solvent ratio. All three were hydrophilic with a contact angle of 0°. Treatment with a base produced the corresponding polymers in a free base form (Poly-1b, Poly-2b, and Poly-3b). Elemental analysis, FTIR, and MALDI mass analyses confirmed the formulation of the salt form and free base form without significant changes in the chemical identity of the polymers. Contact angle

measurements showed that Poly-1b (from Poly-1s) was superhydrophobic (contact angle 154°), whereas Poly-2b (from Poly-2s) was hydrophilic (contact angle 0°). The reversal in hydrophobicity between Poly-1b and Poly-2b indicated a significant change in the orientation of the amine group. Figure 2a shows the mechanism of polymer spheroids formation in two opposite polarity solvents that resulted in different surface morphology (FESEM image) and surface hydrophilicity (contact angle image). The surface area from the BET isotherm also showed the difference in surface property of those three versions of AFC.

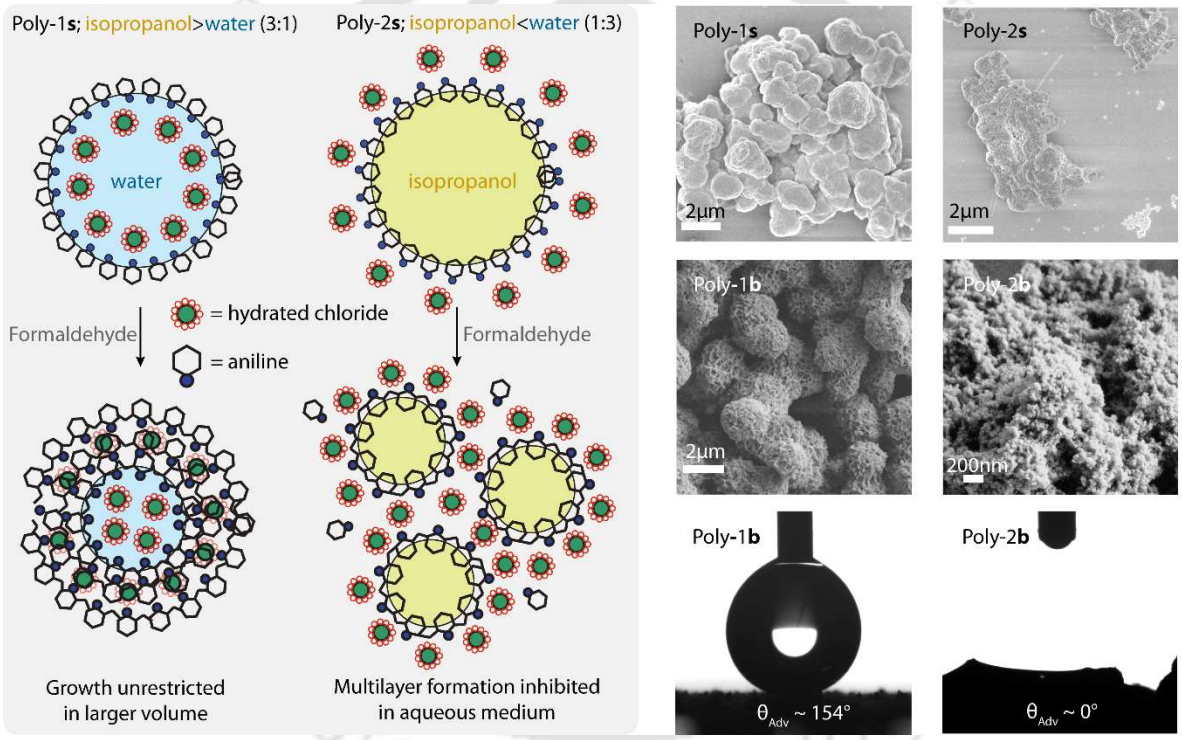

Figure 2a. Scheme of the mechanism of formation of polymer spheres (left); FESEM images of the modified AFC polymers (right-top): Poly1s(isopropanol:water 3:1), Poly-2s(isopropanol:water 1:3); contact angle images of the polymers (right bottom).

We used them to bind chromate from the aqueous solution. It has been found that among the base forms of the AFC (i.e., free amine version), the one with amine groups orientated towards the surface of the polymer spheres (Poly-2b, synthesized from Poly-2s in Figure 2a), showed maximum binding with Cr(VI). The accessibility of the amine groups

in the base forms of AFC varied depending on which solvent mixture was being used during polymer synthesis. On the other hand, almost all the three forms of AFC showed similar Cr(VI) binding among the salt forms. By changing the form of AFC (from free amine to protonated quaternary amine), the Cr(VI) adsorption capacity drastically increased to a maximum value of ~150 mg/g, which is the highest ever reported for AFC. Figure 2b describes how a simple change in solvent ratio results in different orientations of the amine group, which increases the resultant AFC polymer's Cr(VI) adsorption capacity.

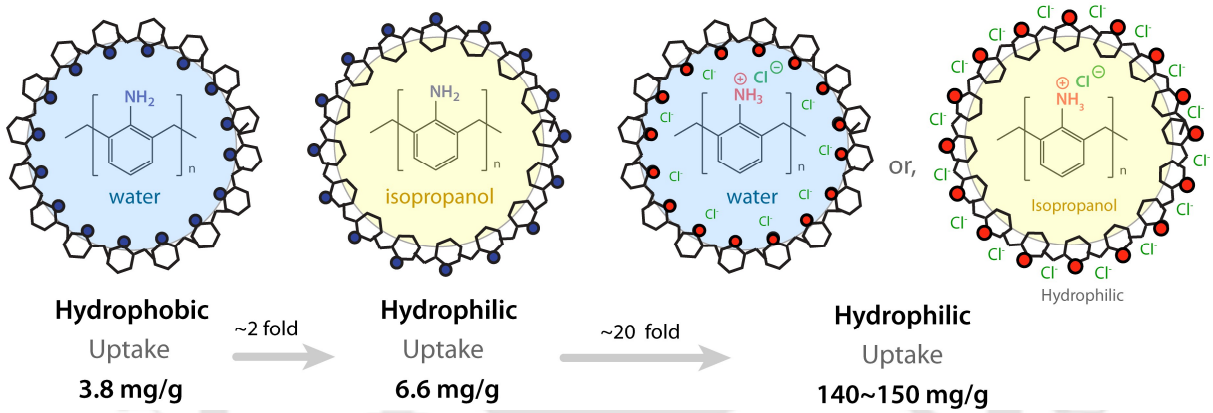

Figure 2b. Reversal of solvent ratio led to a different mechanism of polymer core formation, which in turn affect the surface property, amine site accessibility, and chromate binding.

This work demonstrates that the relationship between surface property and amine site accessibility profoundly impacts chromate binding property.

Chapter 3.

This chapter focused on two topics, (A) long-term storage effect on the salt versions of AFC (which showed the highest ever reported chromate adsorption capacity) in chromate adsorption, and (B) application of the salt versions in another toxic heavy metal, Hg(II) adsorption. Our idea was to make an easy to synthesize material, which can serve as adsorbents for different heavy metals and be stored and used for a long time without losing efficiency.

We found that due to the release of the acid from the protonated form, the morphology and surface area changed drastically over time, making them more similar to the corresponding base forms. This effect is prominent in Poly-1s, and Poly-2s synthesized in a larger solvent volume than the third polymer, Poly-3s. As a result, the chromate adsorption capacity of Poly-1s and Poly-2s decreased with time. Only Poly-3s held its effectivity towards chromate adsorption, showed more than 80% removal of chromate from aqueous solution.

In applying the salt forms of the AFC polymers in Hg(II) removal, we found that they showed excellent Hg(II) adsorption. All three forms showed more than 95% removal at 50 mg/g of Hg(II) concentration. The maximum adsorption capacity was ~150 mg/g at ~74% removal by Poly-2s, with amine groups on the surface.

This chapter has shown that the modification during synthesis increased the chromate adsorption capacity of the resultant versions of AFC and showed excellent Hg(II) removal with high Hg(II) adsorption capacity. The salt versions of AFC can also be stored and used for a longer period for chromate adsorption.

Chapter 4.

In the last two chapters, we focused on synthetic modification of AFC polymer to increase its metal adsorption and effectivity in long-term storage. We wanted to incorporate some other metal coordinating donor sites into the polymeric system. This chapter studied the Hg(II) complexation behavior with some imidazole, pyridine, and thiophene-derived small-molecule ligands before introducing them in the polymeric chain. We synthesized the ligands and their Hg(II) complex, characterize them, and studied which donor site shows better Hg(II) complexation. The Hg(II) complexes' characterization was performed using ^{1}H, COSY NMR, ESI mass, elemental analysis, and single-crystal X-ray diffraction studies. Figure 4a shows the schematic diagram of the Hg(II) complexes of the imidazole and

pyridine-based ligands with the coordination induced shifts obtained from the NMR study and the respective complexes' experimental and stimulated mass spectra.

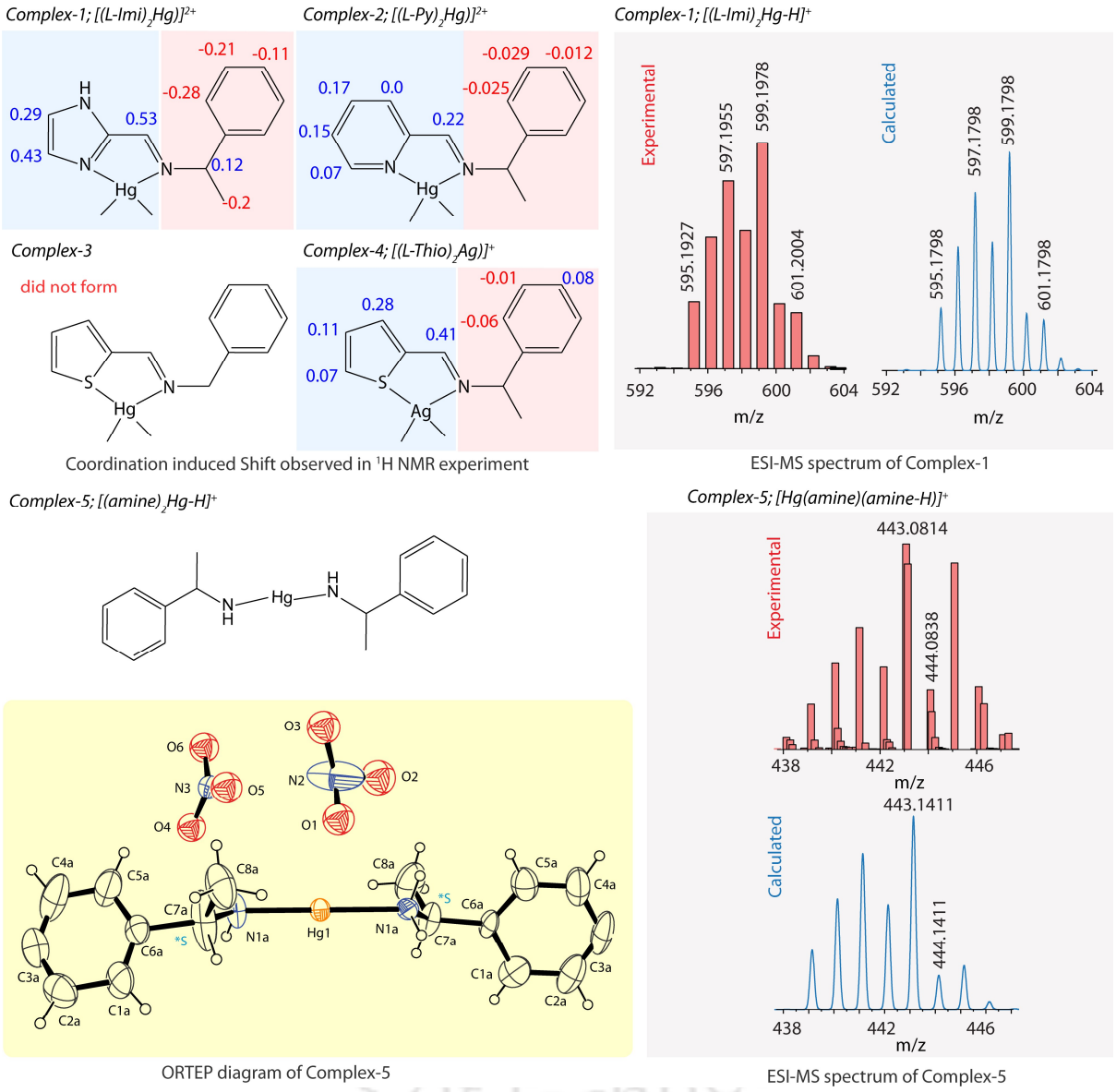

Figure 4a. Coordination induced shift from ^{1}H NMR experiments of the synthesized Hg(II) complexes (top left); ESI mass spectra of Complex-1 (top right); ORTEP diagram of Complex-5 obtained from the reaction of Hg(II) and thiophene ligand (bottom left); ESI mass spectra of Complex-5 (bottom right).

It has been found that the imidazole-derived ligand showed strong complexation with Hg(II) followed by the pyridine-derived ligand. However, the thiophene derived ligand was hydrolyzed while reacted with Hg(II), resulting in the formation of bis-complex of the

starting amine compound, which was used for the ligand synthesis (crystal structure of this amine complex is shown in Figure 4a) and bis-complex of Ag(I) of the thiophene derived ligand. This Ag(I) came as an impurity from the Hg(II) salt we used, and the thiophene ligand preferred that Ag(I) instead of Hg(II).

Chapter 5.

In the second and third chapters, we worked with an aniline-derived polymer, which is not environmentally friendly. Therefore, we wanted to use an environment-friendly system that can be used for areas where our AFC cannot be used. We hence choose chitosan, a biopolymer that has similar free amine groups. We modified chitosan with the same donor sites, imidazole, pyridine, and thiophene donor groups, the schematic diagram shown in Figure 5a.

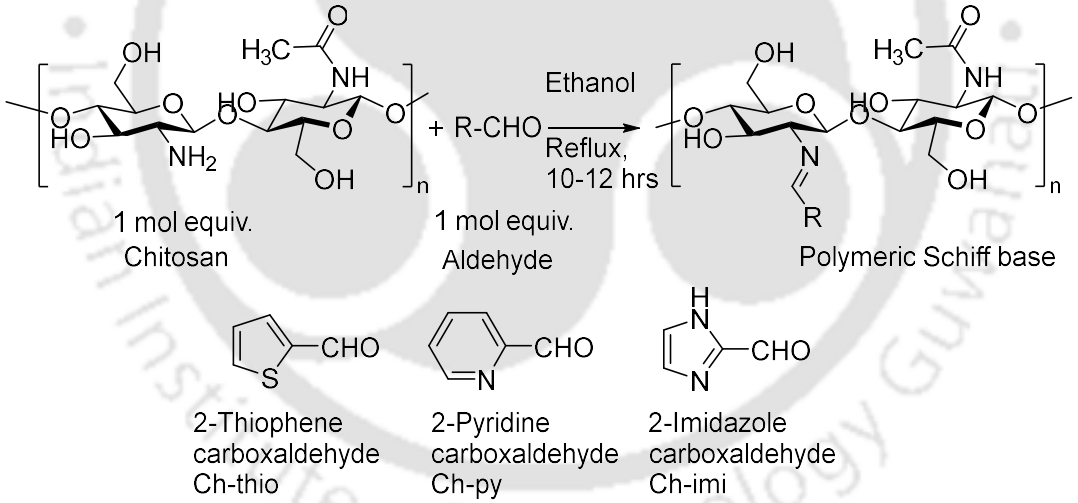

Figure 5a. Scheme describing the chitosan ligands.

In Figure 5b, ^{1}H NMR, ESI mass, TGA-DSC, and elemental analysis data of Ch-imi, the imidazole modified chitosan are shown.

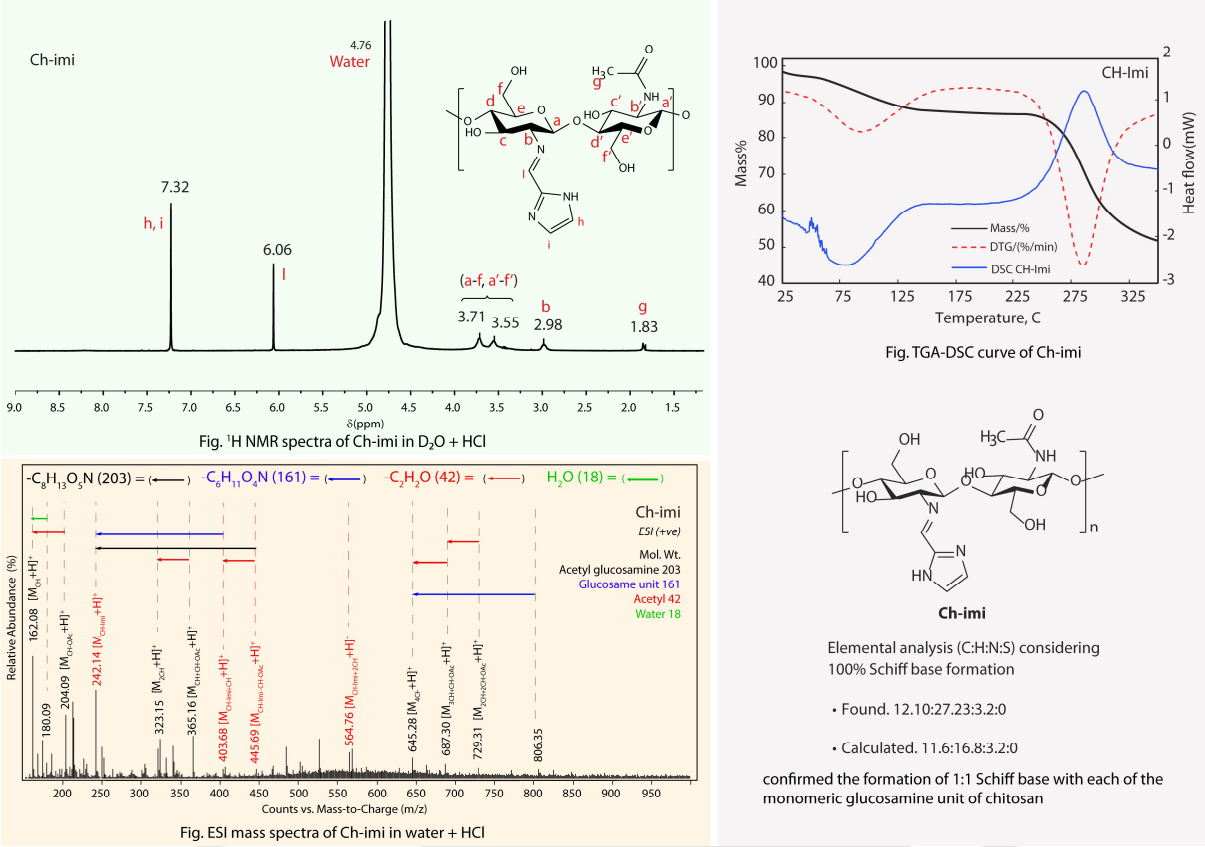

Figure 5b. [1]H NMR spectra of modified polymeric chitosan Schiff base, Ch-imi (left top); TGA-DSC of Ch-imi material (right-top); ESI mass spectra of Ch-imi (left bottom); Elemental analysis scheme of Ch-imi (right bottom).

The three modified chitosan materials were used for the removal of mercury from the aqueous solution. Effect of solution pH, Hg(II) concentration, isotherm analysis of experimental data, the effect of other metal ions on Hg(II) binding, Hg(II) binding kinetics were also examined. Figures 5c shows the variation of Hg(II) removal (%) and adsorption capacity (mg/g) with solution pH and the isotherm analysis of that experimental data by the chitosan polymers. Imidazole derivative of chitosan (Chi-Imi) is significantly more effective than the other two. Chi-Imi removes 90-98% of mercury from 50-200 mg/L solution in the 2-7 pH range (Chi-imi used was 1 g/L, maximum uptake 190 mg/g, 10 min). The preferential binding of mercury with sulfur-containing donor groups is well known. We were

surprised to see that imidazole, common in proteins, is more effective than either pyridine or cyclic thioether.

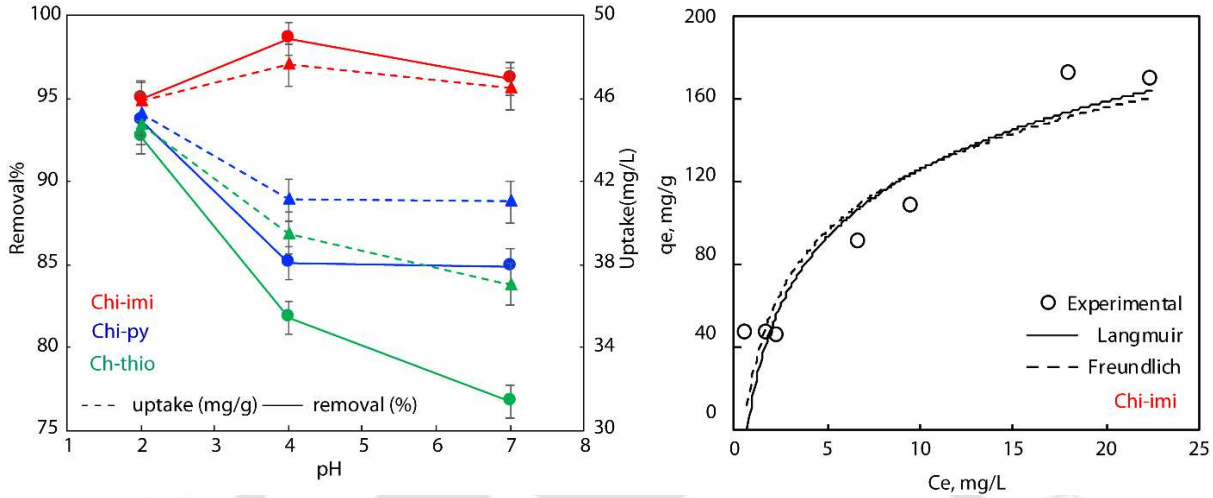

Figure 5c. Hg(II) removal by the modified chitosan materials at 50 mg/L concentration (left); isotherm fitting of the experimental Hg(II) adsorption data of Ch-imi (right).

Characterization data on the complexes helped us understanding the bonding of mercury in the polymer system. By nature, adsorbents have to be insoluble, limiting the understanding of chemical bonds between the materials and the mercury as not all spectroscopy support characterization in an insoluble form. This method of parallel study is simple enough to implement and can lead to more efficient adsorbents in other areas.

Contents

Chapter 1

Introduction: Background & Summary, Literature Survey, Objective

1.1. Purpose of the present investigation

The purpose of the work comprising this thesis is a study of amine group functionalization on heavy metals binding examined using polymers with amine donor sites. Polymeric backbone would act as solid support to remove heavy metals from wastewater, and the functionalization at the amine centers would provide better complexation or binding with the heavy metals.

Heavy metals, in anionic or cationic forms, are the dominant contaminants and multiple industrial such as leather tanning, electroplating, paint, pigments, dyeing, and textile applications led to their wider distribution in the evironment.[1–3] They possess severe water pollution, threatening the environment and human health. WHO recommended a maximum permissible limit of such compounds in wastewater. Therefore, there is an urgent need to develop efficient and practical techniques for removing toxic metals from wastewater before it gets discharged into the environment and from drinking water. Researchers have focused on the selective removal of toxic heavy metal compounds from waste and drinking water during the last few years.[38-51]

In what follows, we briefly summarize the various aspects of the toxicity of heavy metals, various materials used to remove them from wastewater, the mechanism of removing those ions, and the underlying chemistry. This will help to set up the background for going into our work.

1.2. Heavy metal toxicity

Heavy metals are defined chemically based on their atomic weights and specific gravity values. The elements from the fourth period of the periodic table having atomic weights between 64 and 201 with a specific gravity greater than 5.0 are termed as heavy metals.[4] The word-heavy metal, though, refers to the element having a higher density and toxic even

at low concentration. Some heavy metals, e.g., VO_4^{2-}, VO^{2+}, VO_2^{+}, MoO_4^{2-}, MoO_2^{2+}, Mn(II), Fe(II/III), Co(III), Cu(II), Zn(II), etc., are essential in trace amounts, but their excessive levels can be harmful to living organisms.[5] On the other hand, some heavy metals, e.g., Cr(VI), Cd(II), Hg(0/I/II), As(III), Pb(II), etc., are non-essential and are toxic, considered a significant threat to the environment[6]. Unlike organic contaminants, these heavy metals are stable and persistent contaminants, which cannot be degraded or destroyed and accumulate in soil and sediments. Naturally, heavy metals are found in the environment, but the anthropogenic sources contaminate the environment highly compared to the natural sources leading to serious concerns. These led to several catastrophes, e.g., Minamata disaster in Japan due to mercury, Itai-Itai in Japan due to cadmium, Sandoz factory leakage of mercury in Switzerland etc. Heavy metals in wastewater are a major environmental problem as it is challenging to remove them from the water.

Natural sources of these heavy metals include volcanic activity, forest fires, metamorphic rocks and salts, fossil fuels, etc. However, the extent of such natural release of heavy metals is harmless to the environment. The anthropogenic sources sometimes alter heavy metals' geological and biological distribution by altering the chemical forms of the heavy metals being released into the environment. This kind of alteration affects heavy metal's toxicity, making them bioaccumulate in plants and animals[7]. Among the various heavy metals, mercury(II), lead(II), chromium(VI) has much toxicity higher compared to other heavy metals. As they have bioaccumulative properties that increase along the food chain, their toxicity is more pronounced in the animals at higher levels of the food chain. The United States Environmental Protection Agency and the International Agency for Research on Cancer (IARC) have classified these metals as probable human carcinogens based on experimental studies. Some of the heavy metals, their sources, and their toxic effects are summarized in Table 1.1.

Table 1.1. Source common of heavy metal ions and their toxic effect on human

Heavy metal ion	Source	Toxic response	Ref.
Chromium (Cr) *Oxidation states in Nature:* Cr(III), Cr(VI); Ferrochromite ($FeCr_2O_4$) and crocoite ($PbCrO_4$)	*Natural:* Weathering of rock, microbial colonization, volcanic eruption *Anthropogenic:* Electroplating, leather, and tanning, textile, pigments, metalliferous mining, agricultural materials fertilizers	*Ailments in humans:* Genotoxic, epigastric pain, kidney and liver damage, renal failure, intravascular hemolysis, alopecia Effect at the cellular level: Carcinogenic and mutagenic *Uptake mechanism:* mimic the SO_4^{2-} and PO_4^{3-} ions and uptake via Sulfate/phosphate anionic transporters. *Mechanism of toxicity:* Redox cycling	8–12, 13
Mercury (Hg) *Oxidation states in nature:* Hg(0), Hg(I), Hg(II); cinnabar (HgS), corderoite ($Hg_3S_2Cl_2$), and livingstonite ($HgSb_4S_8$)	*Natural:* Weathering of rock, volcanic eruption *Anthropogenic:* Mining, combustion of fossil fuels, oil refinery, battery manufacturing, electrical equipment, smelters, chlorine,	*Ailments in humans:* Embryocidal, cytochemical and histopathological effects, congenital disabilities and miscarriages, allergic reactions, skin rashes, memory loss *Effect at cellular level:* Neurotoxic	14–18, 13

	and chloroalkali manufacturing processes	*Uptake mechanism:* mimic the Mn^{2+} and Zn^{2+} ions and uptake via Specific transport proteins (MerP and MerT) but still not well understood. *Mechanism of toxicity:* Redox-inactive reaction	
Cadmium (Cd) *Oxidation states in nature:* Cd(II); Greenockite (CdS), niedermayrite ($Cu_4Cd(SO_4)_2(OH)_6 \cdot 4H_2O$), otavite ($CdCO_3$), and cadmoselite (CdSe)	*Natural:* sea salt spray, volcanic activities, erosion *Anthropogenic:* Electroplating, batteries, smelting, pigments, iron and steel industry	*Ailments in humans:* Central nervous system damage, bone defects (osteomalacia), lung cancer, inhibited reproduction, lung emphysema, inhibits calcium control in a biological system *Effect at cellular level:* Carcinogenic *Uptake mechanism:* mimic the Ca^{2+}, Zn^{2+}, and other divalent cations and uptake via Essential divalent metal transporters (e.g., Fe^{2+}, Ca^{2+}, and Zn^{2+} channels) and a carrier protein (divalent cation transporter 1 (DCT1)). *Mechanism of toxicity:* Redox-inactive reaction	13, 19–24
Lead (Pb) *Oxidation states in nature:* Pb(II), Pb(IV); galena	*Natural:* Weathering of rock, volcanic eruption	*Ailments in humans:* Effects the synthesis of hemoglobin, disruption of nervous systems and	13, 25–29

(PbS), crocoite ($PbCrO_4$), anglesite ($PbSO_4$), pyromorphite ($Pb_5(PO_4)_3Cl$), coronadite ($PbMn_8O_{16}$), and cerussite ($PbCO_3$)	*Anthropogenic:* Battery, paper and pulp, paints and pigments, mining, electroplating, metallurgical industries	damage of the brain and reproductive system, paralysis of muscles *Effect at cellular level:* Neurotoxic Uptake mechanism: mimic the Ca^{2+}, Zn^{2+}, and other divalent cations and uptake via Essential divalent metal transporters (e.g., Fe^{2+}, Ca^{2+}, and Zn^{2+} channels) and a carrier protein (divalent cation transporter 1 (DCT1)). *Mechanism of toxicity:* Redox-inactive reaction	
Arsenic (As) *Oxidation states in nature:* As(III), As(V); arsenopyrite (FeAsS), cobaltite (CoAsS), niccolite (NiAs), realgar (AsS), orpiment (As_2S_3), and arsenolite (As_2O_3)	*Natural:* Weathering of rock, volcanic eruption *Anthropogenic:* Usage of fossil fuels, fertilizers, mining, semiconductors	*Ailments in humans:* Arsenicosis, cirrhotic portal hypertension, hepatic angiosarcoma, cortical necrosis, *Effect at cellular level:* Carcinogenic and neurotoxic *Uptake mechanism:* mimic the PO_4^{3-} for As(V) and uptake via As(III) through the glycerol and As(V) through phosphate transport *Mechanism of toxicity:* Redox-inactive reaction	13, 30–36, 37

The information obtained from the above discussion of heavy metal toxicity can be summarized as follows:

(a) Most of the heavy metals are carcinogenic and neurotoxic threatening human health.

(b) The anthropogenic industrial works discharge significant amount of various heavy metals into the environment.

Thus, there is an urgent need to develop effective and efficient techniques for reducing heavy metal contamination of wastewater.

1.3. Heavy metal removal techniques

In the previous section, we described various sources and toxic effects of heavy metals released by different industries into the wastewater, which is present in some soluble form. Water pH, oxidation states of the metal, the redox environment of the system, etc., control the solubility of those heavy metals., Different techniques have been utilized to remove them from the wastewater. Screening, settling, and filtration like simple physical separation techniques are inadequate to separate these metal ions. Methods like chemical precipitation, ion exchange, membrane filtration, electrochemical method, adsorption, etc., are the most available techniques. These methods are broadly categorized into three: physical, chemical, and biological methods. Each of these methods has its advantages and limitations. Table 1.2 and Figure 1.1 summarize a listing of the removal methods and their known properties.

Table 1.2. Various heavy metal removal techniques: their advantages, disadvantages

Removal methods	**Method technique**	**Advantages**	**Disadvantages**	**Heavy metals**	**References**
Chemical precipitation	By changing the physical state of the dissolved heavy metals by adding chemicals. Common precipitants include hydroxide, sulfide, carbonate.	Cost-effective	Separation issue in each filtration or sedimentation process. This process requires many chemicals to reduce the heavy metals, a large amount of sludge generation, and sludge disposal cost.	Ni(II), Pb(II), Cr(VI), Cd(II)	38
Coagulation and flocculation	Destabilize the colloidal heavy metals by using a chemical coagulant and results in sedimentation.	Cost-effective, dewatering qualities	Generation of sludge, operational cost due to a large amount of chemical utilization	Cu(II), Pb(II), Cr(VI), As(II)	39
Membrane filtration	Ultrafiltration, nanofiltration, reverse osmosis	High removal efficiency, low space requirement	Complexity in the process, higher cost, membrane	Cu(II), Fe(II), Cd(II)	40

			fouling, and lower permeate flux		
Electrochemical method	Recovery of the heavy metals in the elemental metallic state by using the cathodic and anodic reactions in the electrochemical cell	Efficient for the removal of essential metal ions, low chemical usage	Electrochemical method requires higher initial investments, costly power supply	Cd(II), Cu(II), Hg(II), Ni(II), Pb(II), Zn(II)	41,42
Ion exchange	Ion exchange between a solution and an ion exchanger, an insoluble solid or gel	High efficiency, fast process, synthetic resins are the most common	Removes only limited metal ions, operational cost is high, secondary pollution from regeneration	Cu(II), Zn(II), Cd(II), Pb(II), As(III), As(V)	43
Bioremediation	Bioremediation is a process where the biological systems,	Beneficial for removing heavy metals	Most of the biomasses can remove heavy metals from the wase water, but they	Cd(II), Ni(II), Zn(II)	44,45

	plants, and microorganisms are used to remove toxic pollutants from the aquatic environment		cannot act as alternative materials in actual industrial wastewater treatment		
Adsorption	Activated carbon, carbon nanotubes (CNT), bio adsorbents, synthetic absorbents, etc.	Adsorption method is currently perceived as the most economical, efficient, and selective treatment method for removing heavy metals from wastewater. Easy operation, less sludge production, utilization of low-cost adsorbents	Activated carbon-high price, also efficiency varies depending on the source, depends on the adsorbent type and adsorbent require regeneration	Cd(II), Cu(II), Ni(II), Zn(II), Cr(VI), Hg(II)	46–51

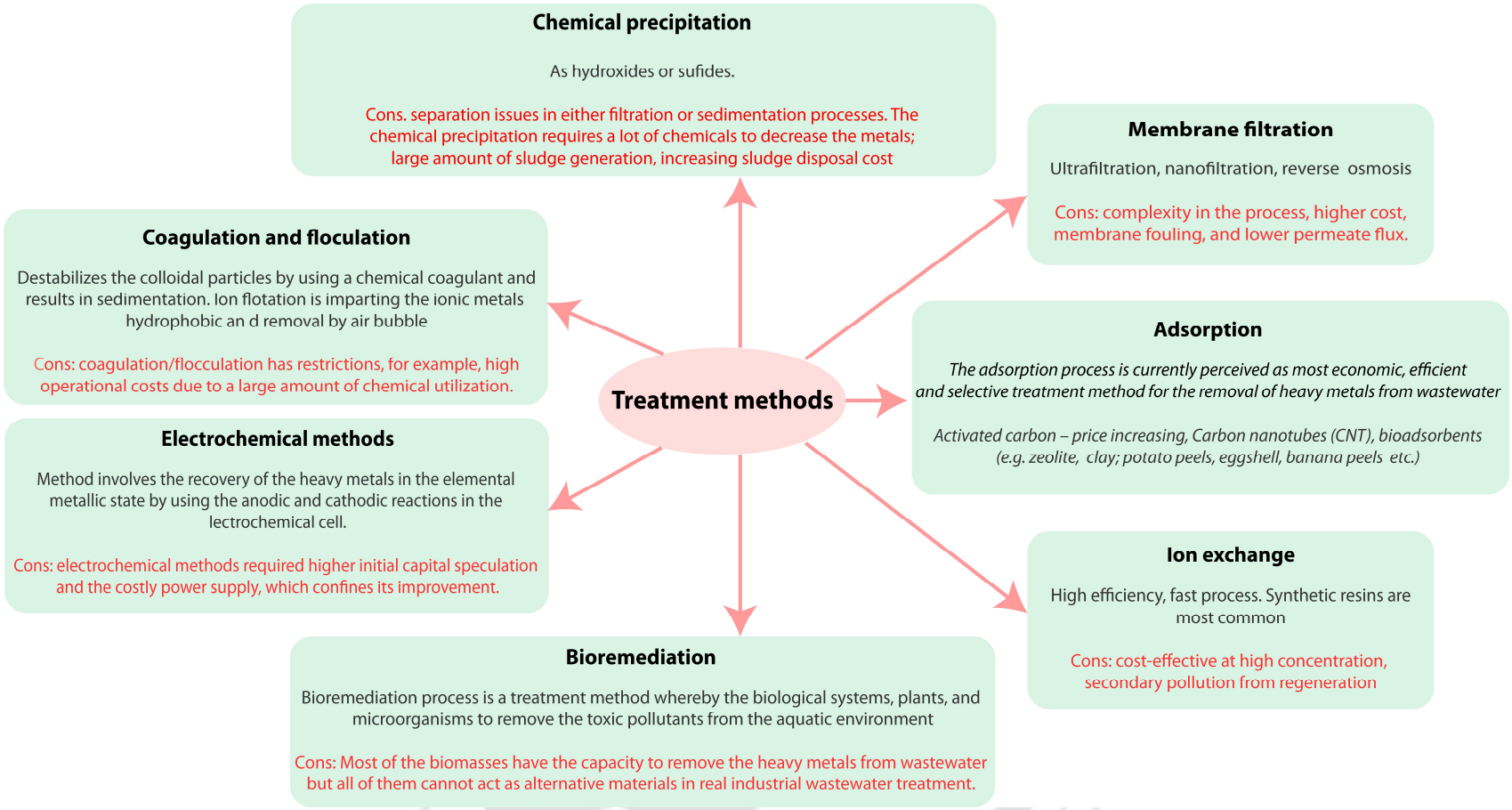

Figure 1.1. Flowchart showing various heavy metal removal methods.

The summary shows that there is still an imperative need to revise effective, efficient, economic and environmentally safe strategies that can minimize the heavy metal ion concentration from toxic to safe limits in the environment. Amongst all the removal methods adsorption process is the most widely used in wastewater treatment due to its simplicity and cost-effectiveness. However, in recent years various types of material have been used as an adsorbent in removing toxic heavy metals from several industrial effluents.

1.4. Heavy metal removal by adsorption technique

Adsorption is accumulation of molecular species onto the surface. Molecules that have been adsorbed on the surface are referred to as adsorbates and the surface to which they are adsorbed as adsorbents. Adsorption differs from absorption in which the absorbate mixes with the absorbent. Adsorption is a surface phenomenon, while absorption involves the whole volume of the material. The adsorption process can occur at the interface between any two phases, such as liquid-liquid, gas-liquid, gas-solid, or liquid-solid interfaces. In the case of liquid-solid interfaces, three types of adsorptions can be possible: (a) physical adsorption, which involves Vander Waal's attraction, (b) chemical adsorption due to the formation of a chemical bond, and (c) exchange adsorption where electrical attraction occurs between the adsorbates and adsorbents. Most of the adsorption phenomena are a combination of the three forms of adsorption. The adsorption process is efficient and most economical for the heavy metal removal from the effluent. In the adsorption process, adsorbents can be regenerated by the desorption process, and the regenerated adsorbent can be reused for several purposes. Adsorption technique is a simple, flexible method that does not produce toxic pollutants, and where the separation of heavy metals is also simple. Surface area, porosity, functional groups determine the efficiency of an adsorbent. A

selective list of different types of adsorbents used for removing various heavy metals is summarized in Table 1.3.

Table 1.3. Various adsorbents used for heavy metal removal

Adsorbents	Heavy metal	Adsorption capacity	Functional group	Reference
Activated Carbon				
Fly ash	Cd(II)	1	Metal oxides	52
Coconut shell	Pb(II)	26	Carboxylates	53
Coal Furfural	Hg(II)	92-174	-	54
Coconut Commercial FS-100	Cr(VI)	74	-	55
Hevea Brasilinesis	Cr(VI)	44	Activated carbon	56
Tree fern	Cu(II)	12	-	57
Peanut husk	Cd(II), Pb(II)	51, 114	Carboxyl, phenolic hydroxyl	58
Herbaceous peat	Cu(II)	5	Lignin, cellulose, and fulvic and humic acid	59
Grafted silica	Pb(II), Cu(II)	38, 16	N-[3-(trimethoxysilyl)propyl]-ethylenediamine	60
Cellulose grafted copolymers	Cu(II), Cd(II)	13, 13	polyacrylonitrile and poly(acrylic acid)	61
Bio-adsorbents				
Papaya wood	Cd(II), Cu(II), Zn(II)	17, 20, 14	Cellulose, protein, lignin	62
Marine algae	Cd(II)	12	Carboxylic	63
Maize bran	Pb(II)	98	Metal oxides	64
Biomass of Rhizopus arrhizus	Cr(VI)	24	Amine, hydroxyl	65

Ulva Lactuca	Hg(II)	149		66
Grape stalks	Cu(II)	10	Lignin	67
Functional polymers				
Herbicide 2,4-dichlorophenoxylicacetic acid	Cu(II), Ni(II), Zn(II), Cd(II)	27, 19, 18, 16	Carboxylic acid	68
Commercial silica grafted with an ethylediamine derivative, N-[3-(trimethoxysilyl) propyl-ethylenediamine]	Cu(II), Pb(II)	17, 38	amine	60
Poly(glycidylmethacrylate-co-methylmethacrylate)	Cr(VI)	2-23	acrylate	69
Aminated polyacrylamides and divinylbenzene	Co(II), Ni(II), Cu(II), Zn(II), Hg(II)	47, 38, 173, 130, 797	amine	70

The information obtained from the above discussion is that adsorbents can be used for the purpose of heavy metal removal, though effectivity and specificity vary with different adsorbents. A flowchart diagram of the above discussion is given in Figure 1.2.

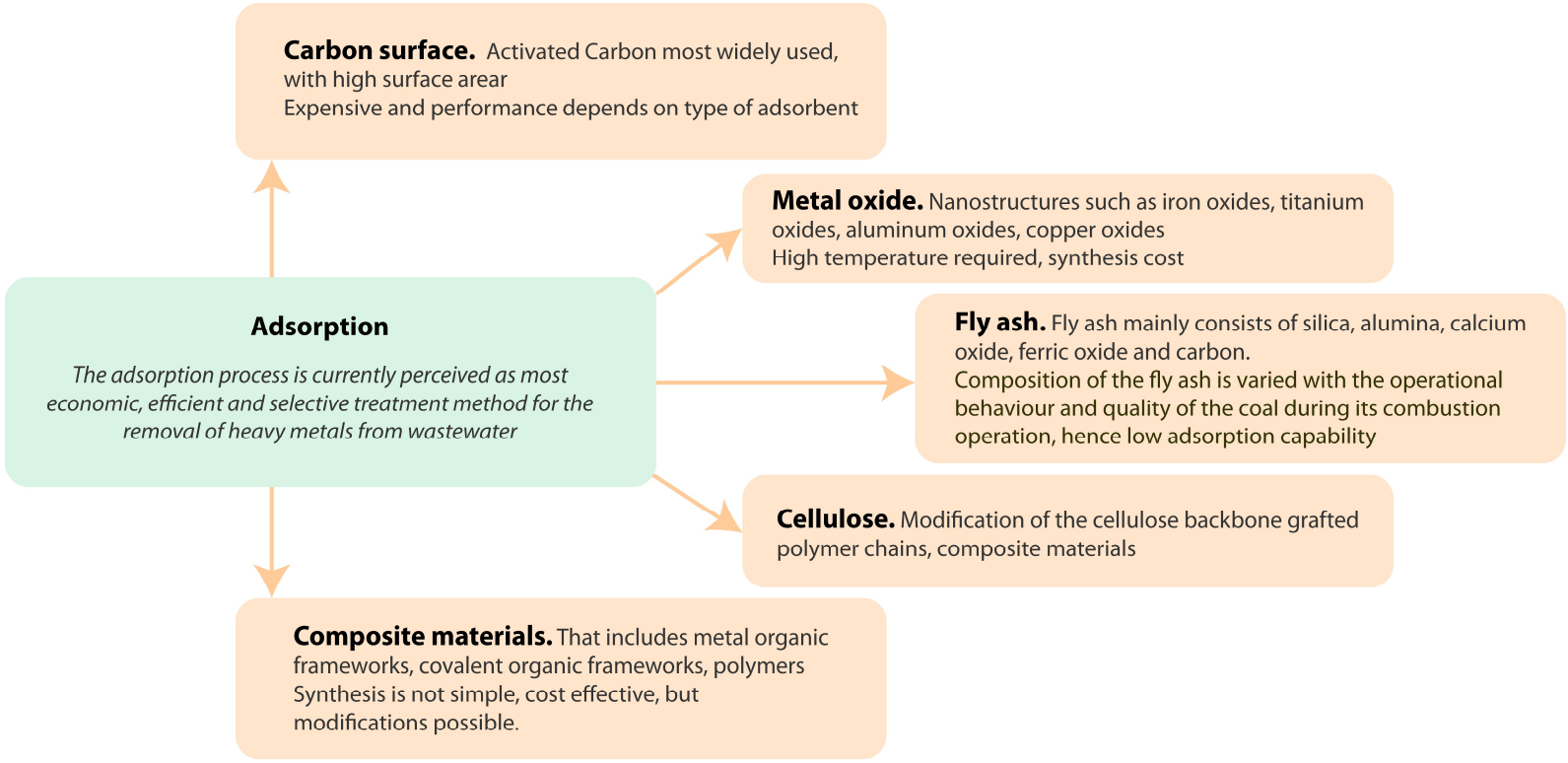

Figure 1.2. Flowchart showing the summary of various adsorbents used to bind heavy metals.

1.5. Functionalized materials as adsorbents for heavy metal removal: Usefulness of the amine functional group

Section 1.2 to 1.4 gave an overview scenario of the toxicity of different heavy metals and various methods used for their removal. The adsorption method was found to be the economically and technically most feasible method. The effectiveness of the adsorption process for the removal of pollutants depends on the adsorbent used.[57,59-62,67,68,70] Polymers containing several functional groups such as amines, carboxylate, ether, hydroxyl, sulfate, phenolic, cyanide, chloride, acetate, etc., have been used to remove a metal ion.[53,58,61-65,69] However, many of the reported functionalized polymers have complex synthesis procedures and are cost-ineffective. Therefore, developing a low-cost, functional polymer with moderate to high metal removal, easy synthesis procedure, modifications could be easy, rapid adsorption kinetics, and reusability is necessary.

Amine functional groups are of utmost importance in the field of industrial applications due to their high reactivity. It is a crucial starting point to many reactions. Amine-functionalized compounds have their application in agrochemical, pest control, pharmaceutical, dye production, food, even in the polymer industry.[71] They are crucial as monomers in various polymer syntheses, e.g., polyamides, polyimides, polyureas, etc. Many reports exist on using amine groups in various forms, e.g., polymeric amines, amines grafted on silica, amine on the surface of reduced graphene oxide, amine-functionalized cellulose, tertiary amine salts, metal-organic framework containing branched amines, modified chitosan, etc., for heavy metals removal. Very few reports are there on the properties that control the selection and binding of heavy metals in designing those materials. A brief

summary of the various amine-based functional polymeric materials used for heavy metal removal is presented in Table 1.4 with some of their chemical structures in Figure 1.3.

Table 1.4. Synthetic amine polymers in metal removal

Adsorbents	**Metals**	**Uptake (mg/g)/ removal (%)**	**Ref.**
- Aminopropyl (H_2N–$(CH_2)_3$–), [2aminoethylamino]-propyl (H_2N–$(CH_2)_2$–NH–$(CH_2)_3$–) and [(2-aminoethylamino)-ethylamino]-propyl (H_2N–$(CH_2)_2$–NH–$(CH_2)_2$–NH–$(CH_2)_3$– grafted silica materials	Cu(II), Ni(II), Pb(II), Cd(II), and Zn(II)	20-40, 30-60, 30-50, 30-75, 90-98	72
- Polyvinyl amine	Co(II), Cu(II), Ni(II), Pb(II), Fe(II), Cd(II), Zn(II), Mn(II)	60%, 97%, 20%, 30%, 99%, 99%, 40%	73
- 1,5-Diaminonaphthalene and 1,4-diaminoanthraquinone on the surface of reduced graphite oxide (RGO).	Pb(II)	0.06 mg/g, 92%; 0.05 mg/g, 76%	74
- Poly(amidoamine) [PAMAM] particles	Cu(II)	-	75
- Polyacrylamide/Sodium Montmorillonite (PAM/Na-MMT) Nanocomposites	Co(II), Ni(II)	98%; 99%	76
- Poly(aniline-co-mphenylenediamine)@Fe_3O_4 Nanocomposite	Pb(II), Cd(II), Co(II)	92%	77
- Amine-functionalized cellulose with abundant amino and carboxyl groups	Cd(II), Pb(II)	218, 139	78

- Graphene oxide/polyamidoamine dendrimers (GO/PAMAMs)	Pb(II), Cd(II), Cu(II), Mn(II)	~250, 75, 50, 20-25	79
- Ethylene Diamine Core Poly(amidoamine) Dendrimers	Cu(II)		80
- Modified Lignin	Cu(II), Zn(II), Cd(II), Pb(II)	20, 11.3, 7.7, 17.5	81
- Micro-hydrogel particles consisting of hyperbranched polyamidoamine (HPAMAM)	Cd(II), Cu(II), Pb(II), Ni(II), Zn(II), Co(II)	170, 270, ~150, <150	82
- Cellulose-Based Solid Amine Adsorbent	Cr(VI)	327.72	83
- Amphoteric Sodium Tertiary Amine Sulfonate Starches	P(II), Cu(II), and Zn(II)	0.050 meq/g	84
- Metal–Organic Framework/Polydopamine Composite	Pb(II), Hg(II)	394, 1634	85
- Aminoethanethiol-Grafted Porous Organic Polymer for	Hg(II)	181-232	86
- Porous Polymer Networks	$(SeO_4)^{2-}$ and $(SeO_3)^{2-}$, Hg(II)	124 (SeO_3^{2-})	87
- Chitosan/Gelatin Hydrogel	Pb(II), Cd(II), Hg(II), and Cr(III)		88
- Amine-Rich Ordered Mesoporous Phenolic Resin	Cr(VI)		89

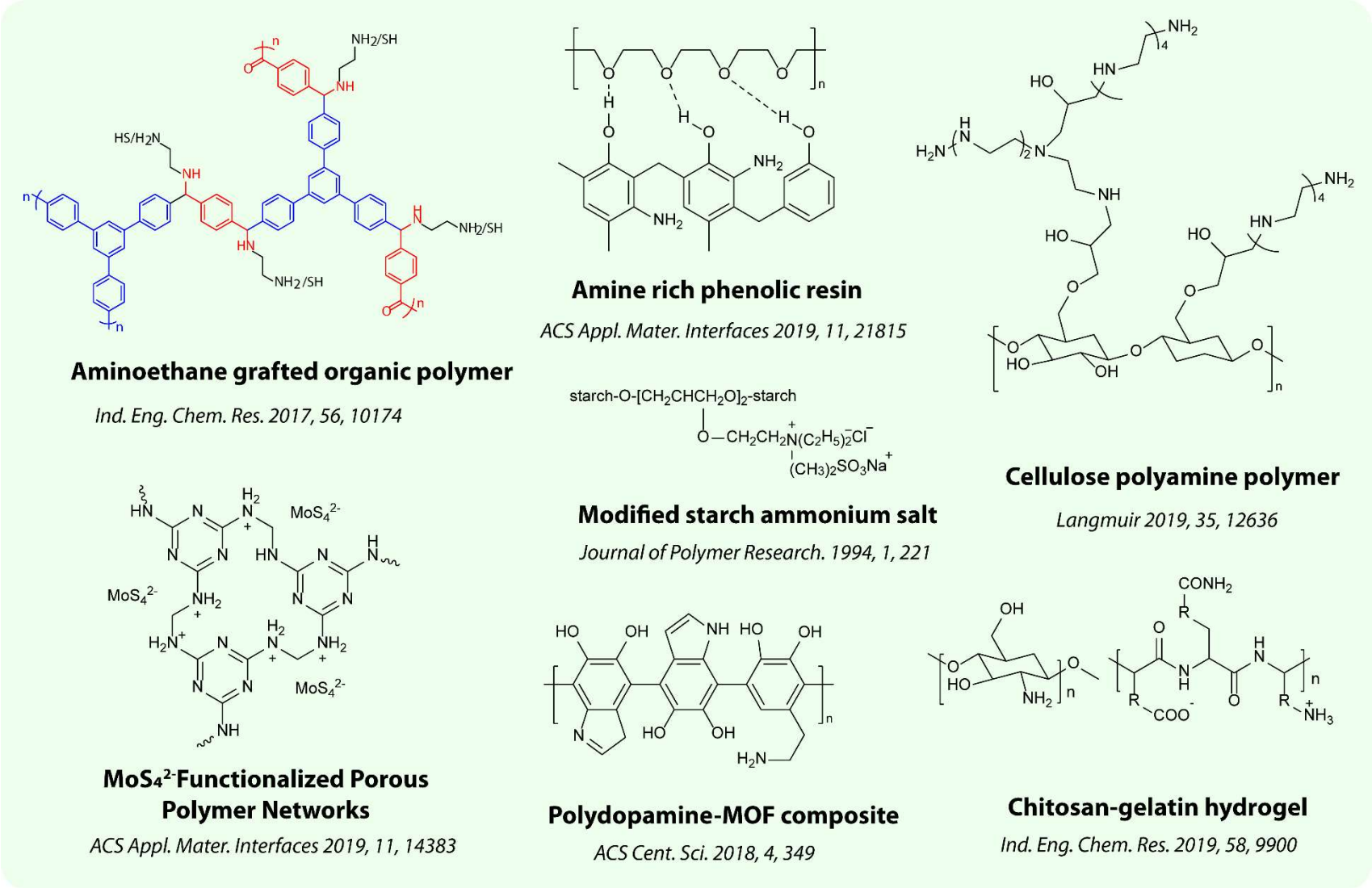

Figure 1.3. Some examples of functionalized amine-based polymer materials used for heavy metal binding.

1.6. Summary

The literature survey and discussions in the previous sections reveal the following facts:

(i) Heavy metals are toxic, and many anthropogenic industrial works have been releasing these metals into the environment.

(ii) Among the various removal techniques available for heavy metal removal, adsorption was found to be the economically and technically most feasible method.

(iii) The amine-based adsorbent materials have multipurpose applications in heavy metal removal. They are potent adsorbents for heavy metals like Cr(VI) and Hg(II).

The lack of literature has been identified as follows:

Many researchers synthesized amine base polymer such as polyacrylonitriles, porous polymeric networks, amine grafted organic polymer, polyacrylamides, polyethyleneimine, etc. and successfully employed for the removal of heavy metal ions from aqueous solution. However, the synthesis procedures of many of these functionalized polymers are complex and involve high costs. Thus, there is a need to synthesize low-cost functionalized polymer material with an easy synthesis procedure and acquire the properties of rapid metal removal kinetics, moderate to high metal removal efficiency, and stability for long-term use.

1.7. Scope of the present work

The information in the previous sections provides a basis to appreciate the scope and limitations of the type of material and heavy metal chosen in the present work. The usage of new material to bind heavy metals successfully from wastewater is essential. It deserves attention, but the ultimate challenge lies in understanding the underlying chemistry, and developing new methods or functionalizing those potent materials is of greater importance to the chemist.

Our group's past research work used amine-based polymer, aniline formaldehyde condensate (AFC) to remove heavy metals, dyes from an aqueous solution.[90–92] Our work showed solvent mixture control morphology of that polymer,[90], but the relationship between morphology, polymer forms, and site accessibility with metal removal remains unexplored.

Scheme 1.1 shows how one can utilize amine functionalization of a system with a polymeric backbone (green sphere) in multiple ways. In this thesis work, I became interested in using an amine polymer and increasing its adsorption capacities primarily because of two reasons. First, the amine functional group is a potential ligand that coordinates many heavy metals' ions. Secondly, these ligands give us a unique opportunity to functionalize them, introducing new donor groups for better metal coordination.

There are two ways to study any environmental process. One is to collect natural samples, analyze the data and correlate several system parameters with one another. The second method is to study model systems in controlled laboratory experiments. For this thesis work, the latter approach has been chosen.

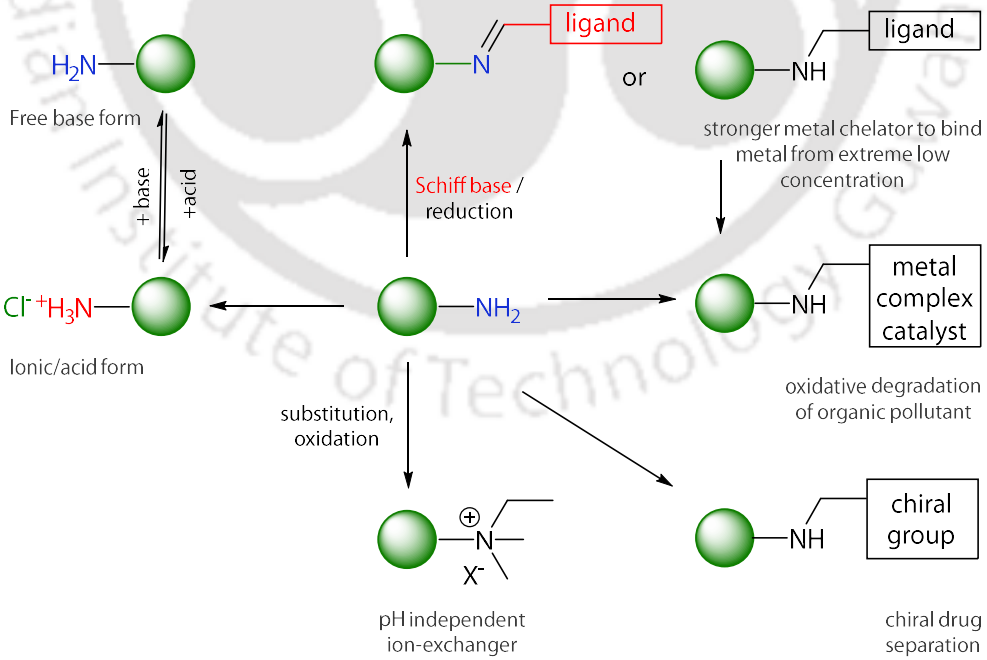

Scheme 1.1. Functionalization of free amine groups of a polymer.

Based on the above facts, the objectives of the thesis have been defined as follows.

- Synthesis of AFC polymer controlling the accessibility of the amine sites and surface property to increase its chromate adsorption capacity. (Chapter 2).
- Leaching and long-term storage properties and exploring another heavy metal, Hg(II) removal by these AFC polymers. (Chapter 3).
- Functionalization of amine with different donor groups to explore its behavior on heavy metal complexation (Chapter 4) and apply them in a polymeric system to study the effect in metal removal (Chapter 5).

1.7. Bibliography

(1) Vandecasteele, C.; Cornelis, G. Oxyanions in Waste: Occurrence, Leaching, Stabilisation, Relation to Wastewater Treatment BT - Water Treatment Technologies for the Removal of High-Toxicity Pollutants; Václavíková, M., Vitale, K., Gallios, G. P., Ivaničová, L., Eds.; Springer Netherlands: Dordrecht, 2010; pp 149–159. https://doi.org/10.1007/978-90-481-3497-7_12.

(2) Verbinnen, B. *Oxyanions In Industrial Waste And Wastewater Formation, Leaching And Adsorption*; 2014.

(3) Bridges, C. C.; Zalups, R. K. Molecular and Ionic Mimicry and the Transport of Toxic Metals. *Toxicol. Appl. Pharmacol.* **2005**, *204* (3), 274–308. https://doi.org/https://doi.org/10.1016/j.taap.2004.09.007.

(4) Srivastava, N. K.; Majumder, C. B. Novel Biofiltration Methods for the Treatment of Heavy Metals from Industrial Wastewater. *J. Hazard. Mater.* **2008**, *151* (1), 1–8. https://doi.org/https://doi.org/10.1016/j.jhazmat.2007.09.101.

(5) Barakat, M. A. New Trends in Removing Heavy Metals from Industrial Wastewater. *Arab. J. Chem.* **2011**, *4* (4), 361–377. https://doi.org/https://doi.org/10.1016/j.arabjc.2010.07.019.

(6) Dincer, I.; Colpan, C. O.; Kizilkan, O.; Ezan, M. A. Progress in Clean Energy. In *Novel Systems and Applications*; Springer, 2015; Vol. 2.

(7) Clemens, S.; Ma, J. F. Toxic Heavy Metal and Metalloid Accumulation in Crop Plants and Foods. *Annu. Rev. Plant Biol.* **2016**, *67* (1), 489–512. https://doi.org/10.1146/annurev-arplant-043015-112301.

(8) Tahar, L. Ben; Oueslati, M. H.; Abualreish, M. J. A. Synthesis of Magnetite Derivatives Nanoparticles and Their Application for the Removal of Chromium (VI) from Aqueous Solutions. *J. Colloid Interface Sci.* **2018**, *512*, 115–126. https://doi.org/https://doi.org/10.1016/j.jcis.2017.10.044.

(9) Kan, C.-C.; Ibe, A. H.; Rivera, K. K. P.; Arazo, R. O.; de Luna, M. D. G. Hexavalent Chromium Removal from Aqueous Solution by Adsorbents Synthesized from Groundwater

Treatment Residuals. *Sustain. Environ. Res.* **2017**, *27* (4), 163–171. https://doi.org/https://doi.org/10.1016/j.serj.2017.04.001.

(10) Services, H. Toxicological Profile for Chromium. *ATSDR's Toxicol. Profiles* **2002**, No. September. https://doi.org/10.1201/9781420061888_ch63.

(11) Robles-Camacho, J.; Armienta, M. A. Natural Chromium Contamination of Groundwater at León Valley, México. *J. Geochemical Explor.* **2000**, *68* (3), 167–181. https://doi.org/https://doi.org/10.1016/S0375-6742(99)00083-7.

(12) O'Brien, T. J.; Ceryak, S.; Patierno, S. R. Complexities of Chromium Carcinogenesis: Role of Cellular Response, Repair and Recovery Mechanisms. *Mutat. Res. Mol. Mech. Mutagen.* **2003**, *533* (1), 3–36. https://doi.org/https://doi.org/10.1016/j.mrfmmm.2003.09.006.

(13) Rahman, Z.; Singh, V. P. The Relative Impact of Toxic Heavy Metals (THMs) (Arsenic (As), Cadmium (Cd), Chromium (Cr)(VI), Mercury (Hg), and Lead (Pb)) on the Total Environment: An Overview. *Environ. Monit. Assess.* **2019**, *191* (7), 419. https://doi.org/10.1007/s10661-019-7528-7.

(14) Mortazavi, S. M. J.; Mortazavi, G.; Paknahad, M. A Review on the Distribution of Hg in the Environment and Its Human Health Impacts. *J. Hazard. Mater.* **2016**, *310*, 278–279. https://doi.org/https://doi.org/10.1016/j.jhazmat.2016.02.043.

(15) Zeng, H.; Wang, L.; Zhang, D.; Yan, P.; Nie, J.; Sharma, V. K.; Wang, C. Highly Efficient and Selective Removal of Mercury Ions Using Hyperbranched Polyethylenimine Functionalized Carboxymethyl Chitosan Composite Adsorbent. *Chem. Eng. J.* **2019**, *358*, 253–263. https://doi.org/https://doi.org/10.1016/j.cej.2018.10.001.

(16) Xu, J.; Bravo, A. G.; Lagerkvist, A.; Bertilsson, S.; Sjöblom, R.; Kumpiene, J. Sources and Remediation Techniques for Mercury Contaminated Soil. *Environ. Int.* **2015**, *74*, 42–53. https://doi.org/https://doi.org/10.1016/j.envint.2014.09.007.

(17) Bernhoft, R. A. Mercury Toxicity and Treatment: A Review of the Literature. *J. Environ. Public Health* **2012**, *2012*, 460508. https://doi.org/10.1155/2012/460508.

(18) Wang, Q.; Kim, D.; Dionysiou, D. D.; Sorial, G. A.; Timberlake, D. Sources and Remediation for Mercury Contamination in Aquatic Systems—a Literature Review. *Environ. Pollut.* **2004**, *131* (2), 323–336. https://doi.org/https://doi.org/10.1016/j.envpol.2004.01.010.

(19) Huang, Y.; Feng, F.; Chen, Z.-G.; Wu, T.; Wang, Z.-H. Green and Efficient Removal of Cadmium from Rice Flour Using Natural Deep Eutectic Solvents. *Food Chem.* **2018**, *244*, 260–265. https://doi.org/https://doi.org/10.1016/j.foodchem.2017.10.060.

(20) Xu, L.; Cao, G.; Xu, X.; Liu, S.; Duan, Z.; He, C.; Wang, Y.; Huang, Q. Simultaneous Removal of Cadmium, Zinc and Manganese Using Electrocoagulation: Influence of Operating Parameters and Electrolyte Nature. *J. Environ. Manage.* **2017**, *204*, 394–403. https://doi.org/https://doi.org/10.1016/j.jenvman.2017.09.020.

(21) Orlowski, C.; Piotrowski, J. K. Biological Levels of Cadmium and Zinc in the Small Intestine of Non-Occupationally Exposed Human Subjects. *Hum. Exp. Toxicol.* **2003**, *22* (2), 57–63.

(22) World Health Organization. Exposure to Cadmium: A Major Public Health Concern. *Prev. Dis. Through Heal. Environ.* **2010**, 3–6.

(23) Richardson, G. M.; Garrett, R.; Mitchell, I.; Mah-Poulson, M.; Hackbarth, T. Critical Review on Natural Global and Regional Emissions of Six Trace Metals to the Atmosphere. *Prep. Int. Lead Zinc Res. Organ. Int. Copp. Assoc. Nickel Prod. Environ. Res. Assoc.* **2001**.

(24) UNEP. Draft Final Review of Scientific Information on Cadmium. United Nations Environment Programme, Chemicals Branch, Nairobi 2008.

(25) Heraldy, E.; Lestari, W. W.; Permatasari, D.; Arimurti, D. D. Biosorbent from Tomato Waste and Apple Juice Residue for Lead Removal. *J. Environ. Chem. Eng.* **2018**, *6* (1), 1201–1208. https://doi.org/https://doi.org/10.1016/j.jece.2017.12.026.

(26) Cataldo, S.; Lazzara, G.; Massaro, M.; Muratore, N.; Pettignano, A.; Riela, S. Functionalized Halloysite Nanotubes for Enhanced Removal of Lead(II) Ions from Aqueous Solutions. *Appl. Clay Sci.* **2018**, *156*, 87–95. https://doi.org/https://doi.org/10.1016/j.clay.2018.01.028.

(27) Gidlow, D. A. Lead Toxicity. *Occup. Med. (Chic. Ill).* **2015**, *65* (5), 348–356.

(28) Abadin, H.; Ashizawa, A.; Stevens, Y.-W.; Llados, F.; Diamond, G.; Sage, G.; Citra, M.; Quinones, A.; Bosch, S. J.; Swarts, S. G. Toxicological Profile for Lead. **2020**, No. August, 582.

(29) World Health, O. *Preventing Disease through Healthy Environments: Exposure to Lead: A Major Public Health Concern (2019 Revision)*; World Health Organization, 2019.

(30) Rasul, S. B.; Munir, A. K. M.; Hossain, Z. A.; Khan, A. H.; Alauddin, M.; Hussam, A. Electrochemical Measurement and Speciation of Inorganic Arsenic in Groundwater of Bangladesh. *Talanta* **2002**, *58* (1), 33–43. https://doi.org/https://doi.org/10.1016/S0039-9140(02)00254-0.

(31) Drahota, P.; Filippi, M. Secondary Arsenic Minerals in the Environment: A Review. *Environ. Int.* **2009**, *35* (8), 1243–1255. https://doi.org/https://doi.org/10.1016/j.envint.2009.07.004.

(32) Mandal, B. K.; Suzuki, K. T. Arsenic Round the World: A Review. *Talanta* **2002**, *58* (1), 201–235. https://doi.org/https://doi.org/10.1016/S0039-9140(02)00268-0.

(33) Bundschuh, J.; Litter, M. I.; Parvez, F.; Román-Ross, G.; Nicolli, H. B.; Jean, J.-S.; Liu, C.-W.; López, D.; Armienta, M. A.; Guilherme, L. R. G.; Cuevas, A. G.; Cornejo, L.; Cumbal, L.; Toujaguez, R. One Century of Arsenic Exposure in Latin America: A Review of History and Occurrence from 14 Countries. *Sci. Total Environ.* **2012**, *429*, 2–35. https://doi.org/https://doi.org/10.1016/j.scitotenv.2011.06.024.

(34) Kruger, M. C.; Bertin, P. N.; Heipieper, H. J.; Arsène-Ploetze, F. Bacterial Metabolism of Environmental Arsenic—Mechanisms and Biotechnological Applications. *Appl. Microbiol. Biotechnol.* **2013**, *97* (9), 3827–3841. https://doi.org/10.1007/s00253-013-4838-5.

(35) Gresser, M. J. ADP-Arsenate. Formation by Submitochondrial Particles under Phosphorylating Conditions. *J. Biol. Chem.* **1981**, *256* (12), 5981–5983. https://doi.org/https://doi.org/10.1016/S0021-9258(19)69115-5.

(36) Rosen, B. P. Biochemistry of Arsenic Detoxification. *FEBS Lett.* **2002**, *529* (1), 86–92. https://doi.org/https://doi.org/10.1016/S0014-5793(02)03186-1.

(37) Mohan, D.; Pittman, C. U. Arsenic Removal from Water/Wastewater Using Adsorbents—A Critical Review. *J. Hazard. Mater.* **2007**, *142* (1), 1–53. https://doi.org/https://doi.org/10.1016/j.jhazmat.2007.01.006.

(38) Metcalf, L. Wastewater Engineering: Treatment and Reuse. Metcalf & Eddy Inc. McGraw-Hill Inc., New York 2003.

(39) Yao, W.; Wang, J.; Wang, P.; Wang, X.; Yu, S.; Zou, Y.; Hou, J.; Hayat, T.; Alsaedi, A.; Wang, X. Synergistic Coagulation of GO and Secondary Adsorption of Heavy Metal Ions on Ca/Al Layered Double Hydroxides. *Environ. Pollut.* **2017**, *229*, 827–836. https://doi.org/https://doi.org/10.1016/j.envpol.2017.06.084.

(40) Feng, Q.; Wu, D.; Zhao, Y.; Wei, A.; Wei, Q.; Fong, H. Electrospun AOPAN/RC Blend Nanofiber Membrane for Efficient Removal of Heavy Metal Ions from Water. *J. Hazard. Mater.* **2018**, *344*, 819–828. https://doi.org/https://doi.org/10.1016/j.jhazmat.2017.11.035.

(41) Ya, V.; Martin, N.; Chou, Y.-H.; Chen, Y.-M.; Choo, K.-H.; Chen, S.-S.; Li, C.-W. Electrochemical Treatment for Simultaneous Removal of Heavy Metals and Organics from Surface Finishing Wastewater Using Sacrificial Iron Anode. *J. Taiwan Inst. Chem. Eng.* **2018**, *83*, 107–114. https://doi.org/https://doi.org/10.1016/j.jtice.2017.12.004.

(42) Zhou, S.-F.; Wang, J.-J.; Gan, L.; Han, X.-J.; Fan, H.-L.; Mei, L.-Y.; Huang, J.; Liu, Y.-Q. Individual and Simultaneous Electrochemical Detection toward Heavy Metal Ions Based on L-Cysteine Modified Mesoporous MnFe2O4 Nanocrystal Clusters. *J. Alloys Compd.* **2017**, *721*, 492–500. https://doi.org/https://doi.org/10.1016/j.jallcom.2017.05.321.

(43) Tavakoli, O.; Goodarzi, V.; Saeb, M. R.; Mahmoodi, N. M.; Borja, R. Competitive Removal of Heavy Metal Ions from Squid Oil under Isothermal Condition by CR11 Chelate Ion Exchanger. *J. Hazard. Mater.* **2017**, *334*, 256–266. https://doi.org/https://doi.org/10.1016/j.jhazmat.2017.04.023.

(44) Fang, W.; Wei, Y.; Liu, J.; Kosson, D. S.; van der Sloot, H. A.; Zhang, P. Effects of Aerobic and Anaerobic Biological Processes on Leaching of Heavy Metals from Soil Amended with Sewage Sludge Compost. *Waste Manag.* **2016**, *58*, 324–334. https://doi.org/https://doi.org/10.1016/j.wasman.2016.07.036.

(45) Ge, J.; Xin-Geng; Du, Y.-H.; Chen, J.-J.; Zhang, L.; Bai, D.-M.; Ji, D.-Y.; Hu, Y.-L.; Li, Z.-H. Highly Sensitive Fluorescence Detection of Mercury (II) Ions Based on WS2 Nanosheets and T7 Exonuclease Assisted Cyclic Enzymatic Amplification. *Sensors Actuators B Chem.* **2017**, *249*, 189–194. https://doi.org/https://doi.org/10.1016/j.snb.2017.04.094.

(46) Peng, L.; Liu, P.; Feng, X.; Wang, Z.; Cheng, T.; Liang, Y.; Lin, Z.; Shi, Z. Kinetics of Heavy Metal Adsorption and Desorption in Soil: Developing a Unified Model Based on Chemical Speciation. *Geochim. Cosmochim. Acta* **2018**, *224*, 282–300. https://doi.org/https://doi.org/10.1016/j.gca.2018.01.014.

(47) Lee, S.-Y.; Choi, H.-J. Persimmon Leaf Bio-Waste for Adsorptive Removal of Heavy Metals from Aqueous Solution. *J. Environ. Manage.* **2018**, *209*, 382–392. https://doi.org/https://doi.org/10.1016/j.jenvman.2017.12.080.

(48) Panda, L.; Das, B.; Rao, D. S.; Mishra, B. K. Application of Dolochar in the Removal of Cadmium and Hexavalent Chromium Ions from Aqueous Solutions. *J. Hazard. Mater.* **2011**, *192* (2), 822–831. https://doi.org/https://doi.org/10.1016/j.jhazmat.2011.05.098.

(49) Yu, J.-G.; Yue, B.-Y.; Wu, X.-W.; Liu, Q.; Jiao, F.-P.; Jiang, X.-Y.; Chen, X.-Q. Removal of Mercury by Adsorption: A Review. *Environ. Sci. Pollut. Res.* **2016**, *23* (6), 5056–5076. https://doi.org/10.1007/s11356-015-5880-x.

(50) Madhavi, V.; Prasad, T. N. V. K. V; Reddy, A. V. B.; Ravindra Reddy, B.; Madhavi, G. Application of Phytogenic Zerovalent Iron Nanoparticles in the Adsorption of Hexavalent Chromium. *Spectrochim. Acta Part A Mol. Biomol. Spectrosc.* **2013**, *116*, 17–25. https://doi.org/https://doi.org/10.1016/j.saa.2013.06.045.

(51) Hayati, B.; Maleki, A.; Najafi, F.; Daraei, H.; Gharibi, F.; McKay, G. Super High Removal Capacities of Heavy Metals (Pb2+ and Cu2+) Using CNT Dendrimer. *J. Hazard. Mater.* **2017**, *336*, 146–157. https://doi.org/https://doi.org/10.1016/j.jhazmat.2017.02.059.

(52) Gupta, V. K.; Jain, C. K.; Ali, I.; Sharma, M.; Saini, V. K. Removal of Cadmium and Nickel from Wastewater Using Bagasse Fly Ash—a Sugar Industry Waste. *Water Res.* **2003**, *37* (16), 4038–4044. https://doi.org/https://doi.org/10.1016/S0043-1354(03)00292-6.

(53) Sekar, M.; Sakthi, V.; Rengaraj, S. Kinetics and Equilibrium Adsorption Study of Lead(II) onto Activated Carbon Prepared from Coconut Shell. *J. Colloid Interface Sci.* **2004**, *279* (2), 307–313. https://doi.org/https://doi.org/10.1016/j.jcis.2004.06.042.

(54) Ekinci, E.; Budinova, T.; Yardim, F.; Petrov, N.; Razvigorova, M.; Minkova, V. Removal of Mercury Ion from Aqueous Solution by Activated Carbons Obtained from Biomass and Coals. *Fuel Process. Technol.* **2002**, *77–78*, 437–443. https://doi.org/https://doi.org/10.1016/S0378-3820(02)00065-6.

(55) Hu, Z.; Lei, L.; Li, Y.; Ni, Y. Chromium Adsorption on High-Performance Activated Carbons from Aqueous Solution. *Sep. Purif. Technol.* **2003**, *31* (1), 13–18. https://doi.org/https://doi.org/10.1016/S1383-5866(02)00149-1.

(56) Karthikeyan, T.; Rajgopal, S.; Miranda, L. R. Chromium(VI) Adsorption from Aqueous Solution by Hevea Brasilinesis Sawdust Activated Carbon. *J Hazard Mater* **2005**, *124* (1–3), 192–199.

(57) Ho, Y.-S. Removal of Copper Ions from Aqueous Solution by Tree Fern. *Water Res.* **2003**, *37* (10), 2323–2330. https://doi.org/https://doi.org/10.1016/S0043-1354(03)00002-2.

(58) Ricordel, S.; Taha, S.; Cisse, I.; Dorange, G. Heavy Metals Removal by Adsorption onto Peanut Husks Carbon: Characterization, Kinetic Study and Modeling. *Sep. Purif. Technol.* **2001**, *24* (3), 389–401. https://doi.org/https://doi.org/10.1016/S1383-5866(01)00139-3.

(59) Gündoğan, R.; Acemioğlu, B.; Alma, M. H. Copper (II) Adsorption from Aqueous Solution by Herbaceous Peat. *J. Colloid Interface Sci.* **2004**, *269* (2), 303–309. https://doi.org/https://doi.org/10.1016/S0021-9797(03)00762-8.

(60) Chiron, N.; Guilet, R.; Deydier, E. Adsorption of Cu(II) and Pb(II) onto a Grafted Silica: Isotherms and Kinetic Models. *Water Res.* **2003**, *37* (13), 3079–3086. https://doi.org/https://doi.org/10.1016/S0043-1354(03)00156-8.

(61) Okieimen, F. E.; Sogbaike, C. E.; Ebhoaye, J. E. Removal of Cadmium and Copper Ions from Aqueous Solution with Cellulose Graft Copolymers. *Sep. Purif. Technol.* **2005**, *44* (1), 85–89. https://doi.org/https://doi.org/10.1016/j.seppur.2004.11.003.

(62) Saeed, A.; Akhter, M. W.; Iqbal, M. Removal and Recovery of Heavy Metals from Aqueous Solution Using Papaya Wood as a New Biosorbent. *Sep. Purif. Technol.* **2005**, *45* (1), 25–31. https://doi.org/https://doi.org/10.1016/j.seppur.2005.02.004.

(63) Matheickal, J. T.; Yu, Q.; Woodburn, G. M. Biosorption of Cadmium(II) from Aqueous Solutions by Pre-Treated Biomass of Marine Alga DurvillAea Potatorum. *Water Res.* **1999**, *33* (2), 335–342. https://doi.org/https://doi.org/10.1016/S0043-1354(98)00237-1.

(64) Singh, K. K.; Talat, M.; Hasan, S. H. Removal of Lead from Aqueous Solutions by Agricultural Waste Maize Bran. *Bioresour. Technol.* **2006**, *97* (16), 2124–2130. https://doi.org/https://doi.org/10.1016/j.biortech.2005.09.016.

(65) Prakasham, R. S.; Merrie, J. S.; Sheela, R.; Saswathi, N.; Ramakrishna, S. V. Biosorption of Chromium VI by Free and Immobilized Rhizopus Arrhizus. *Environ. Pollut.* **1999**, *104* (3), 421–427. https://doi.org/https://doi.org/10.1016/S0269-7491(98)00174-2.

(66) Zeroual, Y.; Moutaouakkil, A.; Zohra Dzairi, F.; Talbi, M.; Ung Chung, P.; Lee, K.; Blaghen, M. Biosorption of Mercury from Aqueous Solution by Ulva Lactuca Biomass. *Bioresour. Technol.* **2003**, *90* (3), 349–351. https://doi.org/https://doi.org/10.1016/S0960-8524(03)00122-6.

(67) Villaescusa, I.; Fiol, N.; Martínez, M.; Miralles, N.; Poch, J.; Serarols, J. Removal of Copper and Nickel Ions from Aqueous Solutions by Grape Stalks Wastes. *Water Res.* **2004**, *38* (4), 992–1002. https://doi.org/https://doi.org/10.1016/j.watres.2003.10.040.

(68) Prado, A. G. S.; Airoldi, C. Adsorption, Preconcentration and Separation of Cations on Silica Gel Chemically Modified with the Herbicide 2,4-Dichlorophenoxyacetic Acid. *Anal. Chim. Acta* **2001**, *432* (2), 201–211. https://doi.org/https://doi.org/10.1016/S0003-2670(00)01372-6.

(69) Bayramoğlu, G.; Yakup Arica, M. Adsorption of Cr(VI) onto PEI Immobilized Acrylate-Based Magnetic Beads: Isotherms, Kinetics and Thermodynamics Study. *Chem. Eng. J.* **2008**, *139* (1), 20–28. https://doi.org/https://doi.org/10.1016/j.cej.2007.07.068.

(70) Mathew, B.; Pillai, V. N. R. Polymer-Metal Complexes of Amino Functionalized Divinylbenzene-Crosslinked Polyacrylamides. *Polymer (Guildf).* **1993**, *34* (12), 2650–2658.

(71) Froidevaux, V.; Negrell, C.; Caillol, S.; Pascault, J.-P.; Boutevin, B. Biobased Amines: From Synthesis to Polymers; Present and Future. *Chem. Rev.* **2016**, *116* (22), 14181–14224. https://doi.org/10.1021/acs.chemrev.6b00486.

(72) Aguado, J.; Arsuaga, J. M.; Arencibia, A.; Lindo, M.; Gascón, V. Aqueous Heavy Metals Removal by Adsorption on Amine-Functionalized Mesoporous Silica. *J. Hazard. Mater.* **2009**, *163* (1), 213–221. https://doi.org/10.1016/j.jhazmat.2008.06.080.

(73) Huang, Y.; Wu, D.; Wang, X.; Huang, W.; Lawless, D.; Feng, X. Removal of Heavy Metals from Water Using Polyvinylamine by Polymer-Enhanced Ultrafiltration and Flocculation. *Sep. Purif. Technol.* **2016**, *158*, 124–136. https://doi.org/10.1016/j.seppur.2015.12.008.

(74) Olanipekun, O.; Oyefusi, A.; Neelgund, G. M.; Oki, A. Synthesis and Characterization of Reduced Graphite Oxide-Polymer Composites and Their Application in Adsorption of Lead. *Spectrochim. Acta - Part A Mol. Biomol. Spectrosc.* **2015**, *149*, 991–996. https://doi.org/10.1016/j.saa.2015.04.071.

(75) Kotte, M. R.; Kuvarega, A. T.; Cho, M.; Mamba, B. B.; Diallo, M. S. Mixed Matrix PVDF Membranes With in Situ Synthesized PAMAM Dendrimer-Like Particles: A New Class of Sorbents for Cu(II) Recovery from Aqueous Solutions by Ultrafiltration. *Environ. Sci. Technol.* **2015**, *49* (16), 9431–9442. https://doi.org/10.1021/acs.est.5b01594.

(76) Moreno-Sader, K.; García-Padilla, A.; Realpe, A.; Acevedo-Morantes, M.; Soares, J. B. P. Removal of Heavy Metal Water Pollutants (Co2+ and Ni2+) Using Polyacrylamide/Sodium Montmorillonite (PAM/Na-MMT) Nanocomposites. *ACS Omega* **2019**, *4* (6), 10834–10844. https://doi.org/10.1021/acsomega.9b00981.

(77) Zare, E. N.; Lakouraj, M. M.; Kasirian, N. Development of Effective Nano-Biosorbent Based on Poly m-Phenylenediamine Grafted Dextrin for Removal of Pb (II) and Methylene Blue from Water. *Carbohydr. Polym.* **2018**, *201*, 539–548. https://doi.org/https://doi.org/10.1016/j.carbpol.2018.08.091.

(78) Fan, H.; Wang, J.; Zhang, Q.; Jin, Z. Tannic Acid-Based Multifunctional Hydrogels with Facile Adjustable Adhesion and Cohesion Contributed by Polyphenol Supramolecular Chemistry. *ACS Omega* **2017**, *2* (10), 6668–6676. https://doi.org/10.1021/acsomega.7b01067.

(79) Zhang, F.; Wang, B.; He, S.; Man, R. Preparation of Graphene-Oxide/Polyamidoamine Dendrimers and Their Adsorption Properties toward Some Heavy Metal Ions. *J. Chem. Eng. Data* **2014**, *59* (5), 1719–1726. https://doi.org/10.1021/je500219e.

(80) Diallo, M. S.; Christie, S.; Swaminathan, P.; Balogh, L.; Shi, X.; Um, W.; Papelis, C.; Goddard, W. A.; Johnson, J. H. Dendritic Chelating Agents. 1. Cu(II) Binding to Ethylene Diamine Core Poly(Amidoamine) Dendrimers in Aqueous Solutions. *Langmuir* **2004**, *20* (7), 2640–2651. https://doi.org/10.1021/la036108k.

(81) Celik, A.; Demirbaş, A. Removal of Heavy Metal Ions from Aqueous Solutions via Adsorption onto Modified Lignin from Pulping Wastes. *Energy Sources* **2005**, *27* (12), 1167–1177. https://doi.org/10.1080/00908310490479583.

(82) Lee, S.; Eom, Y.; Park, J.; Lee, J.; Kim, S. Y. Micro-Hydrogel Particles Consisting of Hyperbranched Polyamidoamine for the Removal of Heavy Metal Ions from Water. *Sci. Rep.* **2017**, *7* (1), 1–9. https://doi.org/10.1038/s41598-017-10066-x.

(83) Xue, F.; He, H.; Zhu, H.; Huang, H.; Wu, Q.; Wang, S. Structural Design of a Cellulose-Based Solid Amine Adsorbent for the Complete Removal and Colorimetric Detection of Cr(VI). *Langmuir* **2019**, *35* (39), 12636–12646. https://doi.org/10.1021/acs.langmuir.9b01788.

(84) Chan, W.-C. Removal of Heavy Metal Ions with Water-Insoluble Amphoteric Sodium Tertiary Amine Sulfonate Starches. *J. Polym. Res.* **1994**, *1* (2), 221–226. https://doi.org/10.1007/BF01374099.

(85) Sun, D. T.; Peng, L.; Reeder, W. S.; Moosavi, S. M.; Tiana, D.; Britt, D. K.; Oveisi, E.; Queen, W. L. Rapid, Selective Heavy Metal Removal from Water by a Metal–Organic Framework/Polydopamine Composite. *ACS Cent. Sci.* **2018**, *4* (3), 349–356. https://doi.org/10.1021/acscentsci.7b00605.

(86) Ravi, S.; Puthiaraj, P.; Row, K. H.; Park, D.-W.; Ahn, W.-S. Aminoethanethiol-Grafted Porous Organic Polymer for Hg2+ Removal in Aqueous Solution. *Ind. Eng. Chem. Res.* **2017**, *56* (36), 10174–10182. https://doi.org/10.1021/acs.iecr.7b02743.

(87) Feng, L.; Chen, W.-M.; Li, J.-L.; Day, G.; Drake, H.; Joseph, E.; Zhou, H.-C. Biological Antagonism Inspired Detoxification: Removal of Toxic Elements by Porous Polymer

Networks. *ACS Appl. Mater. Interfaces* **2019**, *11* (15), 14383–14390. https://doi.org/10.1021/acsami.9b02826.

(88) Perumal, S.; Atchudan, R.; Yoon, D. H.; Joo, J.; Cheong, I. W. Spherical Chitosan/Gelatin Hydrogel Particles for Removal of Multiple Heavy Metal Ions from Wastewater. *Ind. Eng. Chem. Res.* **2019**, *58* (23), 9900–9907. https://doi.org/10.1021/acs.iecr.9b01298.

(89) Wang, K.; Yang, L.; Li, H.; Zhang, F. Surfactant Pyrolysis-Guided in Situ Fabrication of Primary Amine-Rich Ordered Mesoporous Phenolic Resin Displaying Efficient Heavy Metal Removal. *ACS Appl. Mater. Interfaces* **2019**, *11* (24), 21815–21821. https://doi.org/10.1021/acsami.9b03063.

(90) Koner, R. R.; Albino Kumar, P.; Chakraborty, S.; Ray, M. Synthesis of Morphologically Different, Metal Absorbing Aniline-Formaldehyde Polymers Including Micron-Sized Sphere Using Simple Alcohols as Morphology Modifier. *J. Appl. Polym. Sci.* **2008**, *110* (2), 1158–1164. https://doi.org/10.1002/app.28746.

(91) Terangpi, P.; Chakraborty, S. Adsorption Kinetics and Equilibrium Studies for Removal of Acid Azo Dyes by Aniline Formaldehyde Condensate. *Appl. Water Sci.* **2017**, *7* (7), 3661–3671. https://doi.org/10.1007/s13201-016-0510-4.

(92) Terangpi, P.; Chakraborty, S.; Ray, M. Improved Removal of Hexavalent Chromium from 10 mg/L Solution by New Micron Sized Polymer Clusters of Aniline Formaldehyde Condensate. *Chem. Eng. J.* **2018**, *350*, 599–607. https://doi.org/https://doi.org/10.1016/j.cej.2018.05.171.

Chapter 2

Site orientation, accessibility, and surface hydrophobicity control on AFC polymer to increase hexavalent chromium removal performance

2.1. Introduction

Simple mixing of aniline, acid, and formaldehyde readily forms a sticky polymer known as Aniline-Formaldehyde Condensate (AFC).[1,2] The reaction has been known for years. However, besides being used as a classroom demonstration of polymer synthesis or some limited use in the glue industry, it served no useful purpose until recently.[3–5] On the other hand, Bakelite, synthesized by an almost identical reaction using phenol instead of aniline, and polyaniline, synthesized using oxidizer instead of formaldehyde, are synthesized using oxidizer instead of formaldehyde well studied and has several applications.[6,7]

The problem of AFC is multifold. The formation is highly exothermic, resulting in a dark solid rubbery mass with a quick rise in temperature above 40 ℃. Physical and chemical properties vary widely depending on the ratio of the ingredients and reaction temperature.[1,2] Despite these limitations, the availability of the amine functional group, which is amenable to further functionalization through simple organic reactions, is quite attractive for its potential use in multiple areas. However, the bottleneck in achieving these is controlling the reaction to form a chemically and physically uniform polymer where maximum sites are accessible, and the process is well understood.

AFC in different forms showed Cr(VI) removal. Chromium compounds are toxic pollutant with severe health damages found everywhere in the environment because of various industries, which include leather tanning, electroplating, paint, and pigments, dyeing, textile, etc.[8–10] Chromium ions are of mainly two types, one is trivalent Cr(III), and the other one is hexavalent Cr(VI). The toxicity of chromium compounds depends on both their valency and bioavailability. Trivalent Cr(III) and hexavalent Cr(VI) show different chemical and biological activities.[11–13] Cr(III) is the most stable oxidation state of chromium, and it can bind with nucleic acids, proteins at biological pH. However, they are impermeable to biological membranes under physiological conditions. On the other hand, Cr(VI) exists

as strong oxidizing chromate and dichromate ions. The chromate ion, CrO_4^- and dichromate ion, $Cr_2O_7^{2-}$, remain in equilibrium depending on the solution pH and concentration of Cr. The chromate ion, CrO_4^- form predominates under pH 6.5 and pCr value of 1.5.[14,15], which can easily cross the biological membrane and get reduced to Cr(III). Trivalent Cr(III) ions have some biological roles, whereas Cr(VI) ions are hazardous.[16–18] Cr(VI) is five hundred times more toxic and carcinogenic than Cr(III), and it causes skin irritations, lung cancer, liver, kidney damage.[11–13] Therefore, it is essential to remove this toxic metal from wastewater before it gets discharged into the environment and from drinking water. During the last few years, many types of research have been done focusing on the selective removal of Cr(VI) from waste and drinking water. Several methods, including ion exchange, chemical precipitation, filtration, adsorption, and electrodeposition, have been developed for Cr(VI) removal, but adsorption remains the preferred method.[8,18,19]

In the recent past, our group successfully used AFC polymer in different forms as a Cr(VI)/chromate adsorbent.[3,5,20] The work also showed that the solvent mixture in the reaction medium altered the morphology of the polymer.[2] Despite these applications, multiple aspects of the polymer synthesis, control over its morphology, physical properties, and site accessibility were still in infancy for further applications.

AFC polymer with an amine functional group can exist in either an acid salt or free amine form. In this chapter, we synthesized AFC polymer in salt form, Poly-1s, and Poly-2s, by switching the ratio between isopropanol to an aqueous solution in the reaction medium from 3:1 to 1:3. Another version of AFC in salt form, Poly-3s, was prepared in a reduced volume using an intermediate solvent ratio. Treatment with a base produced the corresponding polymers in a free base form (Poly-1b from Poly-1s, Poly-2b from Poly-2s, and Poly-3b from Poly-3s). We characterized them using multiple analytical and spectroscopic tools and studied their chromate removal from aqueous solutions. Reversing

the isopropanol to water ratio reversed the orientation of the amine groups, which significantly altered their physical properties. This work demonstrates that the relationship between surface property and site accessibility profoundly impacts chromate binding property.

2.2. Experimental section

2.2.1. Solvents and reagents

Commercial grade aniline from Merck India was used for polymer synthesis. Aniline was purified by distilling over KOH pellets at 180 ℃. Isopropanol and formaldehyde (37% w/v) from Merck India were used as received. 2,5-Dihydroxybenzoic acid (2,5-DHB) and trifluoroacetic acid (TFA) were purchased from Sigma Aldrich. Other reagents were obtained from commercial sources and used without further purification unless otherwise stated. Water purified by a Merck Direct Q8 ultrapure water purification system was used to prepare all solutions and reactions. Whatman® grade 1 qualitative filter paper was used for filtration during the adsorption experiments.

2.2.2. Measurements

The FTIR spectra were recorded on a Perkin-Elmer Spectrum one FT-IR spectrophotometer with KBr discs in the range 4000-400 cm^{-1}. Elemental analyses were performed using a EuroEA Elemental Analyzer at Biotech Park Guwahati. Particle size was analyzed using a Malvern Panalytical Zetasizer Nano ZS90 dynamic light scattering (DLS) analyzer. Thermogravimetric analysis of the compounds was performed using a Netzsch STA449F3A00 TG analyzer with a heating rate of 10 ℃/min under an Ar atmosphere using a 5-10 mg sample size per run. The Matrix-Assisted Laser Desorption/Ionization mass spectra of the insoluble polymers were obtained using a BRUKER Model: AUTOFLEX SPEED MALDI-TOF spectrometer. To measure the MALDI mass, samples (2-3 mg) were

added to 2 mL of the 2,5-DHB matrix. The matrix was prepared by dissolving 1 mg/mL 2,5-DHB in a solvent mixture containing 30:70 [v/v] acetonitrile and 0.1% TFA in water. 0.5 µL of the matrix-polymer mixture was deposited onto the MALDI target and allowed to dry before analysis. The surface morphologies of the polymers were studied using Zeiss Sigma and Zeiss Gemini Field emission scanning electron microscope (FESEM) instruments, and the polymer samples were coated with gold vapor twice before measurement to reduce charging. The dispersed polymer samples in ethanol were dropped, cast on a silver foil to obtain a thin layer of the polymer surface, and air-dried in a desiccator over silica. Before analysis, the samples were mounted with carbon tape on FESEM stabs. Gas adsorption experiments were performed on a Quantachrome Autosorb-IQ MP instrument to determine the surface area of the samples. The samples were degassed at 50 ℃ before the experiment. The total chromium concentration was measured using a Varian model 55B atomic absorption spectrometer (AAS) using an air-acetylene flame at a wavelength of 429 nm with a slit width of 0.5 nm. The calibration graph was first determined, and then the chromium concentration of the unknown was measured. The calibration curve was linear, with a correlation coefficient of 0.99. All pH measurements were performed using Eutech instruments' EcoScan pH 6 pH-meter. Contact angle measurements were performed using a Kruss Drop Shape Analyser-DSA25 instrument. Solid-state X-Band EPR spectra were recorded using a Jeol JES-FA series spectrometer fitted with a quartz dewar for measurements at room temperature. The spectra were calibrated using an internal manganese (Mn) marker. The solution temperatures were measured using a JSGW Mercury chemical thermometer.

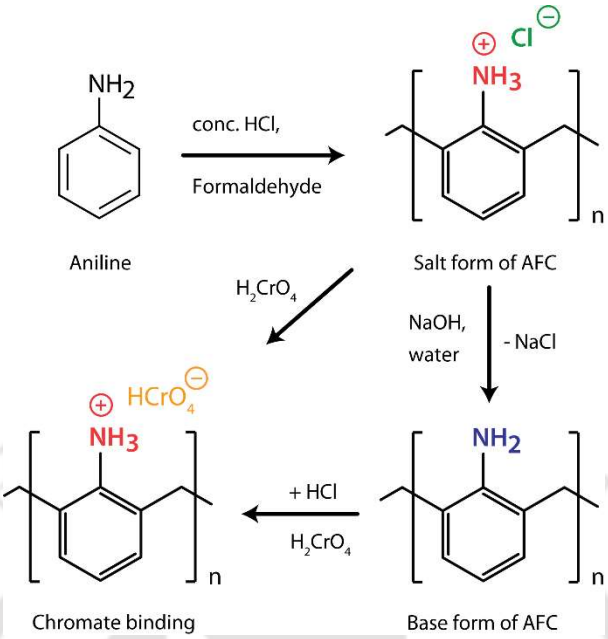

Scheme 2.1. Polymer synthesis of salt and base forms.

2.2.3. Synthesis and characterization

2.2.3.1. Poly-1s. A solution of concentrated HCl (9.66 mL, 96.6 mmol) was added dropwise to distilled aniline (9 g, 96.6 mmol). Isopropanol (120 mL) and water (14.66 mL) were added to this while stirring and cooled in contact with the ice water mixture (3 ℃). The solution was clear at this stage. The temperature of the solution was reduced to 7 ℃ within a few minutes. Formaldehyde (15.68 mL, 193.2 mmol), similarly cooled, was added all at once, and the resulting solution was shaken vigorously to form a uniform solution (Figure 2.1). After approximately 3 min, the solution temperature started rising along with the appearance of cloudiness. The temperature maxima reached about 10 ℃. At this stage, the whole solution appeared to be a frozen lump of a light orange solid. The mixture was kept on ice water for approximately 2 h. After 2 h, the mixture was kept at room temperature for 4 h. The lumps could be easily broken into a slurry with a mortar pastel. 100 mL of 1N HCl was added to the polymer in a beaker and stirred for 3 h. Stirring was used to ensure the solubility of all the acid-soluble low-molecular-weight polymers. The

resulting slurry was filtered through a Büchner funnel to remove the soluble fraction. The polymer was washed first with isopropanol followed by distilled water until the pH of the filtrate was neutral. Isopropanol (50 mL) was added and filtered using a Büchner funnel. The yellow-orange filtrate may have been due to the low molecular weight soluble form of the polymer. The solid was washed with isopropanol until the filtrate became nearly colorless. Finally, it was dried in a vacuum desiccator with a silica gel desiccant for 10 days. The dried polymer was a fine orange powder. It is easily dispersible in water or ethanol upon ultrasonication for a few minutes. The total volume of the solution, the ratio of water to isopropanol, and the aniline, formaldehyde, and HCl ratios were 169 mL, 1:3, and 1:2:1, respectively (Table 2.1). The yield of the product was found to be 26 g. FTIR (KBr, cm^{-1}) 3397(s), 3017(m), 2850(m), 1662(s), 1613(s), 1517(s), and 821(m). Ana. calculated for $(C_7H_7N \bullet HCl)n$: C, 59.38; H, 5.69; N, 9.89. Found C, 59.19; H, 5.63; N, 9.52.

2.2.3.2. Poly-1b. Poly-1s (2 g) synthesized above was placed in a round bottom flask and stirred with 20 ml of 1N NaOH for about 2 h. The orange color of Poly-1s immediately turned into a light brown slurry. It was filtered using filter paper. The slurry was washed with water to remove traces of NaOH and NaCl until the filtrate was neutral to the pH paper. The bulk of the adhered water was removed by soaking in a dry filter paper. It was kept in a vacuum desiccator over anhydrous calcium chloride for two days. The yield of the solid was 1.9 g. FTIR (KBr, cm^{-1}) 3401(s), 2896(m) 1660(s), 1611(s), 1514(s), and 833(m). Ana. calculated for $(C_7H_7N)n$: C, 79.97; H, 6.71; N, 13.32. Found C, 76.92; H, 6.41; N, 12.57.

2.2.3.3. Poly-2s. A solution of concentrated HCl (9.66 mL, 96.6 mmol) was added dropwise to distilled aniline (9 g, 96.6 mmol). Isopropanol (40 mL) and water (94.66 mL) were added while stirring and cooled in contact with the ice water mixture (3 ℃). The solution was clear at this stage. The temperature of the solution was reduced to 7 ℃ within

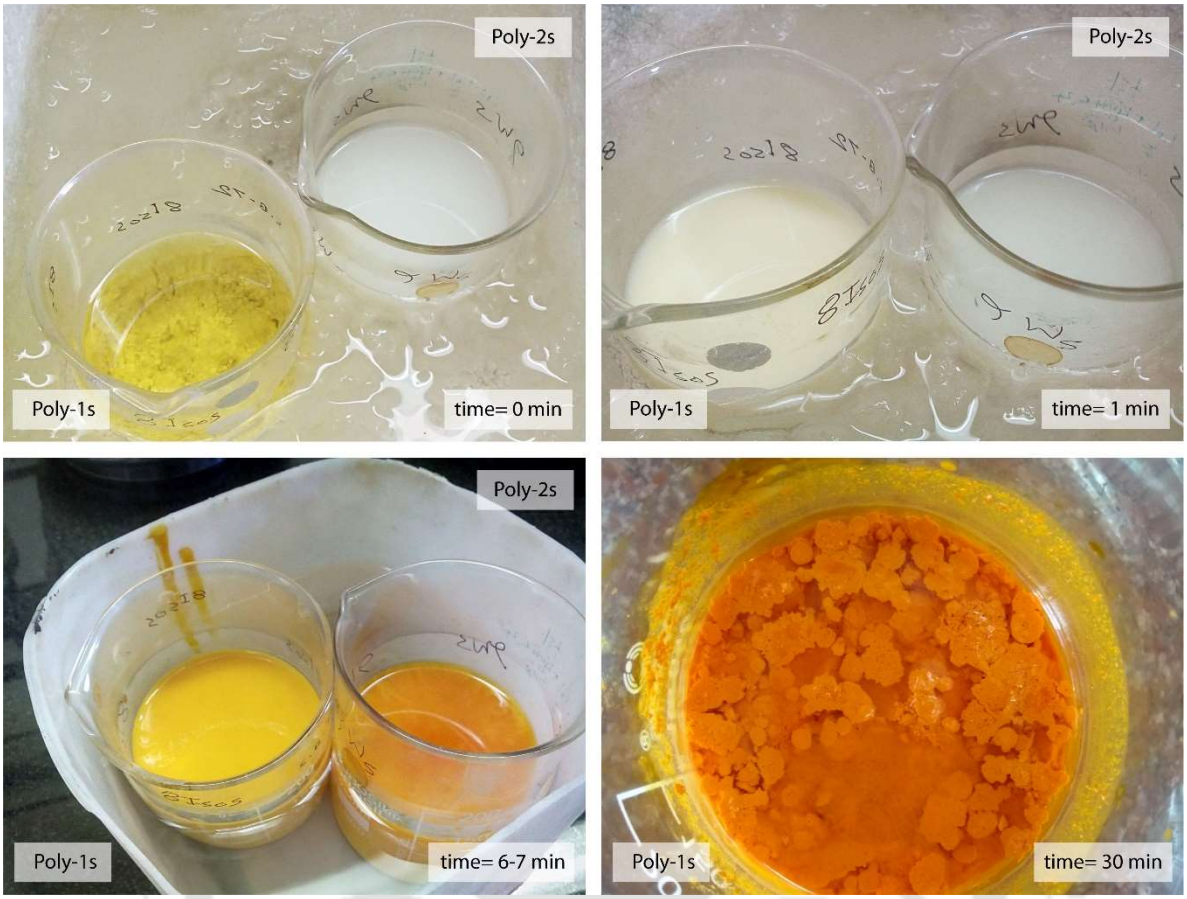

Figure 2.1. Different stages of polymer formation. Poly-1s has more isopropanol, while Poly-2s has more water.

a few minutes. Formaldehyde (15.68 mL, 193.2 mmol), similarly cooled, was added all at once, and the resulting solution was shaken vigorously to form a uniform solution. Within 1 min, the solution temperature started rising along with the appearance of cloudiness (Figure 2.1). The temperature maxima reached approximately 10 ℃ in less than 3 min. The whole solution became a lump of the orange gel after about 7 min. The mixture was kept in ice water for about 2 h. After 2 h, the mixture was kept at room temperature for 4 h. Unlike polymer Poly-1s, this polymer was more gelatinous. 1N HCl was added to the polymer in a beaker and stirred for 3 h. This was to ensure that all the acid-soluble low-molecular-weight polymers came into the solution. It was then filtered through a Büchner funnel and washed with water (50 mL) until the filtrate reached a neutral pH. The solid

was finally dried over anhydrous calcium carbonate for 7 days. The whole material became dried pieces of solid polymer, and it was difficult to form a powder. The lumps were coarsely ground before further use. The color was orange with darker patches. The total volume of the solution, water: isopropanol ratio, and aniline: formaldehyde: HCl ratios were 169 mL, 3:1, and 1:2:1, respectively. Compared to Poly-1s, the solvent ratio was reversed in this case. The yield of the solid was 23 g. FTIR (KBr, cm^{-1}) 3392(s), 2854(m) 1659(s), 1594(s), 1510(s), and 823(m). Ana. calculated for $(C_7H_7N \bullet HCl)n$: C, 59.38; H, 5.69; N, 9.89. Found C, 61.99; H, 5.98; N, 9.53.

2.2.3.4. Poly-2b. It was synthesized using the same procedure as Poly-1b using Poly-2s instead of Poly-1s. The yield of the base treated polymer was 1.63 g. FTIR (KBr, cm^{-1}) 3401(s), 2873(m) 1664(s), 1593(s), 1515(s), 809(m). Ana. calculated for $(C_7H_7N)n$: C, 79.97; H, 6.71; N, 13.32. Found C, 77.56; H, 6.24; N, 12.18.

2.2.3.5. Poly-3s. Concentrated HCl (7 mL, 70.0 mmol) was added to a mixture of aniline (9 g, 96.6 mmol) and 15 mL isopropanol and cooled in an ice bath. Another solution of 37% w/v formaldehyde (15 mL, 184.8 mmol) in 15 mL isopropanol was cooled in an ice bath. This solution was added to the precooled aniline-acid solution under vigorous stirring to obtain a uniform homogeneous solution. The temperature was maintained at 0-5 ℃ for 25 min and allowed to warm to room temperature overnight. The solid lumps were first broken using mortar-pastel, and 100-150 mL of 1N HCl was added to the polymer in a beaker and stirred for 3 h to ensure that all the acid-soluble low-molecular-weight polymer came to the solution, and then filtered through a Büchner funnel. The solid polymer was washed with distilled water until the pH of the filtrate was neutralized. The polymer was then dried in a vacuum desiccator for over four days. The yield of the product was 16.5 g. FTIR (KBr, cm^{-1}) 3414(s), 1659(s), 1597(s), 1509(s), and 821(m). Ana. calculated for $(C_7H_7N \bullet HCl)n$: C, 59.38; H, 5.69; N, 9.89. Found C, 57.88; H, 5.37; N, 9.25.

2.2.3.6. Poly-3b. Poly-3b was synthesized using the same procedure as Poly-1b using Poly-3s instead of Poly-1s. The synthesis of Poly-3b is a modified procedure for the micron-sized polymer reported earlier [18]. Poly-3b is a more thoroughly base treated version of a previously reported polymer. The yield of the solid was 1.7 g. FTIR (KBr, cm^{-1}) 3415(s), 2923, 2855(m) 1661(s), 1614(s), 1517(s), and 812(m). Ana. calculated for $(C_7H_7N)n$: C, 79.97; H, 6.71; N, 13.32. Found C, 76.37; H, 6.27; N, 12.50.

2.2.4. Adsorption experiments

We synthesized three amine-based polymers of similar chemical compositions using different solvent ratios. Accessibilities of the amine groups were studied by performing chromate adsorption of these polymers as we already knew that one particular form of the polymer binds with chromate. All experiments were carried out at a fixed initial pH of 4, and the chromium concentration was varied from 10 mg/L to 100 mg/L. A stock solution of chromium (1000 mg/L) was prepared. The required solutions were prepared from that stock 1000 mg/L solution by diluting it to the required solution. The amount of adsorbent used was 4 to 0.5 g/L. In each experiment, adsorbents with chromate solutions were placed in a specimen tube. The pH of the solution was checked, and if required, the pH was adjusted to 4. It was then shaken in an orbital shaker and filtered through Whatman filter paper. The pH of the filtrate was checked, and the chromium concentration of the filtrate was measured using AAS.

The adsorbed chromium amount (qe) was determined using the following equation,

$$q_t = \frac{(C_o - C_t)}{m} V \qquad (2.1)$$

Where q_t in mg is the amount of chromium adsorbed per g of adsorbent (mg/g), C_0 and C_t are the initial (time is zero), and at time t, the concentration of chromium in solution and m is the mass of the adsorbent used.

The removal percentage was calculated from the following equation (2.2).

$$\text{Removal}(\%) = \frac{(C_o - C_t)}{C_o} \times 100 \qquad (2.2)$$

2.3. Results and discussion

2.3.1. Syntheses

All the polymers were synthesized following a similar general procedure. First, an acidic alcoholic solution of aniline was cooled in an ice bath. The temperature was maintained from 0 ℃ to 5 ℃. Similarly, formaldehyde was cooled. They were mixed, stirred well with a glass rod, and kept in the ice bath for a moment so that polymerization occurs slowly. (Table 2.1) Previously, we observed that adding t-butanol or isopropanol to the reaction mixture formed spherical shaped AFC.[2,20] Our working hypothesis was that anilinium salts in binary solvent mixtures form emulsions or reverse micelles that act as nucleation centers for the spherical growth of polymers.[2,20–23] In this study, three different conditions are selected. In the first two cases, we reversed the solvent ratio to change the conditions suitable for micelles from reverse micelles, keeping the volume constant (Table 2.1).

The volume used was large enough to allow unrestricted growth of the AFC. In the third case, the solvent ratio is intermediate, and the volume is 1/3 of the first two. Accordingly, all three Poly-1s, Poly-2s, and Poly-3s were synthesized following a similar procedure with different solvent mixtures and volume ratios (Table 2.1). Between Poly-1s and Poly-2s, the ratio of isopropanol to the aqueous solution was reversed from 3:1 to 1:3 without changing the volume. Poly-3s were prepared at a much smaller volume with a solvent ratio of 1:1.

During the synthesis, acidic alcoholic solutions of aniline and formaldehyde were cooled separately in an ice bath. The temperature was maintained between 0 ℃ and 5 ℃. They were mixed, homogenized, and kept in an ice bath. The solution gradually transformed from transparent to cloudy within minutes, eventually becoming a completely immobile yellow-orange solid within 30 min (Figure 2.1). The amines in the isolated polymer were HCl salts because of the high concentration of acid used in the reaction (Table 2.1).

Table 2.1. Reagent and solvent ratios used during the synthesis of the polymers

Conditions	**Poly-1s**	**Poly-2s**	**Poly-3s**
Aniline	9 g	9 g	9 g
37% w/v HCHO in water	15.7 mL	15.7 mL	15 mL
Concentrated HCl	9.7 mL	9.7	7 mL
Mole ratio of Aniline:HCHO:HCl	1:2:1	1:2:1	1:2:1.7
Isopropanol	120 mL	40 mL	30 mL
Aqueous medium (HCl+HCHO+water)	40.0 mL	120.0 mL	21 mL
Isopropanol:aqueous solution	3:1	1:3	1.4:1
Total volume	169 mL	169 mL	61 mL

Corresponding base forms, Poly-1b, Poly-2b, and Poly-3b, were synthesized by treating with NaOH.

Treating all three with a base removes the acid and converts the amines to free base form (Scheme 2.1). At a higher volume, the polymer growth is less restricted. As a result, Poly-1s and Poly-2s were loosely held solids, while Poly-3s was a chunky cake that had to be cut into pieces.

2.3.2. FTIR spectroscopy

The FTIR spectra are shown in Figure 2.2 and Figure 2.3. The vibrational stretches are sharp and similar to the AFC polymers reported by Koner et al. synthesized in a mixture of solvents.[2] This is unlike the broad spectrum of AFC when synthesized without an organic solvent.[3] Spectral assignments were compared with 2,6 dimethylaniline and aniline spectra because of their structural similarity with repeating polymer units.[24]

Due to H-bonding and moisture, primary amine stretches were not observed because of the broad absorption with a peak maximum at ~3400 cm^{-1}. Other characteristic peaks were 2800-3000 cm^{-1} (C-H stretching), ~1590-1660 cm^{-1} (very strong, N-H bending of either amine or ammonium), ~1510 cm^{-1} (Strong, C-C stretching), ~1178 cm^{-1} (C-N stretch), and ~810 cm^{-1} (out of plane aromatic C-H stretching).[24,25] Compared to the ~1600 cm^{-1} stretch, the ~1660 cm^{-1} peak intensity decreases in the base form of the polymer, indicating its origin as N-H bending from the ammonium ($-NH_3^+$) form.[25] It is also the region where C=N stretches can occur due to possible imine formation between the amine group of the polymer and formaldehyde.[20,25] The 1660 cm^{-1} peak may have contributed to both imine C=N and N-H bending. The FTIR spectra of all the salt and base forms were very similar, confirming their chemical similarity.

The FTIR spectra of different batches were compared to check the consistency in synthesis and the differences between the acid and base forms.

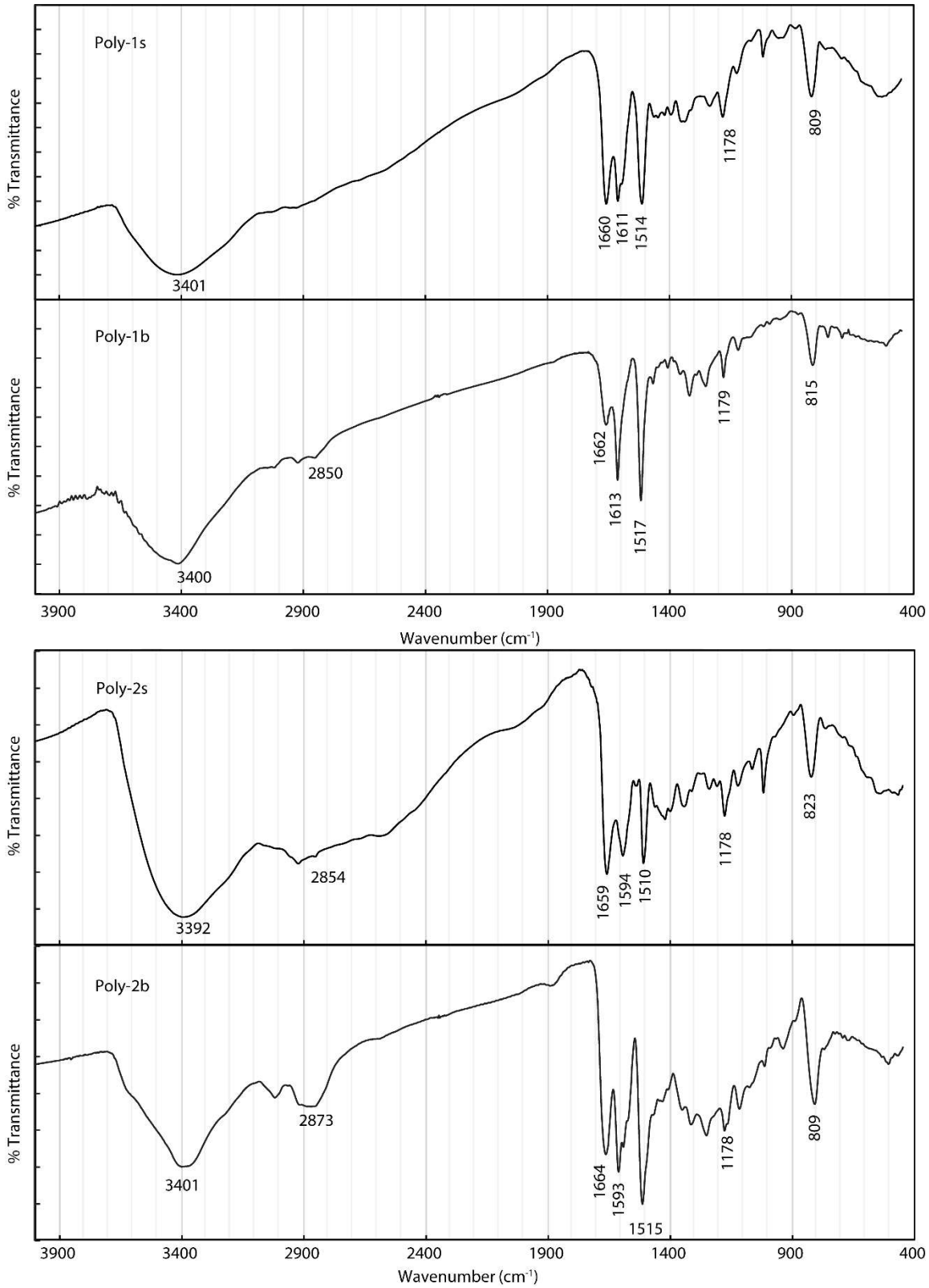

Figure 2.2. FTIR spectra of the polymers Poly-1s, Poly-1b, Poly-2s, and Poly-2b.

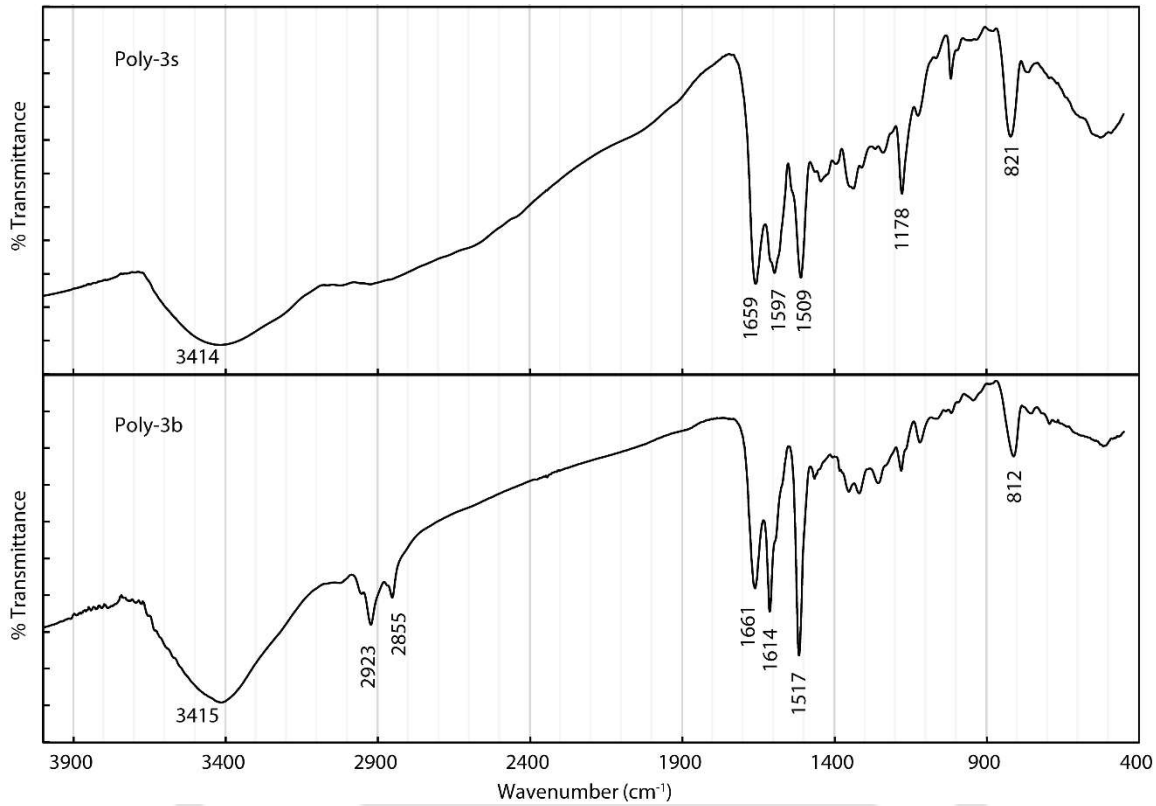

Figure. 2.3. FTIR spectra of the polymers Poly-3s, and Poly-3b.

2.3.3. Thermogravimetric analysis (TGA)

The thermal stabilities were evaluated using TGA. TGA was carried out from 25 ℃ to 300 ℃ at a heating rate of 5°-10 ℃/min. The powdered samples were pre-dried in a vacuum desiccator over anhydrous calcium carbonate at room temperature for several days until a constant weight was reached, were subjected to TGA analysis. The TGA results are shown in Figure 2.4. The salt forms of the polymers showed substantial weight loss between 25 ℃ and 100 ℃. The weight losses in this range were 60%, 33%, and 20% for Poly-1s, Poly-2s, and Poly-3s, respectively. A significant portion of the weight loss is likely to be the loss of HCl from $(C_7H_7N \bullet HCl)n$ to $(C_7H_7N)n$ (calculated as wt. loss ~25%) along with some solvent or water trapped within the polymer. It is not possible to determine the individual contributions from weight loss alone. Compared to this, the base forms of the polymers, Poly-2b and Poly-3b showed only 2%-3% weight loss between 25 ℃ and 130 ℃, indicating

minimal trapped solvent or moisture. Poly-1b showed ~10% weight loss in that temperature range, indicating more trapped solvent.

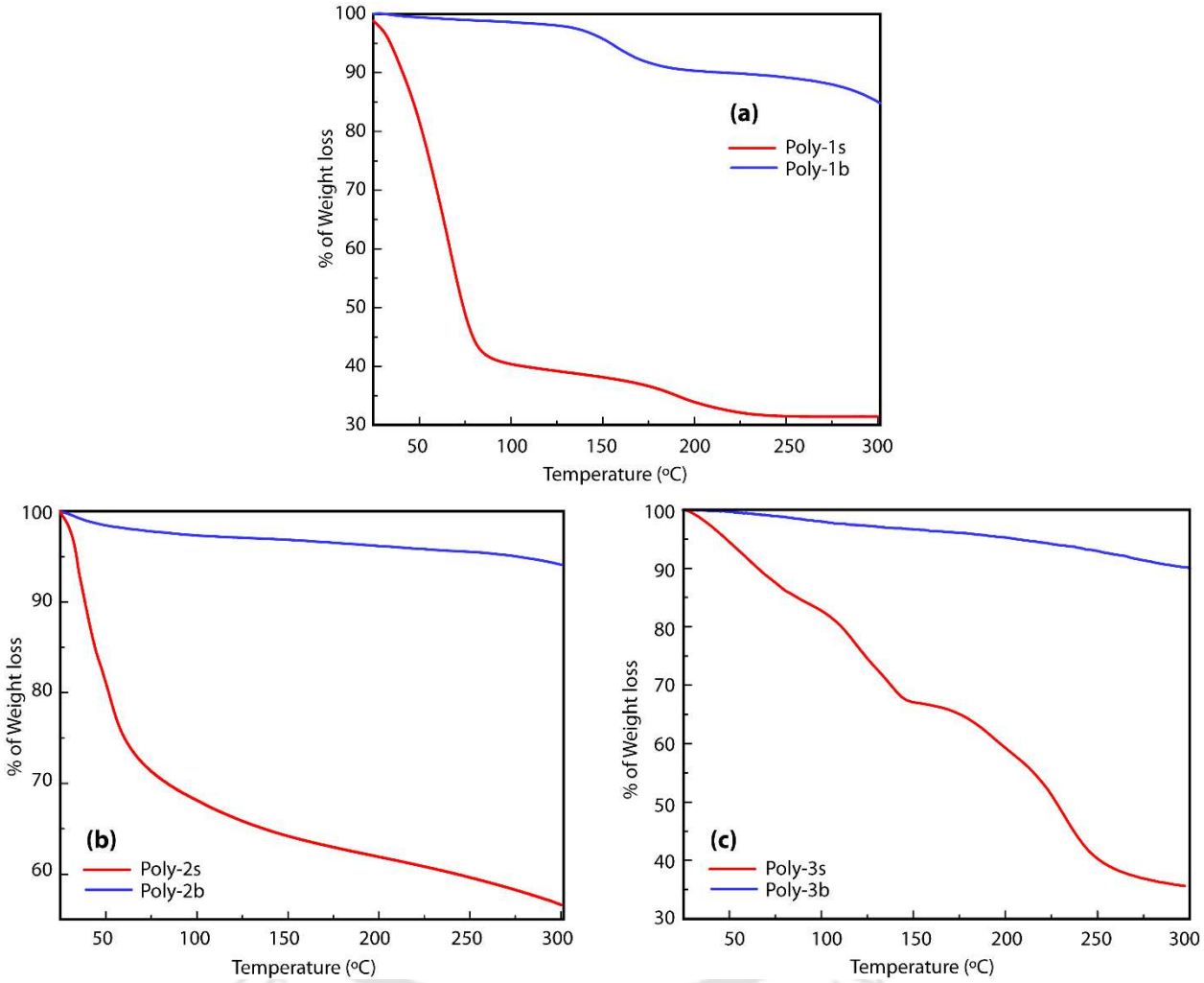

Figure 2.4. TGA plots of the polymers.

2.3.4. Elemental analysis

Elemental analysis was performed to determine the chemical composition of the polymers. The absolute percentage values of the elemental analysis of polymers are difficult

to match with a particular formula; hence we focused on the C:N and C:H:N molar ratio.[2,20] The elemental % and elemental mol ratios of salt or base forms varied within a narrow range. The values were close to the calculated values of the respective forms (Table 2.2).

Table 2.2. Elemental analysis of the polymers

Polymers	C	H	N	C:H:N ratio
Poly-1b	76.92	6.41	12.57	7.1:7.1:1
Poly-2b	77.56	6.24	12.18	7.4:7.1:1
Poly-3b	76.37	6.27	12.50	7.1:7:1
Calcd. $(C_7H_7N)_n$ for base forms	79.97	6.71	13.32	7:7:1
Poly-1s	59.19	5.63	9.52	7.2:8.2:1
Poly-2s	61.99	5.98	9.53	7.6:8.8:1
Poly-3s	57.88	5.37	9.25	7.3:8.1:1
Calcd. $(C_7H_7N \bullet HCl)_n$ for salt forms	59.38	5.69	9.89	7:8:1

The variation within a particular form could be from minute quantities of trapped solvent and moisture even after prolonged drying in a vacuum desiccator. We have noticed that Poly-2 in both forms contains more carbon content than the others, but values are still reasonable for a polymer with trapped solvents. The C:H:N ratios of the salt forms match closely with the calculated ratio containing HCl. Hence, the weight loss in TGA analysis of the salt forms was more likely due to the loss of HCl. The analysis results support the repeating formula $(C_7H_7N)n$ for the base forms and $(C_7H_7N \bullet HCl)n$ in salt form (Scheme 2.1).

2.3.5. Maldi-TOF mass spectral analysis.

The masses of the polymers, Poly-1s, Poly-2s, and Poly-3s were recorded using the positive mode of the matrix-assisted laser desorption (MALDI). These were scanned up to 2000 mass unit; however, mass peaks with significant intensity were observed up to only 1000 mass unit. The spectrum of Poly-1s showed several series of oligomers (Figure 2.5, Table 2.3).

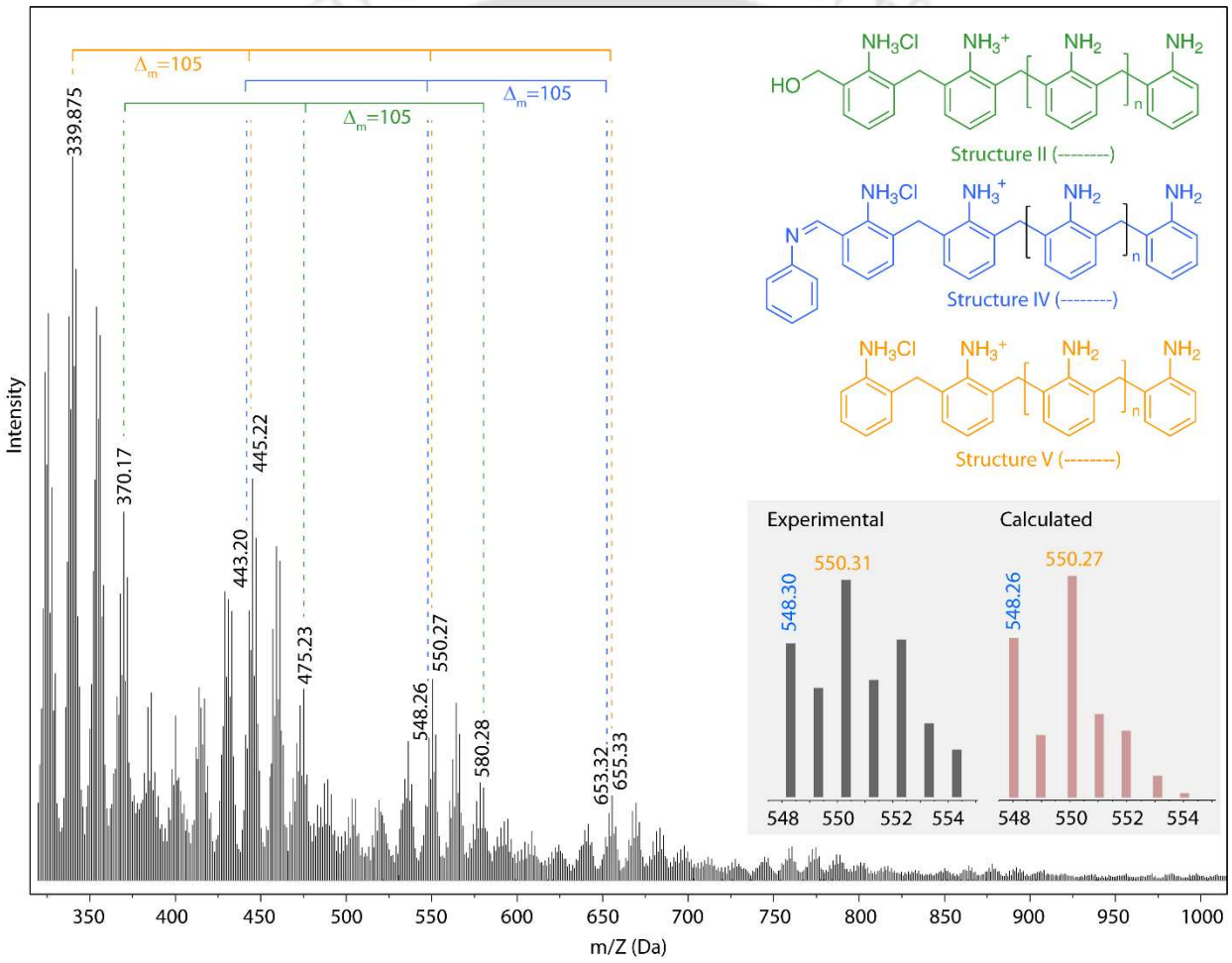

Figure 2.5. MALDI-TOF spectra for the positive ions of Poly-1s. The inset figure of the calculated and experimental isotopic pattern shows that the peaks around 550.27 are a combination of Structure IV (blue) and Structure V (orange). Other structures and a complete analysis table are in the supplementary material.

We identified a total of six interrelated series of oligomers in the MALDI mass spectrum of Poly-1s. Δm, the repeating unit of the polymer, was found to be 105, which is equivalent to the o-methylene aniline unit (C_7H_7N, calcd 105.13). In Figure 2.6, we have presented a set of oligomers' series identified in the MALDI mass spectrum, and in Table 2.3, the series with calculated/expected mass values which comes close to the mass values observed in the MALDI-Mass. The structures of the series of oligomers (Figure 2.6) are based on the products proposed from the mechanism of the formaldehyde aniline polymerization reaction (Figure 2.7) and the fragmentation during the ionization process (Figure 2.8).[26] Apart from molecular ion peaks, it showed a sequential fragmentation pattern with successive loss of 105.13 mass unit, corresponding to a loss of o-methylene aniline unit. The fragmentation pattern shown in the inset of Figure 2.5 is of the oligomer molecular ion (n=2) peak for monocationic form at 550.27 (calcd . for $[M+H]^+$) of structure V, which is the protonated salt form of AFC polymer. Isotopic pattern analysis did not reveal multiply charged species. One possible reason could be that only monocationic oligomers were solubilized in the prepared samples (trifluoroacetic acid, Section 2.2.2).

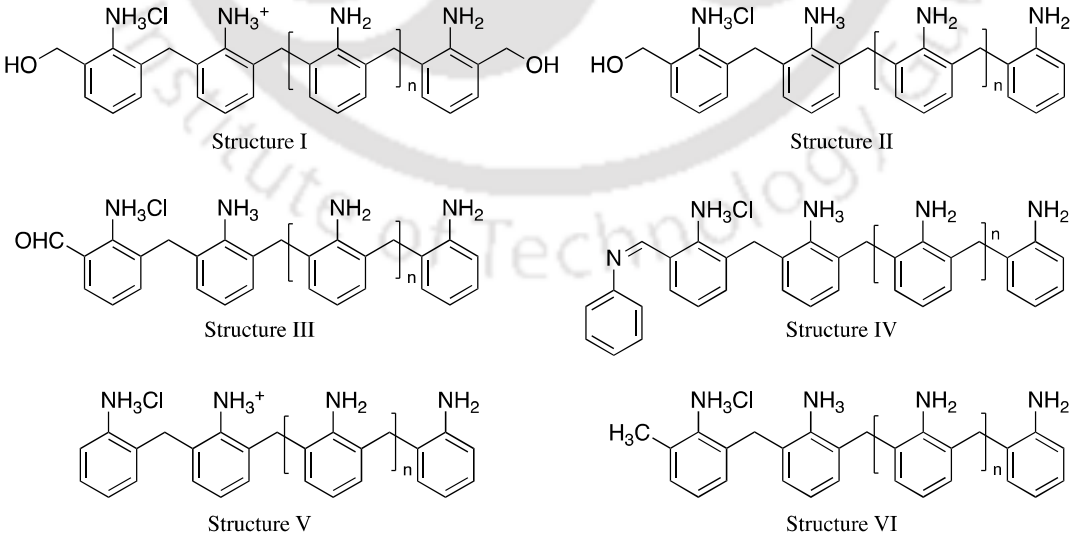

Figure 2.6. Structures of the oligomers identified in MALDI mass spectra.

Table 2.3. Calculated and experimentally found mass values in MALDI mass spectra of polymers.

n	**Structure I**			**Structure II**		
	Formula	*Mass calcd.*	*Mass expt.*	*Formula*	*Mass calcd.*	*Mass expt.*
0	$C_{22}H_{27}ClN_3O_2$	400.18	399.987	$C_{21}H_{25}ClN_3O$	370.17	369.932
1	$C_{29}H_{34}ClN_4O_2$	505.24	505.206	$C_{28}H_{32}ClN_4O$	475.23	475.148
2	$C_{36}H_{41}ClN_5O_2$	610.29	610.434	$C_{35}H_{39}ClN_5O$	580.28	580.381
3	$C_{43}H_{48}ClN_6O_2$	715.35	715.695 *	$C_{42}H_{46}ClN_6O$	685.34	685.621
4	$C_{50}H_{55}ClN_7O_2$	820.41	819.890 *	$C_{49}H_{53}ClN_7O$	790.40	790.876
5	$C_{57}H_{62}ClN_8O_2$	925.47	925.264 *	$C_{56}H_{60}ClN_8O$	895.46	895.795 *
6	$C_{64}H_{69}ClN_9O_2$	1030.53	1030.165 *	$C_{63}H_{67}ClN_9O$	1000.52	1000.087 *

n	**Structure III**			**Structure IV**		
	Formula	*Mass calcd.*	*Mass expt.*	*Formula*	*Mass calcd.*	*Mass expt.*
0	$C_{21}H_{23}ClN_3O$	368.15	368.940	$C_{27}H_{28}ClN_4$	443.20	443.090
1	$C_{28}H_{30}ClN_4O$	473.21	473.151	$C_{34}H_{35}ClN_5$	548.26	548.308
2	$C_{35}H_{37}ClN_5O$	578.27	578.371	$C_{41}H_{42}ClN_6$	653.32	653.539
3	$C_{42}H_{44}ClN_6O$	683.33	683.611	$C_{48}H_{49}ClN_7$	758.37	758.801
4	$C_{49}H_{51}ClN_7O$	788.38	788.867	$C_{55}H_{56}ClN_8$	863.43	863.830 *
5	$C_{56}H_{58}ClN_8O$	893.44	892.837 *	$C_{62}H_{63}ClN_9$	968.49	968.013 *
6	$C_{63}H_{65}ClN_9O$	998.50	997.946 *	$C_{69}H_{70}ClN_{10}$	1073.55	1073.297 *

n	**Structure V**			**Structure VI**		
	Formula	*Mass calcd.*	*Mass expt.*	*Formula*	*Mass calcd.*	*Mass expt.*
0	$C_{20}H_{23}ClN_3$	340.16	339.875	$C_{21}H_{25}ClN_3$	354.17	353.914
1	$C_{27}H_{30}ClN_4$	445.22	445.094	$C_{28}H_{32}ClN_4$	459.23	459.125
2	$C_{34}H_{37}ClN_5$	550.27	550.314	$C_{35}H_{39}ClN_5$	564.29	564.346
3	$C_{41}H_{44}ClN_6$	655.33	655.554	$C_{42}H_{46}ClN_6$	669.35	669.585
4	$C_{48}H_{51}ClN_7$	760.39	760.798	$C_{49}H_{53}ClN_7$	774.41	774.830
5	$C_{55}H_{58}ClN_8$	865.45	865.690 *	$C_{56}H_{60}ClN_8$	879.46	879.798 *
6	$C_{62}H_{65}ClN_9$	970.51	969.827 *	$C_{63}H_{67}ClN_9$	984.52	983.728 *

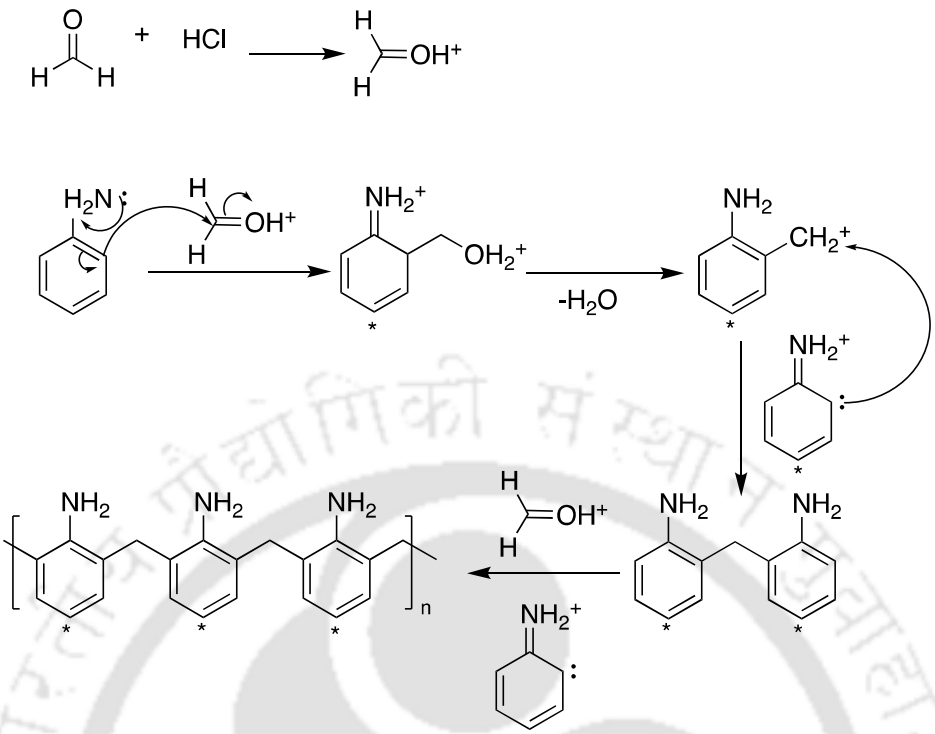

Figure 2.7. A plausible mechanism of AFC polymerization. * para position attack is also possible—mechanism scheme based on Ref [27] and Ref [28].

Aminobenzylalcohol was identified as the first intermediate formed in the reaction. It may be formed due to the attack of formaldehyde at the ortho position of an aniline molecule. Aminobenzyl cation formed in the presence of acid reacts further either at the ortho (which is shown in Figure 2.7) or para position of an aniline molecule leading to polymer chain formation (Structure V). The polymer chain reaction may stop at the aminobenzylalcohol stage, giving rise to the structure I formation detected in the MALDI spectrum. Partial formation of aminobenzylalcohol gave structure II. Oxidation of the alcohol side chain gave structure III. Aldehyde side-chain reacts with aniline to form imine in structure IV. The imine bond in structure IV under MALDI mass condition might break and be reduced to give the corresponding alkane side chain (structure VI). The MALDI spectra of Poly-2s and Poly-3s are given in Figure 2.9. The spectra were very similar with identical fragmentation.

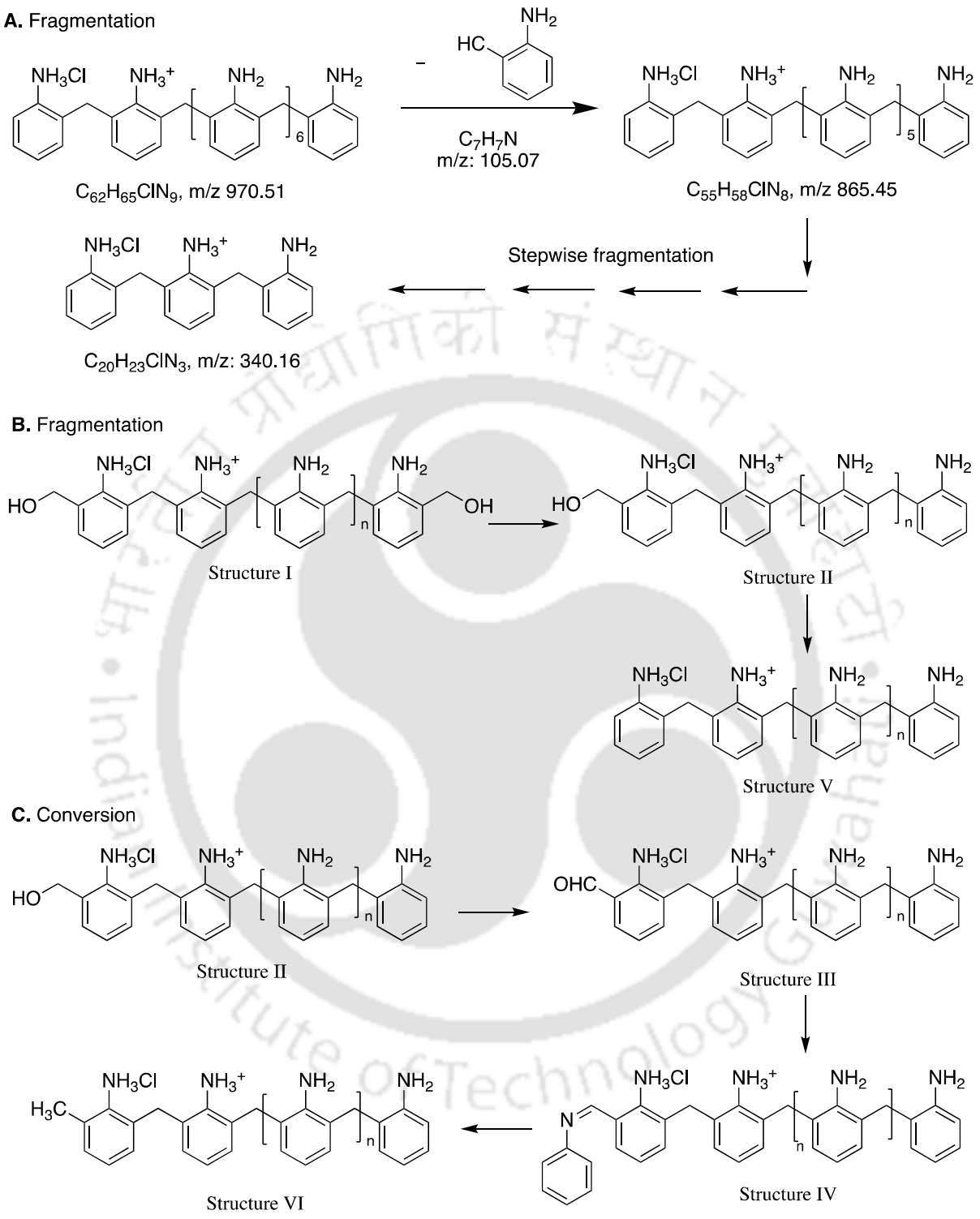

Figure 2.8. Possible ways of fragmentation and conversion have taken place under the MALDI mass condition.

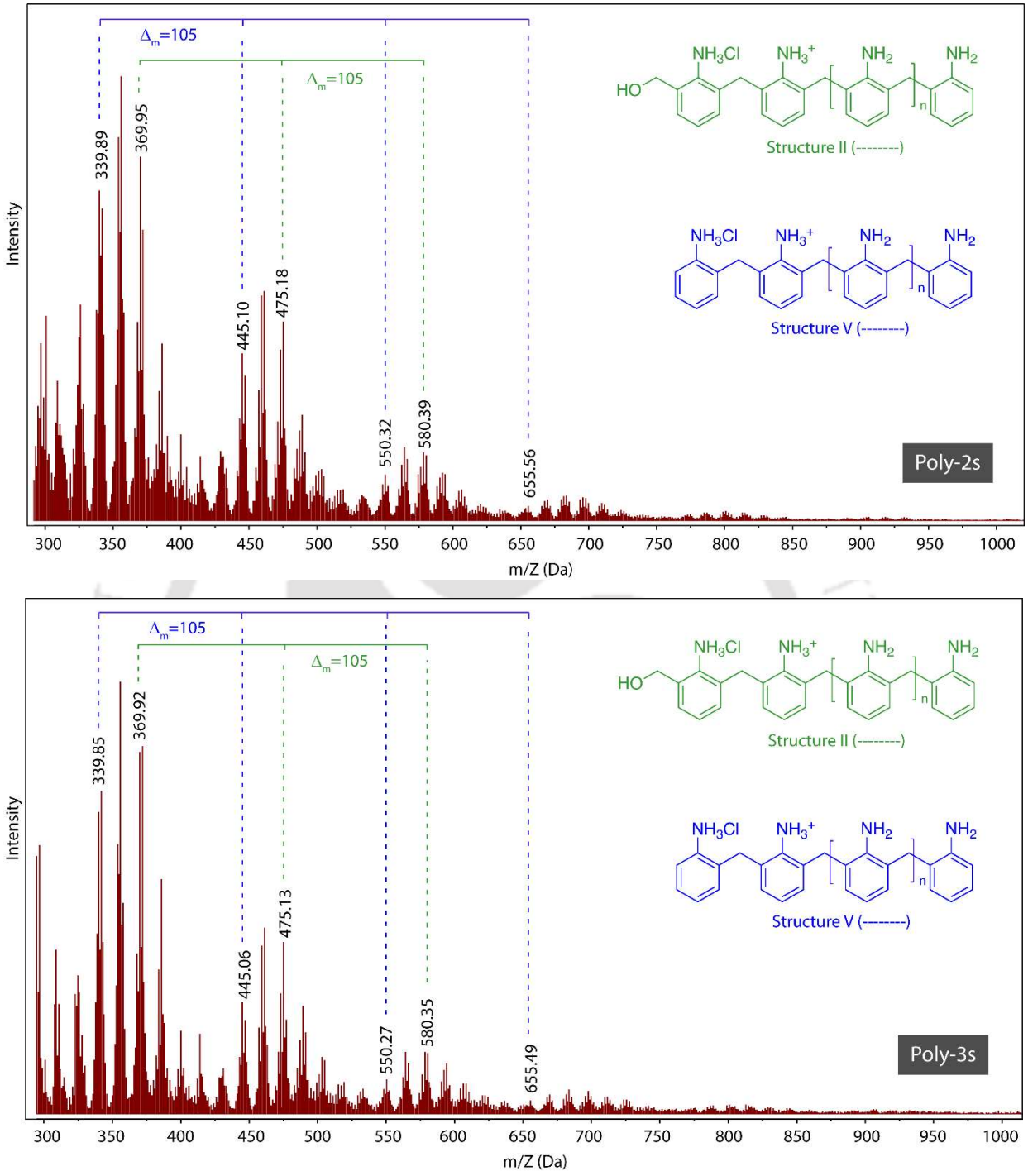

Figure 2.9. MALDI-TOF spectra for the positive ions of Poly-2s and Poly-3s.

Note. Assigned structures are based on the plausible mechanism in Figure 2.7. All the structures are in Figure 2.6, and assignments are in Table 2.3. The origin of the structures through fragmentation and transformations are in Figure 2.8.

From the similar fragmentation pattern with repeating unit, Δm of 105, we conclude that Poly-1s, Poly-2s, and Poly-3s are chemically similar polymers of the o-methylene aniline repeating unit (C_7H_7N, calcd as 105.13). The Structure V oligomers were similar to the fragmentation pattern of an AFC synthesized in t-butanol exclusively.[2]

We did not record the base forms' mass spectra, which are expected to yield similar results as they were prepared from their respective salt forms. Also, samples were prepared in a TFA mixture which eventually converted the base forms into salt forms.

2.3.6. Field emission scanning electron microscopy

Field emission scanning electron microscopy (FESEM) imaging of Poly-1b and Poly-3b showed polymers as spheres with diameters of 1–2 µm attached as clusters (Figure 2.10). Additionally, Poly-1b spheres have a fibrous surface that is missing in Poly-3b. Both were synthesized in an isopropanol and water mixture where the isopropanol quantity was greater than that of water (Table 2.1). Poly-2b, prepared in water: isopropanol ratio of 3:1 is a cluster of fine particles (Figure 2.10). A possibility of the fibrous surface of Poly-1b could be the deposition of low molecular weight polymers on the surface. Their shapes were not resolved in the images. Sphere formation was observed only in the isopropanol or t-butanol rich solution.[2,20] The difference between Poly-3b and Poly-1b is that the total volume used is more than doubled in Poly-1b. This allowed it to grow uninhibited, leading to a fibrous surface with the depletion of reagents over time. There was hardly any difference between the salt forms and the free base forms (Figure 2.10).

Unlike the free base form, the salt forms showed severe materials charging under an electron microscope. Images of salt forms were not as clear as the base forms, despite numerous attempts at different machines due to the charging of the samples. From the images, we concluded that the isopropanol-rich medium promoted spherical formation.

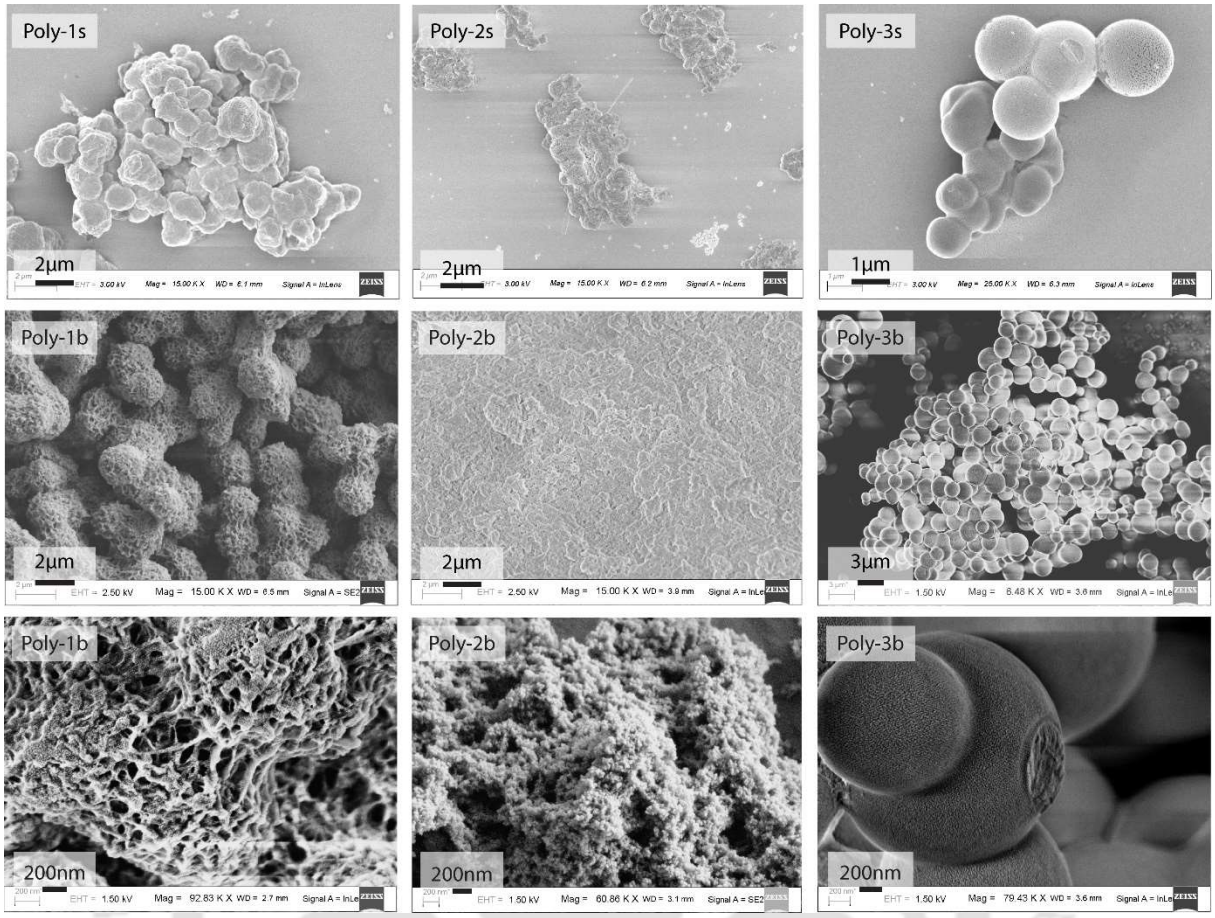

Figure 2.10. Field emission scanning electron microscope images of the polymers; salt forms, base forms, and base form under higher magnification.

Previously, we observed a similar formation in the case of t-butanol.[2] Salts in t-butanol water mixtures are known to form a ring-like structure where polar salts are distributed along with the hydrophobic/hydrophilic interface.[29] Template-free synthesis of polyaniline nanospheres has been reported upon adding salicylic acid to an Aniline-HCL mixture.[22] We believe that in the isopropanol-rich medium, the ionic aniline-HCl salt might have formed a reverse micelle type arrangement that acts as a seed on which the polymer growth occurs (Scheme 2.2). The spherical formation did not occur in the water-rich medium for Poly-2s. Polymer formation requires a cationic intermediate to approach another aniline cation in the ortho or para position (Figure 2.7). In the confined situation of a spherical water pool,

anionic chloride may have facilitated this. However, in the water medium, the chlorides were dispersed, which may have prevented spherical formation. Incidentally, the preparation of AFC in water results in an amorphous sticky solid or powder.[1–3,5]

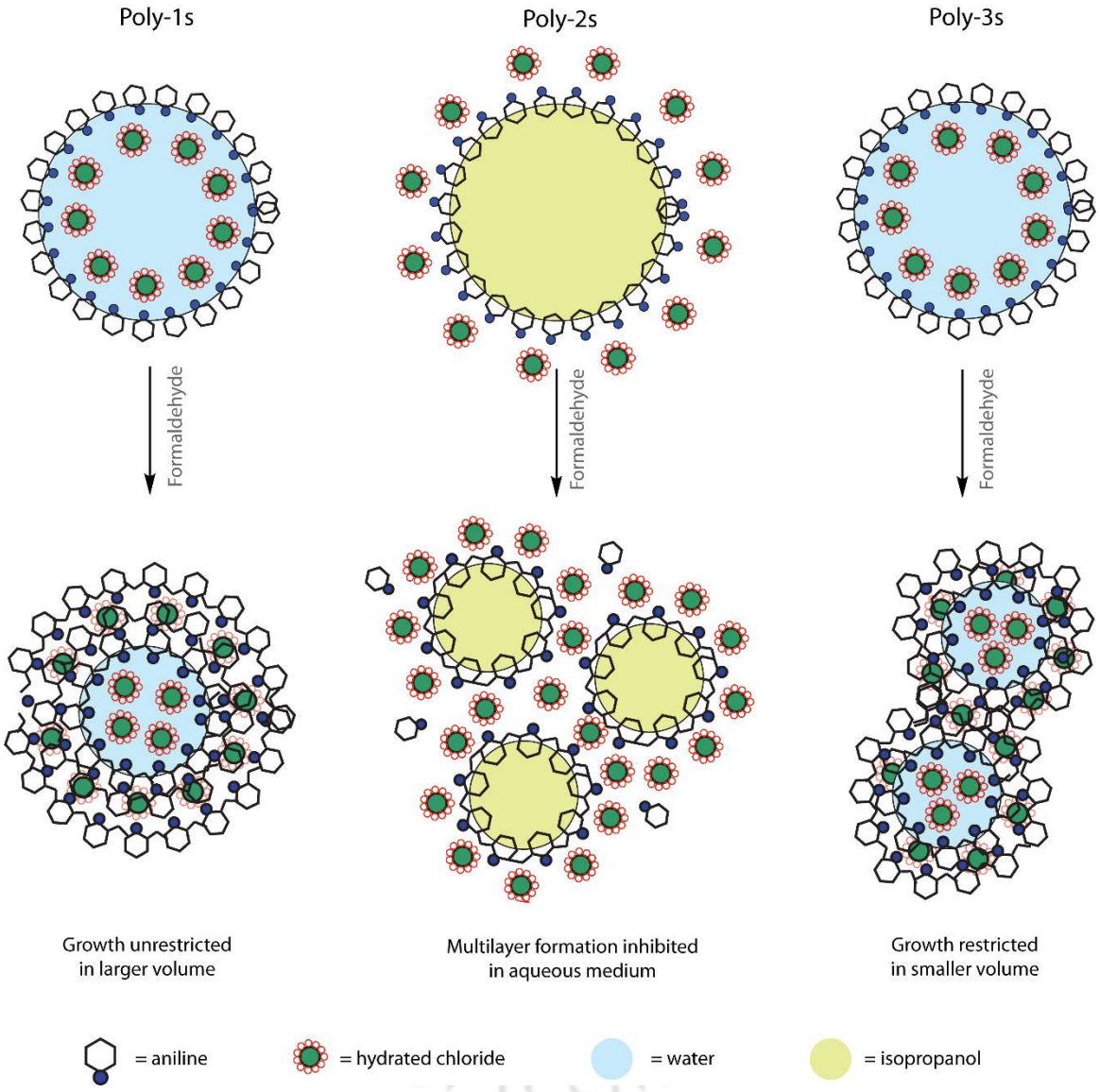

Scheme 2.2. Proposed mechanism of formation of the polymer spheres. Sphere radius in different steps not drawn to scale.

2.3.7. Dynamic light scattering

In the previous section, we hypothesized that micellar or reverse micellar organization occurs in a mixture of solvents. To prove this, we used dynamic light scattering (DLS)

measurements on solutions of aniline, HCl, and an isopropanol/ water mixture. We maintained the ratio precisely as used in the synthesis of the polymers before the addition of formaldehyde (Figure 2.11). The aggregate/micellar formation was measured using a 632.8 nm He-Ne laser using a Zetasizer instrument at 298 K. The sample for measurement was prefiltered to remove any preexisting particles.

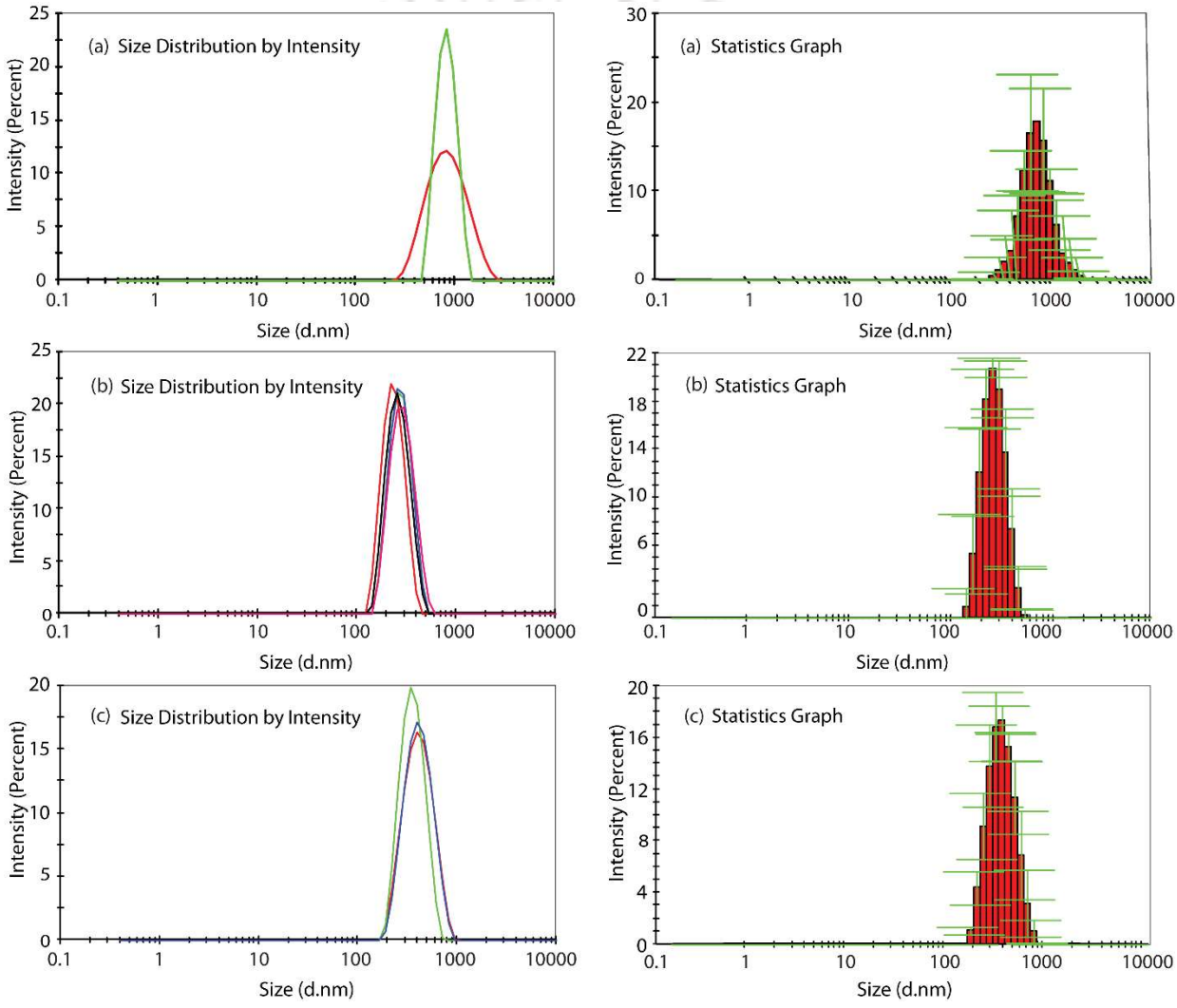

Figure 2.11. DLS plots of the intensity-wise distribution of particles/aggregates formed in the anilinium solution in a mixture of solvents during the preparation of (a) Poly-1s, (b) Poly-2s, and (c) Poly-3s before the addition of formaldehyde.

All three solutions showed aggregate/micelle/reverse micelle formation with a relatively narrow size distribution (Figure 2.11). Micelles or reverse micelles cannot be distinguished using DLS. The average aggregate size diameters obtained from DLS measurements were 723.0 nm, 219.3 nm, and 335.9 nm for preparative solutions without formaldehyde of Poly-1s, Poly-2s, and Poly-3s, respectively. Barring the differences in diameter, all had aggregates irrespective of the quantity of isopropanol, but the average particle size increased with higher concentrations of isopropanol (Figure 2.10). This observation confirms the formation of micellar or reverse micellar formation, as shown in Scheme 2.2.

2.3.8. Contact angle measurements

Reversal of solvent ratio should change the orientation of the polar amine groups in the polymers (Scheme 2.2). The surface properties, namely hydrophobicity, and hydrophilicity were measured by measuring the contact angles. The air-water contact angles were measured using a Kruss Drop Shape analyzer fitted with an optical and computer system. In powder form, Poly-1b showed superhydrophobicity with an air-water advancing contact angle (θ_{Adv}) of 154°, and Poly-3b showed moderate hydrophobicity with θ_{Adv} of 114°. Poly-2b was hydrophilic, and θ_{Adv} was 0° (Figure 2.12). The substantial hydrophobic property of Poly-1b and the hydrophilic property of Poly-2b support their respective aromatic and polar surface (Scheme 2.2). Poly-2b has intermediate property reflecting the intermediate condition used in the synthesis (Table 2.1). When these powders were pressed into pellets, θ_{Adv} changed significantly. θ_{Adv} of the pressed forms were 79°, 0°, and 85° for Poly-1b, Poly-2b, and Poly-3b, respectively. In pressed form, the shift of Poly-1b and Poly-3b towards a more hydrophilic contact angle is likely to be due to the exposure of the inner surface. The shift of contact angle of Poly-2b from 114° to 85° means the difference between interior and the exterior surface is less. The salt forms of all three polymers are hydrophilic in powder

form with a contact angle of ~0° (Figure 2.12). This means that salt forms are more porous and protonated -NH_3Cl groups are accessible from the surface. Removing HCl and forming -NH_2 somewhat closes the pores on spherical Poly-1b and Poly-3b, making the polar surface

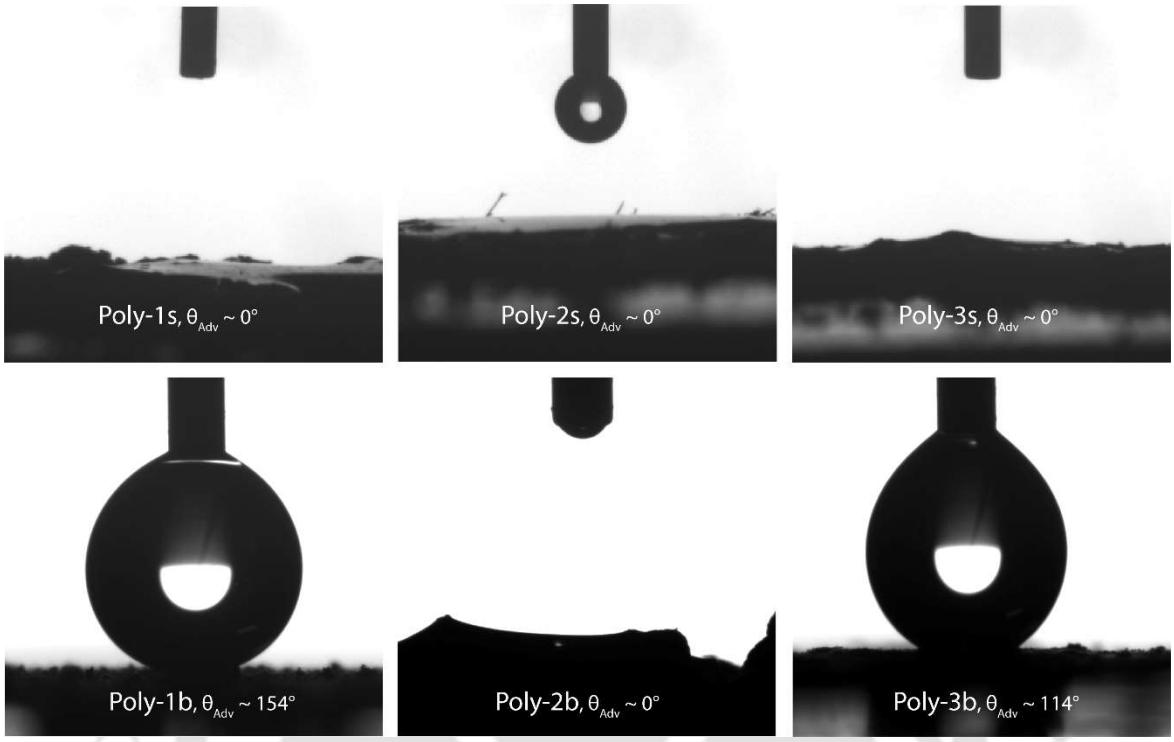

Figure 2.12. Advancing contact angle images of a water droplet on the polymer surface.

less accessible unless pressed into a pellet. Comparing both salt and free base forms, we found that Poly-1b and Poly-3b are spheres with more hydrophobic (aromatic rings) groups on the outer surface, and hydrophilic amine or ammoniums are inside (Scheme 2.2). Poly-2b has smaller particles with most of the amines on the surface, making it hydrophilic irrespective of the form.

2.3.9. Surface area measurements

The specific surface areas of the polymers were measured using the standard nitrogen adsorption technique, the BET method. The isotherm patterns of all six polymers were

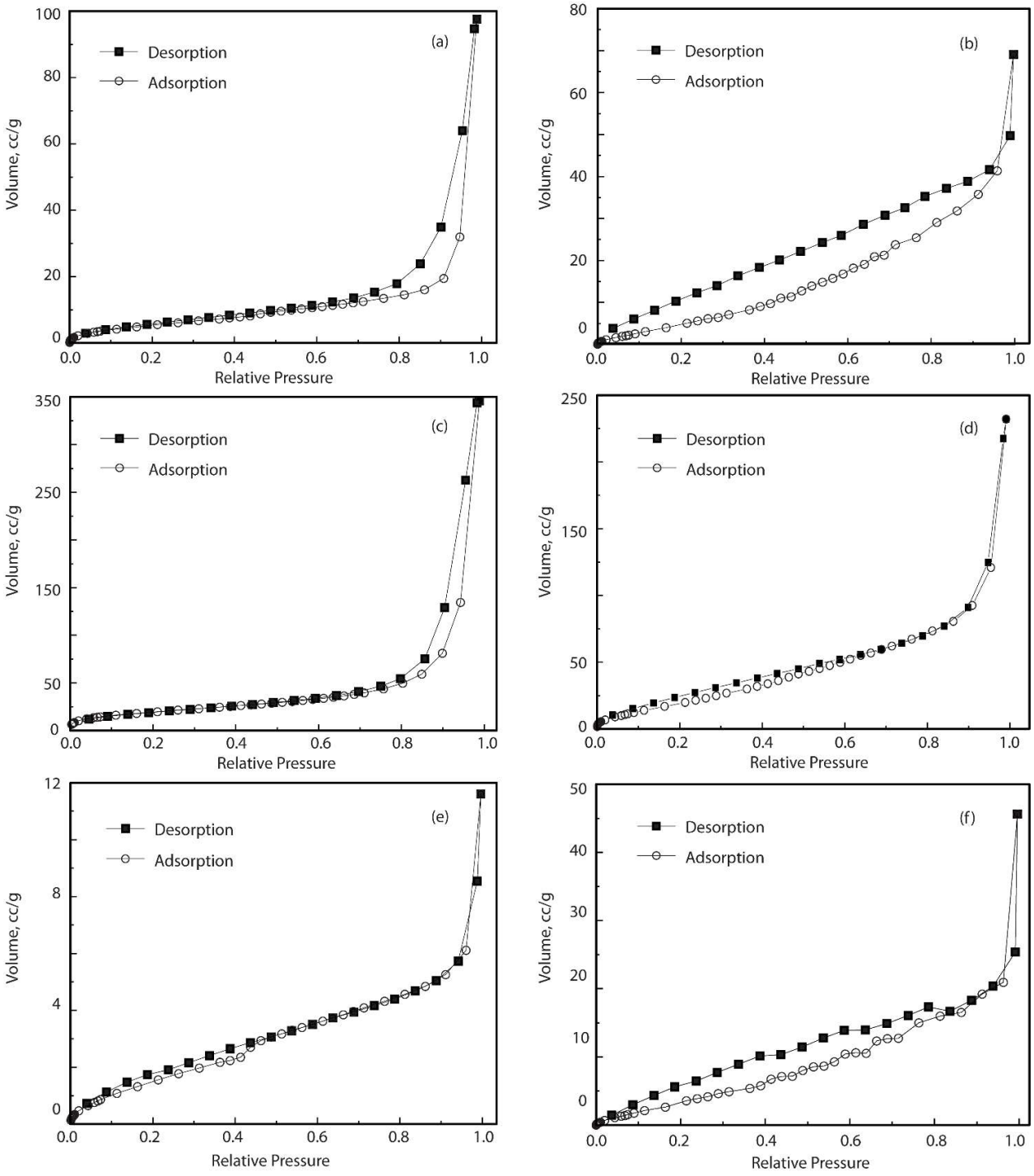

Figure 2.13. BET isotherm of the polymer base forms (a) Poly-1b, (c) Poly-2b, (e) Poly-3b and salt forms (b) Poly-1s, (d) Poly-2s, (f) Poly-3s.

similar (Figure 2.13). The adsorption isotherms showed a complex hysteresis loop without showing any limiting adsorption at high P/Po, similar to the H3 type.[30,31] This

behavior can usually be caused by the existence of non-rigid aggregates or assemblages of slit-shaped pores.

In principle, it should not be expected to provide a reliable assessment of either the pore size distribution or the total pore volume.[30,31] The pore diameter varied between a narrow range of 13–30 nm (Table 2.4). Thus, all are mesoporous solids (2-50 nm).[30,31] Adsorption on mesoporous solids proceeds via multilayer formation and capillary condensation. This type of isotherm at the initial stage appeared similar to that of mesoporous solids, and with increasing pressure, it rose steeply due to capillary condensation in the mesopores. Capillary condensation and capillary evaporation might not occur at the same pressure, owing to which such hysteresis loops appeared. The calculated surface areas are presented in Table 2.4.

Table 2.4. BET isotherm results

	Free amine forms			***Salt forms***		
Parameters	**Poly-1b**	**Poly-2b**	**Poly-3b**	**Poly-1s**	**Poly-2s**	**Poly-3s**
Surface Area (m^2/g)	21.779	72.268	6.027	29.130	93.390	21.079
Pore diameter (nm)	27.78	29.52	13.56	14.66	15.37	13.38
Total pore volume (cc/g)(dia. < XXX nm)	0.151 (165.9)	0.537 (161.7)	0.020 (370.1)	0.107 (743.6)	0.359 (210.2)	0.070 (456.5)
at P/P_o	0.98827	0.98796	0.99704	0.99742	0.99080	0.99579

Surface areas are calculated from multipoint BET data.

The surface area of both Poly-1 and Poly-2 in either form is higher than that of Poly-3b and the previously reported version.[20] This might be because their synthesis was performed at a higher volume (Table 2.1). Poly-3s/b synthesized in 1/3 volume had the

lowest surface area. Poly-2s/b with smaller particles (Figure 2.10) had the highest surface area. The salt forms had a slightly higher surface area than the corresponding base forms. Salt forms had additional HCl, which might be the reason for the larger surface area.

2.3.10. Effect of initial Cr(VI) concentration and adsorbent dose

The accessibility of the binding sites in these amine-containing polymers was studied based on their chromate binding capacities. In previous studies, this type of polymer showed maximum removal of chromate between 3-4 pH.[20] All the investigations presented here were performed at a fixed initial pH of 4.[2,5,20] In each experiment, 15 mL (for a dose of 4 g/L and 1 g/L) or 30 mL (0.5 g/L) solution of chromate (prepared with pH adjusted Millipore deionized water) and 0.060 g (for a dose of 4 g/L) or 0.015 g (for a dose of 1 g/L and 0.5 g/L) were used in specimen tubes. The adsorbent experiments were carried out at initial chromate concentrations of 10, 20, 50, and 100 mg/L. The pH of the salt forms of the polymer was found to change with time to pH 3.1- 3.5 due to hydrolysis of acidic anilinium salt.

On the other hand, the base forms of polymers change to pH 5-5.5, owing to the absorption of protons to form anilinium ions. In each case, three independent sets of experiments were performed. Standard deviations were calculated based on three sets, and the data were plotted with standard deviations. All experiments were performed in an orbital shaker at 300 rpm for 3 h.

The hydrophilic Poly-2b removed 56% of the 10 mg/L chromates among the base forms when the adsorbent dose was 4 g/L (Figure 2.14). At higher chromate concentrations, the removal percentage fell sharply to 27% (Table 2.5). The chromate removal of superhydrophobic Poly-1b and hydrophobic Poly-3b varied between 16% and 23 % over the entire range. In general, all the polymers in their base form are weak chromate absorbents.

Chemically, these three are the same (Thermogravimetric analysis (TGA), Maldi-TOF mass spectral analysis). Hence the difference in removal must be due to the hydrophobicity. The

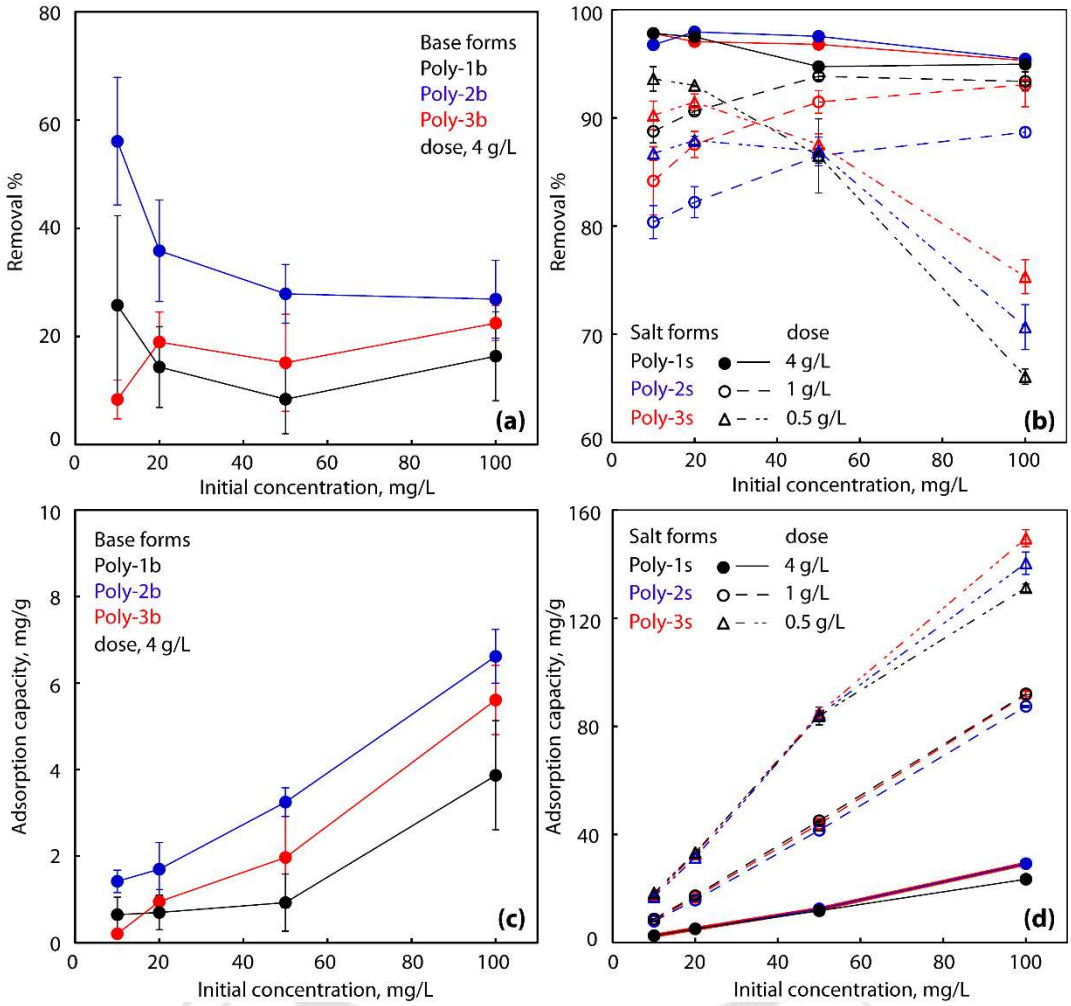

Figure 2.14. Comparison of chromate removal and adsorption capacity by base (a, c) and salt (b, d) forms of the polymers at different initial concentrations with a dose of 4-0.5 g/L.

higher the hydrophobicity, the weaker is the adsorbent. In contrast, all the polymers in their acid forms at the same dose showed 80%-98% removal over the entire range of chromate concentrations of 10-100 mg/L (Figure 2.14 and Table 2.5, 2.6). This also indicates that their adsorption capacity was not saturated at the 4 g/L dose. To view the differences between the individual polymers, we reduced the dose to 1 g/L and 0.5 g/L. At a low

adsorbent dose of 0.5 g/L, the differences between the polymers above 20 mg/L of chromate are narrow. This is especially observable in the adsorption capacity vs. initial chromate concentration plot (Figure 2.14). The adsorption capacity increases with a lower dose as expected, but the capacities of all three polymers remain quite close (Table 2.7, 2.8). All three salt forms are hydrophilic, chemically similar and have virtually similar adsorption properties irrespective of the orientation of the functional amine groups. All have much higher removal and adsorption capacity than their respective base forms. We conclude that both the interior and exterior surfaces are almost equally accessible to chromate in acid form.

From a practical utility point, salt forms showed very high removal (95%-98%) over the entire range of initial chromate concentrations (10-100 mg/L) at 4 g/L (Figure 2.14b). When the adsorbent dose was reduced to 1g/L, the removal was still practical between 80% and 93%. At 0.5 g/L, the removal properties of Poly-2s and Poly-2b were above 70%. The maximum adsorption capacity of Poly-2s and Poly-2b at 0.5 mg/L dose lies between 140-149 mg/g for removal between 70%-75% (Table 2.8). It not only overtook our previous results but was better than the commercially available ion exchanger Amberlite IRA-400 and other reported materials (Table 2.9).

Table 2.5. Comparison of chromate uptake (mg/g) and removal capacity (%) of the base form of the polymers at a dose of 4 g/L

Initial Conc.		**Poly-1b**	**Poly-2b**	**Poly-3b**	**Polymer from ref [20]**
10 ppm	Uptake, mg/g	0.65 (±0.40)	1.42 (±0.26)	0.21 (±0.09)	5.32 (±0.04)
	Removal %	25.75 (±16.55)	56.07 (±11.78)	8.34 (±3.69)	97.60 (±0.60)
20 ppm	Uptake, mg/g	0.70 (±0.40)	1.70 (±0.62)	0.95 (±0.28)	4.31 (±0.61)
	Removal %	14.34 (±7.47)	35.84 (±9.37)	18.97 (±5.53)	94.33 (±0.63)

50ppm	Uptake, mg/g	0.93 (±0.66)	3.25 (±0.33)	1.97 (±1.17)	11.18 (±1.02)
	Removal %	8.39 (±6.38)	27.87 (±5.43)	15.13 (±8.99)	94.23 (±0.81)
100 ppm	Uptake, mg/g	3.87 (±1.26)	6.62 (±0.62)	5.61 (±0.80)	23.73 (±3.40)
	Removal %	16.33 (±8.23)	26.87 (±7.21)	22.46 (±3.22)	92.61 (±0.88)

Table 2.6. Chromate removal (%) and uptake (mg/g) of the salt form of the polymers in different initial concentrations at a dose of 4 g/L

Initial Concentration		**Poly-1s**	**Poly-2s**	**Poly-3s**
10 ppm	Uptake, mg/g	2.59 (±0.00)	2.56 (±0.01)	2.59 (±0.01)
	Removal %	97.81 (±0.17)	96.76 (±0.37)	97.81 (±0.19)
20 ppm	Uptake, mg/g	5.13 (±0.19)	5.10 (±0.15)	5.15 (±0.24)
	Removal %	97.48 (±0.09)	97.95 (±0.14)	97.05 (±0.05)
50ppm	Uptake, mg/g	11.83 (±0.05)	12.52 (±0.02)	12.43 (±0.03)
	Removal %	94.75 (±0.41)	97.54 (±0.18)	96.80 (±0.26)
100 ppm	Uptake, mg/g	23.45 (±0.02)	29.26 (±0.07)	29.23 (±0.02)
	Removal %	94.96 (±0.05)	95.43 (±0.22)	95.30 (±0.06)

Table 2.7. Chromate removal (%) and uptake (mg/g) of the salt form of the polymers in different initial concentrations at a dose of 1 g/L

Initial Concentration		**Poly-1s**	**Poly-2s**	**Poly-3s**
10 ppm	Uptake, mg/g	8.75 (±0.1)	7.92 (±0.15)	8.3 (±0.31)
	Removal %	88.76 (±1.06)	80.37 (±1.52)	84.17 (±3.14)
20 ppm	Uptake, mg/g	17.36 (±0.06)	15.75 (±0.27)	16.77 (±0.23)
	Removal %	90.61 (±0.3)	82.21 (±1.43)	87.54 (±1.2)
50ppm	Uptake, mg/g	45.11 (±0.15)	41.58 (±0.32)	43.97 (±0.49)
	Removal %	93.84 (±0.31)	86.5 (±0.67)	91.47 (±1.03)
100 ppm	Uptake, mg/g	91.98 (±0.87)	87.36 (±0.45)	91.68 (±2.01)
	Removal %	93.37 (±0.88)	88.68 (±0.46)	93.07 (±2.04)

Table 2.8. Chromate removal (%) and uptake (mg/g) of the salt form of the polymers in different initial concentrations at a dose of 0.5 g/L

Initial Concentration		Poly-1s	Poly-2s	Poly-3s
10 ppm	Uptake, mg/g	18.38 (±0.22)	17.03 (±0.13)	17.72 (±0.26)
	Removal %	93.6 (±1.12)	86.71 (±0.64)	90.23 (±1.31)
20 ppm	Uptake, mg/g	33.32 (±0.04)	31.5 (±0.14)	32.77 (±0.27)
	Removal %	93 (±0.11)	87.92 (±0.38)	91.46 (±0.76)
50ppm	Uptake, mg/g	83.83 (±3.31)	84.24 (±1.29)	84.86 (±0.94)
	Removal %	86.49 (±3.42)	86.91 (±1.33)	87.56 (±0.97)
100 ppm	Uptake, mg/g	131.21 (±1.4)	140.33 (±4.13)	149.54 (±3.12)
	Removal %	66.08 (±0.71)	70.67 (±2.08)	75.31 (±1.57)

Table 2.9. Comparison of adsorption capacities with other adsorbents

Adsorbent	**Initial concentration (mg/L)**	**Dose (g/L)**	**Adsorption capacity (mg/g)**	**Removal (%)**	**Reference**
AFC on silica gel	10	8	0.62	43	3
Micron size AFC	10	2	4.50	80	20
Polyaniline on Jute	10	2	3.52	72	32
Cellulose-based anion exchanger	10	2	4.99	99	33
Amberlite IRA-400	10	6	3	60	19
Chitosan-graphene oxide nanocomposite	10	5	1.96	98	34
Poly-1s	10	4	2.59	98	This work

Poly-2s	10	4	2.56	97	This work
Poly-3s	10	4	5.59	98	This work
Poly-1s	10	0.5	18.38	94	This work
Poly-2s	10	0.5	17.03	87	This work
Poly-3s	10	0.5	17.72	90	This work
AFC on silica gel	50-200	8	60-65	60	3
Tamarind hull	50-150	1	95	99	35
Nanocrystalline akageneite	10-50	-	80	-	36
Polyacrylamide grafted sawdust	100	2	45	91	37
Chitosan-graphene oxide nanocomposite	10	5	1.96	98	34
Polyacrylonitrile fibres	50	1	35	70	38
Poly-1s	100	4	23.45	95	This work
Poly-2s	100	4	29.26	96	This work
Poly-3s	100	4	29.23	96	This work
Poly-1s	100	0.5	131.21	66	This work
Poly-2s	100	0.5	140.33	70.67	This work
Poly-3s	100	0.5	149.54	75	This work

2.3.11. Mechanism of Removal.

The mechanism of removal by AFC polymer coated on silica[3] and a powder form[20] similar to Poly-3b has been addressed before based on speciation of Cr(VI) and aniline at different pH values (Figure 2.15b) and desorption studies with different anions.[20]. Chemically the AFC polymers used in this work were the same as those used in previous studies.[3,20] Thus, the mechanism of removal was not expected to be different. Between pH 2-7, the predominant species of potassium dichromate in water is $HCrO_4^-$, a strong oxidizer.[20,39,40] The amine functional group in AFC exist in two different forms in equilibrium $Ar\text{-}NH_3^+Cl^- \longleftrightarrow Ar\text{-}NH_2 + HCl$ (Ar = aromatic). The relative concentration of the two

forms will depend on the pH of the solution and pKa of the amine. The pKa of the polymer, which is structurally close to 2,6 dimethylaniline than aniline, is expected to be ~4 (pKa of 2,6 dimethylaniline is 3.89). Hence, at pH 4, both the free base (Ar-NH_2) and the ionic salt forms (Ar-$NH_3^+Cl^-$) of the polymers will coexist.[20,39]

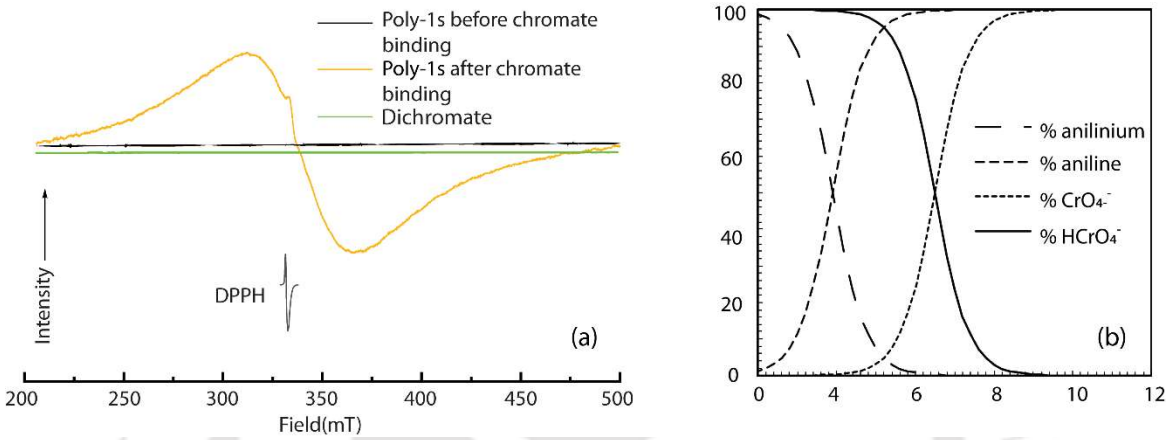

Figure 2.15. EPR spectra of the virgin Poly-1s, dichromate solution, and Poly-1s after binding with chromate (a) and speciation of aniline and chromate at different pH (b).

The Ar-NH_3^+ is harder to oxidize due to its positive charge compared to the free base form, Ar-NH_2. The removal of chromate can occur by (a) ion exchange of $HCrO_4^-$ with chloride ion of Ar-$NH_3^+Cl^-$ and (b) oxidation of Ar-NH_2 followed by coordination of Cr(III) with the remaining Ar-NH_2. The ion exchange path would mean that competition with other anions will reduce the removal of chromate. This is observed with phosphate and nitrate with an AFC very similar to Poly-3s. The effect is negligible with chloride and sulfate (Section 2.3.13). The high desorption with HCl also supports the ion-exchange mechanism in the case of the salt form (Section 2.3.13). The oxidation of free base form would reduce Cr(VI) to Cr(III). Cr(III) has a characteristic EPR spectrum.[41] To test this, the polymer, 4 g/L dose, was treated with 100 mg/L initial concentration of Cr(VI) at pH 4 for 3 h. The dose of 4 g/L was chosen as at this dose, and the polymer does not get saturated, increasing the sensitivity of the EPR spectra. The polymers were thoroughly washed and dried. The

EPR spectra showed a characteristic EPR signal at g = 1.98, which was absent in the virgin polymer and chromate solution (Figure 2.15a). This confirms that the oxidation of the polymer occurred. The quantity cannot be determined using the EPR. Thus, both ion-exchange and oxidation of polymer are possible reasons behind the chromate removal.

The significant difference between salt forms (Poly-1s to 3s) and the free base forms (Poly-1b to 3b) is related to the accessibility of the amines and hydrophobicity. If all the amine sites were equally available in water and sufficient times are given to reach equilibrium, all six would have the same number of Ar-NH_2 and Ar-NH_3^+ sites at a given pH due to hydrolysis. Among Poly-1b and 3b, the hydrophobicity prevents protonation of the interior sites. Hydrophilic Poly-2b showed better removal. However, its removal is still not comparable to any of the salt forms. We think the neutral amines on the surface of Poly-2b (Ar-NH_2) take a long time to reach equilibrium by either absorbing acid or undergoing hydrolysis (Ar-NH_2 + H_2O $\longleftrightarrow$ R-$NH_3^+OH^-$). Absorption of acid did take place, evident from the shift in pH of the solution from 4 to 5–6 at the end of the 3 h experiment. Salt forms are already in ionic form and hydrophilic. This polar nature allows penetration of water to interior groups, and ion-exchange can take place faster. The final pH after removal in salt form lies ~3.5.

All AFC forms have the same hydrolysable amine functionality, but the morphology and surface property changes the ratio between Ar-NH_2 and Ar-$NH_3^+Cl^-$ sites. More number of ionic sites in salt forms show higher removal. Base versions could not reach the same number of ionic sites, even after absorbing acids (final pH 5–6) which lowers the chromate removal.

2.3.12. Adsorption isotherm.

Langmuir and Freundlich's isotherm model fitting were tested with the experimental data of chromate adsorption by the polymers to determine the appropriate isotherm of

adsorption. Isotherm fitting results and plots of total chromium uptake (qe, mg/g) versus chromium concentration (Ce, mg/L) of the three polymers are given in Table 2.10 and Figure 2.16. Langmuir adsorption isotherm is

$$q=q_{max}\frac{K_L C_e}{1+K_L C_e} \qquad 2.3$$

Where C_e (mg/L) is the equilibrium concentration of Chromate, q_e (mg/g) is the adsorption capacity at equilibrium, q_{max} (mg/g) is the monolayer adsorption capacity of the adsorbent, and K_L (L/mg) is the affinity constant of adsorption in the Langmuir model.

Freundlich isotherm has the following general form,

$$q_e=K_f C_e^{\frac{1}{n}} \qquad 2.4$$

Here, K_f is the Freundlich capacity factor, and n is the index of heterogeneity.

Nonlinear regression was done to determine the isotherm parameters. The fitness of the isotherm model with the experimental data was verified using correlation coefficient (R^2) and average relative error (ARE). The equation used to determine ARE is as follows,

$$ARE=\frac{100}{n}\sum_{i=0}^{n}\left[\frac{q_{eexp}-q_{ecal}}{q_{eexp}}\right] \qquad 2.5$$

Where q_{eexp} and q_{ecal} are the experimental and calculated using isotherm chromium uptake values, respectively.

Table 2.10. Estimated isotherm parameters for adsorption of Chromate by the salt forms of the three polymers at pH 4.

Polymers	Model	Model parameters	Values	R^2	ARE (%)
Poly-1s	Langmuir	q_{max} (mg/g)	47.12	0.91	15.156
		K_L (L/mg)	0.22		
	Freundlich	K_f	16.54	0.91	9.948
		1/n	0.40		
Poly-2s	Langmuir	q_{max} (mg/g)	98.68	0.92	12.371
		K_L (L/mg)	0.096		
	Freundlich	K_f	12.41	0.87	9.614
		1/n	0.53		
Poly-3s	Langmuir	q_{max} (mg/g)	106.16	0.92	8.47

	K_L (L/mg)	0.10		
Freundlich	K_f	12.57	0.89	9.21
	1/n	0.57		

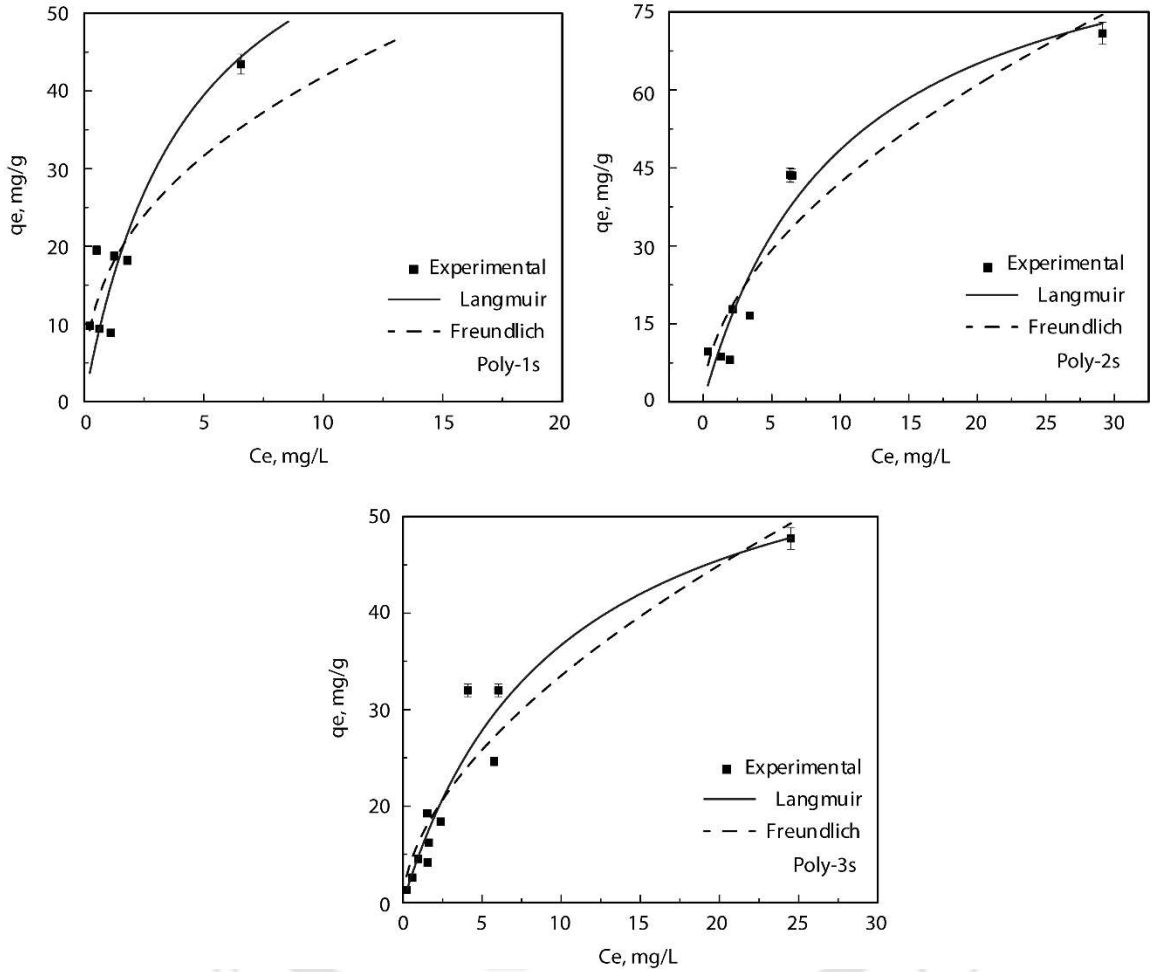

Figure 2.16. Isotherm plot of total chromium uptake by the polymers.

The results showed that the R^2 values for the two-isotherm fitting in each of the three polymers are very close. The maximum uptake achieved was ~150 mg/g for Poly-3s, although the values for other polymers are also comparable. The parameter values suggest that both the isotherm are applicable for the adsorption of chromate on the polymer surfaces.

2.3.13. Effect of other ions, desorption studies, and reuse of polymer.

The effect of competing ions on chromate adsorption of Poly-1s was examined at 50 mg/L of initial chromium concentration with a dose of 1 g/L at pH 4. The study was carried out separately using four ions, Ca^{2+}, Mg^{2+}, Cl^{-}, and SO_4^{2-}. Concentrations of other ions chosen were 25, 50, and 100 mg/L. Results are shown in Fig. 2.17a. No change in the removal capacity of Poly-1s was observed.

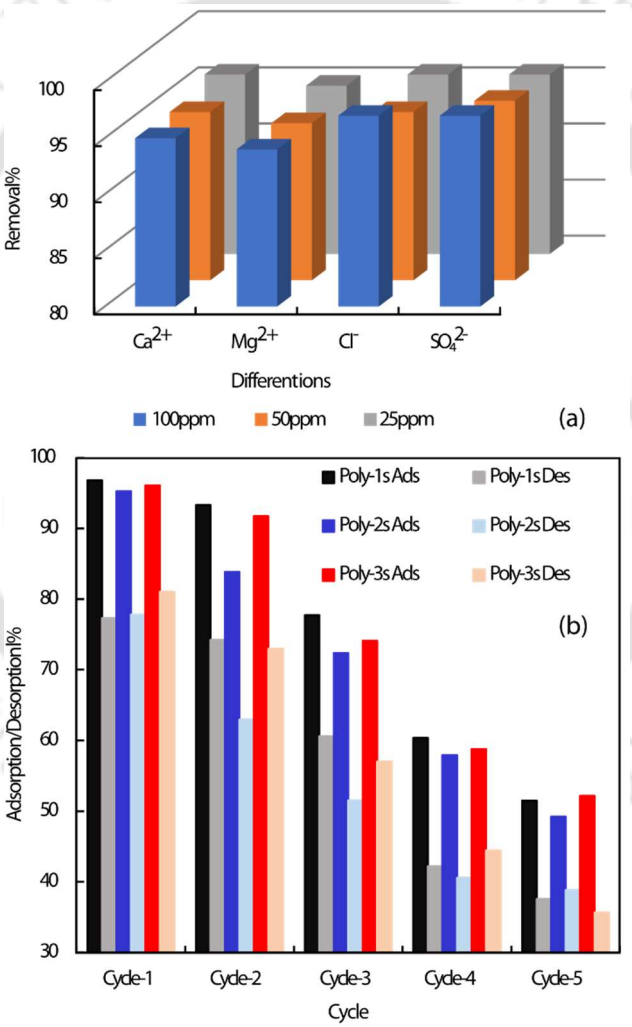

Fig. 2.17. (a) Effect of other ions on total chromate uptake of Poly-1s and (b) adsorption–desorption of chromate from salt forms of AFC in several cycles (Ads: adsorption, Des: desorption).

Regeneration and reusability were studied at 50 mg/L of initial chromium concentration with a dose of 1 g/L of Poly-1s, Poly-2s, and Poly-3s at pH 4. Desorption of the chromium load from salt forms of the polymers was performed using 1 N HCl, digestion time 12 h, 300 rpm. An earlier report of a desorption experiment on a form of AFC similar to Poly-3s showed maximum desorption by 1 N HCl. The results are shown in Fig. 2.17b. Reusability experiments were performed up to 5 cycles. Maximum desorption was observed (greater than 90%) for Poly-1s and Poly-3s up to 2 cycles, and for Poly-2s, it was more than 80%. As the adsorption of chromate, in this case, is a combination of ion-exchange and oxidation of the polymer, gradually more sites became occupied due to the binding of Cr(III) upon reduction. Hence the recyclability decreases gradually after each cycle.

2.3.14. Energy-dispersive X-ray analysis

EDAX analysis of the polymers was performed to determine the presence of any metals in the adsorbent before the adsorption experiments and after the adsorption experiments. The results are shown in Figure 2.18. The EDAX spectra showed no other metals and even chromium on the polymer surface before adsorption. The presence of Cr on the polymers' surface confirmed the metal adsorption. Al and Au came as the sample preparation was done on an aluminum foil, and the sample was coated with gold to reduce charging. Elemental composition showed the presence of chlorine, which came from the quaternary ammonium chloride of the salt version of the polymers.

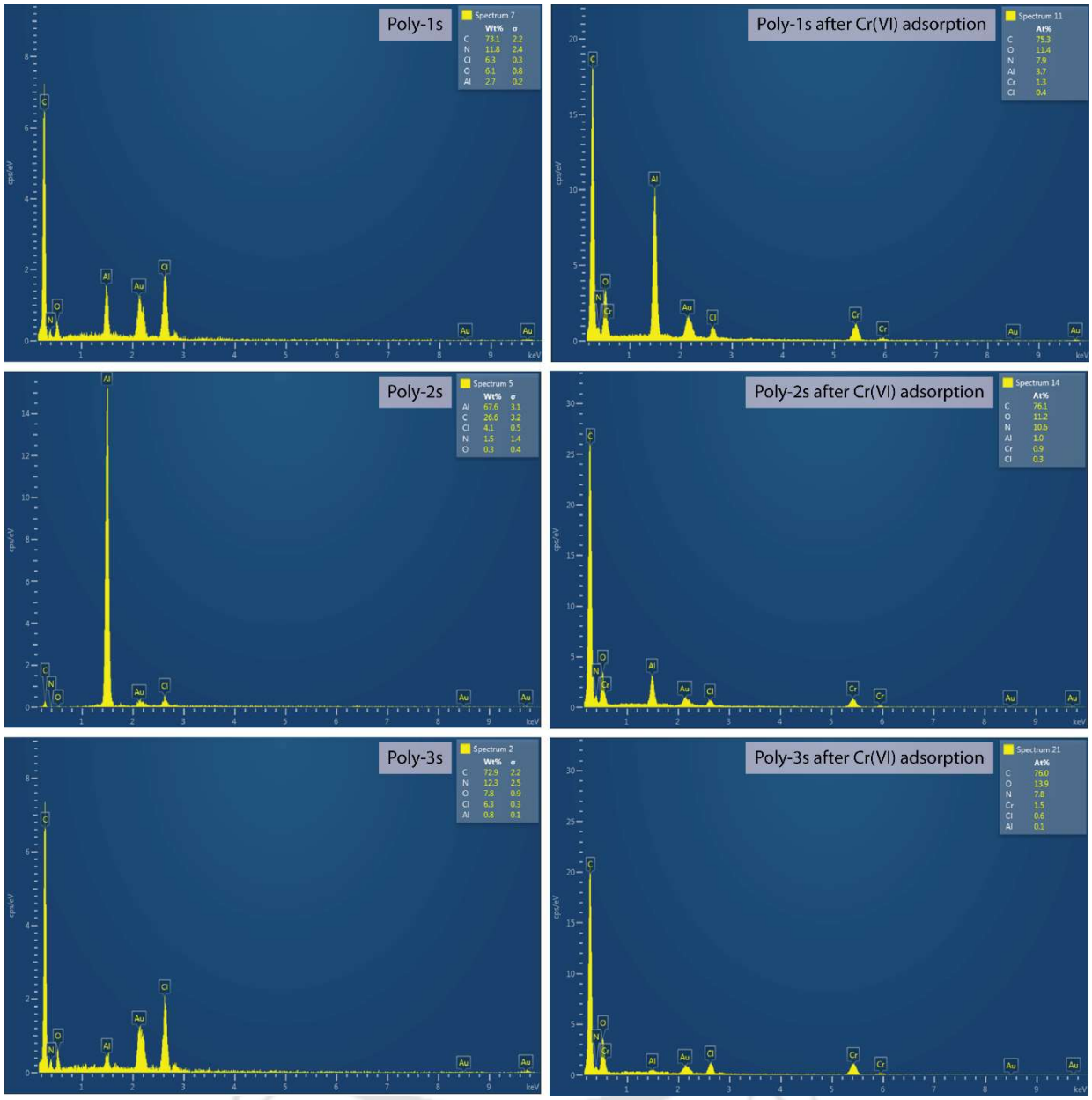

Figure 2.18. EDAX spectra of the polymers before and after the chromate adsorption.

2.3.15. Cost analysis

Cost for the first cycle calculated for 1kg and then converted in terms of cost for 1gm material. The cost of raw materials was calculated using (a) cost of research-grade chemicals from reputed Indian supplier (upper limit) and (b) cost of industrial-grade bulk chemicals from Indian Business to business supplier (lower limit). The power requirement is to make

1 kg ice required for synthesis at the local prevailing rate. Other than ice to cool, recipe does not need heating or stirring. Filtration is by filter paper. Labor cost is taken for my work hour wages. This is on the higher side. The recipe does not need a well-qualified chemist. All prices were converted to US$ at the current rate (1 US$ = 75 Rs.).

Cost calculated for the costlier Poly-1s due to use of a larger amount of isopropanol. To estimate cost to remove 1gm chromium, qe value used at conditions where removal is above 93% (dose 1 g/L, pH 4, initial chromate 200 ppm). The maximum qe was with 0.5 g dose, but at that condition, removal is 75% for initial chromate 200 ppm. This was not used in the calculation.

Recipe cost = Raw material cost + Energy cost + Labor cost

Recipe cost of 1kg Poly-1s using research grade chemicals = 79 $ + 0.04 $ + 12.5 $ = 91.5 $

Recipe cost of 1kg Poly-1s using industrial grade chemicals = 13 $ + 0.04 $ + 12.5 $ = 25.5 $

Thus, 1 kg of Poly-1s costing between 25-91 $ can remove 93% of chromate from 1000 L of water containing 100 ppm chromate.

Compared to this:

1 kg Amberlite IRA 400 (non-branded), ion exchange resin cost 26 $ which can remove 90% of chromate from 1000 L of water containing 100 ppm chromate.[42] Ion-exchange resins are capable of multiple cycles, thereby reducing the cost further.

1 kg of Amberlite IRA 900 (branded, Aldrich) ion exchange resin cost 280 $ which can remove 97% of chromate from 1000 L of water containing 100 ppm chromate.[42] Ion-exchange resins are capable of multiple cycles, thereby reducing the cost further.

1 kg of chitosan derivative costs between 9870 – 25392 $,[43] depending on the type of derivative. A recent report showed 1 kg chitosan biochar composite can remove 90% of chromate from 1000 L of water containing 55 ppm chromate.[44]

1 kg of Agro-based (Tea and Ginger mix) cost 0.45 $ which removes 75% of chromate from 100 L of water containing 30 ppm chromate or 10 kg costing 4.5 $ can remove 75% or chromate from 1000 L of water having 30 ppm.[45]

2.4. Conclusions

The major findings in this chapter are the following:

(i) The goal of increasing the amine site's accessibility and chromate removal performance of AFC polymer has been achieved.

(ii) Three different versions of the AFC polymer, each in salt and free base forms, were synthesized by controlling the solvent ratio and total volume. Reversal of the solvent ratio resulted in different polymer morphologies (Figure 2.10). Chemical analysis confirmed that the salt forms as HCl salts of the corresponding free amine forms (Table 2.2). They are chemically similar; the only difference is their morphology and surface property.

(iii) The salt form and one of the base forms were hydrophilic. The spherical base forms were either hydrophobic (Poly-3s) or superhydrophobic (Poly-1s). DLS supports polymer formation on top of a micellar or reverse micellar core, which changes the orientation of the amine functional groups (Scheme 2.2). This effect was prominent in the base form. In salt forms, the polarity of the functional group made the sites more accessible to water, irrespective of their orientation, as evidenced by the contact angles.

(iv) The accessibility of the sites and hydrophilicity profoundly improved the chromate removal properties of the polymers.

(v) The adsorption capacities shown by the salt form of the polymers are the best reported for AFC polymers. These are the most efficient when compared with different adsorbents (Table 2.9).

(vi) Chromium removal was the worst (1/30th of Poly-1s) with the superhydrophobic Poly-1b, where the functional groups are inside the polymer spheres. Poly-2b, with functional groups on the surface, fares well with twice the efficiency of Poly-1b. Thus, the orientation of the functional group matters but cannot compensate for the high efficiency shown by the polar salt forms.

(vii) The high efficiency of salt forms is due to the higher accessibility of the sites. In conclusion, using a simple solvent polarity control to change the orientation of amine functional groups, we have engineered AFC polymers as efficient chromate adsorbents, effective over a broader range of concentrations than before.[3,20]

(viii) In terms of cost, a rudimentary analysis put the recipe cost of the Poly-1s between ion exchange resin (IRA 900) and bio-adsorbents.

2.5. Bibliography

(1) Liu, G.; Freund, M. S. New Approach for the Controlled Cross-Linking of Polyaniline: Synthesis and Characterization. *Macromolecules* **1997**, *30* (19), 5660–5665. https://doi.org/10.1021/ma970469n.

(2) Koner, R. R.; Kumar, P. A.; Chakraborty, S.; Ray, M. Synthesis of Morphologically Different, Metal Absorbing Aniline-Formaldenyde Polymers Including Micron-Sized Sphere Using Simple Alcohols as Morphology Modifier. *J. Appl. Polym. Sci.* **2008**. https://doi.org/10.1002/app.28746.

(3) Kumar, P. A.; Ray, M.; Chakraborty, S. Hexavalent Chromium Removal from Wastewater Using Aniline Formaldehyde Condensate Coated Silica Gel. *J. Hazard. Mater.* **2007**, *143* (1–2), 24–32. https://doi.org/10.1016/j.jhazmat.2006.08.067.

(4) Kumar, G. P.; Kumar, P. A.; Chakraborty, S.; Ray, M. Uptake and Desorption of Copper Ion Using Functionalized Polymer Coated Silica Gel in Aqueous Environment. *Sep. Purif. Technol.* **2007**, *57* (1), 47–56. https://doi.org/10.1016/j.seppur.2007.03.003.

(5) Kumar, P. A.; Ray, M.; Chakraborty, S. Adsorption Behaviour of Trivalent Chromium on Amine-Based Polymer Aniline Formaldehyde Condensate. *Chem. Eng. J.* **2009**, *149* (1–3), 340–347. https://doi.org/10.1016/j.cej.2008.11.030.

(6) Baekeland, L. H. The Synthesis, Constitution, and Uses of Bakelite. *J. Ind. Eng. Chem.* **1909**, *1* (3), 149–161. https://doi.org/10.1021/ie50003a004.

(7) Crespy, D.; Bozonnet, M.; Meier, M. 100 Years of Bakelite, the Material of a 1000 Uses. *Angew. Chemie Int. Ed.* **2008**, *47* (18), 3322–3328. https://doi.org/10.1002/anie.200704281.

(8) Pakade, V.; Chimuka, L. Polymeric Sorbents for Removal of Cr (VI) from Environmental Samples *. *Pure Appl. Chem.* **2013**, *85* (12), 2145–2160.

(9) (IARC), I. A. for R. on C. Monographs on the Evaluation of Carcinogenic Risks to Humans. *http://monographs.iarc.fr/ENG/Classification/index.php* **2006**.

(10) Services, U. S. D. of H. and H. Toxicological Profile for Chromium. *Public Heal. Serv. Agency Toxic Subst. Dis. Regist. Washington, DC* **1991**.

(11) Straif, K.; Benbrahim-Tallaa, L.; Baan, R.; Grosse, Y.; Secretan, B.; El Ghissassi, F.; Bouvard, V.; Guha, N.; Freeman, C.; Galichet, L.; Cogliano, V. A Review of Human Carcinogens—Part C: Metals, Arsenic, Dusts, and Fibres. *Lancet Oncol.* **2009**, *10* (5), 453–454. https://doi.org/10.1016/S1470-2045(09)70134-2.

(12) Vincent, J. B. Chromium: Biological Relevance. *Encyclopedia of Inorganic Chemistry*. September 7, 2005. https://doi.org/https://doi.org/10.1002/0470862106.ia042.

(13) von Burg, R.; Liu, D. Chromium and Hexavalent Chromium. *J. Appl. Toxicol.* **1993**, *13* (3), 225–230. https://doi.org/https://doi.org/10.1002/jat.2550130315.

(14) Greenwood, N. N.; Earnshaw, A. *Chemistry of the Elements*; Elsevier, 2012.

(15) Hummel, W.; Filella, M.; Rowland, D. Where to Find Equilibrium Constants? *Sci. Total Environ.* **2019**, *692*, 49–59. https://doi.org/https://doi.org/10.1016/j.scitotenv.2019.07.161.

(16) WHO, G. Guidelines for Drinking-Water Quality. *World Heal. Organ.* **2011**, *216*, 303–304.

(17) SEDMAN, R. M.; BEAUMONT, J. A. Y.; MCDONALD, T. A.; REYNOLDS, S.; KROWECH, G.; HOWD, R. Review of the Evidence Regarding the Carcinogenicity of Hexavalent Chromium in Drinking Water. *J. Environ. Sci. Heal. Part C* **2006**, *24* (1), 155–182. https://doi.org/10.1080/10590500600614337.

(18) Ruotolo, L. A. M.; Gubulin, J. C. Reduction of Hexavalent Chromium Using Polyaniline Films. Effect of Film Thickness, Potential and Flow Velocity on the Reaction Rate and Polymer Stability. *J. Appl. Electrochem.* **2003**, *33* (12), 1217–1222. https://doi.org/10.1023/B:JACH.0000003856.63371.73.

(19) Kusku, O.; Rivas, B. L.; Urbano, B. F.; Arda, M.; Kabay, N.; Bryjak, M. A Comparative Study of Removal of Cr(VI) by Ion Exchange Resins Bearing Quaternary Ammonium Groups. *J. Chem. Technol. Biotechnol.* **2014**, *89* (6), 851–857. https://doi.org/10.1002/jctb.4320.

(20) Terangpi, P.; Chakraborty, S.; Ray, M. Improved Removal of Hexavalent Chromium from 10 mg/L Solution by New Micron Sized Polymer Clusters of Aniline Formaldehyde Condensate. *Chem. Eng. J.* **2018**, *350*, 599–607. https://doi.org/https://doi.org/10.1016/j.cej.2018.05.171.

(21) Kim, B.-J.; Im, S.-S.; Oh, S.-G. Investigation on the Solubilization Locus of Aniline-HCl Salt in SDS Micelles with 1H NMR Spectroscopy. *Langmuir* **2001**, *17* (2), 565–566. https://doi.org/10.1021/la0012889.

(22) Wang, R.; Wang, C.; Liu, K.; Bei, F.; Lu, L.; Han, Q.; Wu, X. Nucleation of Polyaniline Nano-/Macrotubes from Anilinium Composed Micelles. *J. Phys. Chem. B* **2014**, *118* (9), 2544–2552. https://doi.org/10.1021/jp411235u.

(23) Wan, M. A Template-Free Method Towards Conducting Polymer Nanostructures. *Adv. Mater.* **2008**, *20* (15), 2926–2932. https://doi.org/10.1002/adma.200800466.

(24) Ojha, J. K.; Venkatram Reddy, B.; Ramana Rao, G. Vibrational Analysis and Valence Force Field for Nitrotoluenes, Dimethylanilines and Some Substituted Methylbenzenes. *Spectrochim. Acta Part A Mol. Biomol. Spectrosc.* **2012**, *96*, 632–643. https://doi.org/https://doi.org/10.1016/j.saa.2012.06.035.

(25) Fleming, I.; Williams, D. Infrared and Raman Spectra BT - Spectroscopic Methods in Organic Chemistry; Fleming, I., Williams, D., Eds.; Springer International Publishing: Cham, 2019; pp 85–121. https://doi.org/10.1007/978-3-030-18252-6_3.

(26) Lenghaus, K.; Qiao, G. G.; Solomon, D. H. The Effect of Formaldehyde to Phenol Ratio on the Curing and Carbonisation Behaviour of Resole Resins. *Polymer (Guildf).* **2001**, *42* (8), 3355–3362. https://doi.org/https://doi.org/10.1016/S0032-3861(00)00710-2.

(27) Nayar, M. R. G.; Francis, J. D. Kinetics and Mechanism of the Aniline-Formaldehyde Reaction in Acid Medium. *Die Makromol. Chemie* **1978**, *179* (7), 1783–1790. https://doi.org/https://doi.org/10.1002/macp.1978.021790713.

(28) Gürses, A.; Eroğlu, Z.; Güneş, K.; Doğar, Ç. Synthesis and Thermal and Textural Characterization of Aniline Formaldehyde-Organoclay Composites. *Acta Phys. Pol. A* **2016**, *129*, 853–856.

(29) Paschek, D.; Geiger, A.; Hervé, M. J.; Suter, D. Adding Salt to an Aqueous Solution of T-Butanol: Is Hydrophobic Association Enhanced or Reduced? *J. Chem. Phys.* **2006**, *124* (15), 154508. https://doi.org/10.1063/1.2188398.

(30) Kruk, M.; Jaroniec, M. Gas Adsorption Characterization of Ordered Organic−Inorganic Nanocomposite Materials. *Chem. Mater.* **2001**, *13* (10), 3169–3183. https://doi.org/10.1021/cm0101069.

(31) Thommes, M. Physical Adsorption Characterization of Nanoporous Materials. *Chemie-Ingenieur-Technik* **2010**, *82* (7), 1059–1073. https://doi.org/10.1002/cite.201000064.

(32) Albino, P.; Chakraborty, S.; Ray, M.; Kumar, P. A.; Chakraborty, S.; Ray, M. Removal and Recovery of Chromium from Wastewater Using Short Chain Polyaniline Synthesized on Jute Fiber. *Chem. Eng. J.* **2008**, *141* (1–3), 130–140. https://doi.org/10.1016/j.cej.2007.11.004.

(33) Anirudhan, T. S.; Jalajamony, S.; Suchithra, P. S. Improved Performance of a Cellulose-Based Anion Exchanger with Tertiary Amine Functionality for the Adsorption of Chromium(VI) from Aqueous Solutions. *Colloids Surfaces A Physicochem. Eng. Asp.* **2009**, *335* (1–3), 107–113. https://doi.org/10.1016/j.colsurfa.2008.10.035.

(34) Ali, M. E. A. Synthesis and Adsorption Properties of Chitosan-CDTA-GO Nanocomposite for Removal of Hexavalent Chromium from Aqueous Solutions. *Arab. J. Chem.* **2018**, *11* (7), 1107–1116. https://doi.org/https://doi.org/10.1016/j.arabjc.2016.09.010.

(35) Verma, A.; Chakraborty, S.; Basu, J. K. Adsorption Study of Hexavalent Chromium Using Tamarind Hull-Based Adsorbents. *Sep. Purif. Technol.* **2006**, *50* (3), 336–341. https://doi.org/10.1016/j.seppur.2005.12.007.

(36) Lazaridis, N. K.; Bakoyannakis, D. N.; Deliyanni, E. A. Chromium(VI) Sorptive Removal from Aqueous Solutions by Nanocrystalline Akaganeite. *Chemosphere* **2005**, *58* (1), 65–73.

(37) Raji, C.; Anirudhan, T. S. Batch Cr(VI) Removal by Polyacrylamide-Grafted Sawdust: Kinetics and Thermodynamics. *Water Res.* **1998**, *32* (12), 3772–3780. https://doi.org/10.1016/S0043-1354(98)00150-X.

(38) Deng, S.; Bai, R. Removal of Trivalent and Hexavalent Chromium with Aminated Polyacrylonitrile Fibers: Performance and Mechanisms. *Water Res.* **2004**, *38* (9), 2424–2432. https://doi.org/10.1016/j.watres.2004.02.024.

(39) Lide, D. R. *CRC Handbook of Chemistry and Physics*; CRC press, 2004; Vol. 85.

(40) Gao, B.; Li, Y.; Chen, Z. Adsorption Behaviour of Functional Grafting Particles Based on Polyethyleneimine for Chromate Anions. *Chem. Eng. J.* **2009**, *150* (2), 337–343. https://doi.org/https://doi.org/10.1016/j.cej.2009.01.012.

(41) Que, L. *Physical Methods in Bioinorganic Chemistry: Spectroscopy and Magnetism*; Sterling Publishing Company, 2000.

(42) Pratima, M.; Ghosh, A.; Ramamurthy, Y.; Pandey, B.D.; Abhilash; Torem, M.L. Removal of Hexavalent Chromium from Mine Effluents by Ion Exchange Resins-Comparative Study of Amberlite IRA 400 and IRA 900. *Russian Journal of Non-Ferrous Metals.* **2018,** *59* (5), 533-542. https://doi.org/10.3103/S1067821218050103.

(43) Gkika, D.; Liakos, E.V.; Vordos, N.; Kontogoulidou, C.; Magafas, L.; Bikiaris, D.N.; Bandekas, D.V.; Mitropoulos, A.C.; Kyzas, G.Z. Cost Estimation of Polymeric Adsorbents. *Polymers (Basel).* **2019,** *11* (5), 925. https://doi.org/10.3390/polym11050925.

(44) Altun, T.; Ecevit, H.; Kar, Y.; Çiftçi, B. Adsorption of Cr(VI) onto cross-linked chitosan-almond shell biochars: equilibrium, kinetic, and thermodynamic studies. *Journal of Analytical Science and Technology.* **2021,** *12* (1), 38. https://doi.org/10.1186/s40543-021-00288-0.

(45) Sharma, P.K.; Ayub, S. The cost analysis and economic feaibility of AGRO wastes to adsorb chromium (VI) from wastewater. *International journal of civil engineering and technology.* **2019,** *10* (2), 2387.

Chapter 3

Long term storage property and Hg(II) adsorption behavior of the salt version of the AFC polymers

3.1. Introduction

In the previous chapter, we have seen that the aniline formaldehyde condensate polymers were easy to synthesize. They were very effective in removing chromate from the aqueous solution with good adsorption capacity. In this chapter, we have focused on three things.

(i) Leaching of chemicals from the polymers;

(ii) Effect of long-term storage of the polymeric material in their chromate removal capacity and chemical changes due to storage;

(iii) Effectivity in any other metal removal, e.g., Hg(II).

There have been multiple amine materials for the effective removal of chromate or other heavy metals from water at different conditions.[1–8] But hardly, people have studied the leaching of chemicals and long-term storage properties of those materials. We thus examined the leaching property of the salt form of AFC. Further, we repeated the chromate adsorption experiment with one-year-old polymers, checked their chromate removal capacity, and compared it with the freshly prepared polymers from chapter two. We recharacterized the old polymers to understand the results obtained to determine if any physical or chemical change occurred over one year.

Next, we extended our focus on the adsorption of any other toxic heavy metal by the salt versions of AFC polymer. Our polymers have amine functional groups. In their salt form, they remain as ammonium, which can act as an ion exchanger in acidic conditions or as a coordinating donor site depending on the pH of the medium. Amine functional groups usually bind Hg(II) to form relatively less soluble amine complexes. Hg(II) is regarded as one of the most toxic pollutants due to its high bioaccumulative properties.[9–11] Almost all mercury species, or organic mercury compounds are toxic. Because of usage in many products and processes, e.g., alkali production, pharmaceutical, cosmetic preparations, combustion of fossil fuels, electrical and electronics manufacturing plants, metal processing,

metal plating, metal finishing, and pulp and paper industries, it results in the contamination of aquatic systems.[12,13] The materials that have been used for adsorption varied from low-cost materials such as clay particles, activated carbon to carbon nanotubes, functionalized polymer, and ion-exchange resins.[8,12,14–19]

We used the salt forms of the polymer to study the removal of Hg(II). We have investigated the removal of Hg(II) at different initial metal concentrations using the polymer against various parameters, including- pH, isotherms, and emphasis was given to identify the adsorption mechanism during the removal process.

Part A: Leaching and storage property

3.2A. Experimental Section

3.2.1A. Solvents and reagents

Potassium dichromate from Merck India was used for the chromium removal studies. Other reagents were obtained from commercial sources and used without further purification unless otherwise stated. Water purified by Merck Direct Q8 ultrapure water purification system was used to prepare all solutions and reactions. Whatman® grade 1 qualitative filter paper was used for filtration purposes during adsorption experiments.

3.2.2A. Measurements

The UV visible spectra were recorded on a Perkin Elmer Lambda 25 UV–vis spectrophotometers. FTIR spectra were recorded with KBr discs on Perkin-Elmer Spectrum one FT-IR spectrophotometer in the range of 4000-400 cm^{-1}. Thermogravimetric analysis of the compounds was performed using a Netzsch STA449F3A00 TG analyzer with a heating rate of 10 ℃ per min. under N_2 atmosphere using a sample size of 5-10 mg per run. FESEM images were recorded using Zeiss Sigma and Zeiss Gemini instruments. The polymer samples

were first dispersed in ethanol, drop cast on a silver foil to get a thinner layer of the polymer surface, and air-dried in a desiccator over silica. Before analysis, it was mounted with the help of carbon tape on the stabs, coated with gold vapor twice before measurement to reduce charging. The BET surface area was obtained from the N_2 adsorption isotherm. Gas adsorption experiments were performed on a Quantachrome Autosorb-IQ MP instrument. Samples were degassed at 80 ℃ before the experiment. Total chromium concentration was measured using a Varian model-AA240 atomic absorption spectrometer (AAS) using air-acetylene flame at a wavelength of 429 nm with a slit width of 0.5 nm. The calibration graph was first determined, and then the chromium concentration of the unknown was measured. All the pH measurements were done using Eutech instruments' EcoScan pH 6 pH-meter.

3.2.3A. Leaching experiment

The salt forms of the polymer were subjected to the adsorption condition in an aqueous solution of pH ~4. In specimen tubes, 30 mL of pH adjusted Millipore deionized water with the same amount of polymers used for adsorption experiments (Section 2.2.4) were shaken in an orbital shaker at 300 rpm for 3 hours. The solutions were filtered, we analyzed the filtrate in a UV-Visible spectrophotometer. On the other hand, we took 17 mg (0.18 mmol) of aniline in 10 mL of 1N HCl and checked its UV-Vis absorption.

3.2.4A. Adsorption experiment

Chromate adsorption experiments under a similar condition as studied in Chapter two (Section 2.2.4) were performed with the one-year-old salt version of the polymers instead of freshly prepared polymers. The polymers were stored in a calcium carbonate desiccator under a vacuum. Here, we kept all the experimental variables the same as our previous experiments (initial pH of the solutions was kept as 4, the dose of the polymers taken was 4 g/L, digestion time 3hours, adsorption experiments were carried out in an orbital shaker

at 300 rpm) except the initial chromate concentration. The initial chromate concentration was varied from 10 mg/L to 100mg/L. In each experiment, 15 mL solution of chromate (prepared with pH adjusted Millipore deionized water) was used in specimen tubes along with 0.060 g of polymer.

3.3A. Results and discussion

3.3.1A. Leaching study

We synthesized polymers, characterized them, and found that their salt forms removed chromate from an aqueous solution with high adsorption capacity (mg of metal ion removed per gram of the polymer). So, the next question arose automatically, did it leach any chemicals in the medium? As the polymers can contain starting materials or low molecular weight polymer which are soluble in acidic condition. To find the answer, we digested the polymers in pH 4 water for 3 hours at 300 rpm, filtered, and took UV-Vis spectra of the filtrates. We compared the spectra with that of aniline in a dilute HCl medium with a known concentration. A comparison of the UV-vis spectra is shown in Figure 3.1A.

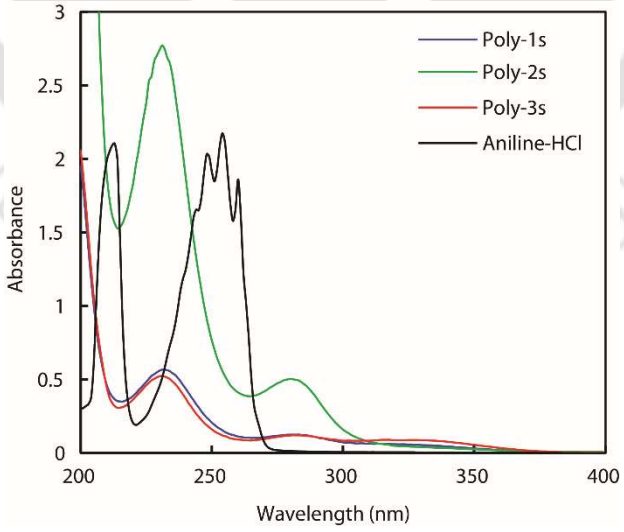

Figure 3.1A. UV-Visible spectra of aniline in HCl and the leached product of the polymers at the experimental condition.

The filtrate showed similar UV-Vis absorption in the UV region for all three polymers. The filtrate of Poly-1s showed maximum absorbance. This indicates the leaching of chemicals into the solution. We took 17 mg (0.18 mmol) of aniline in 10 mL of 1N HCl and checked its UV-Vis absorption. We wanted to compare the spectra of the filtrates with that of anilinium hydrochloride in known concentration to estimate the leached chemicals. However, the aniline in HCl spectra and the polymer extract spectra came different. This could be due to the polymeric nature of the leached chemicals; it did not show an exact absorbance pattern as the anilinium hydrochloride molecule. Since UV-visible is a very sensitive instrument, high absorbance in the spectra of the polymer extract does not mean a high amount of chemical leaching. Although quantitative estimation of the leached chemicals could not be done, the experiment tells us the salt form of the AFC polymers leach chemicals in a small quantity.

3.3.2A. Chromate removal

The salt forms of the freshly prepared polymers showed excellent chromate binding capacity at a dose of 0.5 g/L, even from a solution where the concentration of chromate was low (Figure 2.14). We used a dose of 4 g/L for the old polymers. The chromate removal data are shown in Figure 3.2A and Table 3.1A.

The adsorption capacity of the old polymers decreased. The effectivity of Poly-1s decreased the most, followed by Poly-2s and Poly-3s. Only Poly-3s showed moderate to good chromate removal for 10 mg/L to 100 mg/L chromate solutions at dose 4 g/L.

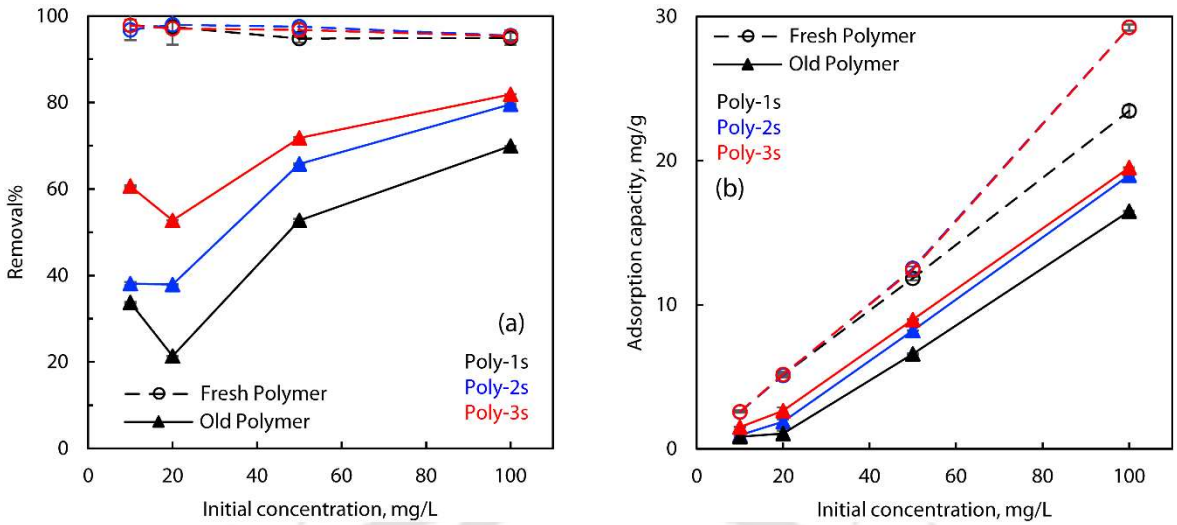

Figure 3.2A. Adsorption capacity and removal percent variation with initial Chromate concentration of the polymers at dose 4g/L, before and after one year.

Table 3.1A. Comparison of chromate removal (%) and uptake (mg/g) by the old polymers with that of the freshly prepared polymers at a dose of 4 g/L

Initial Concentration	Parameters	Poly-1s Old	Poly-1s	Poly-2s Old	Poly-2s	Poly-3s Old	Poly-3s
10 ppm	Uptake, mg/g	0.84 (±0.13)	2.59 (±0.00)	0.95 (±0.08)	2.56 (±0.01)	1.52 (±0.03)	2.59 (±0.01)
	Removal %	33.72 (±5.16)	97.81 (±0.17)	38.15 (±3.4)	96.76 (±0.37)	60.67 (±1.33)	97.81 (±0.19)
20 ppm	Uptake, mg/g	1.07 (±0.09)	5.13 (±0.19)	1.89 (±0.07)	5.10 (±0.15)	2.64 (±0.18)	5.15 (±0.24)
	Removal %	21.35 (±1.73)	97.48 (±0.09)	37.09 (±1.42)	97.95 (±0.14)	52.75 (±3.64)	97.05 (±0.05)
50ppm	Uptake, mg/g	6.59 (±0.08)	11.83 (±0.05)	8.22 (±0.12)	12.52 (±0.02)	8.97 (±0.22)	12.43 (±0.03)
	Removal %	52.70 (±0.61)	94.75 (±0.41)	65.75 (±0.95)	97.54 (±0.18)	71.76 (±1.73)	96.80 (±0.26)
100 ppm	Uptake, mg/g	16.48 (±1.07)	23.45 (±0.02)	18.98 (±0.39)	29.26 (±0.07)	19.51 (±0.21)	29.23 (±0.02)
	Removal %	69.90 (±4.53)	94.96 (±0.05)	79.59 (±1.65)	95.43 (±0.22)	81.91 (±0.87)	95.30 (±0.06)

The decrease in adsorption capacity could be because of either any chemical change that happened to them or any physical change within this one year. To understand these better, we did a chemical analysis of the old polymers. We compared their FTIR spectra (if any chemical change) and isotherm parameters (physical change), also looked for their surface morphology.

3.3.3A. FTIR Spectra

Chromate removal capacity of the polymers decreased with time. These polymers were chemically the same when they were synthesized (FTIR spectra were almost similar). Therefore, to check whether, within a year, there occurred any chemical change to the polymers, we took FTIR spectra of the year-old polymers.

The FTIR spectra of the one-year-old polymers looked almost similar to that of the base forms of the polymers (Figure 3.3A). The expected peaks for primary amine (two N-H stretch expected) were under the broad absorption with a peak maximum at ~3440 cm^{-1} due to H-bonding and moisture. Other characteristic peaks were ~1660 cm^{-1} (-NH_4^+ stretching), ~1584 cm^{-1} (very strong, N-H bending), ~1510 cm^{-1} (Strong, C-C stretching), ~1177 cm^{-1} (strong), ~812 cm^{-1} (out of plane aromatic C-H).[20] Peak at ~1660 cm^{-1} was shorter in base form, and the peak at the same position was shorter in the one-year-old salt forms of the polymers. This peak was assigned to ammonium stretching.[20] The decrease in intensity of this particular peak in the one-year-old polymers might be due to the release of the trapped acid from the polymeric core. Thus, they became more like the basic form of polymers. As a result, their chromate binding capacity decreased significantly. The least affected polymer from the FTIR spectra was Poly-3s, and Poly-3s is the one that showed moderate to good (more than 80%) chromate removal after one-year storage. The FTIR data thereby support the removal result.

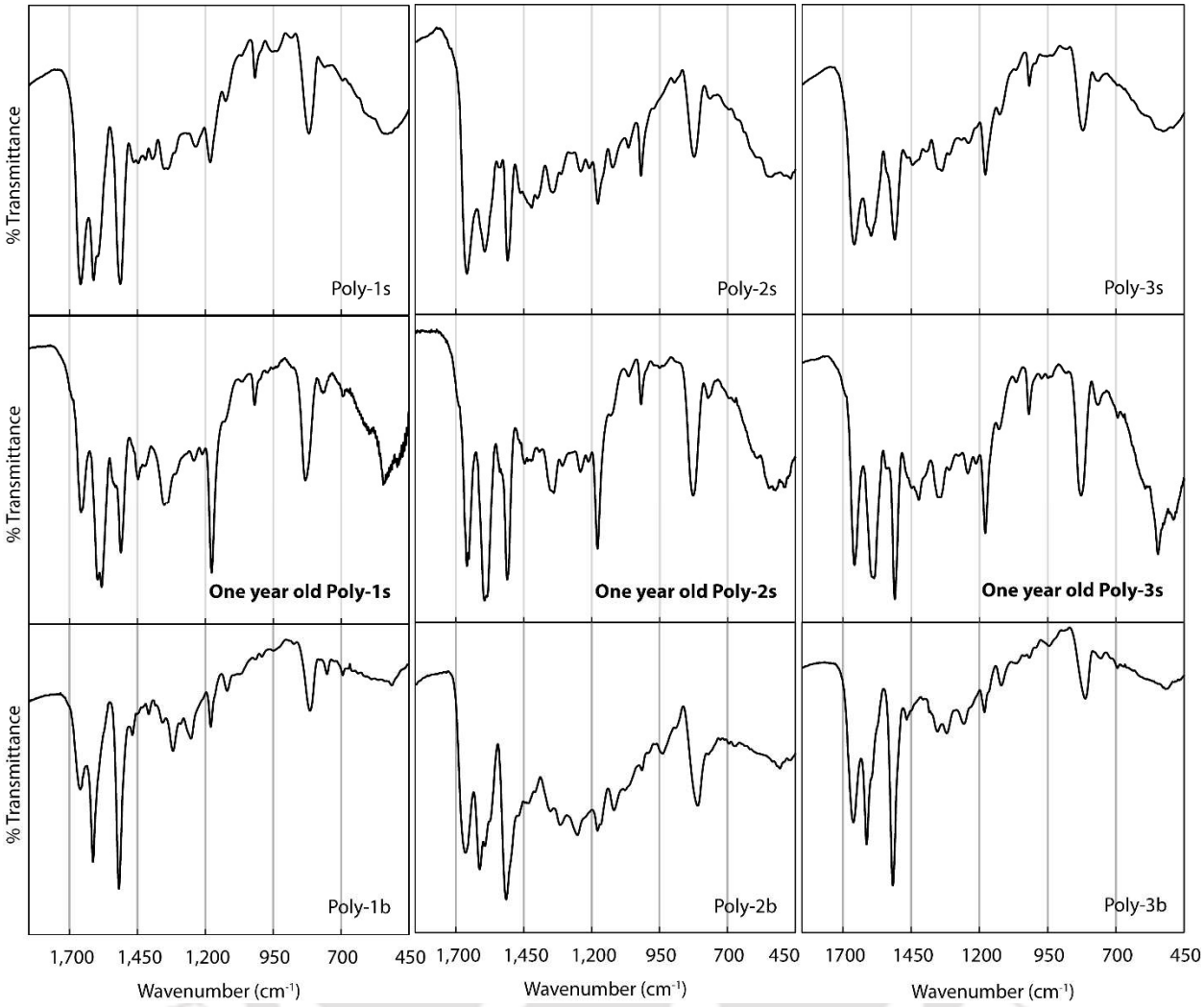

Figure 3.3A. Comparison of the FTIR spectra of the polymers before and after one year (S-Salt form, B-Base form) with that of the corresponding base forms.

3.3.4A. Surface area measurement (BET Isotherm)

Gas adsorption experiments were performed on a Quantachrome Autosorb-IQ MP instrument with the previously dried solid powdered samples. The isotherms patterns (Figure 3.4A) of the polymers did not change much. They are of type-II and type-IV according to IUPAC nomenclature.[21,22] As it could be seen, surface area and total pore volume of the one-year polymers decreased significantly with time. We were storing the polymers in a vacuum desiccator. The release of the trapped solvents and acids could happen

with time, reducing the polymers' porous nature. The surface got shrunk, resulting in a decrease in surface areas (Table 3.2A).

Table 3.2A. Isotherm parameters of the polymers by the BET method

Parameters	**Fresh polymers**			**One-year-old polymers**		
	Poly-1s	**Poly-2s**	**Poly-3s**	**Poly-1s**	**Poly-2s**	**Poly-3s**
Multipoint BET						
Surface Area (m^2/g)	29.130	93.390	21.079	5.302	29.484	4.660
Pore diameter (nm)	14.66	15.37	13.38	15.83	28.85	11.58
Total Pore Volume						
TPV (cc/g)	0.1068	0.3589	0.7053	0.02099	0.2127	0.01350
at P/P_o	0.99742	0.99080	0.99579	0.99625	0.98879	0.99729

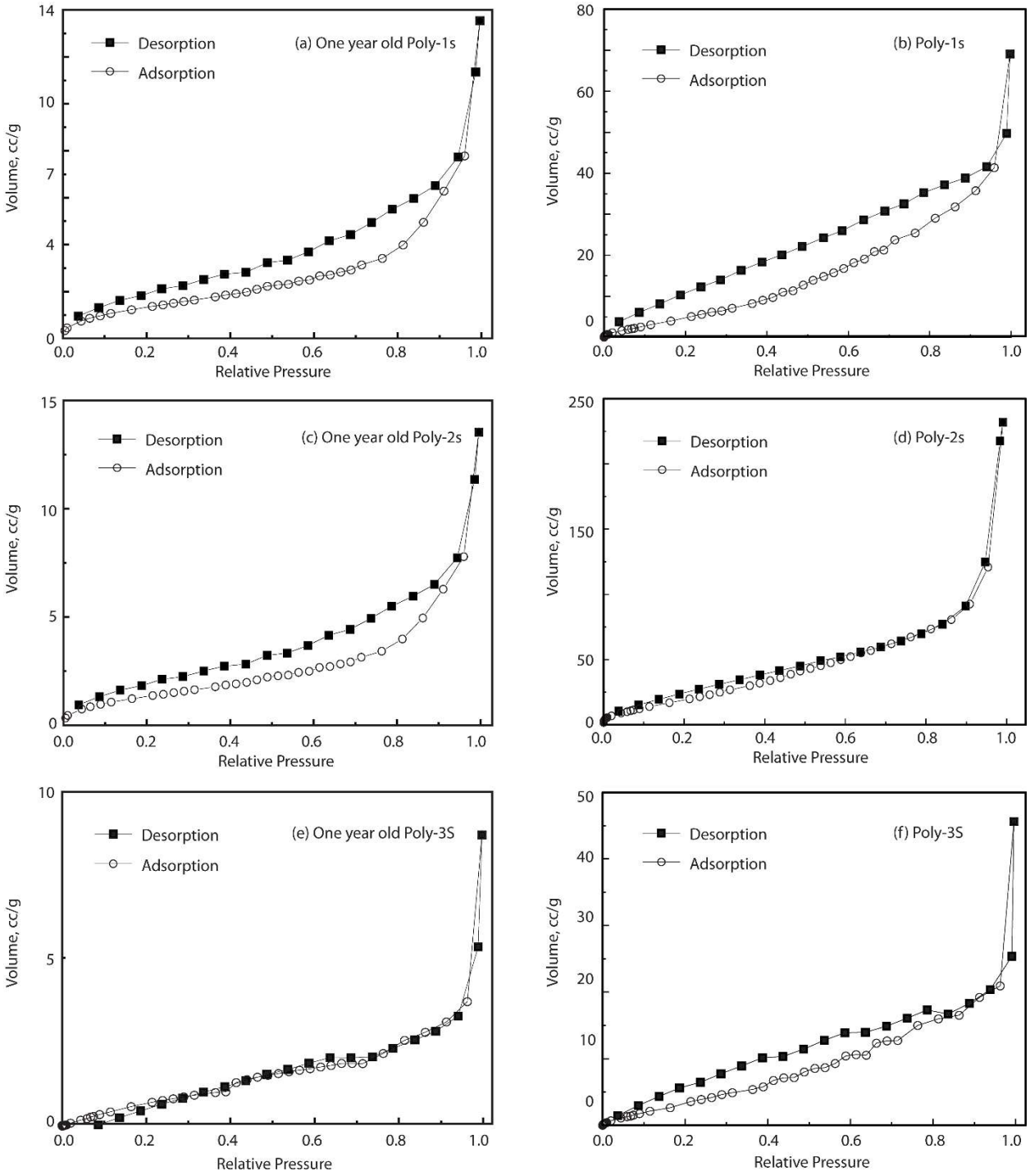

Figure 3.4A. BET isotherm of the one-year-old polymers compared with that of fresh polymers.

With the decrease in surface area, if there was physical adsorption, that also decreased with time. Hence the decrease in chromate binding.

3.3.5A. Surface morphology (FESEM imaging)

For FESEM studies, well-dried samples, dispersed in absolute ethanol (so that the dehydration occurred), were used, though charging the samples happened. The images are shown in Figure 3.5A. Samples were doubly coated with gold; operating accelerating voltage was kept as low as possible at 3 kV while capturing the images with an In-lens detector. Unfortunately, we could not stop the charging problem. Comparison with the freshly prepared sample (Figure 2.10), the significant visual difference in the morphology of the salt forms of the polymers is that the shape of the surface of one-year-old polymers changed (Figure 3.5A). The effect is most prominent in Poly-1s. We have seen that the chromate adsorption capacity of the Poly-1s polymer is affected most over time.

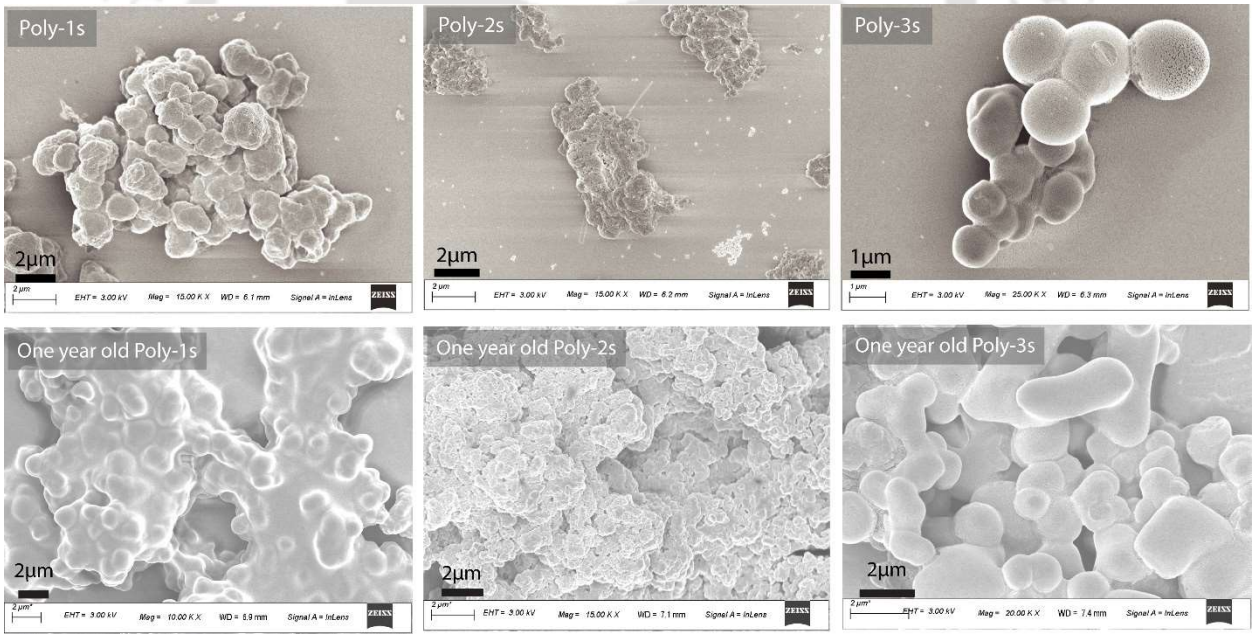

Figure 3.5A. FESEM images of the salt version of the one-year-old polymers (a) Poly-1s, (b) Poly-3s, and (c) Poly-2s.

Due to the loss of the trapped acids and solvents over time, the surface of the polymer became more polished. Loss of acids made the polymers non-conducting, because of which

there might be a charge accumulation during image capture, hence the charging. From the FESEM images, it is clear that surface morphology drastically changed with time. Loss of acids, solvents converted the quaternary ammonium to amine, resulting in loss of porosity and a decrease in its ion-exchanging capacity.

Part B: Hg(II) adsorption study

3.2B. Experimental Section

3.2.1B. Reagents and solvents

Mercuric nitrate [$Hg(NO_3)_2.H_2O$] was purchased from HiMedia and used as received. Other reagents were obtained from commercial sources and used without further purification. Water purified by Merck Direct Q8 ultrapure water purification system was used to prepare all solutions and reactions. Whatman® grade 1 qualitative filter paper was used for filtration purposes during adsorption experiments.

3.2.2B. Measurements

The FTIR spectra were recorded on Perkin-Elmer Spectrum one FT-IR spectrophotometer with KBr discs in the range of 4000-400 cm^{-1}. Surface morphology and energy dispersive X-ray spectra were studied using Zeiss Sigma and Zeiss Gemini instruments equipped with energy dispersive X-ray spectrometer. The polymer samples were coated with gold vapor twice before measurement to reduce charging. Total mercury concentration was analyzed using an Atomic Absorption spectrometer (model-AA240, Varian); flame ionization technique (Flame AAS) with a wavelength of 253.7 nm, slit width of 0.5 nm, optimum working range between 2-400 mg/L. All pH measurements were done using Eutech instruments' EcoScan pH 6 pH-meter. Chloride ion concentration in the solutions after pH adjustment and after adding the polymers was measured using Thermo Scientific™ Orion™ Chloride Electrodes.

3.2.3B. Adsorption study

A stock solution of 1000 mg/L of Hg(II) was prepared by dissolving analytical-grade $Hg(NO_3)_2.H_2O$ salt in distilled water in the presence of 300 µL of concentrated nitric acid.

Successive dilutions obtained desired concentration of Hg(II) solution with distilled water. The adsorption experiments were carried out to determine the adsorbent's optimum pH and adsorption capacity for maximum adsorption. All adsorption experiments were performed using a 15 mL volume of Hg(II) solution with 15 mg of polymer dose. The pH of the solutions was adjusted using either 1N HCl/1N NaOH solutions. An adsorption experiment was performed in an orbital shaker (300 rpm) for 3 hours. The amount of mercury ion adsorbed on polymer was obtained using the following equation (3.1B)

$$q_t = \frac{(C_o - C_t)}{m} V \qquad 3.1B$$

Where q_t is the amount of Hg(II) adsorbed per gram of polymer at time t (mg/g); C_o and C_t are the initial concentration and concentration at time t of Hg(II) ion in aqueous solution, respectively; V is the volume of the solution (L), and m is the mass of the adsorbent (g).

The removal percentage of mercury ions from aqueous solutions was calculated from the following equation (3.2B).

$$\text{Removal}(\%) = \frac{(C_o - C_t)}{C_o} \times 100 \qquad 3.2B$$

3.3B. Results and discussion

3.3.1B. FTIR spectroscopy

FTIR spectra of the polymers were taken before and after the Hg(II) adsorption and compared. No significant changes were observed after adsorption except the appearance of a sharp and intense peak at around 1384 cm^{-1}, which confirmed the presence of nitrate that came after Hg(II) adsorption.[20] The FTIR spectra are given in Figure 3.1B.

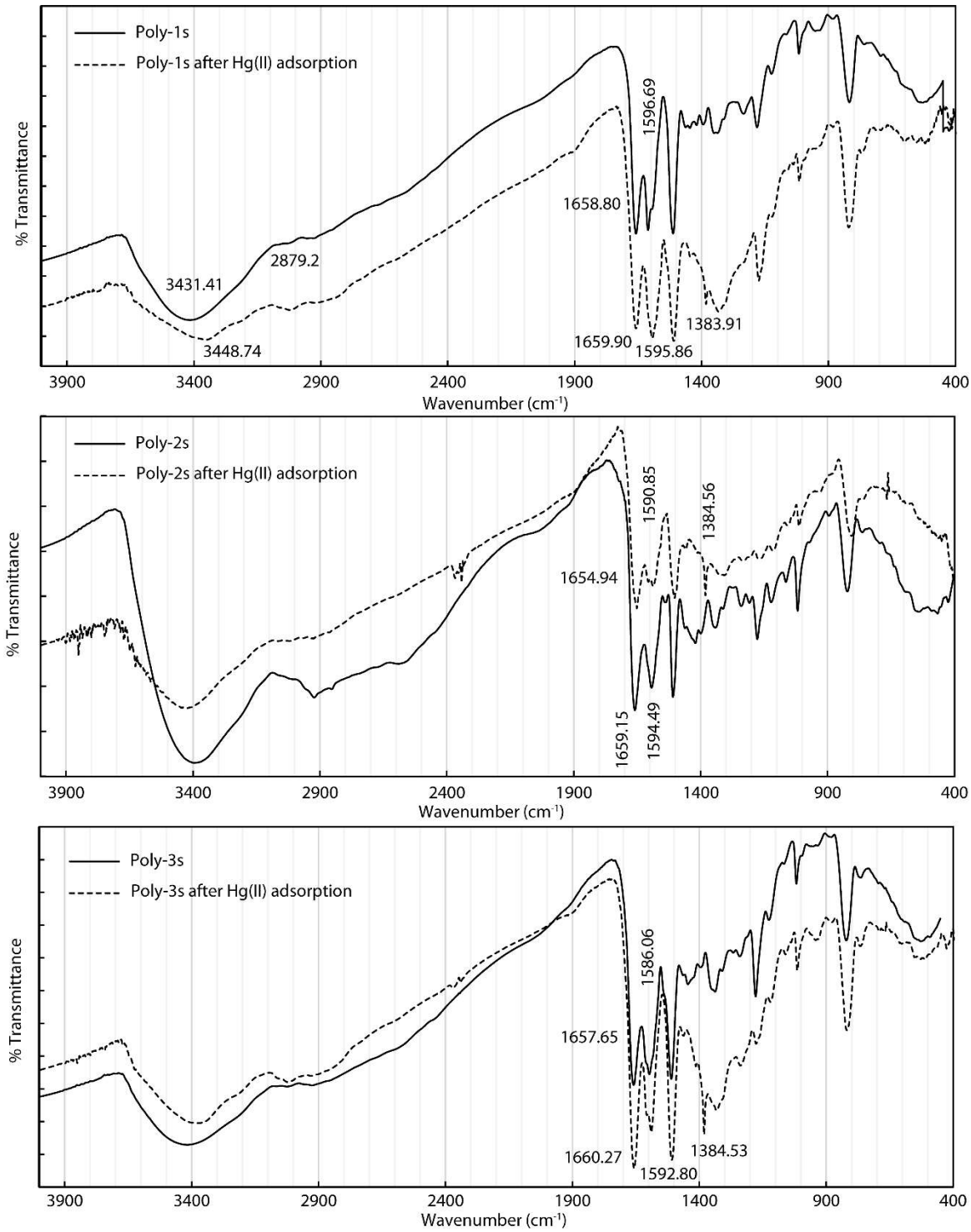

Figure 3.1B. Comparison of FTIR spectra of the polymers before and after Hg(II) adsorption.

3.3.2B. Hg(II) adsorption: Effect of pH

The influence of the solution pH on the removal efficiency was examined at an initial Hg(II) concentration of 50-200 mg/L using a 1 g/L polymer dose. The experiments were carried out at three controlled pH conditions, and experimental pH was varied from 2 to 7 to avoid any precipitation effect in pH greater than 7. Results are shown in Figure 3.2B and Table 3.1B-3.3B. The results indicate that removal efficiency was maximum at pH 4. Above and below pH 4, a decrease in removal was observed.

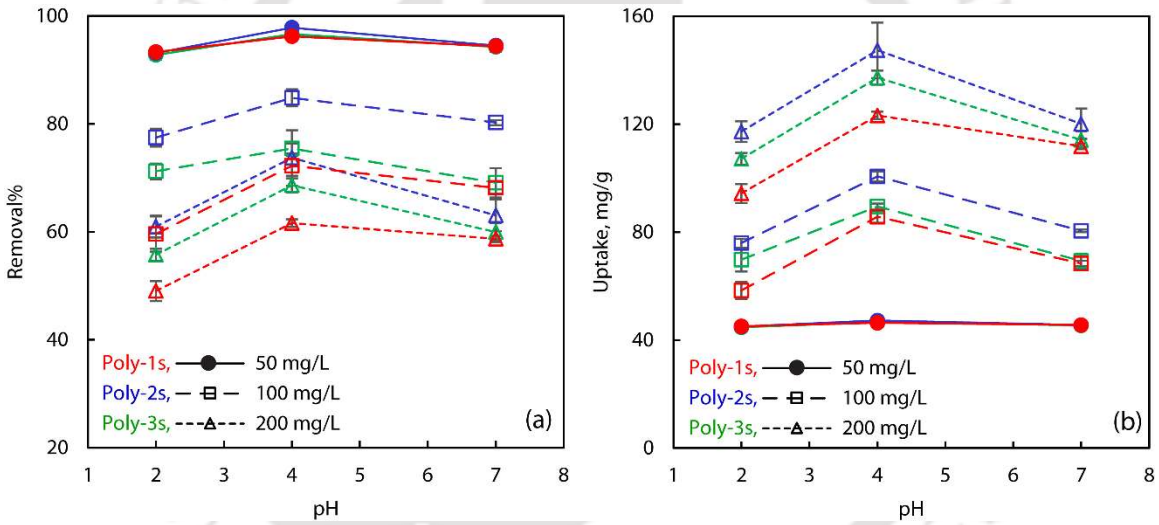

Figure 3.2B. Hg(II) removal efficiency and adsorption capacities of the polymers at different pHs at three initial concentrations with a dose of 1 g/L.

To understand this observation, we looked into the speciation of anilinium form of the polymer at different pH (Figure 2.5b). Also, we looked into the speciation of Hg(II) at that condition. The % of the anilinium form was calculated using respective pKa values. The anilinium form of the polymer is known to behave as an anion exchanger for the removal of chromate anion, as was observed previously (Chapter 2). At pH 2, it remains as anilinium. At pH 4, both aniline and anilinium are present in a 1:1 ratio, and at higher pH 7, the only

aniline remains. Now, pH control of the Hg(II) solutions was done with 1(N) HCl and 1(N) NaOH. The chloride ions enhance the formation of the Hg(II)-chloride complex, always competing with the Hg(II)-hydroxy complexes.[23] According to Hahne et al. 1973 at pH 2, the predominant forms are Hg(II) and $Hg(OH)^+$ when the pCl value is greater than 9, with a decrease in the pCl value (i.e., increase in Cl^- ion concentration), the predominant forms changed to $HgCl^+$, $HgCl_2$, $HgCl_3^-$ and $HgCl_4^{2-}$ depending on the pCl value.[23] Similar speciation occurs at pH 4 and pH 7, where we did our adsorption experiments. We measured the concentration of Cl^- ions at the experimental conditions and found that the chloride ion concentrations were 113 mg/L, 329 mg/L, and 12-20 mg/L at pH 2, 4, and 7, respectively. According to the speciation diagram reported by Hahne et al. 1973, the predominant forms of the Hg(II) at that respective pH must be $HgCl_2$, $HgCl_3^-$ and a mixture of $HgOH^+$, $HgOH_2$, and $HgCl_2$.[23] As there remained some amount of $HgCl_3^-$ at pH 2, the polymers showed removal of those anionic form of mercuric chlorides. At higher pH 7, because of the complexation of Hg(II) with the amine groups of the polymers, they showed some amount of mercury removal. At pH 4, both complexation and ion exchange are possible by the polymers. Therefore, it showed maximum Hg(II) uptake at that pH.

Table 3.1B. Hg(II) removal by the polymers at dose 1g/L at pH 2

Initial Concentration	Parameters	Poly-1s	Poly-2s	Poly-3s
50 ppm	Uptake, mg/g	45.09 (±0.21)	44.97 (±0.29)	44.8 (±0.43)
	Removal %	93.31 (±0.43)	93.10 (±0.59)	92.75 (±0.89)
100 ppm	Uptake, mg/g	58.40 (±3.20)	75.93 (±1.64)	69.80 (±4.36)
	Removal %	59.59 (±3.27)	77.48 (±1.67)	71.22 (±1.45)
200 ppm	Uptake, mg/g	94.33 (±3.52)	117.27 (±3.84)	107.17 (±2.15)
	Removal %	49.06 (±1.83)	60.98 (±2.00)	55.73 (±1.12)

Table 3.2B. Hg(II) removal by the polymers at dose 1g/L at pH 4

Initial Concentration	Parameters	Poly-1s	Poly-2s	Poly-3s
50 ppm	Uptake, mg/g	46.47 (±0.25)	47.23 (±0.05)	44.67 (±0.33)

	Removal %	96.20 (±0.52)	97.79 (±0.10)	96.62 (±0.68)
100 ppm	Uptake, mg/g	85.67 (±2.17)	100.63 (±1.86)	89.47 (±1.13)
	Removal %	72.23 (±1.83)	84.85 (±1.57)	75.44 (±0.95)
200 ppm	Uptake, mg/g	123.23 (±1.38)	147.4 (±10.26)	137.20 (±2.62)
	Removal %	61.62 (±0.69)	73.70 (±5.13)	68.60 (±1.31)

Table 3.3B. Hg(II) removal by the polymers at dose 1g/L at pH 7

Initial Concentration	**Parameters**	**Poly-1s**	**Poly-2s**	**Poly-3s**
50 ppm	Uptake, mg/g	45.63 (±0.19)	45.63 (±0.12)	45.53 (±0.45)
	Removal %	94.40 (±0.3)	94.48 (±0.26)	94.27 (±0.93)
100 ppm	Uptake, mg/g	66.33 (±0.70)	80.67 (±0.41)	79.60 (±0.49)
	Removal %	63.78 (±0.68)	77.56 (±0.40)	76.54 (±0.47)
200 ppm	Uptake, mg/g	111.83 (±1.06)	120.16 (±5.63)	114.23 (±3.11)
	Removal %	58.71 (±0.56)	63.07 (±2.96)	59.97 (±1.63)

3.3.3B. Hg(II) adsorption: Effect of initial concentration

Initial Hg(II) concentration was varied from 50 to 200 mg/L with a polymer dose of 1 g/L at pH 2-7 (Table 3.1B-3.3B). In terms of Hg(II) removal efficiency, removals were > 90%, up to initial Hg(II) concentrations of 50 mg/L and 80-70% at Hg(II) of 100 mg/L. The difference in removal efficiency started showing at an initial concentration of 100 mg/L, which further increased at 200 mg/L initial concentration. Similar trends of variation of removal (%) and adsorption capacity were observed at the three experimental pH.

When initial Hg(II) concentration was very low, amine sites on polymer greatly outnumbered Hg(II) ions. So, Hg(II) removal efficiency was almost similar among the three forms of the polymers. With an increase in Hg(II) concentrations, amine sites on polymer surfaces getting saturated. As a result, the removal percentage decreased. As adsorption capacity depends on the initial metal concentration and dose, it increases with increasing initial Hg(II) concentration.

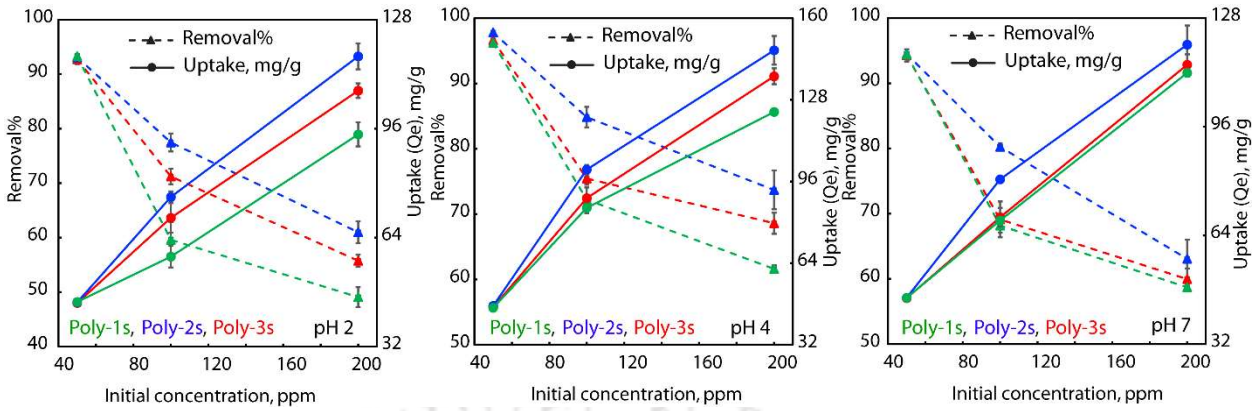

Figure 3.3B. Hg(II) removal efficiency and adsorption capacities of the polymers at different initial concentrations with a dose of 1 g/L.

Among the three polymers, we have seen Poly-2s has the amine groups at the outer surface of the polymeric core, and in the case of Poly-1s, it is inside the polymeric core. As a result, the surface of the Poly-2s has more amine sites than Poly-1s, Poly-3s being intermediate. This effect of amine site orientation is reflected on the respective polymer's Hg(II) removal capacity. Poly-2s showed the maximum Hg(II) removal at a definite initial concentration and pH.

A comparison table of Hg(II) removal by some known amine-based materials is given in Table 3.4B. It shows that none of the materials have shown high removal percentage with a high uptake value than our salt forms of the AFC.

Table 3.4B. Comparison of adsorption capacities with other known amine-based materials

Adsorbent	**Initial concentration (mg/L)**	**dose (g/L)**	**Removal (%)**	**Uptake (mg/g)**	**References**
New ultra-stable mesoporous adsorbent and on a commercial ion exchange resin	10	3	78.9	2.63	24
Chitosan-alginate nanoparticles (CANPs)	4	20	89	0.178	25
Polyaniline/Humic acid	50	0.5	98.3	98.3	26
Polyaniline nanocomposite coated on rice husk	100	10	95~	9.5~	27
Poly(1-amino-5-chloroanthraquinone) (PACA) nanofibrils	10 mM/L	1.6	51.2~	3.2~mM/g	28
Mesoporous silica/polyacrylamide composite	100	0.4	70.8	177	29
Amide functionalized cellulose from sugarcane bagasse	250	1	71.2~	178~	30
Chitosan derivatives	100	1	79	79	31
Novel amidoamine functionalized multi-walled carbon nanotubes	50	1	55~	27.5~	32
Activated coke by thiol-functionalization	1	0.1	98~	9.8~	33

Amine group-containing chelating fiber	100	1	95~	95~	34
Nanoporous carbon impregnated with surfactants	10	1	92~	9.2~	35
Polyamidoamine dendrimers functionalized magnetic graphene oxide	50	0.5	94~	94~	36
Chitosan coated magnetic nanoparticles	50	6g/L	84.5	7.04	37
Aminated chelating fiber	2000	1	32.9	657.9	38
Aminoethanethiol-Grafted Porous Organic Polymer	2000~	1	96~	181, 232 (estimation from isotherm)	39
Chitosan/Gelatin and glutaraldehyde hydrogel particles	561		98, 84, 58		40
PPN-150-MoS4	500	1	60.6	303	41
Poly-1s	50	1	97	46.47	This work
Poly-2s	50	1	98	47.23	This work
Poly-2s	200	1	74	147.4	This work

3.3.4B. Adsorption isotherm

Isotherms are beneficial for explaining the theoretical uptake capacity of different adsorptive materials. Langmuir and Freundlich's equations were used to analyze the experimental data of the Hg(II) removal in our study. Langmuir isotherm equation is given below (3.3B), and linear form is given in equation 3.4B.

$$q_e = \frac{q_m K_L C_e}{(1+bC_e)} \qquad 3.3B$$

$$\frac{1}{q_e} = \frac{1}{q_m} + \frac{1}{q_m K_L C_e} \qquad 3.4B$$

where Ce is the equilibrium concentration of a metal ion in mg/L, qt is the amount of metal ion adsorbed at equilibrium (mg/L). q_m and K_L is Langmuir constants related to adsorption capacity and energy of adsorption, respectively.

Freundlich equation is given in equation 3.5B and its linear form in equation 3.6B.

$$q_e = K_f C_e^{\frac{1}{n}} \qquad 3.5B$$

$$\log q_e = \log K_f + \frac{1}{n} \log C_e \qquad 3.6B$$

Where, K_f, 1/n are the adsorption capacity and adsorption intensity, respectively. The parameter values calculated from the Langmuir and the Freundlich models are listed in Table 3.5B. Figure 3.4B shows the isotherm fitting plots of the experimental equilibrium uptake (qe, mg/g) at equilibrium (Ce, mg/L).

Table 3.5B. Estimated isotherms parameters of adsorption of Hg(II) by the salt forms of the polymers

Material	Model	Model parameters	Values	R^2	ARE (%)
Poly-1s	Langmuir	q_m (mg/g)	115.78	0.87	-3.10
		K_L (L/mg)	0.24		
	Freundlich	K_f	34.73	0.97	-1.73

		1/n	0.27		
Poly-2s	Langmuir	q_m (mg/g)	112.94	0.74	2.80
		K_L (L/mg)	0.25		
	Freundlich	K_f	38.09	0.89	-1.84
		1/n	0.26		
Poly-3s	Langmuir	q_m (mg/g)	107.57	0.86	0.85
		K_L (L/mg)	0.26		
	Freundlich	K_f	36.39	0.97	-0.69
		1/n	0.25		

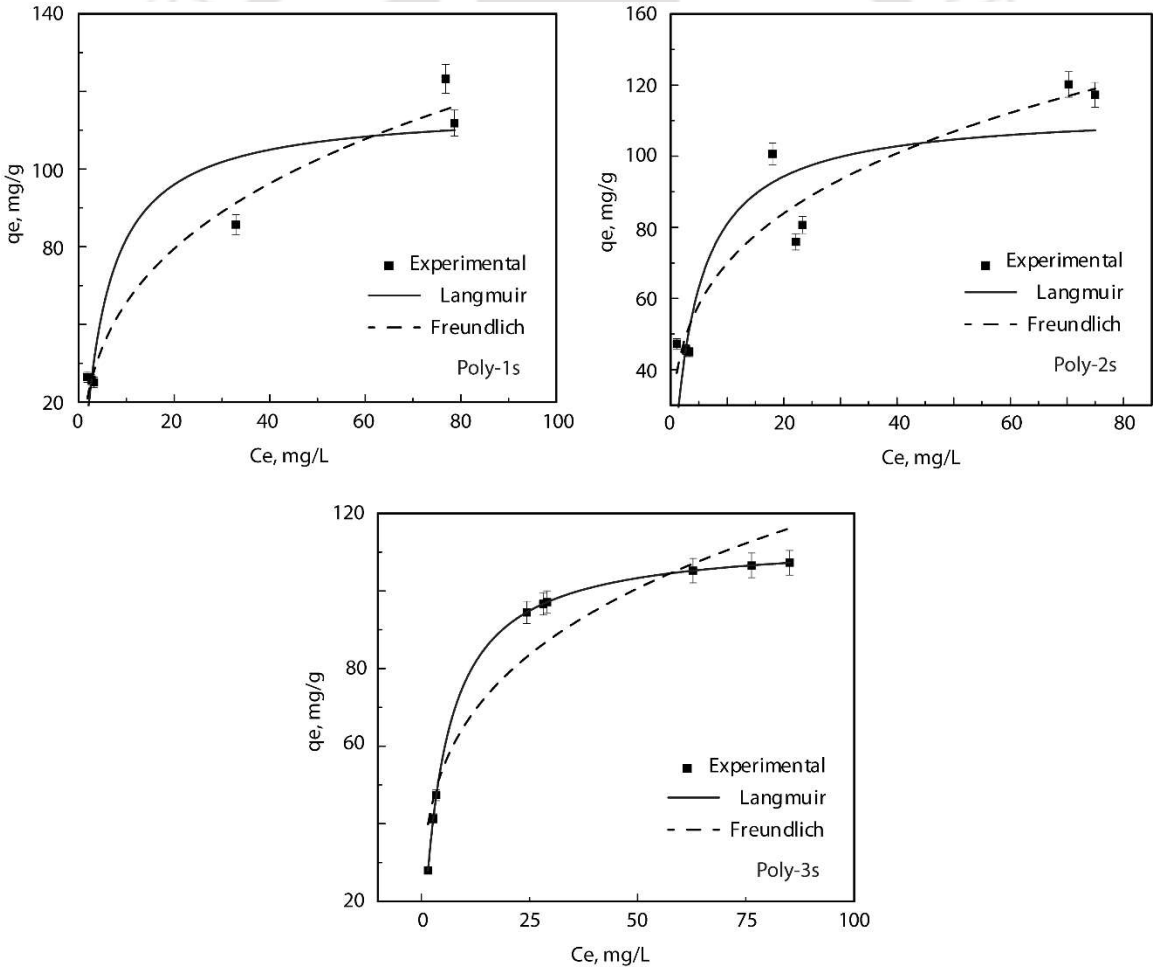

Figure 3.4B. Isotherm plot of Hg(II) uptake by the polymers.

Comparing the data obtained from the two isotherm models, it can be concluded that both the isotherm models fitted equally, in some cases Freundlich isotherm predominates. When 1/n values are in the range $0.1 < 1/n < 1$, the adsorption process is favorable. In this study, the value of 1/n values were 0.25 (Poly-3s), 0.26 (Poly-2s), and 0.27 (Poly-1s), suggesting favorable multilayer adsorption of Hg(II) when equilibrium Hg(II) concentration was more than 1 mg/L.

3.3.5B. Energy-dispersive X-ray spectra from FESEM

Energy-dispersive X-ray analysis was performed to investigate the presence of any metals in the adsorbent before the adsorption experiment. The EDAX spectra of the polymers before and after Hg(II) adsorption are given in Figure 3.5B.

As shown in the figure, the presence of any metals before adsorption was very negligible. The presence of mercury X-ray peak in EDX spectra of the polymers after the adsorption experiments confirmed the adsorption of Hg(II) onto the surface of the polymers. However, the elemental compositions obtained from this FESEM-EDX were quantitative enough to estimate the amount of Hg(II) present on that surface. It is because analysis of particles smaller than 1 μ m is a limitation for FESEM-EDX. The X-ray signals of smaller particles are difficult to detect against the discrete background lines from the substrate and the broad continuum background.[42] That is why the elemental composition percentage from EDX spectra differed from the composition obtained from elemental analysis.

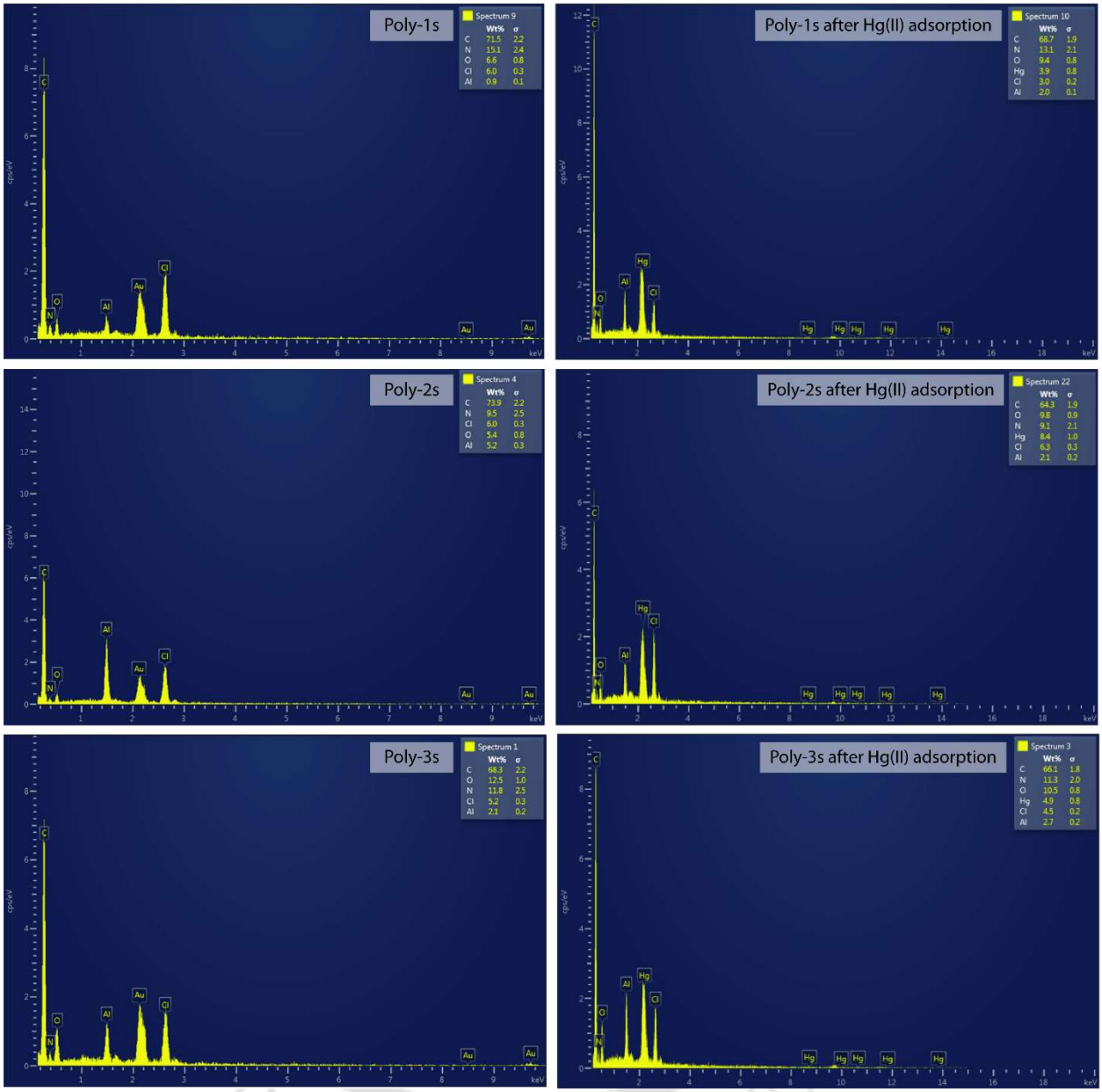

Figure 3.5B. EDX spectra of the polymers before and after Hg(II) adsorption.

3.4. Conclusion

The significant findings in this chapter are the following.

(i) The salt version of the amine-based AFC polymers loses their adsorption capacity with time (13-25% in terms of removal). The decrease in adsorption capacity is mainly due to converting the active salt form to the inactive base form.

(ii) Among the three polymers, Poly-3s remains active as observed from its chromate removal efficiency, even after one year. That means we can keep the polymers in a closed container, and it can be used to remove chromate from a range of chromate solutions with an excellent removal capacity. We used a calcium chloride desiccator for the storage, which might have helped absorb the acid from the salt forms. $CaCl_2$ should not be used, and we would like to study the storage property of the polymers without $CaCl_2$ desiccant in the future.

(iii) The polymers can effectively remove toxic heavy metal, Hg(II), from the aqueous medium.

(iv) Maximum adsorption observed at pH 4, and the polymer (Poly-2s) with amine groups on the surface showed somewhat better binding with the metal, Hg(II).

(VI) Isotherm studies showed the Freundlich isotherm the more favourable adsorption isotherm for the Hg(II) removal from the aqueous solutions suggesting the process to be a multilayer adsorption process.

3.5. Bibliography

(1) Dinker, M. K.; Kulkarni, P. S. Recent Advances in Silica-Based Materials for the Removal of Hexavalent Chromium: A Review. *Journal of Chemical and Engineering Data*. American Chemical Society September 10, 2015, pp 2521–2540. https://doi.org/10.1021/acs.jced.5b00292.

(2) Kumar, P. A.; Ray, M.; Chakraborty, S. Hexavalent Chromium Removal from Wastewater Using Aniline Formaldehyde Condensate Coated Silica Gel. *J. Hazard. Mater.* **2007**, *143* (1–2), 24–32. https://doi.org/10.1016/j.jhazmat.2006.08.067.

(3) Awad, F. S.; Abouzeid, K. M.; El-Maaty, W. M. A.; El-Wakil, A. M.; El-Shall, M. S. Efficient Removal of Heavy Metals from Polluted Water with High Selectivity for Mercury(II) by 2-Imino-4-Thiobiuret-Partially Reduced Graphene Oxide (IT-PRGO). *ACS Appl. Mater. Interfaces* **2017**, *9* (39), 34230–34242. https://doi.org/10.1021/acsami.7b10021.

(4) Xue, F.; He, H.; Zhu, H.; Huang, H.; Wu, Q.; Wang, S. Structural Design of a Cellulose-Based Solid Amine Adsorbent for the Complete Removal and Colorimetric Detection of Cr(VI). *Langmuir* **2019**, *35* (39), 12636–12646. https://doi.org/10.1021/acs.langmuir.9b01788.

(5) Fu, F.; Wang, Q. Removal of Heavy Metal Ions from Wastewaters: A Review. *J. Environ. Manage.* **2011**, *92* (3), 407–418. https://doi.org/https://doi.org/10.1016/j.jenvman.2010.11.011.

(6) Bailey, S. E.; Olin, T. J.; Bricka, R. M.; Adrian, D. D. A Review of Potentially Low-Cost Sorbents for Heavy Metals. *Water Res.* **1999**, *33* (11), 2469–2479. https://doi.org/10.1016/S0043-1354(98)00475-8.

(7) Varma, A. J.; Deshpande, S. V; Kennedy, J. F. Metal Complexation by Chitosan and Its Derivatives: A Review. *Carbohydr. Polym.* **2004**, *55* (1), 77–93. https://doi.org/https://doi.org/10.1016/j.carbpol.2003.08.005.

(8) Sharma, A.; Sharma, A.; Arya, R. K. Removal of Mercury(II) from Aqueous Solution: A Review of Recent Work. *Sep. Sci. Technol.* **2015**, *50* (9), 1310–1320. https://doi.org/10.1080/01496395.2014.968261.

(9) Patra, M.; Bhowmik, N.; Bandopadhyay, B.; Sharma, A. Comparison of Mercury, Lead and Arsenic with Respect to Genotoxic Effects on Plant Systems and the Development of Genetic

Tolerance. *Environ. Exp. Bot.* **2004**, *52* (3), 199–223. https://doi.org/https://doi.org/10.1016/j.envexpbot.2004.02.009.

(10) Kim, K.-H.; Kabir, E.; Jahan, S. A. A Review on the Distribution of Hg in the Environment and Its Human Health Impacts. *J. Hazard. Mater.* **2016**, *306*, 376–385. https://doi.org/https://doi.org/10.1016/j.jhazmat.2015.11.031.

(11) Risher, J.; DeWoskin, R. Report: Toxicological Profile for Mercury. *U.S. Dep. Heal. Hum. Serv. Public Heal. Serv. Agency Toxic Subst. Dis. Regist.* **1999**, No. March, 1–676.

(12) Bernhoft, R. A. Mercury Toxicity and Treatment: A Review of the Literature. *J. Environ. Public Health* **2012**, *2012*, 460508. https://doi.org/10.1155/2012/460508.

(13) Wang, Q.; Kim, D.; Dionysiou, D. D.; Sorial, G. A.; Timberlake, D. Sources and Remediation for Mercury Contamination in Aquatic Systems—a Literature Review. *Environ. Pollut.* **2004**, *131* (2), 323–336. https://doi.org/https://doi.org/10.1016/j.envpol.2004.01.010.

(14) Elhami, S.; Shafizadeh, S. Removal of Mercury (II) Using Modified Nanoclay. *Mater. Today Proc.* **2016**, *3* (8), 2623–2627. https://doi.org/10.1016/j.matpr.2016.06.005.

(15) Nouri, R.; Tahmasebi, E.; Morsali, A. Capability of Magnetic Functional Metal-Organic Nanocapsules for Removal of Mercury(II) Ions. *Mater. Chem. Phys.* **2017**, *198*, 310–316. https://doi.org/https://doi.org/10.1016/j.matchemphys.2017.06.018.

(16) Xu, J.; Bravo, A. G.; Lagerkvist, A.; Bertilsson, S.; Sjöblom, R.; Kumpiene, J. Sources and Remediation Techniques for Mercury Contaminated Soil. *Environ. Int.* **2015**, *74*, 42–53. https://doi.org/https://doi.org/10.1016/j.envint.2014.09.007.

(17) Ahmad, M.; Ahmed, S.; Ikram, S. ADSORPTION OF HEAVY METAL IONS: ROLE OF CHITOSAN AND CELLULOSE FOR WATER TREATMENT. *Int. J. Pharmacogn.* **2015**, *2* (6), 280–289. https://doi.org/10.13040/IJPSR.0975-8232.IJP.2(6).280-89.

(18) Saad, A.; Bakas, I.; Piquemal, J.-Y.; Nowak, S.; Abderrabba, M.; Chehimi, M. M. Mesoporous Silica/Polyacrylamide Composite: Preparation by UV-Graft Photopolymerization, Characterization and Use as Hg(II) Adsorbent. *Appl. Surf. Sci.* **2016**, *367*, 181–189. https://doi.org/https://doi.org/10.1016/j.apsusc.2016.01.134.

(19) Hadi, P.; To, M. H.; Hui, C. W.; Lin, C. S. K.; McKay, G. Aqueous Mercury Adsorption by Activated Carbons. *Water Res.* **2015**, *73*, 37–55. https://doi.org/10.1016/j.watres.2015.01.018.

(20) Fleming, I.; Williams, D. Infrared and Raman Spectra BT - Spectroscopic Methods in Organic Chemistry; Fleming, I., Williams, D., Eds.; Springer International Publishing: Cham, 2019; pp 85–121. https://doi.org/10.1007/978-3-030-18252-6_3.

(21) Kruk, M.; Jaroniec, M. Gas Adsorption Characterization of Ordered Organic-Inorganic Nanocomposite Materials. *Chem. Mater.* **2001**, *13* (10), 3169–3183. https://doi.org/10.1021/cm0101069.

(22) Thommes, M. Physical Adsorption Characterization of Nanoporous Materials. *Chemie-Ingenieur-Technik* **2010**, *82* (7), 1059–1073. https://doi.org/10.1002/cite.201000064.

(23) Hahne, H. C. H.; Kroontje, W. The Simultaneous Effect of PH and Chloride Concentrations upon Mercury(II) as a Pollutant. *Soil Sci. Soc. Am. J.* **1973**, *37* (6), 838–843. https://doi.org/https://doi.org/10.2136/sssaj1973.03615995003700060016x.

(24) De Clercq, J. Removal of Mercury from Aqueous Solutions by Adsorption on a New Ultra Stable Mesoporous Adsorbent and on a Commercial Ion Exchange Resin. *Int. J. Ind. Chem.* **2012**, *3* (1), 1. https://doi.org/10.1186/2228-5547-3-1.

(25) Dubey, R.; Bajpai, J.; Bajpai, A. K. Chitosan-Alginate Nanoparticles (CANPs) as Potential Nanosorbent for Removal of Hg (II) Ions. *Environ. Nanotechnology, Monit. Manag.* **2016**, *6*, 32–44. https://doi.org/https://doi.org/10.1016/j.enmm.2016.06.008.

(26) Zhang, Y.; Li, Q.; Sun, L.; Tang, R.; Zhai, J. High Efficient Removal of Mercury from Aqueous Solution by Polyaniline/Humic Acid Nanocomposite. *J. Hazard. Mater.* **2010**, *175* (1), 404–409. https://doi.org/https://doi.org/10.1016/j.jhazmat.2009.10.019.

(27) Ghorbani, M.; Lashkenari, M. S.; Eisazadeh, H. Application of Polyaniline Nanocomposite Coated on Rice Husk Ash for Removal of Hg(II) from Aqueous Media. *Synth. Met.* **2011**, *161* (13), 1430–1433. https://doi.org/https://doi.org/10.1016/j.synthmet.2011.05.016.

(28) Huang, S.; Ma, C.; Liao, Y.; Min, C.; Du, P.; Jiang, Y. Removal of Mercury(II) from Aqueous Solutions by Adsorption on Poly(1-Amino-5-Chloroanthraquinone) Nanofibrils:

Equilibrium, Kinetics, and Mechanism Studies. *J. Nanomater.* **2016**, *2016*, 7245829. https://doi.org/10.1155/2016/7245829.

(29) Saad, A.; Bakas, I.; Piquemal, J.-Y.; Nowak, S.; Abderrabba, M.; Chehimi, M. M. Mesoporous Silica/Polyacrylamide Composite: Preparation by UV-Graft Photopolymerization, Characterization and Use as Hg(II) Adsorbent. *Appl. Surf. Sci.* **2016**, *367*, 181–189. https://doi.org/https://doi.org/10.1016/j.apsusc.2016.01.134.

(30) Sun, N.; Wen, X.; Yan, C. Adsorption of Mercury Ions from Wastewater Aqueous Solution by Amide Functionalized Cellulose from Sugarcane Bagasse. *Int. J. Biol. Macromol.* **2018**, *108*, 1199–1206. https://doi.org/10.1016/j.ijbiomac.2017.11.027.

(31) Kyzas, G. Z.; Bikiaris, D. N. Recent Modifications of Chitosan for Adsorption Applications: A Critical and Systematic Review. *Mar. Drugs* **2015**, *13* (1), 312–337. https://doi.org/10.3390/md13010312.

(32) Singha Deb, A. K.; Dwivedi, V.; Dasgupta, K.; Musharaf Ali, S.; Shenoy, K. T. Novel Amidoamine Functionalized Multi-Walled Carbon Nanotubes for Removal of Mercury(II) Ions from Wastewater: Combined Experimental and Density Functional Theoretical Approach. *Chem. Eng. J.* **2017**, *313*, 899–911. https://doi.org/10.1016/j.cej.2016.10.126.

(33) Li, Z.; Wu, L.; Liu, H.; Lan, H.; Qu, J. Improvement of Aqueous Mercury Adsorption on Activated Coke by Thiol-Functionalization. *Chem. Eng. J.* **2013**, *228*, 925–934. https://doi.org/https://doi.org/10.1016/j.cej.2013.05.063.

(34) Ma, N.; Yang, Y.; Chen, S.; Zhang, Q. Preparation of Amine Group-Containing Chelating Fiber for Thorough Removal of Mercury Ions. *J. Hazard. Mater.* **2009**, *171* (1–3), 288–293. https://doi.org/10.1016/j.jhazmat.2009.06.001.

(35) Anbia, M.; Amirmahmoodi, S. Removal of Hg (II) and Mn (II) from Aqueous Solution Using Nanoporous Carbon Impregnated with Surfactants. *Arab. J. Chem.* **2016**, *9*, S319–S325. https://doi.org/https://doi.org/10.1016/j.arabjc.2011.04.004.

(36) Ma, Y.-X.; Xing, D.; Shao, W.-J.; Du, X.-Y.; La, P.-Q. Preparation of Polyamidoamine Dendrimers Functionalized Magnetic Graphene Oxide for the Adsorption of Hg(II) in Aqueous

Solution. *J. Colloid Interface Sci.* **2017**, *505*, 352–363. https://doi.org/https://doi.org/10.1016/j.jcis.2017.05.104.

(37) Nasirimoghaddam, S.; Zeinali, S.; Sabbaghi, S. Chitosan Coated Magnetic Nanoparticles as Nano-Adsorbent for Efficient Removal of Mercury Contents from Industrial Aqueous and Oily Samples. *J. Ind. Eng. Chem.* **2015**, *27*, 79–87. https://doi.org/10.1016/j.jiec.2014.12.020.

(38) Ma, N.; Yang, Y.; Chen, S.; Zhang, Q. Preparation of Amine Group-Containing Chelating Fiber for Thorough Removal of Mercury Ions. *J. Hazard. Mater.* **2009**, *171* (1), 288–293. https://doi.org/https://doi.org/10.1016/j.jhazmat.2009.06.001.

(39) Ravi, S.; Puthiaraj, P.; Row, K. H.; Park, D.-W.; Ahn, W.-S. Aminoethanethiol-Grafted Porous Organic Polymer for Hg2+ Removal in Aqueous Solution. *Ind. Eng. Chem. Res.* **2017**, *56* (36), 10174–10182. https://doi.org/10.1021/acs.iecr.7b02743.

(40) Perumal, S.; Atchudan, R.; Yoon, D. H.; Joo, J.; Cheong, I. W. Spherical Chitosan/Gelatin Hydrogel Particles for Removal of Multiple Heavy Metal Ions from Wastewater. *Ind. Eng. Chem. Res.* **2019**, *58* (23), 9900–9907. https://doi.org/10.1021/acs.iecr.9b01298.

(41) Feng, L.; Chen, W. M.; Li, J. L.; Day, G.; Drake, H.; Joseph, E.; Zhou, H. C. Biological Antagonism Inspired Detoxification: Removal of Toxic Elements by Porous Polymer Networks. *ACS Appl. Mater. Interfaces* **2019**, *11* (15), 14383–14390. https://doi.org/10.1021/acsami.9b02826.

(42) Atkins, P.; Overton, T.; Rourke, J.; Weller, M.; Armstrong, F. *Shriver and Atkins' Inorganic Chemistry*; Oxford University Press, 2010.

Chapter 4

Complexation of thiophene, pyridine, and imidazole derived Schiff base ligands with Mercury(II)

4.1. Introduction

Mercury is a health hazard in all forms.[1,2] The binding of mercury with chelating ligands or within a polymer having a functional group is being studied for a long time.[3–8] The first one provides electronic and structural information, while the latter functions as an adsorbent of mercury from polluted water. In both the case, the donor group plays a vital role in binding mercury. In the previous two chapters (Chapter 2 and 3), we have used functionalized amine polymers by modifying their form in removing chromate, Cr(VI), and mercury, Hg(II) from an aqueous medium. In this chapter, we chose three bidentate Schiff base ligands with three different donor groups, keeping the other groups identical. The three different groups were imidazole, pyridine, and cyclic thioether, thiophene (Scheme 4.1). Imidazole moiety of L-histidine is common in metalloenzyme active sites, whereas pyridine is common in biomimetic complexes.[9,10] The preferential binding of mercury with sulfur-containing donor groups is well known. Ligands were reacted with $Hg^{2+,}$ and the resultant complexes were characterized to identify their respective binding capabilities. We will use the resulting knowledge in the next chapter, where similar functionalization will be made on polymer.

4.2. Experimental Section

4.2.1. Solvents and reagents

Solvents and acids were obtained from Merck and used without further purifications unless otherwise stated. Pyridine-2-carboxaldehyde, imidazole-2-carboxaldehyde, thiophene-2-carboxaldehyde, and 1-phenylethylamine were purchased from Sigma Aldrich Chemical Co. and used as received. Mercuric nitrate and mercuric chloride were purchased from HiMedia and used as received.

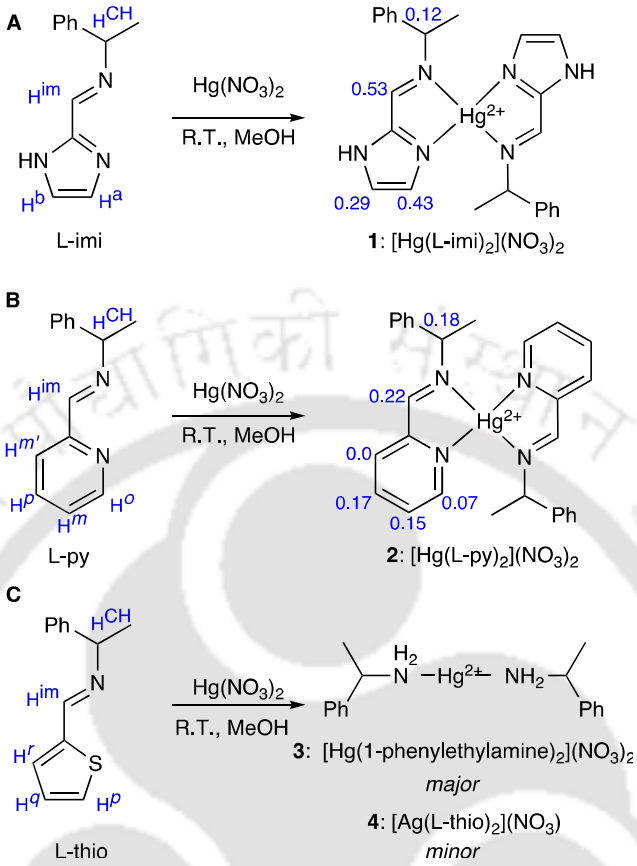

Scheme 4.1. Ligands with NMR labeling and corresponding mercury(II) complexes.

4.2.2. Measurements

The FTIR spectra were recorded on PerkinElmer Spectrum One FT-IR spectrophotometer with KBr discs in the range 4000-400 cm^{-1}. Elemental analyses were performed using the Eurovector EA3000 CHNS analyzer at Biotech Park Guwahati. Electrospray Ionization mass (ESI-MS) recorded on an AGILENT Q-TOF 6520 High-Resolution Mass Spectrometer. For ESI-MS measurement, compounds were dissolved in 2 ml of methanol. This solution was filtered through a 0.2 µm membrane filter before measurement. ^{1}H NMR spectra were recorded using Bruker 400 MHz instruments. Circular Dichroism measurement was performed using JASCO J-1500CD Spectrometer, and the spectra were analyzed using JASCO spectra manager version 2.0. The CD spectra were

recorded under inert N_2 atmosphere using DMSO as a solvent and a high Precision Cell made of Quartz SUPRASIL cuvette having a path length of 1 mm.

4.2.3. Syntheses

The ligands L-imi and L-py were synthesized following the reported procedure.[11]

4.2.3.1. 1-(1H-imidazol-2-yl)-N-(1-phenylethyl)methanimine (L-imi). 1-phenylethylamine (0.500 g, 4.13 mmol) was stirred in 10 mL methanol. A solution of imidazole-2-carboxaldehyde (0.396 g, 4.13 mmol) in 10 mL methanol was added dropwise to it. The solution turned yellowish. The mixture was stirred for 3 h at room temperature. The solvent was evaporated to obtain a white solid. Solid was washed with 10 mL of n-hexane followed by 10 mL of diethyl ether. The solid was dried in a desiccator to obtain the product as an off-white solid. Yield, 0.62 g. FTIR (KBr, cm^{-1}): υ (C=N)stretch 1642 (s). ^{1}H NMR (400 MHz, DMSO, ppm): 8.30 (H^{imi}, s, 1H), 7.42 (H^{Ph}, d, 2H, J=6.8Hz), 7.35 (H^{Ph}, t, 2H, J=7.2Hz), 7.25 (H^{Ph}, t, 1H, J=7.2Hz), 7.22 (H^{b}, s, 1H,), 7.08 (H^{a}, s, 1H), 4.63 (H^{CH}, q, 1H, J = 6.6Hz), 1.51 (H^{Me}, d, 3H, J = 6.6Hz). ESI-MS ($[C_{12}H_{13}N_3 + H]^+$): calcd 200.119; found 200.131.

4.2.3.2. N-(1-phenylethyl)-1-(pyridin-2-yl) methanimine (L-py). This was synthesized following the same procedure as L-imi using imidazole-2-carboxaldehyde (0.442 g, 4.13 mmol) instead of 2-thiophenecarboxaldehyde. In this case, the Schiff base was obtained as yellow liquid. Yield, 0.92 g. FTIR (KBr, cm^{-1}): $\upsilon(C{=}N)_{stretch}$ 1646 (s). ^{1}H NMR (400 MHz, DMSO, ppm): 8.51 (H^{imi}, s, 1H), 8.68 (H^{o}, d, 1H, J = 4.4Hz), 8.06 ($H^{m'}$, d, 1H, J = 8Hz), 7.91 (H^{m}, dt, 1H, J = 7.6Hz, 1.6Hz), 7.50 (H^{p}, t, 1H, J=4.4Hz), 7.47 (H^{Ph}, d, 2H, J=7.6Hz), 7.39 (H^{Ph}, t, 2H, J=7.6Hz), 7.29 (H^{Ph}, t, 1H, J=7.2Hz), 4.74 (H^{CH}, q, 1H, J = 6.8Hz), 1.55 (H^{Me}, d, 3H, J = 6.8Hz). ESI-MS ($[Hg(C_{14}H_{14}N_2)Cl]+$): calcd 447.049; found 447.050.

4.2.3.3. N-(1-phenylethyl)-1-(thiophene-2-yl)methanimine (L-thio). (S)-(-)-1-Phenylethylamine (0.500 g, 4.13 mmol) was taken in 10 mL of methanol. 2-Thiophenecarboxaldehyde (0.463 g, 4.13 mmol) in 5 mL of methanol was added to the first solution and was stirred. The solution turned brownish with no precipitation. The solution was stirred for 3 hours at room temperature. The solvent was evaporated, and ethyl acetate was added to it. It was then extracted 5-7 times with the brine solution. The organic layer was dried over anhydrous sodium sulfate and then evaporated to get a pale brown-colored crystalline solid. Yield, 0.87 g. FTIR (KBr, cm^{-1}): $\upsilon(C{=}N)_{stretch}$ 1634 (s). ^1H NMR (400 MHz, DMSO, ppm): 8.58 (H^{imi}, s, 1H), 7.67 (H^{p}, d, 1H, J = 5.2Hz), 7.48 (H^{r}, dd, 1H, J = 3.6Hz, 0.8Hz), 7.15 (H^{q}, dd, 1H, J = 4.4Hz, 3.6Hz), 7.38 (H^{Ph}, d, 2H, J=6.8Hz), 7.34 (H^{Ph}, t, 2H, J=7.6Hz), 7.24 (H^{Ph}, t, 1H, J=7.2Hz), 4.55 (H^{CH}, q, 1H, J = 6.8Hz), 1.47 (H^{Me}, d, 3H, J = 6.8Hz). ESI-MS ($[C_{13}H_{13}NS + H]+$): calcd 216.085; found. 216.087.

4.2.3.4. [Hg(L-imi)2](NO₃)₂ (1). The ligand L-imi (0.150 g, 0.75 mmol, 2 eq.) was dissolved in 10 mL of methanol and stirred at room temperature. To the stirred solution, $Hg(NO_3)_2.H_2O$ (0.128 g, 0.38 mmol, 1 eq.) in 5 mL of methanol-water (10:1) was added dropwise, which turned it to a cloudy solution. Immediately it was filtered through celite, and the filtrate was stirred for 3 hrs. Off-white precipitation formed, was filtered, washed with methanol, dried under vacuum in a desiccator. Yield, 0.160g. FTIR (KBr, cm^{-1}): $\upsilon(C{=}N)_{stretch}$ 1631 (s), 1384.8, 555. ^1H NMR (400 MHz, DMSO, ppm): 8.83 (H^{imi}, s, 1H), 7.51 ($H^{a,b}$, s, 2H), 7.14 (H^{Ph}, m, 5H), 4.75 (H^{CH}, q, 1H, J = 6.4Hz), 1.31 (H^{Me}, d, 3H, J = 6.4Hz). ESI-MS ($[Hg(C_{12}H_{13}N_3)_2 - H]^+$): calcd 599.185; found 599.198.

4.2.3.5 [Hg(L-py)₂](NO₃)₂ (2a). The ligand L-py (0.150 g, 0.71 mmol, 2 eq.) was dissolved in 10 mL of methanol and stirred at room temperature. To the stirred solution, $Hg(NO_3)_2.H_2O$ (0.122 g, 0.36 mmol, 1 eq.) in 5 mL of methanol-water (10:1) was added dropwise. Immediately a cloudy solution formed, which was filtered, and the filtrate was

stirred for 3 hrs. No precipitation was formed this time. Evaporation of the solvent yielded an oily liquid Yield, 0.12g. FTIR (KBr, cm^{-1}): $\upsilon(C{=}N)_{stretch}$ 1644 (s), 1311, 536. ESI-MS ($[Hg(C_{14}H_{14}N_2)_2NO_3]^+$): calcd 684.0693; found 684.1923.

[Hg(L-py)]Cl_2 (2b). The complexation reaction of L-py with Hg(II) was repeated using $HgCl_2$ instead of $Hg(NO_3)_2$. To a solution of L-py in methanol (0.150 g, 0.71 mmol, 2 eq.), $HgCl_2$ (0.098 g, 0.36 mmol, 1 eq.) solution in methanol was added dropwise and stirred for 3 hrs. This time crystalline precipitate came, which was filtered and washed with methanol. Yield, 0.09 g. FTIR (KBr, cm^{-1}): $\upsilon(C{=}N)_{stretch}$ 1647 (s), 539. ^1H NMR (400 MHz, DMSO, ppm): 8.73 (H^{imi}, s, 1H), 8.75 (H^{o}, d, 1H, J = 4.8Hz), 8.06 ($H^{m,p}$, m, 2H), 7.67 ($H^{m'}$, m, 1H), 7.45 (H^{Ph}, d, 2H, J=7.6Hz), 7.36 (H^{Ph}, t, 2H, J=7.4Hz), 7.28 (H^{Ph}, t, 1H, J=7.2Hz), 4.92 (H^{CH}, q, 1H, J = 6.8Hz), 1.61 (H^{Me}, d, 3H, J = 6.8Hz). ESI-MS ($[Hg(C_{14}H_{14}N_2)Cl]^+$): calcd 447.049; found 447.050.

4.2.3.6. Product of reaction between L-thio + $Hg(NO_3)_2$ (3). The ligand L-thio (0.150 g, 0.70 mmol, 2 eq.) was dissolved in 10 mL of methanol and stirred at room temperature. To the stirred solution, $Hg(NO_3)_2$ (0.119 g, 0.35 mmol, 1 eq.) in 5 mL of methanol-water (10:1) was added dropwise, which initially turned into a cloudy solution, and the mixture was stirred for 3 hours. It was filtered through a G-4 crucible. The filtrate is kept for slow evaporation. Within 3 days, colorless block-shaped crystals formed. Yield, 0.070g (crystalline compound). FTIR (KBr, cm^{-1}): 1579 (s), 1379 (br), 552. ESI mass found 443.081, 539.068.

4.2.3.7. [Hg(1-phenylethylamine)2]$(NO_3)_2$ (4). The ligand (S)-(-)-1-Phenylethylamine (0.200 g, 1.65 mmol, 2 eq.) was dissolved in 10 mL of methanol and stirred at room temperature. To the stirred solution, $Hg(NO_3)_2$ (0.282 g, 0.82 mmol, 1 eq.) in 5 mL of methanol-water (10:1) was added dropwise. Initially, white precipitation was formed, and the mixture was stirred for 3 hours. It was filtered through a G-4 crucible, and

the filtrate was kept for slow evaporation. After 3 days, colorless rod-shaped crystals formed. Yield, 0.180g. FTIR (KBr, cm^{-1}): 1582 (s), 1379 (br), 551. ESI-Mass ($[Hg(C_8H_{11}N)_2\text{-}H]^+$): calcd 443.070; found 443.126.

4.2.3.8. $[Ag(L\text{-}thio)_2](NO_3)$ (5). The ligand L-thio (0.100 g, 0.46 mmol, 2 eq.) was dissolved in 10 mL of methanol and stirred at room temperature. To the stirred solution, $Ag(NO_3)$ (0.039 g, 0.23 mmol, 1 eq.) in 5 mL of methanol was added dropwise. It was stirred for 3 hours. It was filtered through G-4 crucible, and addition of diethyl ether to the filtrate afforded white precipitate. Yield, 0.070g. FTIR (KBr, cm^{-1}): 1631 (s), 1385, 555. ^1H NMR (400 MHz, DMSO, ppm): 8.94 (H^{imi}, s, 1H), 7.62 (H^p, d, 1H, J = 5.2Hz), 7.72 (H^r, dd, 1H, J = 3.6Hz, 1.2Hz), 7.21 (H^q, dd, 1H, J = 5Hz, 3.6Hz), 7.27-7.35 ($H^{o,m,p\text{-}Ph}$, m, 5H), 4.85 (H^{CH}, q, 1H, J = 6.4Hz), 1.67 (H^{Me}, d, 3H, J = 6.8Hz). ESI-Mass ($[Ag(C_{13}H_{13}NS)_2]^+$): calcd 539.058; found 539.062.

4.2.4. X-ray Data Collection, Structure Solvation, and Refinement

Crystals of 3 were subjected to single-crystal X-ray diffraction analysis to get structure-related information. Crystals were mounted on a glass fiber with silicone oil. The crystals' geometric and intensity data were collected at room temperature using a Bruker APEX-II CCD diffractometer equipped with a fine focus 1.75 kW sealed tube Mo-K (= 0.71073 Å) X-ray source. The Bruker APEX2 software was used for data acquisition and the Bruker SAINT V8.38A software for data extraction.[12] Absorption corrections were done using SADABS-2016/2.[12] After the initial solution and refinement with SHELXL[13], and the final refinements were performed on Olex2[14] environment using olex2.refine. All non-hydrogen atoms were refined anisotropically. Nitrate molecules were refined isotropically. Wherever possible, the hydrogen atoms were located from the difference Fourier maps and refined isotropically. Thus, some of the C-H bonds will not be ideal and may vary. Crystallographic

data and details of refinements are listed in Table 4.3, and selected bond distances and angles are listed in Table 4.4.

4.3. Results and Discussion

4.3.1. Syntheses

Three Schiff bases were synthesized; (a) the thiophene, pyridyl, and imidazolyl are potential donor ligands, and (b) creation of strong chelating sites in the Schiff base structure. The Schiff base ligands were synthesized by condensing the chiral 1-phenylethylamine and the aldehyde in methanol. The L-py and L-thio were isolated as an oily liquid, while the L-imi was isolated as an off-white solid. However, after some days, L-thio yielded yellowish block-shaped crystals. A strong vibration near 1650 cm^{-1} in the FTIR spectra of the ligands is assigned to the C=N stretch of the newly formed imine bonds. These ligands' Hg(II) complexes were synthesized by adding the metal to the ligand's solution at room temperature (Scheme 4.1). The metal to ligand ratio maintained was 1:2. The addition of Hg(II) to L-py and L-imi resulted in immediate cloudiness, which was filtered through celite. The filtrate was stirred, precipitation formed, washed, dried under vacuum, and used for further characterization. The reaction of L-py with $Hg(NO_3)_2$ did not yield any solid compound; hence the complexation reaction was repeated with the $HgCl_2$ salt. On the other hand, L-thio initially gave little precipitation, but the solid dissolved and gave a clear solution. Slow evaporation of the filtered solution yielded nice rod-shaped colorless crystals.

4.3.2. ^{1}H NMR analysis

^{1}H NMR spectra of the ligands and the complexes were taken in DMSO-d_6. The proton NMR spectra of the free ligands and their Hg(II) complexes are shown in Figures 4.1-4.3. Chemical shifts of the imidazole, pyridine, and thiophene ring protons in the corresponding ligands have been determined by analysis of the respective AB, ABCD, and ABX systems.

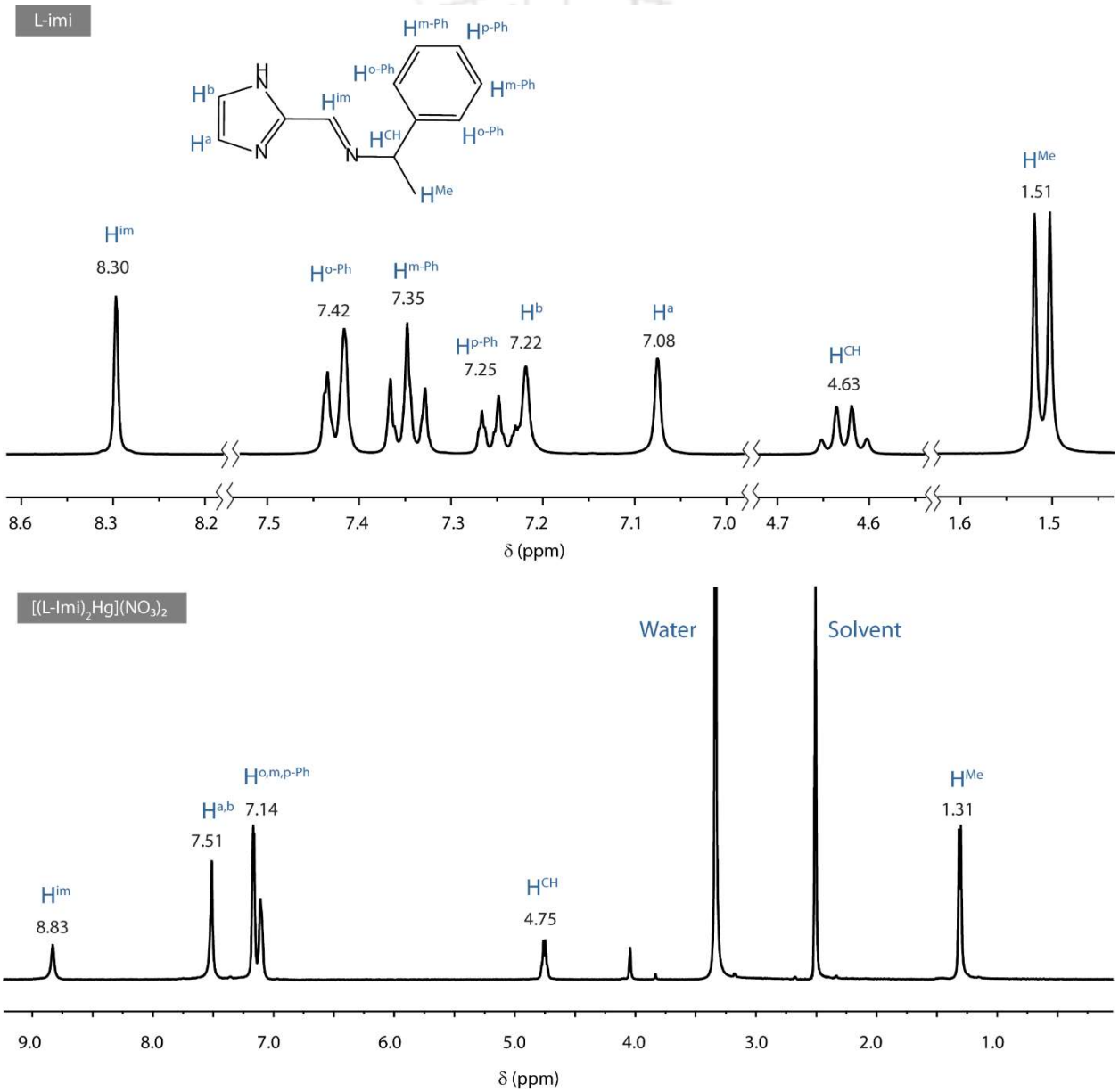

Figure 4.1. ^{1}H NMR spectra of ligand, L-imi, and its Hg^{2+} complex in d_6-DMSO.

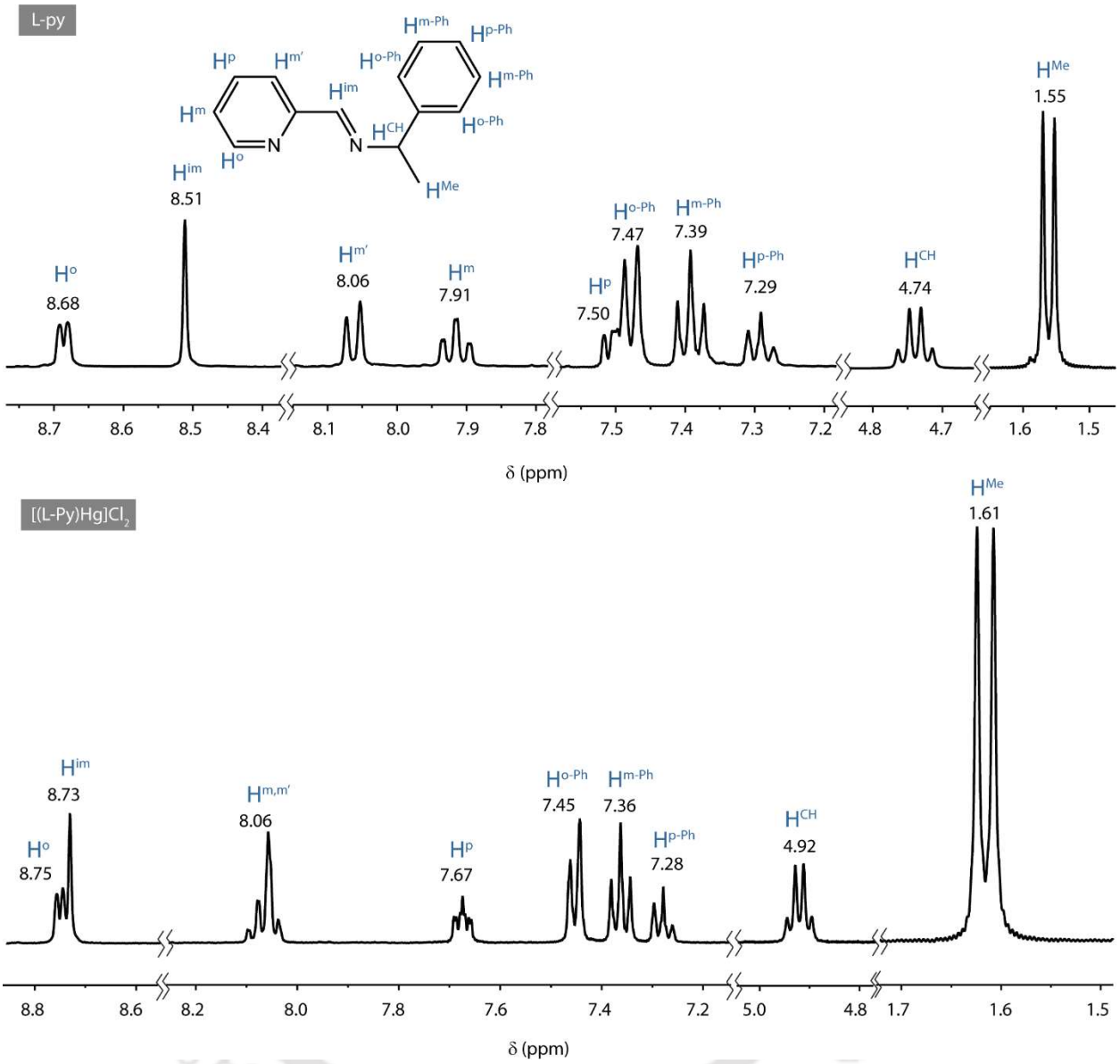

Figure 4.2. ^{1}H NMR spectra of ligand, L-py, and its Hg^{2+} complex in d_6-DMSO.

The protons of these heterocyclic rings were assigned from the corresponding chemical shift and proton-proton coupling constant values. For the Hg(II) complexes of L-imi and L-py, the assignments were done from those of the free ligands' chemical shifts and coupling constants. With the thiophene-derived ligand, L-thio, the complexation reaction with Hg^{2+} ended up with colorless crystal whose ^{1}H NMR spectra differed from that of the free L-thio ligand where peaks corresponding to the thiophene rings were missing (Figure 4.3).

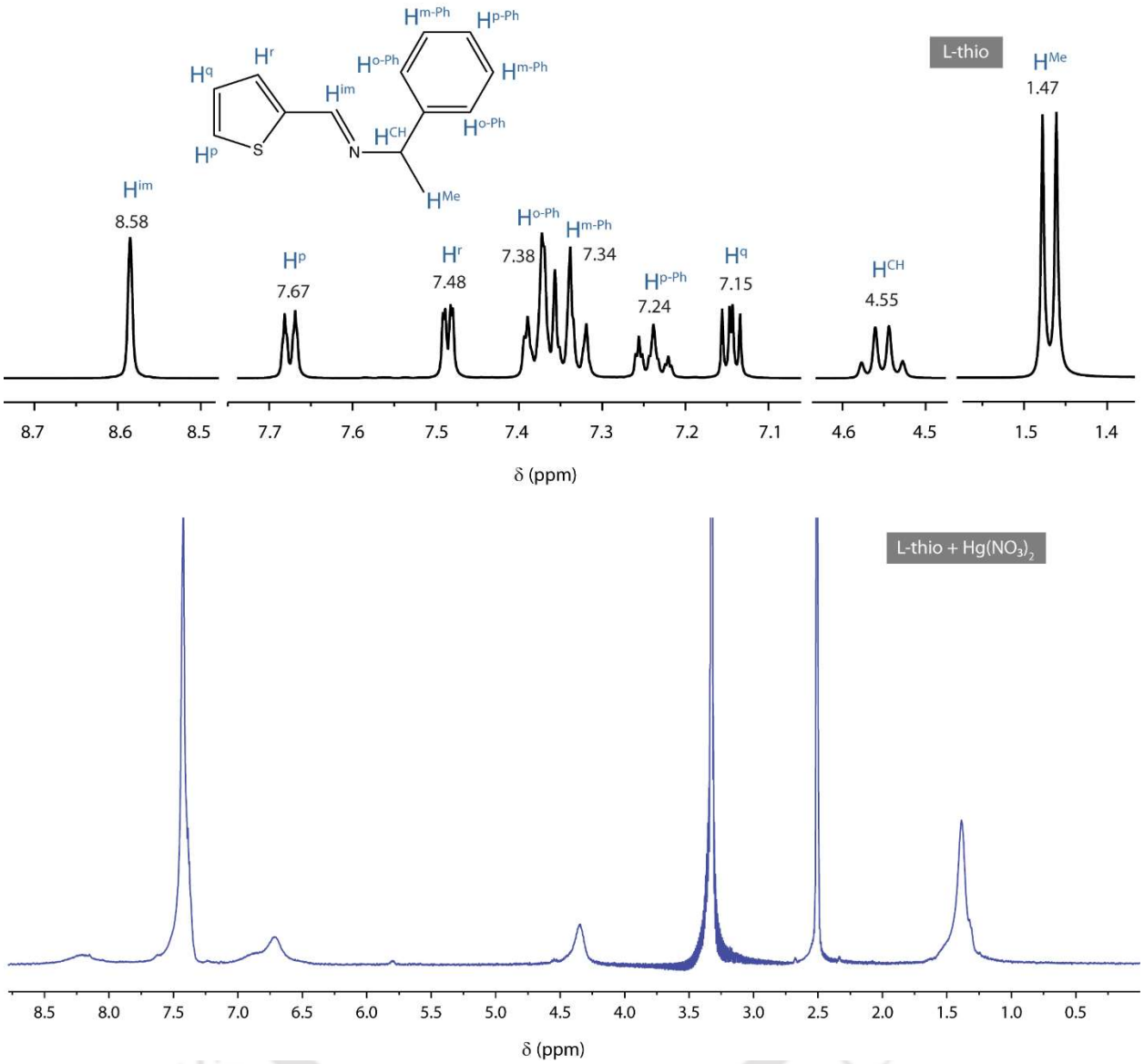

Figure 4.3. ^{1}H NMR spectra of ligand, L-thio, the product (complex **3**) of reaction L-thio and $Hg(NO_3)_2$ in d_6-DMSO.

Now, positive coordination-induced shifts (CIS) were observed with Hg^{2+} complexes of L-imi and L-py (Table 4.1). Positive CISs (complexed free) refer to the downfield shift of the corresponding protons. The maximum positive shifts were observed for the protons of the heterocyclic ring of imidazole, followed by the pyridine ring. Withdrawal of electron density from the nitrogen via -donation is the main reason that is responsible for the

deshielding effect. This effect spreads over the heterocyclic ring through the sigma bond (inductive effect) and pi bonding (resonance effect) predominant in the position. Positive CIS values of the imidazole, pyridine ring protons and the corresponding ligand's imine protons confirmed the coordination of Hg(II) with the ligands through N-N donor sites.

4.3.3. ESI Mass analysis

Mass spectra of the ligands, their Hg(II) complexes were recorded using the electrospray ionization technique (ESI-Mass). The ligands easily accept protons, hence positive ion mode was used. The spectra are shown in Figures 4.4-4.5.

ESI mass spectra of the Complex **1** showed molecular ion peak for monocationic form of the corresponding bis-complexes at 599.198 (calculated for $[Hg(L\text{-}imi)_2\text{-}H]^+$, 599.185). A comparison of the experimental and simulated fragmentation patterned is shown in the inset of Figure 4.4a, which confirmed the formation of the bis-complex, $[Hg(L\text{-}imi)_2](NO_3)_2$. The mass spectra of complex **2a** showed a molecular ion peak at 684.192 (calculated for $[Hg(L\text{-}py)_2{+}NO_3]^+$, 684.069)., along with the bis-complex, the spectrum showed the molecular ion peak for the monocationic mono-complex of Hg^{2+} with L-py at 457.086 and 474.069 (calculated for $[Hg(L\text{-}py){+}HCOO]^+$, 457.079 and $[Hg(L\text{-}py){+}NO_3]^+$, 474.069). We found a molecular ion peak for the bis-complex of L-py with Ag(I), $[Ag(L\text{-}py)_2]^+$ at 527.139 in the mass spectra of complex **2a**. These peaks were absent in the mass spectra of complex **1**. In all the above cases of Hg^{2+} and Ag^+ bis-complexes of L-py, the fragmentation patterns matched well exactly with the simulated ones as shown in the inset of Figure 4.4b. ESI mass spectra of complex **2b** showed molecular ion peak for $[Hg(L\text{-}py)]Cl^-$ at 447.050. No other significant peaks, as in the case of complex **2a,** were observed in the mass spectra of complex **2b**.

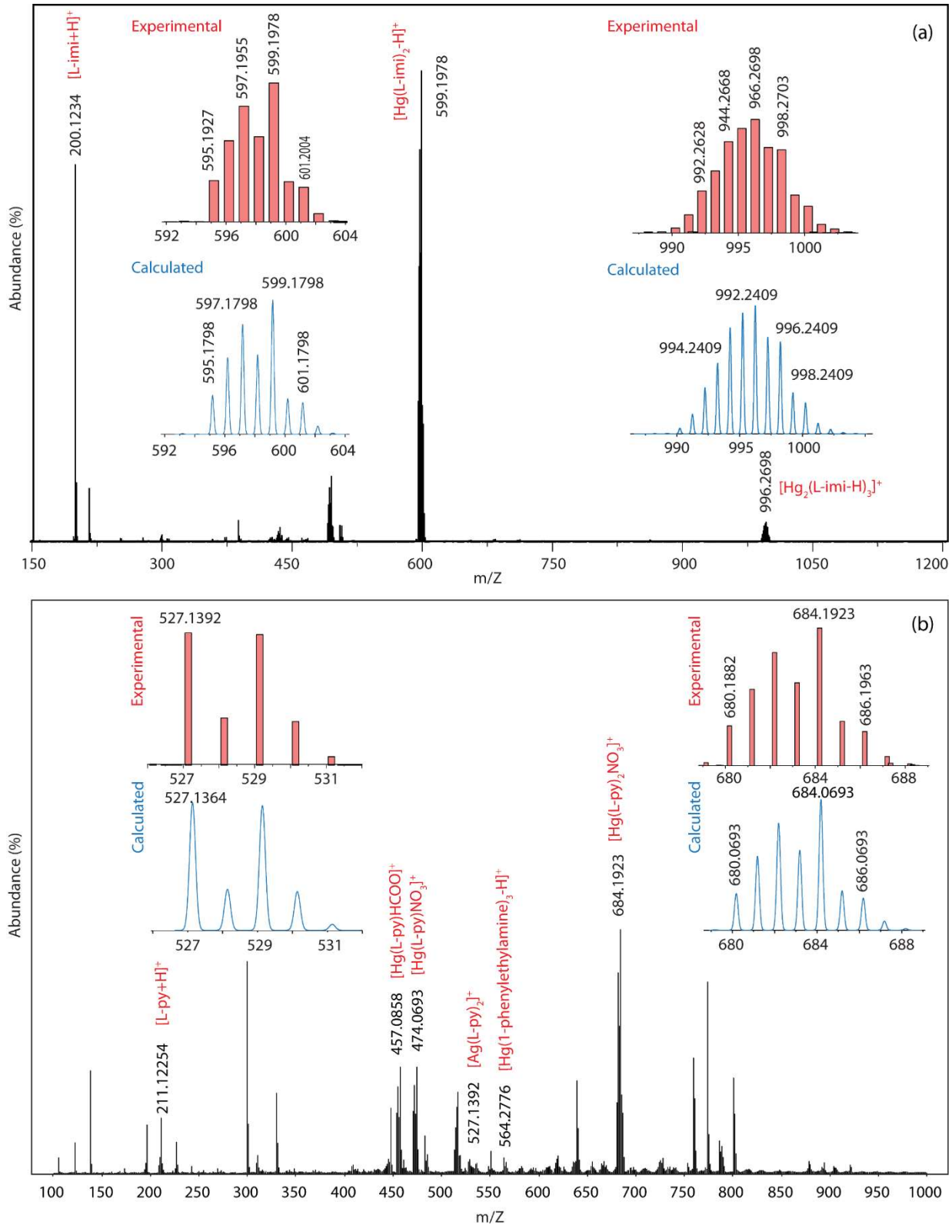

Figure 4.4. ESI-MS spectrum for positive ions of complex **1** and **2a** along with the comparison of molecular ion peaks among experimental isotopic pattern and its calculated isotopic pattern.

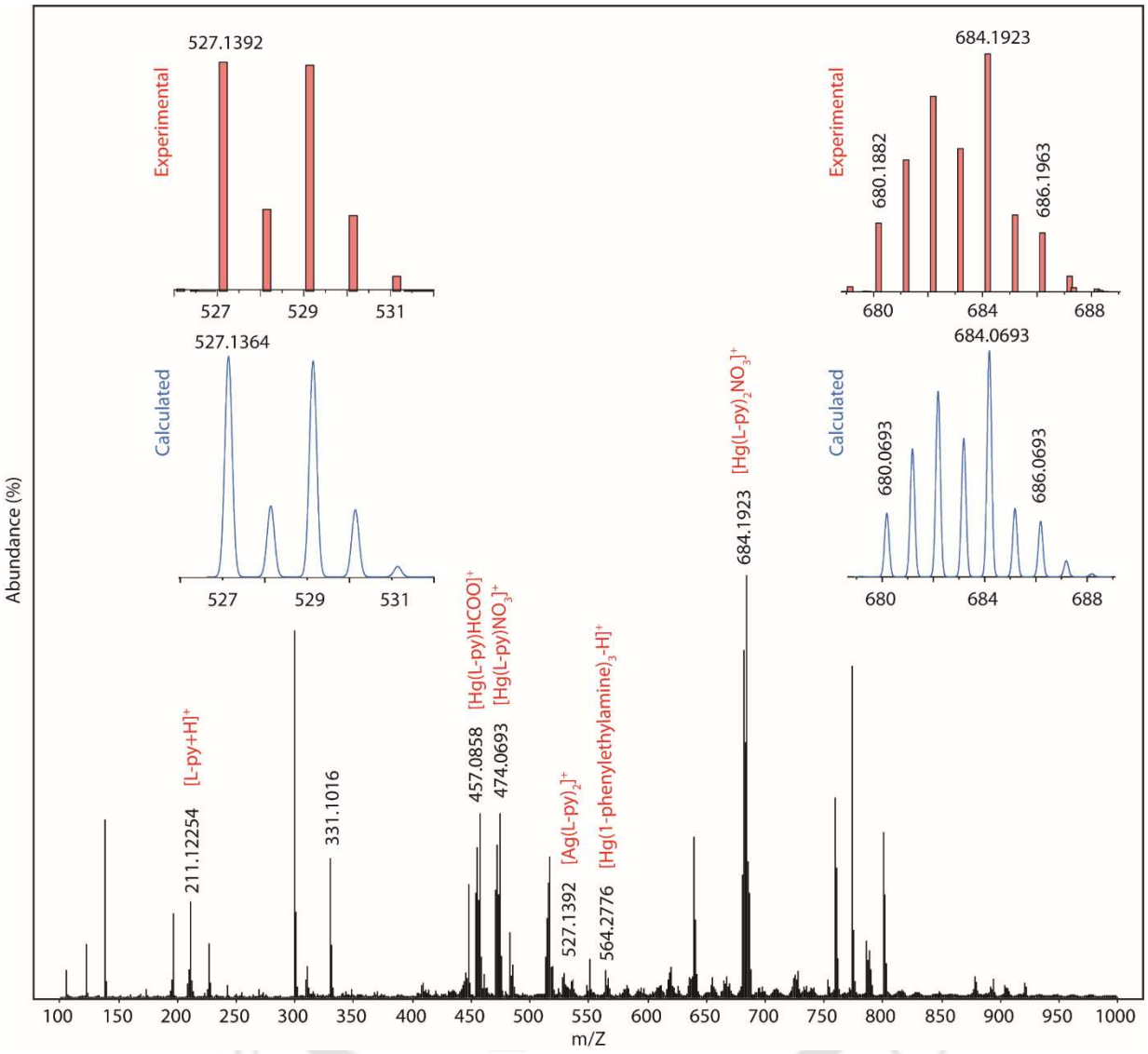

Figure 4.5. ESI-MS spectrum for positive ions of 2a along with the comparison of molecular ion peaks among experimental isotopic pattern and its calculated isotopic pattern.

The ESI mass spectra of complex **3** (product of the reaction between L-thio and Hg^{2+}) did not reveal any peak corresponding to the Hg^{2+} complex of L-thio. Instead, it showed peaks corresponding to the monocationic bis-complex of the starting amine, $[Hg(1\text{-phenylethylamine})_2\text{-H}]^+$ at 434.0814 (calculated m/Z, 434.141) and monocationic mono and bis-complex of L-thio with Ag^+ at 321.987 and 539.087 (calculated for $[Ag(\text{L-thio})]^+$, 321.982 and $[Ag(\text{L-thio})_2]^+$, 539.058). The fragmentation pattern of those peaks matched well with

their simulated versions. To understand this, we synthesized two other complexes separately; first, the Hg^{2+} complex of starting amine, 1-phenylethylamine (complex **4**), and second, the Ag^{+} complex of the ligand, L-thio (complex **5**). Comparison of the ^{1}H NMR spectra of the product of reaction 3 and complex **4** showed that the spectra matched exactly (Figure 4.6).

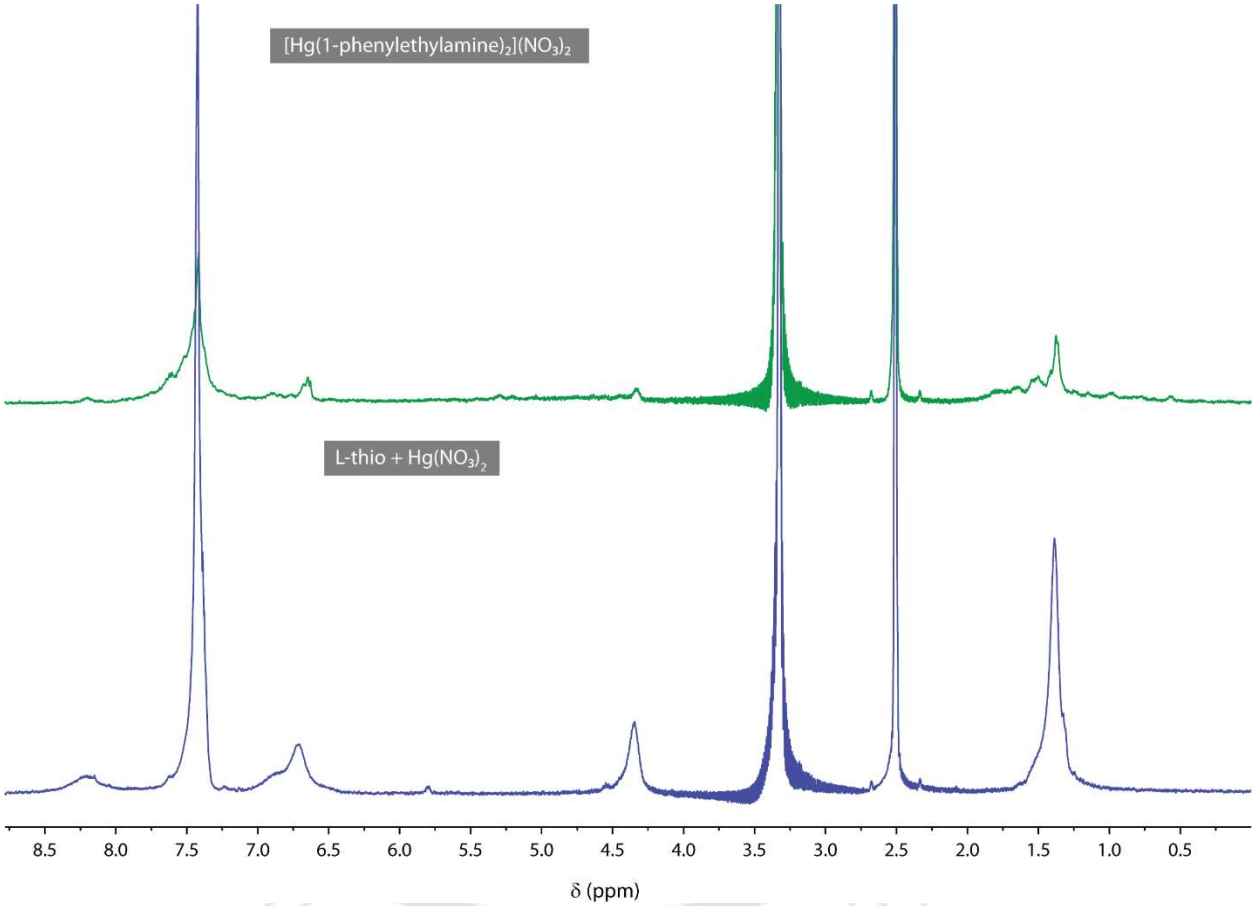

Figure 4.5. ^{1}H NMR spectra of the product (complex **3**) of reaction L-thio and $Hg(NO_3)_2$ and complex **4** in d_6-DMSO.

This confirmed that the crystalline product of reaction 3 is nothing but the bis-complex of starting 1-phenylethylamine and indicates the ligand (L-thio) hydrolysis. The Proton NMR spectrum of complex **5** is shown in Figure 4.7. The spectrum indicates the coordination of the L-thio ligand with Ag^{+}. Assignments of the protons in the complex were

done comparing the free ligands' chemical shifts and coupling constants. Positive CIS values from the ^{1}H NMR spectra of complex **5** confirmed the strong coordination of Ag^{+} with L-thio (Table 4.1).

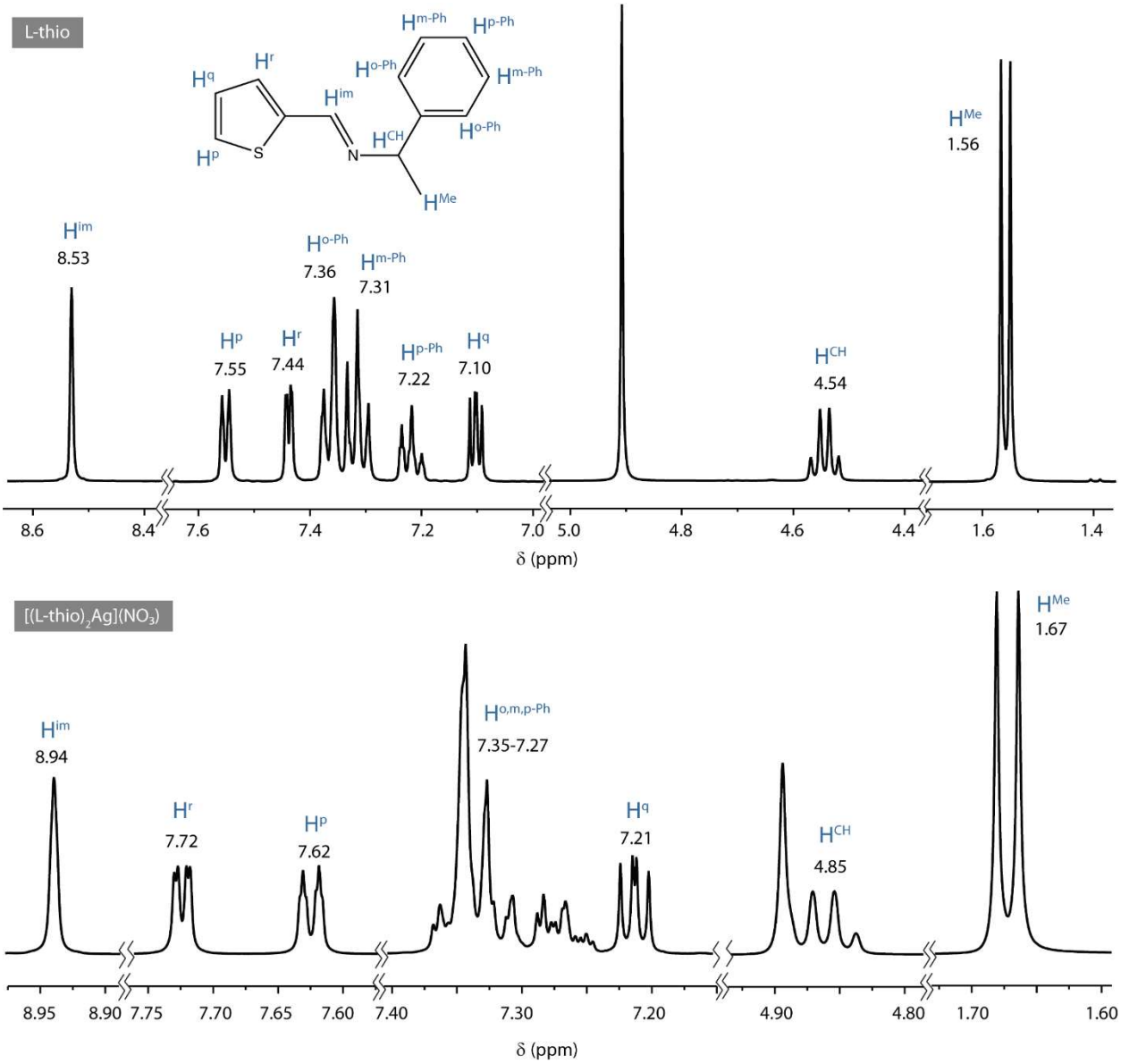

Figure 4.6. ^{1}H NMR spectra of ligand, L-imi, and its Ag^{+} complex in d_4-methanol.

Complex formation with Ag^{+} and formation of amine complex of Hg^{2+} indicates the preference of thioether ligand towards silver instead of mercury. The Ag^{+} in the case of complex **3** might have come from as impurity in the commercial $Hg(NO_3)_2.H_2O$ salt.

Table 4.1. Selected 1H NMR and molecular ion peaks from ESI-mass data of the ligands and complexes

Ligands	**^{1}H NMR**						**ESI-Mass**	**In methanol**	
	H^{im}	**H^{CH}**	**H^a**	**H^b**			M.F.	Found	Calc.
L-imi in d_6-DMSO	8.30	4.63	7.22	7.08			$\{C_{12}H_{13}N_3 + H\}^+$	200.131	200.119
$[Hg(L\text{-}imi)_2](NO_3)_2$ in d_6-DMSO	8.83	4.75	7.51				$\{Hg(C_{12}H_{13}N_3)_2 - H\}^+$	599.198	599.185
CIF	+0.53	+0.12	+0.29	+0.43					
			H^o	**H^m**	**H^p**	**$H^{m'}$**			
L-py in d_6-DMSO	8.51	4.74	8.68	8.06	7.91	7.50	$\{C_{14}H_{14}N_2 + H\}^+$	211.125	211.123
$[Hg(L\text{-}py)]Cl_2$ in d_6-DMSO	8.73	4.92	8.75	8.06	8.06	7.67	$\{Hg(C_{14}H_{14}N_2)Cl\}^+$	447.050	447.049
CIF	+0.22	+0.18	+0.07	0.00	+0.15	+0.17			
			H^p	**H^q**	**H^r**				
L-thio in d_6-DMSO	8.58	4.55	7.67	7.48	7.15		$\{C_{13}H_{13}NS + H\}^+$	216.087	216.085
L-thio $+Hg(NO_3)_2$ in d_6-DMSO		4.35						443.081 539.068	
$[Hg(1\text{-phenylethylamine})_2](NO_3)_2$ in d_6-DMSO		4.35					$\{Hg(C_8H_{11}N)_2 - H\}^+$		443.141
L-thio in d_4-methanol	8.53	4.54	7.55	7.44	7.10		$\{C_{13}H_{13}NS + H\}^+$	216.087	216.085
$Ag(L\text{-}thio)_2$ in d_4-methanol	8.94	4.85	7.62	7.72	7.21		$\{Ag(C_{13}H_{13}NS)_2\}^+$		539.058

4.3.4. Elemental analysis

Elemental analyses of dried samples were done to confirm the molecular composition. The expected and calculated elemental ratios are given in Table 4.2.

Table 4.2. Elemental analysis of the complexes

Complexes	Found (%)				Calculated	Experimental
	C	H	N	S	C:H:N:S	C:H:N:S
1 $[(\text{L-imi})_2\text{Hg}](NO_3)_2$	32.6	3.6	12.6	0	24:26:8:0	24.1:31.7:8:0
2b $[(\text{L-py})\text{Hg}]Cl_2$	35.8	3.8	5.9	0	14:14:4:0	14.2:17.9:2:0
3 L-thio + $Hg(NO_3)_2$	34.2	5.1	9.7	0	26:26:4:2	16.5:29.4:4:0
4 $[(\text{1-Phenylethylamine})_2\text{Hg}](NO_3)_2$	34.8	4.8	10.0	0	16:22:4:0	16.1:26.7:4:0

The result showed that the experimental and calculated C:N:S ratio matched well, except the amount of H came higher. This could probably be due to the hydrogen-bonded water molecules as the metal complexes have a tendency to acquire moisture. The calculated amount of water molecules for complex 1 and 2b is 3 and 2, respectively. The ratio of C:H:N:S found for product 3 obtained from the reaction of L-thio with $Hg(NO_3)_2$ was similar to that of complex 4, confirming the hydrolysis of L-thio in the presence of Hg^{2+} and formation of starting amine complex of Hg^{2+}. Such hydrolysis of Schiff base compound by Hg^{2+} was reported earlier.[15,16]

4.3.5. FTIR of the compounds

Comparison of the FTIR spectra of the ligands and their Hg^{2+} complexes are shown in Figures 4.8 and 4.9. All the monomeric Schiff base ligands showed a characteristic peak at around 1640 cm^{-1} for the C=N stretching of the imine bonds.[17] Shift in the imine (-C=N)

stretching in the Hg^{2+} complexes of L-imi and L-py confirmed the complexation of Hg^{2+} through the imine group (Figure 4.8).

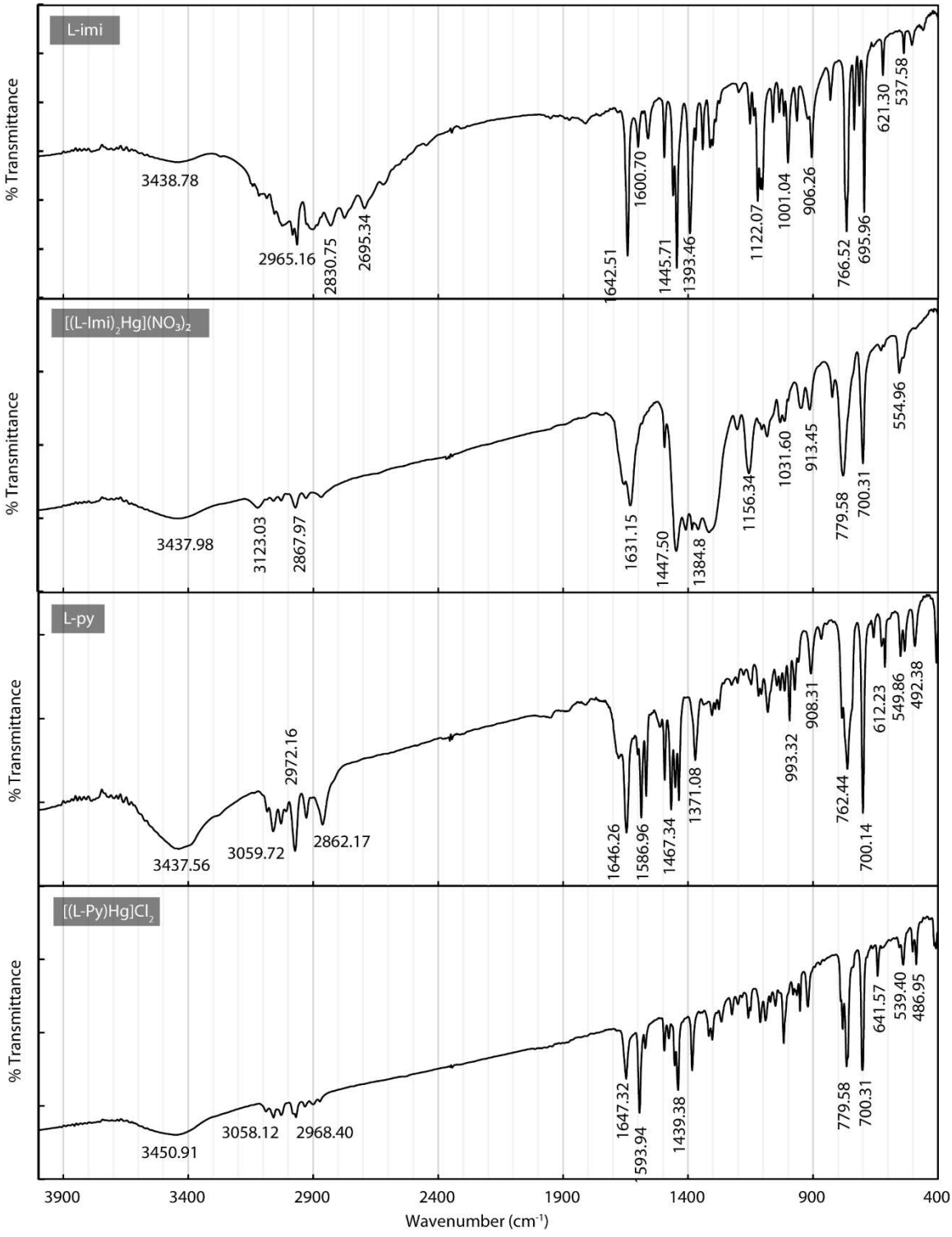

Figure 4.8. FTIR spectra of ligands, L-imi, L-py and their Hg^{2+} complexes, **1** and **2b**.

Hg^{2+} complex of the L-thio ligands showed a broad absorption at 1379 cm^{-1} which is identical with that of the product of reaction 4 along with other identical peaks (Figure 4.9).

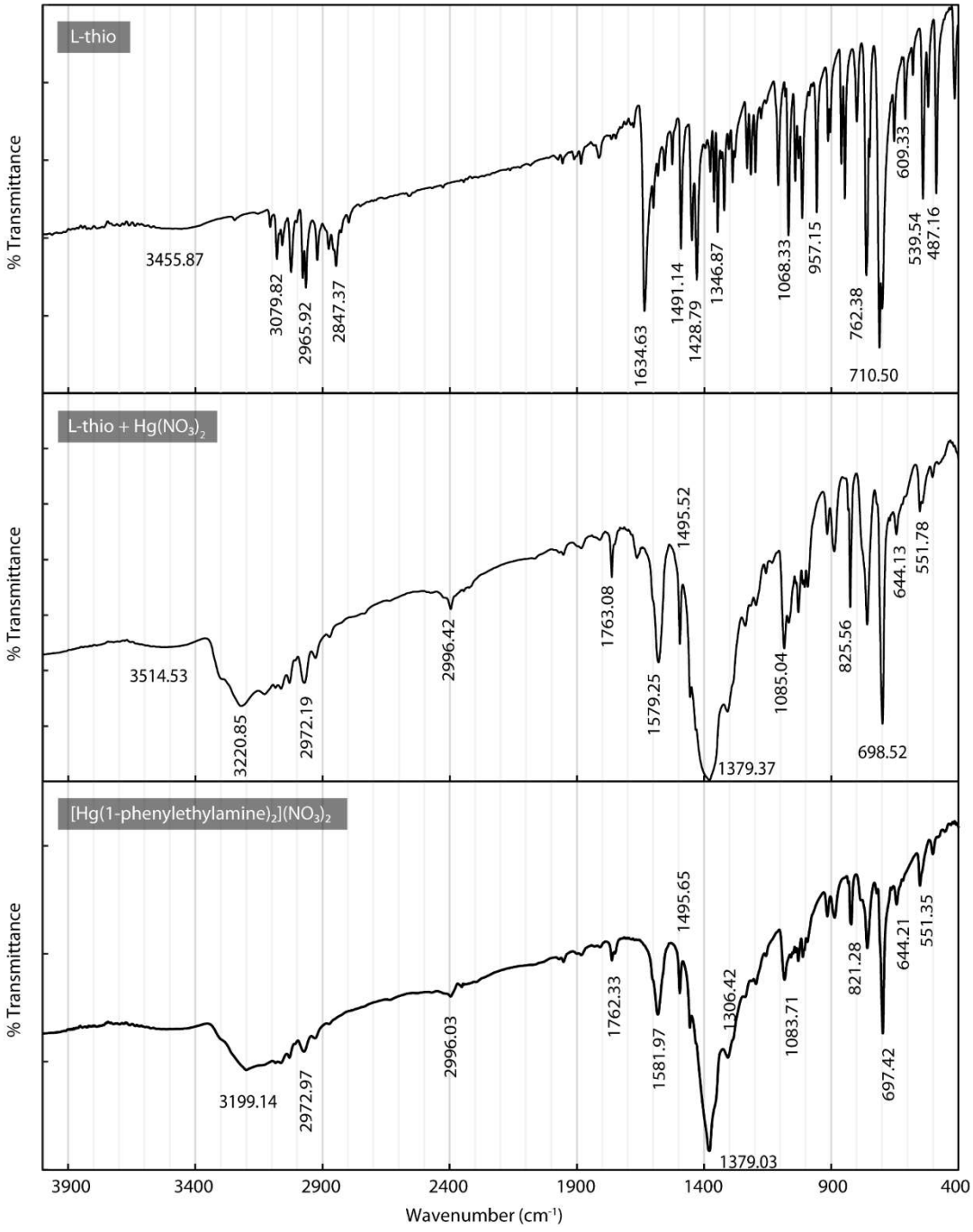

Figure 4.9. FTIR spectra of ligand, L-thio, the product of reaction L-thio and $Hg(NO_3)_2$ and complex **4**.

This result supports the ^{1}H NMR, ESI mass, and elemental percentage obtained from the CHNS analysis. Hg(II) complex of all the ligands showed a characteristic peak at around 550 cm^{-1} which is assigned to the Hg-N stretching vibration.[17]

4.3.6. Molecular structures of the complex 3

Compound **3**, obtained from the reaction of L-thio and $Hg(NO_3)_2$, formed a colorless block-shaped crystal. The X-ray diffraction data showed it crystallized in chiral space group $P2_2$ with one molecule of the cationic complex, two nitrate anions in the asymmetric unit. The final structural parameters are in Table 4.3, and selected bond length and bond angles are in Table 4.4. ORTEP diagram of the complex is shown in Figure 4.10.

Table 4.3. Crystallographic data and refinement parameters of crystal formed in the reaction between L-thio and $Hg(NO_3)_2$ (in 2:1 ratio).[a]

	[Hg(1-Phenylethylamine)$_2$](NO$_3$)$_2$
Empirical formula	C_{16} H_{22} Hg N_4 O_6
FW	566.97
crystal system	Trigonal
space group	$P2_2$
a, A°	6.3399(4)
b, A°	6.3399(4)
c, A°	42.719(3)
a(°)	90
°	90
°	120
V, Å^3	1487.04(16)
Z/ρ (g cm^{-3})	3/1.899
μ (mm^{-1})	7.803
coll.reflns	5044
indep reflns	2522
FLACK para.	0.39(3)

GOF on F^2	1.030
Residuals (e Å^{-3})	1.7057, -3.5278
R1[b], wR2[b]	0.0628/0.1692
R1[c], wR2[c]	0.0760/0.1770

[a]Data collected at 296.15(2) K. [b]I >2σ. [c]All data

Table 4.4. Selected bond distances (Å) and angles (°) of Hg(II) complex of 1-phenylethylamine obtained from reaction 3

Hg1-N1	2.1210(1)	Hg1-N1A	2.0317(1)
O1-N2	1.1753(1)	O4-N3	1.3110(1)
O2-N2	1.2473(1)	O5 -N3	1.1116(1)
O3-N2	1.2681(1)	O6-N3	1.3212(1)
N1-C7	1.5175(1)	N1A-C7A	1.4754(1)
N1-Hg1-N1A	179.24(1)	Hg1-N1A-C7A	119.02(1)
Hg1-N1-C7	115.06(1)	O1-N2-O2	101.50(1)
O1-N2-O3	123.12(1)	O2-N2-O3	116.89(1)
O4-N3-O5	126.54(1)	O4-N3-O6	103.36(1)
O5-N3-O6	130.1(1)		

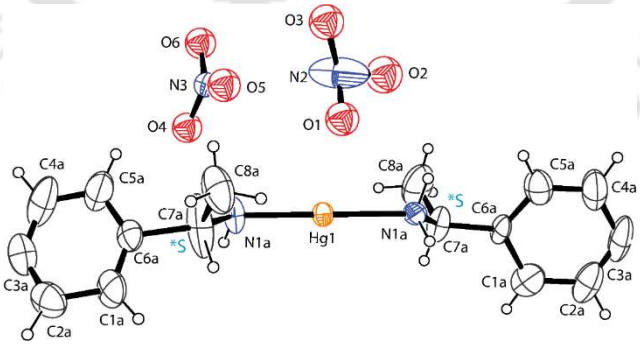

Figure 4.10. The ORTEP diagram (with 30% ellipsoid probability) of the Hg(II) complex of 1-phenylethylamine obtained from reaction 3.

The ORTEP diagram (Figure 4.10) of the cationic complex showed a linear Hg(II) complex of 1-phenylethylamine, which was the starting material for ligand synthesis. The Hg-N (primary amine) bond lengths in the complex are slightly shorter (~2.0-2.1 Å) compared to Hg-N (secondary amine). The crystal contains H-bonded interactions between the amine NH and the nitrate oxygen. Ligand synthesis was done using enantiopure S-(-)-1-phenylethylamine. The two chiral carbon centers of the two ligands have S configuration, further confirmed from the circular dichroism spectra of complex **3** (Figure 4.11).

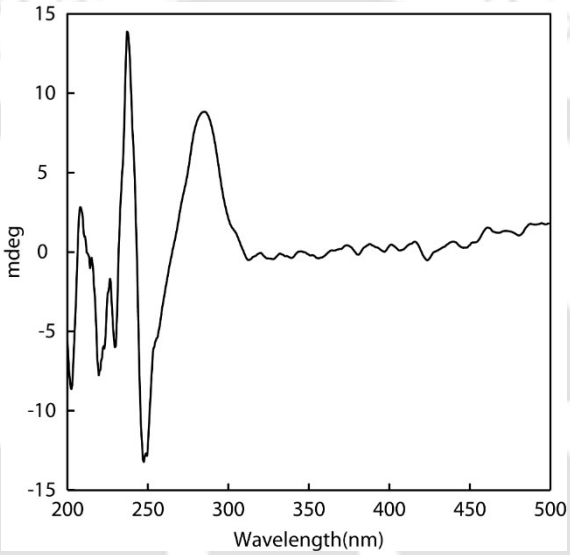

Figure 4.11. Circular dichroism spectra of complex **3**.

The structural data from the X-ray diffraction further confirmed that the thioether ligand, L-thio, hydrolyzed in the presence of Hg^{2+} to give the bis-complex of starting 1-phenylethylamine. It suggests cyclic thioether is a poor ligand for Hg(II), although acyclic thio groups are a potential donor for Hg(II).

4.4. Conclusions

The significant results which emerge from this chapter are the following:

(i) The imidazole and pyridine-based ligands showed complex formation with Hg^{2+} in the ratio of 2:1 (ligand to metal). ESI mass and elemental analysis confirmed the molecular formulation.

(II) Coordination induced shift values calculated from the NMR spectra showed strong coordination of L-imi with Hg^{2+} followed by L-py.

(iii) L-thio, besides being a thioether, did not form any complex with Hg^{2+}. Instead, the ligand hydrolyzed to form bis-complex of the starting amine and a tiny amount of Ag^{+} complex of L-thio. The formation of $[Ag(L\text{-thio})_2]_+$ suggests using the thiophene donor group in Ag^{+} detection or capture.

(iv) This work gives an impetus for the necessary modification of the amine donor sites with potential ligand for better Hg(II) complexation.

4.5. Bibliography

(1) Kim, K.-H.; Kabir, E.; Jahan, S. A. A Review on the Distribution of Hg in the Environment and Its Human Health Impacts. *J. Hazard. Mater.* **2016**, *306*, 376–385. https://doi.org/https://doi.org/10.1016/j.jhazmat.2015.11.031.

(2) Risher, J.; DeWoskin, R. Report: Toxicological Profile for Mercury. *U.S. Dep. Heal. Hum. Serv. Public Heal. Serv. Agency Toxic Subst. Dis. Regist.* **1999**, No. March, 1–676.

(3) Tripathi, S.; Bardhan, D.; Chand, D. K. Multistimuli-Responsive Hydrolytically Stable "Smart" Mercury(II) Coordination Polymer. *Inorg. Chem.* **2018**, *57* (18), 11369–11381. https://doi.org/10.1021/acs.inorgchem.8b00964.

(4) Wang, X.-F.; Lv, Y.; Okamura, T.; Kawaguchi, H.; Wu, G.; Sun, W.-Y.; Ueyama, N. Structure Variation of Mercury(II) Halide Complexes with Different Imidazole-Containing Ligands. *Cryst. Growth Des.* **2007**, *7* (6), 1125–1133. https://doi.org/10.1021/cg060814c.

(5) Skyllberg, U.; Bloom, P. R.; Qian, J.; Lin, C.-M.; Bleam, W. F. Complexation of Mercury(II) in Soil Organic Matter: EXAFS Evidence for Linear Two-Coordination with Reduced Sulfur Groups. *Environ. Sci. Technol.* **2006**, *40* (13), 4174–4180. https://doi.org/10.1021/es0600577.

(6) Govindaswamy, N.; Moy, J.; Millar, M.; Koch, S. A. A Distorted Mercury [Hg(SR)4]2- Complex with Alkanethiolate Ligands: The Fictile Coordination Sphere of Monomeric [Hg(SR)x] Complexes. *Inorg. Chem.* **1992**, *31* (26), 5343–5344. https://doi.org/10.1021/ic00052a001.

(7) Bebout, D. C.; DeLanoy, A. E.; Ehmann, D. E.; Kastner, M. E.; Parrish, D. A.; Butcher, R. J. Characterization of Mercury(II) Complexes of Bis[(2-Pyridyl)Methyl]Amine by X-Ray Crystallography and NMR Spectroscopy. *Inorg. Chem.* **1998**, *37* (12), 2952–2959. https://doi.org/10.1021/ic971499+.

(8) Bjørklund, G.; Crisponi, G.; Nurchi, V. M.; Cappai, R.; Buha Djordjevic, A.; Aaseth, J. A Review on Coordination Properties of Thiol-Containing Chelating Agents Towards Mercury, Cadmium, and Lead. *Molecules* . 2019. https://doi.org/10.3390/molecules24183247.

(9) Narasimhan, B.; Sharma, D.; Kumar, P. Biological Importance of Imidazole Nucleus in the New Millennium. *Med. Chem. Res.* **2011**, *20* (8), 1119–1140. https://doi.org/10.1007/s00044-010-9472-5.

(10) Pandey, Y. H. E.-P. P. Role of Pyridines in Medicinal Chemistry and Design of BACE1 Inhibitors Possessing a Pyridine Scaffold; IntechOpen: Rijeka, 2018; p Ch. 2. https://doi.org/10.5772/intechopen.74719.

(11) Bhattacharya, S.; Ray, M. Chiral Resolution of 1-Phenylethylamine in Schiff Base Form within a Mixed Ligand Complex of Ni(II). *Inorganica Chim. Acta* **2020**, *502*, 119338. https://doi.org/https://doi.org/10.1016/j.ica.2019.119338.

(12) Bruker, A. X. S. Apex2, Saint and Sadabs. *Bruker AXS Inc., Madison* **2009**.

(13) Sheldrick, G. M. SHELXT - Integrated Space-Group and Crystal-Structure Determination. *Acta Crystallogr. Sect. A Found. Crystallogr.* **2015**, *71* (1), 3–8. https://doi.org/10.1107/S2053273314026370.

(14) Dolomanov, O. V; Bourhis, L. J.; Gildea, R. J.; Howard, J. A. K.; Puschmann, H. OLEX2: A Complete Structure Solution, Refinement and Analysis Program. *J. Appl. Crystallogr.* **2009**, *42* (2), 339–341.

(15) Kumar, A.; Dubey, M.; Pandey, R.; Gupta, R. K.; Kumar, A.; Kalita, A. C.; Pandey, D. S. A Schiff Base and Its Copper(II) Complex as a Highly Selective Chemodosimeter for Mercury(II) Involving Preferential Hydrolysis of Aldimine over an Ester Group. *Inorg. Chem.* **2014**, *53* (10), 4944–4955. https://doi.org/10.1021/ic403149b.

(16) Tekuri, V.; Sahoo, S. K.; Trivedi, D. R. Hg2+ Induced Hydrolysis of Thiazole Amine Based Schiff Base: Colorimetric and Fluorogenic Chemodosimeter for Hg2+ Ions in an Aqueous Medium. *Spectrochim. Acta Part A Mol. Biomol. Spectrosc.* **2019**, *218*, 19–26. https://doi.org/https://doi.org/10.1016/j.saa.2019.03.106.

(17) Fleming, I.; Williams, D. Infrared and Raman Spectra BT - Spectroscopic Methods in Organic Chemistry; Fleming, I., Williams, D., Eds.; Springer International Publishing: Cham, 2019; pp 85–121. https://doi.org/10.1007/978-3-030-18252-6_3.

Chapter 5

Effect of functionalization of Chitosan, a biological macromolecule with thiophene, pyridine, and imidazole derived groups on its Hg(II) uptake

5.1. Introduction

Materials capable of binding and thus removing mercury from aqueous solution is an active research area due to the hazardous nature of mercury salts.[1–5] The preferential binding of mercury with sulfur-containing donor groups is well known.[6–11] As a result, a significant number of materials that are effective towards mercury incorporate some forms of sulfur as the donor. Other donor groups such as imidazole, a part of histidine amino acid in proteins, are less often used. In the previous chapter, we studied the complexation of mercury with three ligands having different donors, namely imidazole, pyridine, and thiophene. The imidazole donor set worked best among the three. Characterization data on the complexes helped us understand the underlying chemistry of mercury bonding in those ligand structures.

By nature, adsorbents have to be insoluble, limiting the understanding of chemical bonds between the materials and the mercury as not all spectroscopy support characterization in an insoluble form. In this chapter, we have made similar functionalization in a polymer system named chitosan. Chitosan is a natural polysaccharide obtained by partial deacetylation of chitin. It is one of the most abundant polysaccharides in nature, like cellulose.[12,13] It is a linear copolymer composed of N-acetylglucosamine units and glucosamine units. The main difference between cellulose and chitosan is one amino group at the C-2 position instead of the hydroxyl group. Due to the presence of this amine group (high % of nitrogen), as amine groups can be easily functionalized, chitosan is of high commercial interest.[14–16] Most of the presently used materials are synthetic materials that lack biocompatibility and biodegradability. Because of Chitosan's biocompatibility, biodegradation property, and non-toxicity, it has been used in many industries, e.g., food processing, cosmetics, catalysis, water management, wound healing, drug delivery, etc.[12,15] However, naturally found non-functionalized chitosan polymers exhibit some limitations in

practical usage.[13,15] We functionalized chitosan's amine group into imidazole, pyridine, and thiophene-based chelate ligands (Scheme 5.1) and applied them in removing Hg(II) from aqueous solution. We used Hg(II) complexation knowledge with those donor sites from the previous chapter here on a polymer. This method of parallel study is simple enough to implement and can lead to more efficient adsorbents in other areas as well.

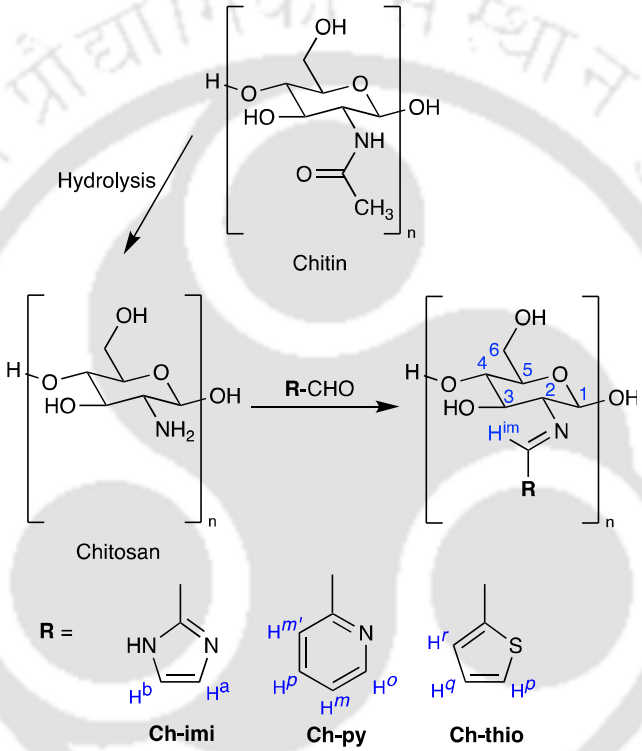

Scheme 5.1. Molecular diagram of chitin, chitosan, and three chitosan derivatives along with proton numbering scheme.

5.2. Experimental Section

5.2.1. Materials and Methods

Solvents and acids were obtained from Merck India and used without further purifications unless otherwise stated. Chitosan-low-molecular weight, 2-pyridinecarboxaldehyde, 2-imidazolecarboxaldehyde, and 2-thiophenecarboxaldehyde were

purchased from Sigma Aldrich Chemical Co. and used as received. Mercuric nitrate [$Hg(NO_3)_2.H_2O$] was purchased from HiMedia and used as received. Water purified by Merck Direct Q8 ultrapure water purification system was used to prepare all solutions and reactions. Whatman® grade 1 qualitative filter paper was used for filtration purposes during adsorption experiments.

5.2.2. Measurements

The FTIR spectra were recorded on PerkinElmer Spectrum One FT-IR spectrophotometer with KBr discs in the range 4000-400 cm^{-1}. Ionization mass (ESI-MS) recorded on an AGILENT Q-TOF 6520 High-Resolution Mass Spectrometer. For ESI-MS measurements of the polymeric chitosan derivative compounds: samples were dissolved in 2 ml of distilled water in the presence of 10 µL of concentrated HNO_3. The solution was filtered through a 0.2-micron membrane filter before the measurement. Proton NMR spectra were recorded using Bruker 400 MHz instruments. Samples of the polymeric chitosan derivative compounds for NMR were prepared in appropriate 0.7mL D_2O using 10 µL of concentrated HNO_3. Elemental analysis was carried out on the Eurovector EA3000 CHNS analyzer at Guwahati Biotech Park. The materials' surface morphology and chemical characterization were studied by Gemini Field Emission Scanning Electron Microscope (FESEM) equipped with an energy-dispersive X-ray spectrometer. The polymeric materials were first dispersed in ethanol, drop cast on a silver foil to get a thinner layer of the polymer surface, and air-dried in a desiccator over silica. Prior to analysis, it was mounted with the help of carbon tape on the stabs, coated with gold vapor twice before measurement to reduce charging. Mercury concentration was analyzed using an Atomic Absorption spectrometer (model-AA240, Varian); flame ionization technique (Flame AAS) with a wavelength of 253.7nm, slit width of 0.5nm, optimum working range between 2-400 mg/L. For all experiments and reagents preparation, Milli-Q deionized water was used. All pH

measurements were done using Eutech instruments' EcoScan pH 6 pH-meter. Chloride ion concentration in the solutions after pH adjustment was measured using Thermo Scientific™ Orion™ Chloride Electrodes.

5.2.3. Syntheses

The ligands L-imi and L-py (Scheme 2) were synthesized following a reported procedure.[17]

5.2.3.1. ((1H-imidazol-2-yl)methylene)amino-chitosan (Ch-imi). Low molecular weight chitosan (0.500 g, 3.12 mmol) was stirred in 10 mL ethanol. A solution of 2-imidazolecarboxaldehyde (0.300 g, 3.12 mmol) in 10 mL ethanol was added dropwise to the first mixture. The whole mixture was then subjected to reflux for 6 hours. The mixture turned yellowish. It was filtered, washed with ethanol, kept in a vacuum desiccator. The chitosan Schiff base material is an insoluble solid; hence, it was made soluble in water in the presence of acid before the NMR and mass analysis experiments. Yield. 0.9 g. FTIR (KBr, cm^{-1}): $\upsilon(C{=}N)_{stretch}$ 1655(s). ^1H NMR (400 MHz, $D_2O{+}HNO_3$, ppm): 6.27 (H^{imi}, s, 1H), 7.44 ($H^{a,b}$, s, 2H), 3.19 (H^2, s, 1H), 3.72-3.90 ($H^{1,\ 3\text{-}6}$, br, 5H), 2.06 (H^{Me}, s). ESI-MS ($[C_{10}H_{15}N_3O_4 + H]^+$): calculated 242.11; found 242.14.

5.2.3.2. ((pyridin-2-yl)methylene)amino-chitosan (Ch-py). This was prepared following the same procedure as Ch-imi using 2-pyridinecarboxaldehyde instead of 2-imidazolecarboxaldehyde. Yield. 0.71 g. FTIR (KBr, cm^{-1}): $\upsilon(C{=}N)_{stretch}$ 1649(s). ^1H NMR (400 MHz, $D_2O{+}$ HNO_3, ppm): 6.27 (H^{imi}, s, 1H), 8.69 (H^o, d, 1H, J = 5.6Hz), 8.61 (H^p, t, 1H, J = 8Hz), 8.14 ($H^{m'}$, d, 1H, J = 8Hz), 8.01 (H^m, t, 1H, J=5.6), 3.14 (H^2, s, 1H), 3.66-3.85 ($H^{1,\ 3\text{-}6}$, br, 5H), 2.01 (H^{Me}, s). ESI-MS ($[C_{24}H_{29}N_4O_8 + H]^+$): calculated 502.21; found 502.22.

5.2.3.3. ((thiophen-2-yl)methylene)amino-glucosamine (Ch-thio). This was prepared following the same procedure as Ch-imi using 2-thiophenecarboxaldehyde instead of 2-imidazolecarboxaldehyde. Yield. 0.502g. FTIR (KBr, cm^{-1}): $\upsilon(C{=}N)_{stretch}$ 1629(s). ^1H

NMR (400 MHz, D_2O+HNO_3, ppm): 7.33 (H^{imi}, s, 1H), 9.84 (H^{p}, s, 1H), 8.03 ($H^{q,r}$, s, 2H), 3.19 (H^{2}, s, 1H), 3.72-3.90 ($H^{1, 3-6}$, br, 5H), 2.06 (H^{Me}, s). ESI-MS ($[C_{27}H_{40}N_3O_{14}S+H]^+$): calculated 663.23; found 663.30.

5.2.4. Adsorption experiments

Mercury adsorption experiments were done at room temperature. At first, a stock solution of Hg(II) of 1000 mg/L was prepared using the required amount of $Hg(NO_3)_2.H_2O$ salt in the presence of 300 µL of concentrated nitric acid. This was diluted with Milli-Q water to get the required concentration of Hg(II) solution ranging from 50 to 200 mg/L. The pH of these solutions was adjusted at the desired value by 1N HCl/NaOH solutions. Before the adsorbent addition and after the adsorption experiment, the pH of all the solutions was measured and noted. We did the adsorption experiments at three different pH values with three different initial Hg(II) concentrations and a fixed adsorbent dose. We used 0.15 mg of our material in 15 mL of Hg(II) solution, adjusted the pH of the solutions by dropwise addition of either 1(N) NaOH or 1(N) HCl solution. Adsorption experiment was performed in an orbital shaker (300rpm) for 3hours. We did Hg(II) adsorption experiments at a single dose of 1 g/L at three different pH and with three different initial concentrations. The amount of mercury adsorbed on the material was obtained by the following equation.

$$q_t = \frac{C_0 - C_t}{m} V \qquad 5.1$$

Here,

q_t = amount of Hg(II) adsorbed per gram of the material at time t (mg/g)

C_0 = initial concentration

C_t = concentration at time t.

V = volume of the solution (L); and

m = mass of the adsorbent (g).

The removal percentage of mercury ion was calculated using the following equation.

$$\text{Removal } (\%) = \frac{C_0 - C_t}{C_0} \times 100 \qquad 5.2$$

5.3. Results and Discussion

5.3.1. Syntheses

Polymeric Schiff base materials were synthesized by condensation between the corresponding aldehydes and chitosan in ethanol under reflux conditions (Scheme 5.1). Mixing aldehyde with chitosan did not immediately change the color of chitosan. The color changed to darker brownish on heating. The reaction introduced an imine functional group at the C-2 position of the chitosan polysaccharide ring. All the modified chitosan Schiff bases are soluble in an acidic aqueous solution. ^{1}H NMR and ESI mass analysis of the chitosan polymers were performed with soluble samples in an acidic aqueous solution.

5.3.2. FTIR of the compounds

The FTIR spectra of the chitosan Schiff base compounds before and are shown in Figure 5.1. Among the typical vibrations of chitosan, the broad band around 3430 cm^{-1} indicates –OH/–NH stretching, intermolecular hydrogen bonding. The peak at 2919 cm^{-1} corresponds to the symmetric stretching vibration of $–CH_2$ in the pyranose ring, 1651 cm^{-1} corresponds to the -C=O stretching vibration in the amide group and 1593 cm^{-1} corresponds to the $–NH_2$ bending vibration.[13,18] The FTIR spectra of the polymeric chitosan Schiff base ligands other than the vibrations as mentioned above exhibited a sharp peak at 1640-1650 cm^{-1} corresponding to the (C=N) stretching mode of the imine bonds.[18] After Hg(II) adsorption, the polymeric materials showed a sharp peak at around 550 cm^{-1}, which is due to the Hg(II)-

N bond formation after the adsorption. Further assignments of the other peaks are given in Table 5.1.

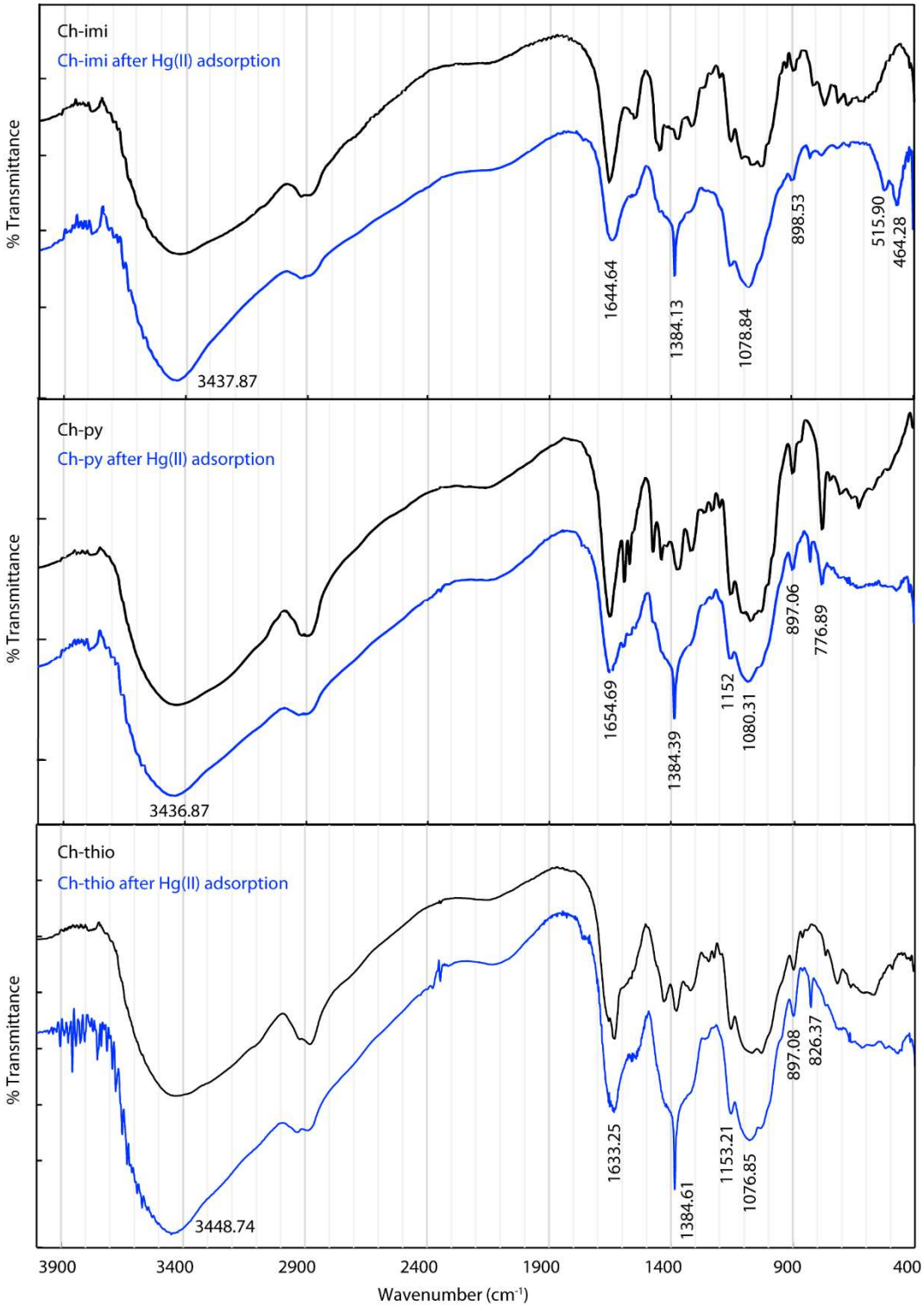

Figure 5.1. FTIR spectra of Ch-imi before and after Hg(II) adsorption.

Table 5.1. IR frequencies for Chitosan and Chitosan materials

Groups	Chitosan	Ch-imi	Ch-py	Chi-thio
-OH/-NH stretching	3436	3427	3436	3373
-C-H stretching	2919	2921, 2883	2900	2870
-C=O of amide	1651		-	
-C=N stretching	-	1655	1649	1629
-N-H bending	1593, 1561	1549	1592, 1570	
>C-H deformation	-	1446	1472	
$-CH_3$ sym deformation, -C-N-stretching	1383	1375	1374	1369
$-NO_3^-$ sharp	-	-	-	
-OH bending	1318	1316	1314	
-C-O stretching	1076, 1034	-	1071, 1024	1022
-C-O-C- asym stretching	1114	1124	1116	
CH bending out of the plane of the ring of monosaccharides	898	896	898	
Aromatic Pyridine ring C-H stretching	-	-	777	
C-H out-of-plane-bending of Imidazole ring	-	767	-	
C-H out-of-plane-bending of Thiophene ring				715

5.3.3. NMR analysis

The functionalized chitosan materials are insoluble in any solvent; hence proton and ^{1}H-^{1}H correlation spectrum (COSY) NMR experiments were recorded in acidic D_2O solution. Both Schiff-bases and the heterocyclic rings can be protonated in an aqueous medium and give the ternary and secondary amines. Hence, these ^{1}H NMR spectra are rather of the protonated form of the Schiff bases.

From the ^{1}H NMR analysis, the chemical shifts of the H atoms of chitosan are located within the range of 2.00 to 4 ppm. The peaks for the chitosan carbohydrate ring protons were assigned following a reported procedure.[19–21]

The chemical shifts of the H atoms of the imidazole, pyridine, and thiophene ring are located within the range of 7–9 ppm. The successful conjugation of the heterocyclic moiety to the chitosan backbone is evident from the chemical shift at around 6.30 ppm. The imine proton peak here came at an upfield position. This was compared with the spectra of ligand, L-imi synthesized in acidic D_2O. Proton NMR spectra of L-imi in acidic D_2O showed a singlet peak at ~6.3. In the COSY spectrum of L-imi in acidic D_2O, the peak at ~6.3 did not show any correlation with other protons, which is also evident in the COSY spectra of Ch-imi. This confirmed the assignment of the imine proton peak. The protons of the heterocyclic rings were assigned from the corresponding chemical shift and proton-proton coupling constant values. The ^{1}H NMR and COSY spectra of the functionalized materials are given in Figure 5.2-5.6. Some selected assignments of the Schiff base materials are given in Table 5.2.

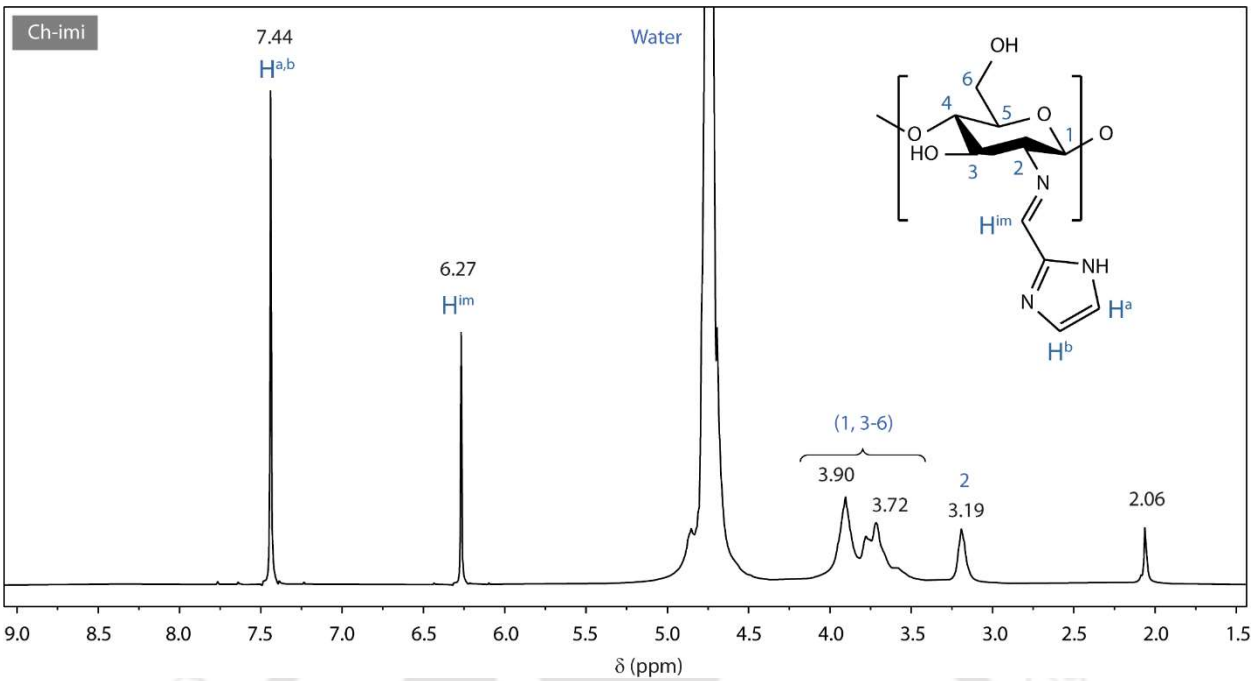

Figure 5.2. ^{1}H NMR spectra of Ch-imi in acidic D_2O solution.

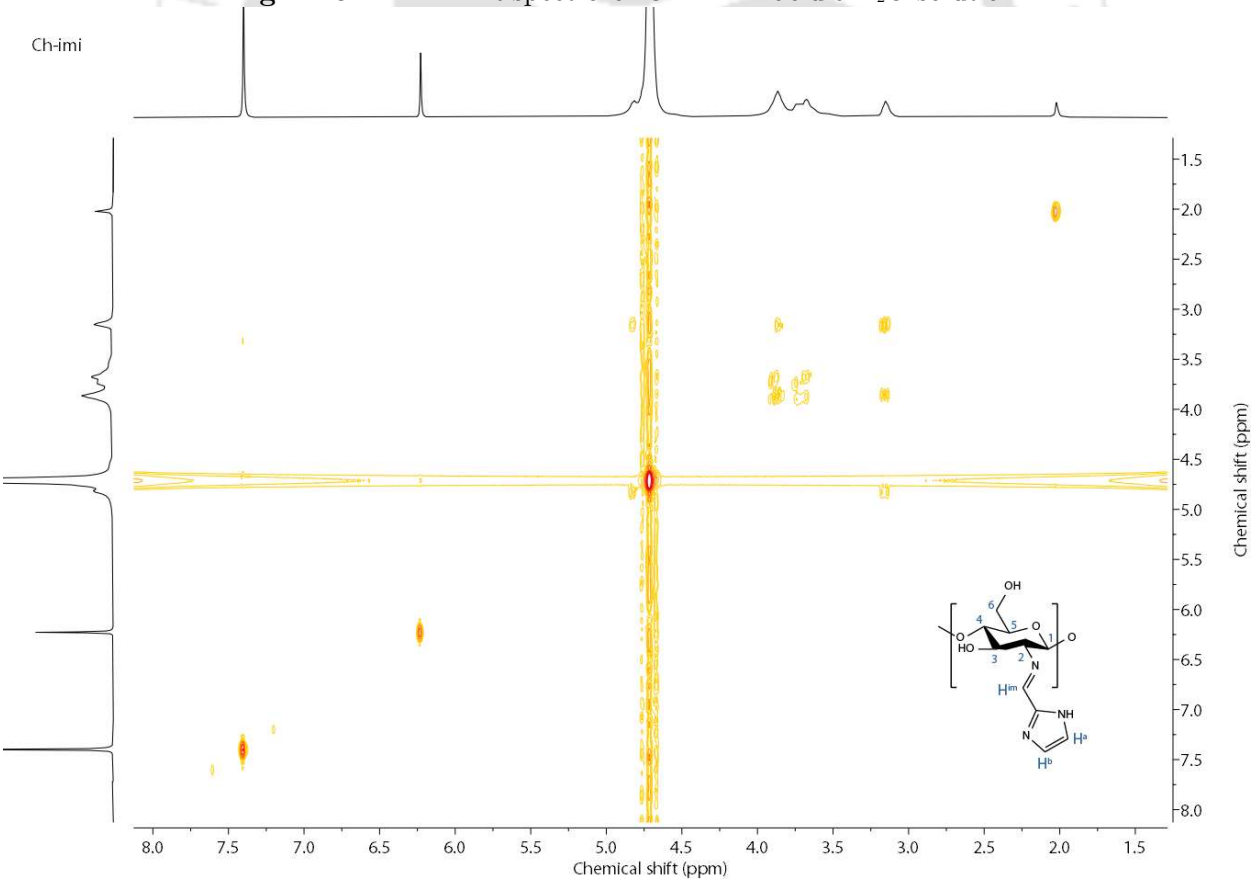

Figure 5.3. ^{1}H - ^{1}H COSY NMR spectra of Ch-imi in acidic D_2O solution.

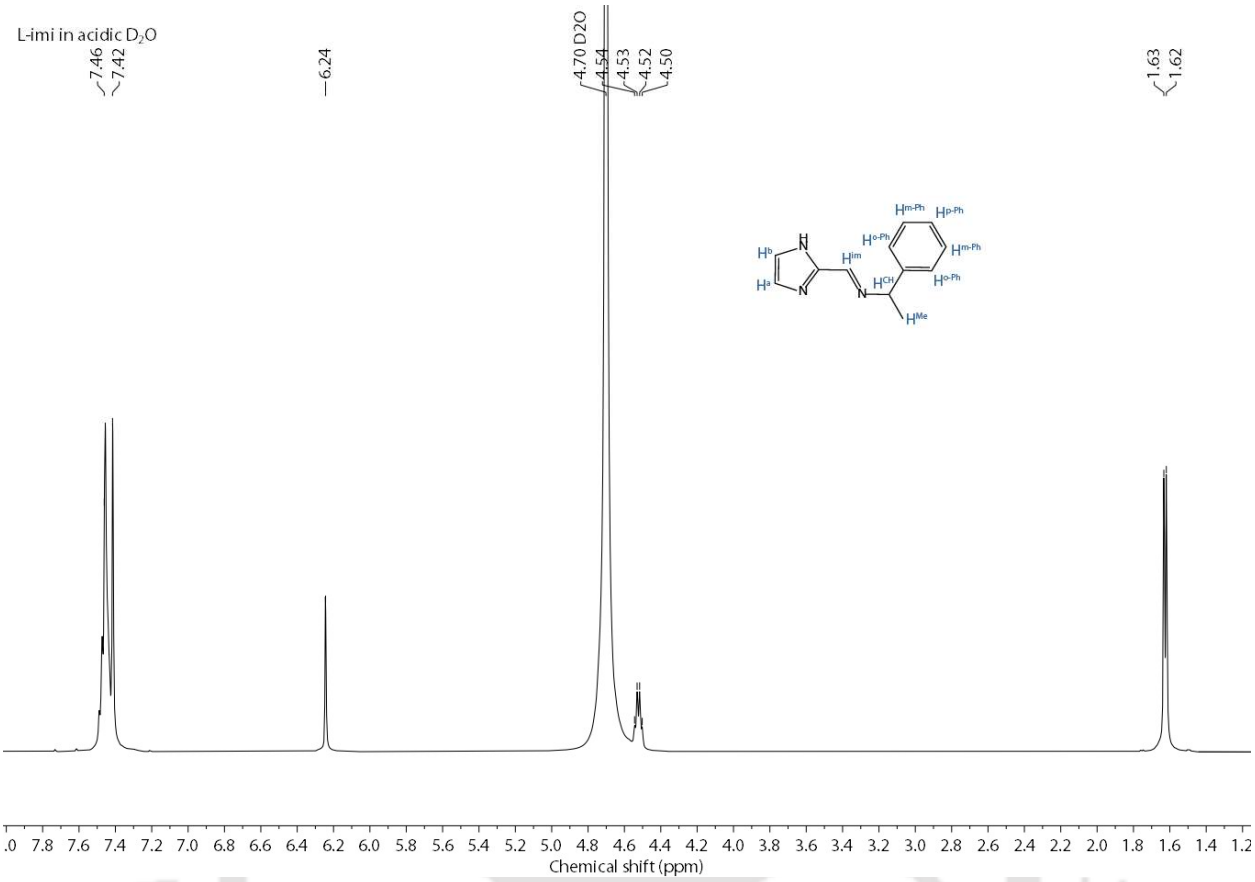

Figure 5.4. ^{1}H NMR spectra of L-imi (Section 5.2.3.1) in acidic D_2O solution.

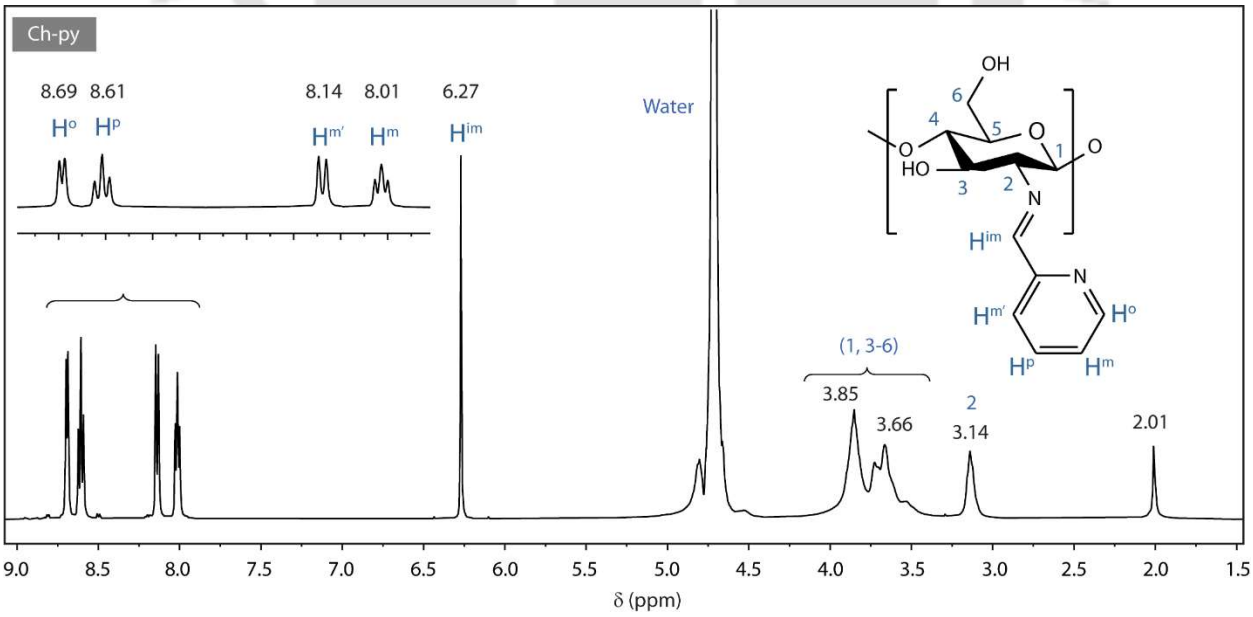

Figure 5.5. 1H NMR spectra of Ch-py in acidic D_2O solution.

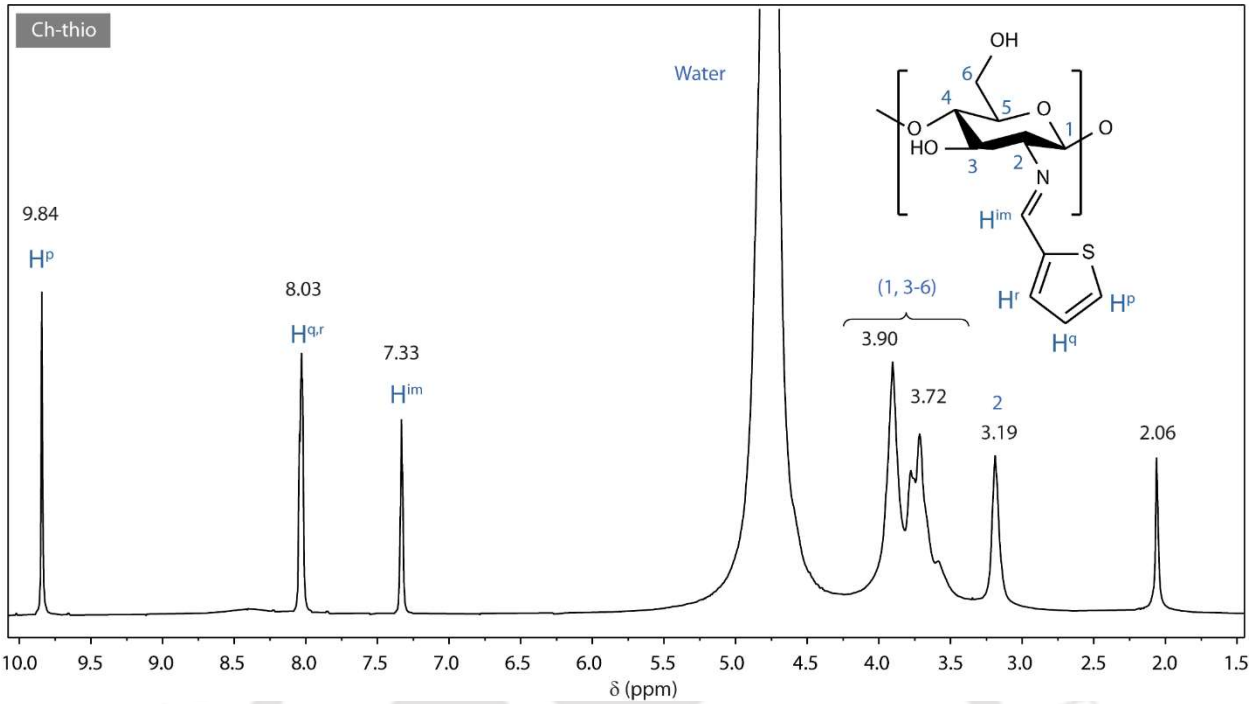

Figure 5.6. ^{1}H NMR spectra of Ch-thio in acidic D_2O solution.

Table 5.2. Selected ^{1}H NMR of chitosan derivatives and L-imi as reference in acidic D_2O solution.

Compounds	**H^2**	**$H^{1,\ 3\text{-}6}$**	**H^{im}**	**H^{CH}**	**H^a**	**H^b**			**-CH_3**
Ch-imi	3.19	3.90, 3.72	6.27		7.44	7.44			2.06
Ch-imi+ $Hg(NO_3)_2$	3.20	3.92, 3.75	6.27		7.44	7.44			2.06
L-imi			6.24	4.52	7.44				1.62
					H^o	**H^m**	**H^p**	**$H^{m'}$**	
Ch-py	3.14	3.85, 3.66	6.27		8.69	8.01	8.61	8.14	2.01
Ch-py+ $Hg(NO_3)_2$	3.17	3.90, 3.65	6.32		8.74	8.06	8.66	8.19	2.06

				H^p	H^q	H^r	
Ch-thio	3.19	3.90, 3.72	7.33	9.84	8.03	8.03	2.06
Ch-thio +$Hg(NO_3)_2$	3.18	3.90, 3.72	7.34	9.84	8.03	8.03	2.06

Hydrogen numbering sequences are in Scheme 5.1. M.F. is the molecular formula. -CH_3 is from the residual acetyl group (Chitin in Scheme 5.1). Corresponding ligands NMR in acid and D_2O were compared to identify imine hydrogen location.

^{1}H NMR spectra of the chitosan materials after Hg(II) binding were taken similarly in acidic D_2O solution. Unfortunately, no coordination-induced shifts were observed in the NMR spectra (Table 5.4). This could be due to the fact that in the presence of an acid, the coordination bond hydrolyzed, and Hg(II) remains in the solution.

The degrees of Schiff base formation, free amine, and acetylation in the modified chitosan materials were calculated from the ^{1}H NMR data of the respective materials. Calculation procedure for % of free amine and unhydrolyzed acetylated in chitosan from ^{1}H NMR has been reported by Lavertu et al. as well as Hirai et al.[19,20] For Schiff base derivatives of chitosan reported here, and we used a similar method utilizing the NMR integration values of the highlighted protons in Figure 5.7. Unlike previous reports, we used H^2 as a reference as strong HOD signal masks the H^1 signal and affects the integration of $H^{3\text{-}6}$ in our case. This and lower intensity of the acetyl methyl group introduces 2-3% error in the quantity of acetylated unit.

Method. We considered the presence of all three types of units. We further considered that the integration value of H^2 is a sum of all three type units multiplied by the fraction of each type. Detailed calculations are given below. The value of free amine is determined by deducting acetylation and Schiff base values from 100%.

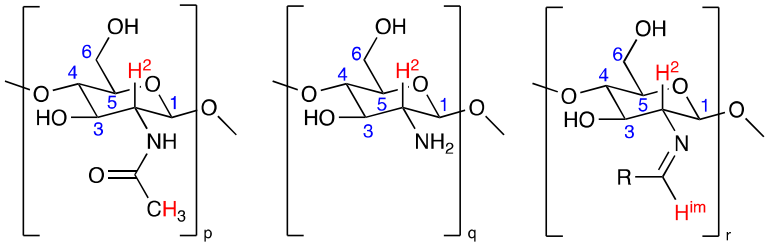

Figure 5.7. Three types of units bearing acetyl from unhydrolyzed chitin, free amine in chitosan, and Schiff base in synthesized material. The integration value of the highlighted protons was used in the calculation.

Table 5.3. Integration values of -CH_3, $H^{2.}$ and imine H from ^{1}H NMR of chitosan and chitosan derivatives dissolved in 0.7mL D_2O and 0.01mL HNO_3.

Integration of →	**-CH_3**	**H^2**	**H^{im}**
chitosan	0.41	1	-
Ch-imi	0.434	1	0.835
Ch-py	0.49	1	0.78
Ch-thio	0.41	1	0.37

Calculation for Chitosan. It has first two structural units

Total no. of proton for -CH_3 = 3p,

Total no. of proton for H^2 = 1p+1q

From integration of ^{1}H NMR spectra, 3p/(1p+1q) = 0.41/1 5.3

% of sites with acetyl group = p/(p+q) x 100 = 0.41/3 x 100 = 14% using eq. (1)

Calculation for Ch-imi. It has all three structural units.

Total no. of proton for -CH_3 = 3p

Total no. of proton for H^2 = 1p+1q+1r

No. of Him = r

From integration of 1H NMR spectra, 3p/(1p+1q+1r) = 0.434/1 5.4

From integration of 1H NMR spectra, r/(1p+1q+1r) = 0.835/1 5.5

% of sites with chitin = p/(p+q+r) x 100 = 14%

% of sites with Schiff base = r/(p+q+r)x 100 = 83%

% of sites with free amine = 100-(83+14) = 3%

Calculation for Ch-py. It has all three structural units.

Total no. of proton for $-CH_3$ = 3p

Total no. of proton for H^2 = 1p+1q+1r

No. of Him = r

From integration of 1H NMR spectra, 3p/(1p+1q+1r) = 0.49/1 5.5

From integration of 1H NMR spectra, r/(1p+1q+1r) = 0.78/1 5.6

% of sites with chitin = p/(p+q+r) x 100 = 16%

% of sites with Schiff base = r/(p+q+r)x 100 = 78%

Calculation for Ch-thio. It has all three structural units.

Total no. of proton for $-CH_3$ = 3p

Total no. of proton for H^2 = 1p+1q+1r

No. of Him = r

From integration of 1H NMR spectra, 3p/(1p+1q+1r) = 0.41/1 5.7

From integration of 1H NMR spectra, r/(1p+1q+1r) = 0.37/1 5.8

% of sites with chitin = p/(p+q+r) x 100 = 14%

% of sites with Schiff base = r/(p+q+r)x 100 = 37%

Following a similar procedure, the degrees of Schiff base and free amine present in the Schiff base materials after Hg(II) binding were determined (Table 5.4). Calculation showed after Hg(II) complexation, the amount of Schiff base in the material reduced, indicating hydrolysis of the imine bond in the presence of Hg^{2+}. Similar hydrolysis of the ligands was observed in the previous chapter with L-thio and reported earlier.[22,23]

5.3.4. ESI Mass analysis

Mass of the chitosan Schiff base materials was analyzed using time of flight electron spray ionization mass spectrometry. The mass data were collected in positive mode ranging from 100-1000 m/Z and illustrated in Figure 5.8-5.10. Δm, the repeating unit of the chitosan polymer, was found to be ~161 and ~203, which are equivalent to the deacetylated chitosan, glucosamine units [Ch($C_6H_{11}O_4N$)] and acetylated chitosan, chitin units [Ch-OAc($C_8H_{13}O_5N$)] were detected in the mass spectrum of the chitosan materials. As the chitosan's polysaccharide backbone is likely to undergo dehydration and glycosidic dissociation, fragmentation patterns related to change of m/Z values of ~18 (for H_2O) and ~161 (for Ch, $C_6H_{11}O_4N$, the repeating unit) were observed. The decrease in intensity pattern with an increase in m/Z was observed. That might be due to the breaking of glycosidic linkages in ESI mode. Isotopic pattern analysis did not reveal multiply charged species.

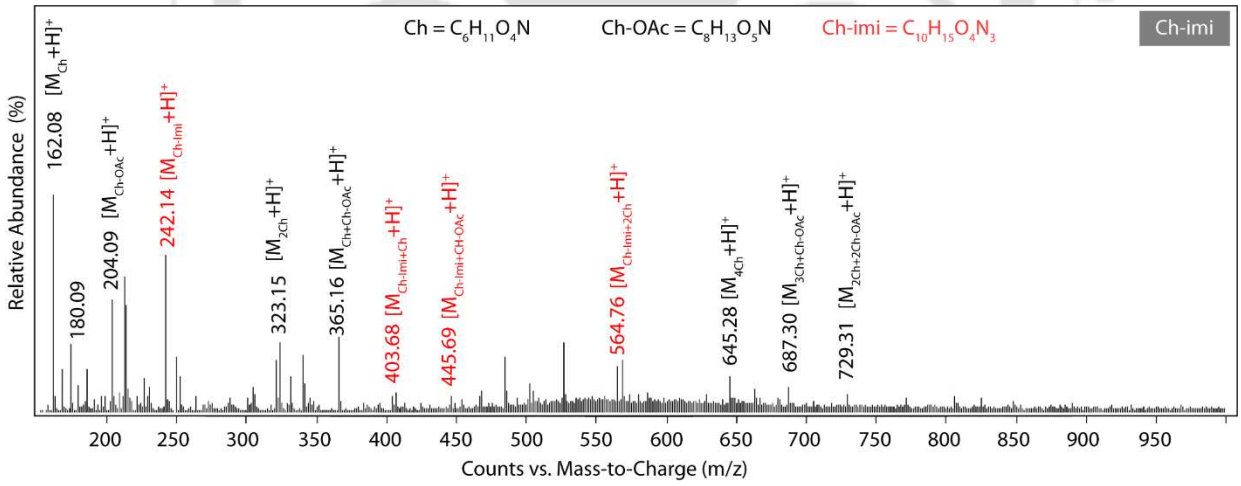

Figure 5.8. ESI mass spectra of Ch-imi in acidic aqueous solution.

The ESI mass spectra of the corresponding Schiff base material shows molecular ion peak for the monocationic form at 242.14, 403.68, 445.69, 564.76 [Ch-imi, $\{C_{10}H_{15}N_3O_4+H\}^+$, Ch-imi+Ch $\{C_{16}H_{26}N_4O_8+H\}^+$, Ch-imi+2Ch $\{C_{22}H_{37}N_5O_{12}+H\}^+$, Ch-imi+Ch $\{C_{16}H_{26}N_4O_4$

+H}$^+$], 273.21, 502.22 [Ch-py, {$C_{12}H_{14}N_2O_4$ +Na}$^+$, 2Ch-py, {$C_{24}H_{29}N_4O_8$ +H}$^+$] and 663.30 [Ch-thio, {$C_{27}H_{40}N_3O_{14}S$ +H}$^+$]. Apart from molecular ion peaks, the Schiff base materials showed sequential fragmentation patterns with successive losses of ~161 (Ch unit), ~203 (Ch-OAc unit), and ~18 (water). These peaks came from the polysaccharide backbone of the chitosan. The FTIR, elemental analyses, proton, and COSY NMR, and the results from the mass spectra all together confirm the formation of the Schiff base of chitosan (Table 5.4).

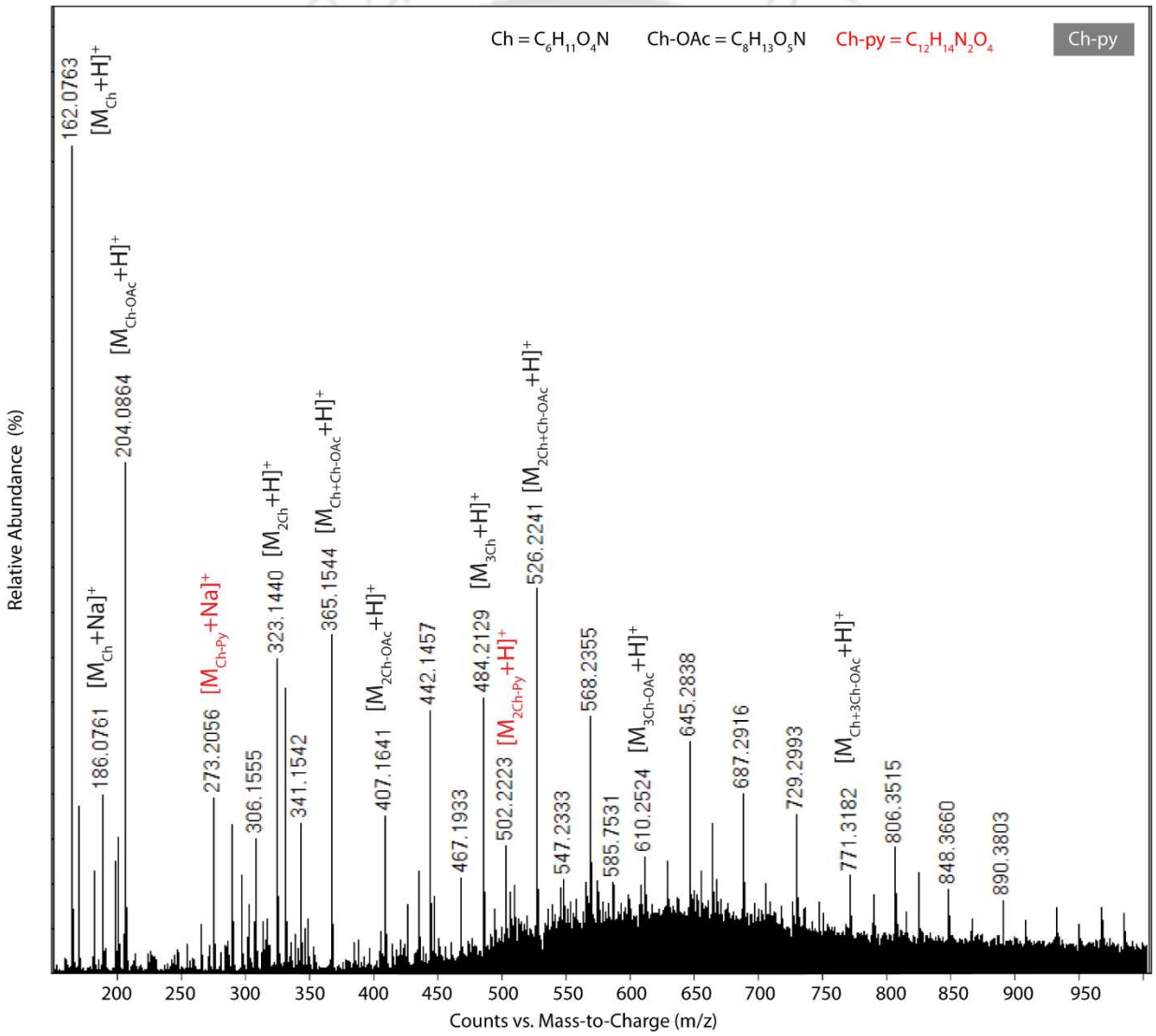

Figure 5.9. ESI mass spectra of Ch-imi in acidic aqueous solution.

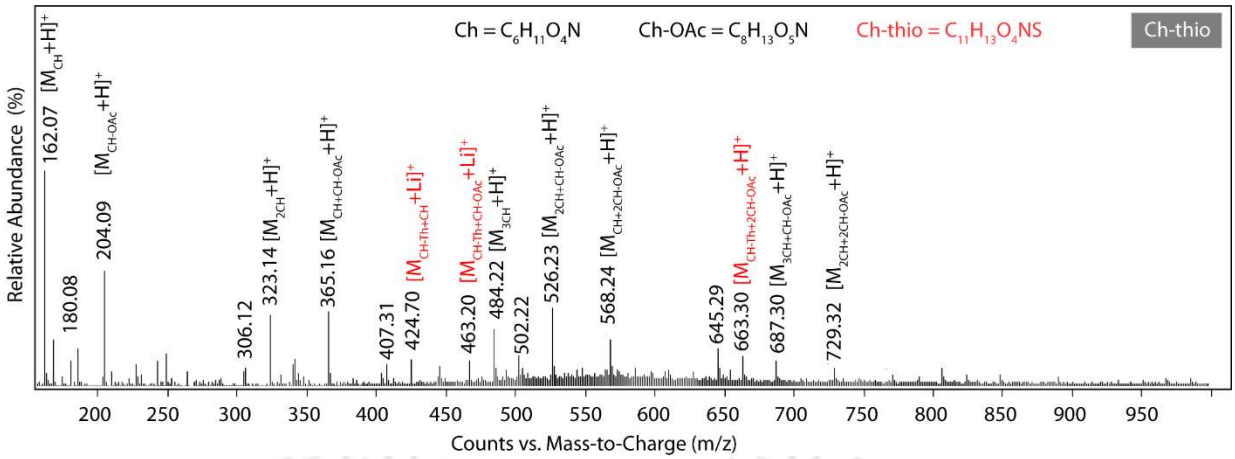

Figure 5.10. ESI mass spectra of Ch-imi in acidic aqueous solution.

Molecular ion peaks for the higher molecular weight units could not be observed in our experimental condition and machine setup. This might be because of the solubility issue, and the voltage we used to excite the molecule was insufficient. We tried with matric assisted laser desorption ionization (MALDI) technique using dihydroxy benzoic acid as a matrix to identify the higher molecular fragments. Unfortunately, we could not ionize it.

5.3.5. Elemental analysis

Elemental analyses were done with the well-dried samples. Data were collected multiple times from different batches, compared, and analyzed. The absolute percentage values of elemental analysis of solid polymers, especially of the hydrogen was difficult to match with a formula. This is because the materials absorbed moisture. However, the mole ratio of C:N:S was a reliable indicator of composition as either of these elements cannot come from either salt or water, or moisture. The C:N:S ratio for the polymer measured was close to the expected ratio of the proposed formula (Table 5.4). The elemental analysis result supports the Schiff base formation as evident in the FTIR, NMR, and ESI mass spectra.

Table 5.4. Selected properties of the chitosan derivatives.

	Chitosan content in %			ESI-mass in acid and water		Atomic mole ratio from analysis		FTIR in KBr	
	Schiff base	***Free amine***	***Residual chitin***	**MF**	**Found (Calc.)**	**Found**	**Calculated**	$n_{C=N}$, cm^{-1}	n_{NO3}, cm^{-1}
Chitosan	0	86	14	$\{C_6H_{11}NO_4+H\}^+$	162.08 (162.07)	C6:H10:N1	C6:H11:N1		
Ch-imi	83	3	14	$\{C_{10}H_{15}N_3O_4+H\}^+$	242.14 (242.11)	C11:H25:N3	C10:H14:N3	1655	
Ch-imi+ $Hg(NO_3)_2$	78	8	14					1645	1384
Ch-py	78	6	16	$\{C_{24}H_{29}N_4O_8+H\}^+$	502.22 (502.21)	C12:H19:N2	C12:H15:N2	1649	
Ch-py+ $Hg(NO_3)_2$	42	47	11					1655	1384
Ch-thio	37	49	14	$\{C_{27}H_{40}N_3O_{14}S+H\}^+$	663.30 (663.23)	C7.4:H13:N1:S0.5	C11:H14:N1:S1	1631	
Ch-thio +$Hg(NO_3)_2$	25	60	15					1633	1385

Amount of Schiff base, free mine and residual amine in the polymers were calculated from ^1H NMR of the materials in D_2O and HNO_3 solution. Electrospray ionization Mass spectra (ESI-Mass) were recorded in H_2O and HNO_3 solution. Atomic mole ratio and FTIR data are of solid powder without addition of HNO_3.

5.3.6. Thermogravimetric and differential scanning calorimetric Analysis (TGA-DSC)

The thermal stability of the materials was analyzed by thermogravimetric analysis (TGA). TG analysis of the polymeric materials was done with samples of ~7-10 mg, placed in an alumina crucible, and heated from 25 to 350 °C at 5 °C/min heating rate under nitrogen atmosphere (50 mL/min). All samples were stored in a desiccator before analysis. It showed two-step weight loss of the Schiff base materials (Figure 5.11). The first step, weight loss of around 5-12%, occurred between 60 ℃ to 160 ℃, which accounted for the loss of hydrogen-bonded water molecules. Chitosan-imi being showed the maximum weight loss of 12.45% in this region, leading to the highest moisture content, which is also evident from elemental analysis (more than 4 molecules of water from elemental analysis compared to more than two molecules from TGA). Weight losses of the other Schiff base materials (Ch-thio of 4.64% and Ch-py of 7.76%) are also inconsistent with the elemental analysis result. Since unmodified chitosan contains many hydroxyl groups, there is a chance of the presence of hydrogen-bonded water molecules even after prolong drying under vacuum. The presence of imine -NH ring proton could be the reason for higher water content in the imidazole-modified chitosan. Thiophene, being a comparable hydrophobic moiety, had a lesser moisture amount in its polymer material, Ch-py being intermediate. The second weight-loss step showed a maximum weight loss of more than 40%, which might be due to the decomposition of the material as melting point checking of the polymer materials showed visual charring of the materials at around 270 ℃.

DSC analysis of the polymeric materials was done using aluminum pans and heated from 25 to 350 ℃ at 5 ℃/min heating rate under nitrogen atmosphere (50 mL/min). A broad endothermic peak was observed close to 70-100 ℃ in the DSC plot of the materials

due to the evaporation of the hydrogen-bonded water molecules, which is in agreement with the TGA results.

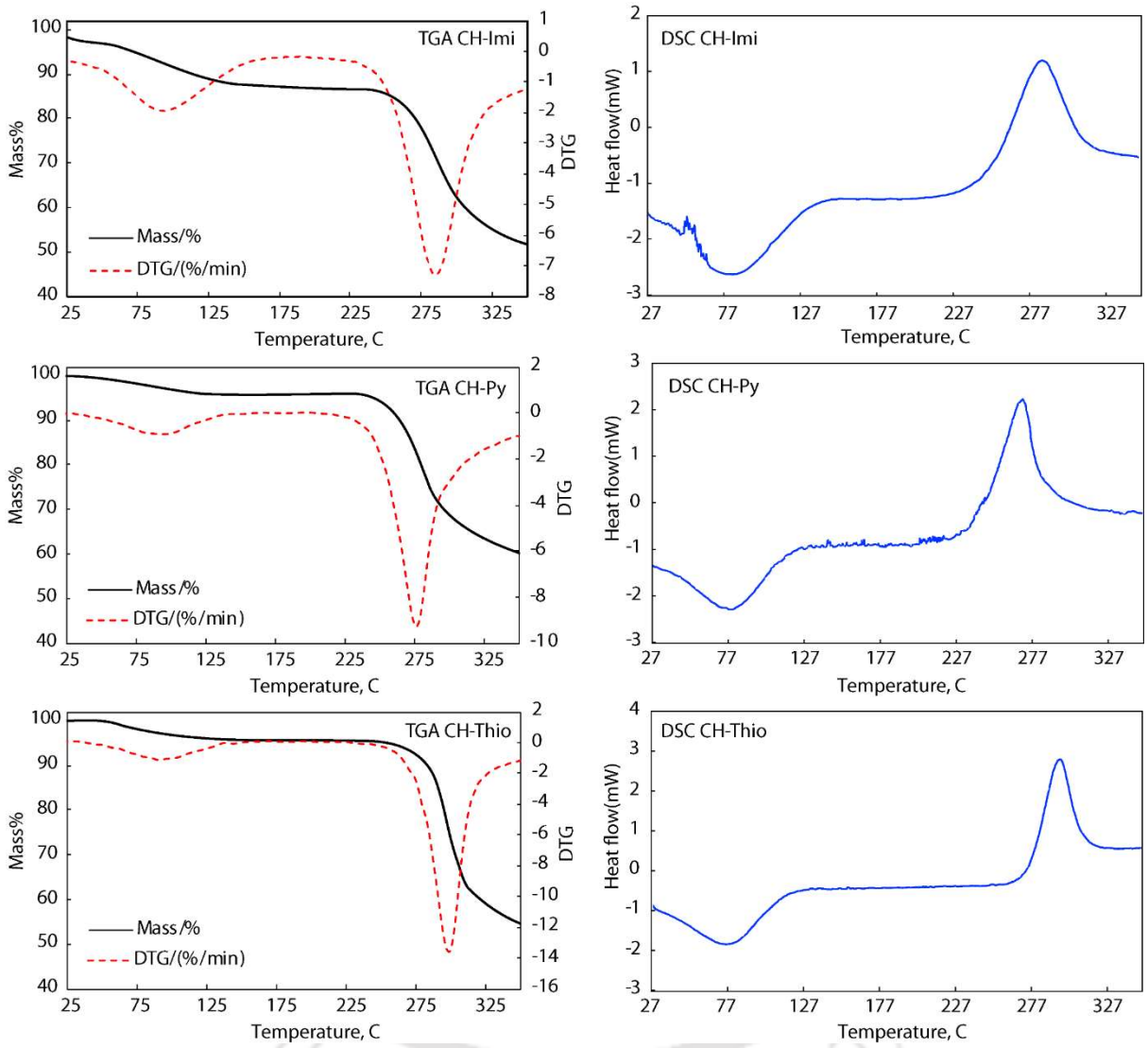

Figure 5.11. TGA-DSC plot of Ch-imi.

A shift in the position of endotherm might be due to the difference in their water holding capacity and strength of water-polymer interaction.[24–26] The endothermic jump in the DSC curve near 300 ℃ indicated the molecular chain breaking, which means the decomposition of the materials. The glass transition temperature is usually obtained by DSC. Some people reported it to be ranged from 30℃ to even higher temperature, like 200 ℃, depending on

the source of the chitosan or amount of water content, as water has a plasticizing effect.[24] But, in our case, we did not observe any such significant stepwise change of the specific heat that could favor the presence of a glass transition temperature.

2.3.7. Field emission scanning electron microscopy

Field emission scanning electron microscopy (FESEM) imaging of the chitosan Schiff base materials showed non-uniform polymer surfaces. The unmodified chitosan exhibits a smoother surface, whereas the Schiff base modifications created agglomerates, and the surface becomes rougher. The FESEM images are shown in Figure 5.12.

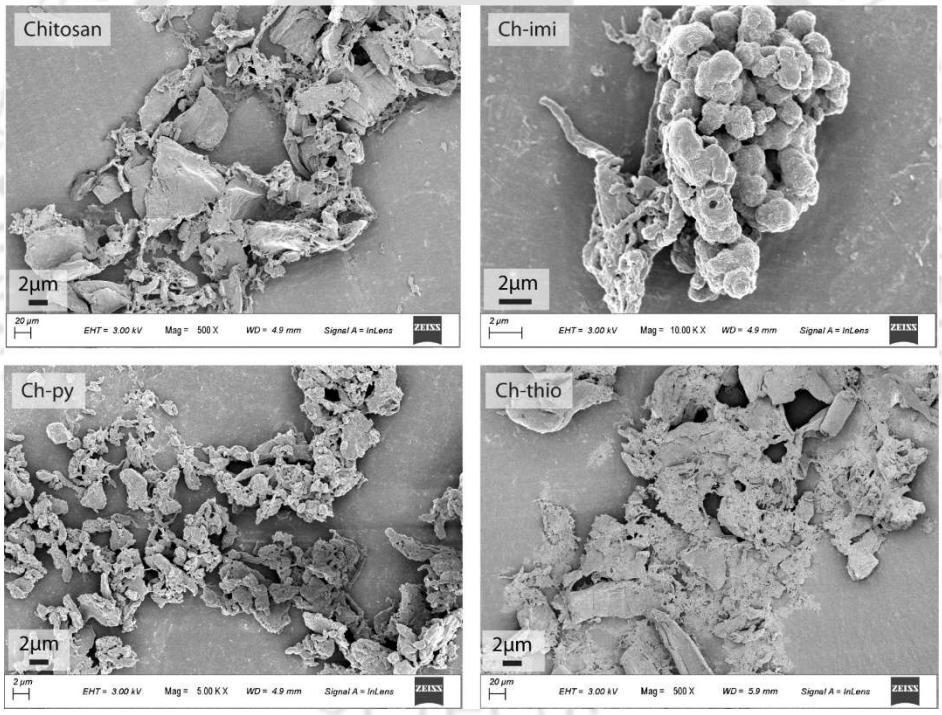

Figure 5.12. FESEM images of the chitosan and chitosan-Schiff base polymers.

The images showed the changes of the surface morphology is more in the case of Ch-imi and Ch-py than the Ch-thio.

2.3.8. Determination of Zero Point Charge (pHzpc).

The surface chemistry of a material is primarily governed by the acidic or basic nature of its surface. We know that a positive surface charge means acidic and a negative surface charge means basic. Thus, it is very important to have an understanding of the surface charge of the material in the case of adsorption studies in an aqueous medium. The pHzpc of the polymeric modified chitosan materials was determined by the salt addition method. The point of zero charge (pHzpc) estimates the pH at which the surface charge of the material is zero in the aqueous media. In this method, pHzpc was determined by different pH variations with a dose of 3 g/L. The graph (Figure 5.13) showed the pHzpc of the materials to be around 6.5-7.

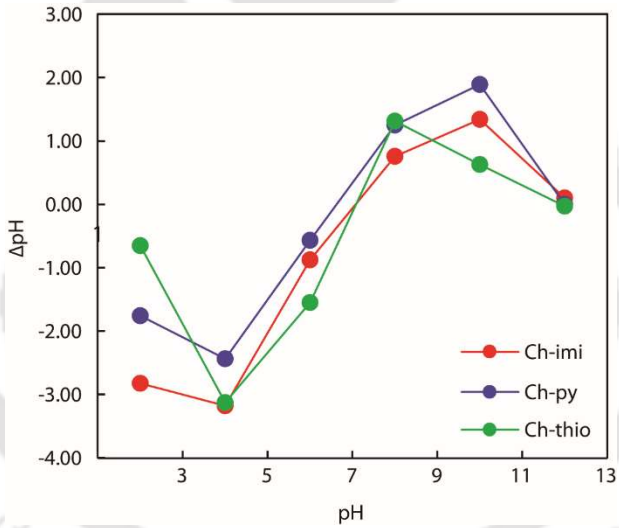

Figure 5.13. Determination of pHzpc of the chitosan and chitosan-Schiff base polymers.

This experiment shows that at below pH ~6.5, the surface of the materials is positively charged.

5.3.9. Mercury(II) adsorption

5.3.9.1 Effect of pH on Hg(II) adsorption

The effect of the solution pH on the removal efficiency of the modified chitosan polymers was investigated within a pH range of 2-7 at an initial Hg(II) concentration of 50-200 mg/L

using 1 g/L polymer dose and digestion time of 3 hours. Experiments were carried out by maintaining the initial pH of the Hg(II) solutions using dilute HCl or dilute NaOH solutions. Maximum Hg(II) uptake was observed at acidic pH 2 by Ch-thio and Ch-py. No such pH effect was found with Ch-imi;> 90% removal of Hg(II) was observed at all pH variances. Figure 5.14. and Table 5.5-5.7. shows the Hg(II) removal data.

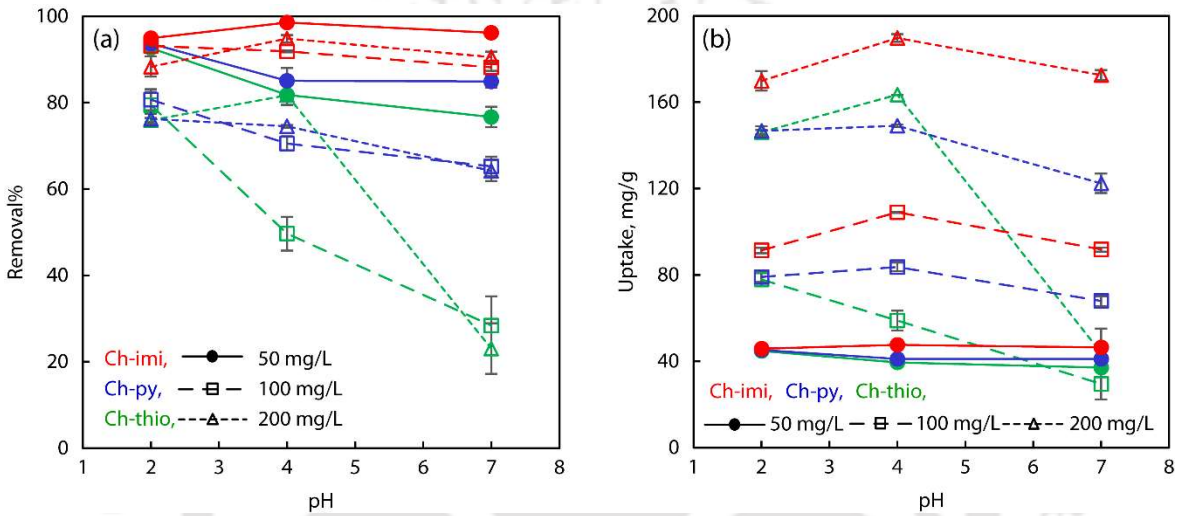

Figure 5.14. Comparison of Hg(II) removal (a) and adsorption capacity (b) by the modified chitosan Schiff base polymers at different pH and initial concentrations with a dose of 1 g/L.

The surface charge is an important parameter that controls the adsorption process. We looked into the speciation of Hg(II) at the experimental conditions.[27] We found that Cl^- ions can interact with Hg(II) and make different chloro complexes. The form varies from $HgCl^+$, $HgCl_2$, $HgCl_3^-$ and $HgCl_4^{2-}$ depending on the extent of Cl^- ion concentration.[27] We measured chloride ion concentration of the solution and found the pCl values to be equal to 1.5-1.2 at pH 2 and 4. The predominant form from the speciation was thereby either $HgCl_3^-$ and $HgCl_4^{2-}$. Zero-point charge value and speciation diagram calculated from the respective pKa values of the corresponding aldehydes showed the materials were protonated at lower pH. Ion exchange could occur, and thus the maximum removal at lower pH by all the modified

chitosan Schiff base materials. Only Ch-imi showed >90% removal over the range of pH from 2-7. This can be explained based on the strong complexation of Hg(II) to the L-imi, as observed in the previous chapter.

Table 5.5. Mercury removal by the modified chitosan Schiff base polymers at 50 mg/L initial Hg(II) concentration at dose 1g/L at three pH from 2-7

pH of the solution	Parameters	Ch-imi	Ch-py	Ch-thio
2	Uptake, mg/g	45.87 (±0.09)	45.23 (±0.12)	44.73 (±0.25)
	Removal %	94.96 (±0.2)	93.65 (±0.26)	92.62 (±0.52)
4	Uptake, mg/g	47.6 (±0.29)	41.1 (±1.44)	39.5 (±1.1)
	Removal %	98.55 (±0.61)	85.09 (±2.97)	81.78 (±2.29)
7	Uptake, mg/g	46.47 (±0.42)	41.0 (±0.7)	37.03 (±1.15)
	Removal %	96.2 (±0.87)	84.89 (±1.44)	76.67 (±2.37)

Table 5.6. Mercury removal by the modified chitosan Schiff base polymers at 100 mg/L initial Hg(II) concentration at dose 1g/L at three pH from 2-7

Initial Concentration	Parameters	Ch-imi	Ch-py	Ch-thio
2	Uptake, mg/g	91.3 (±1.24)	79.07 (±2.38)	77.87 (±2.92)
	Removal %	93.16 (±1.26)	80.68 (±2.43)	79.46 (±2.98)
4	Uptake, mg/g	92.78 (±0.24)	71.25 (±2.01)	50.15 (±4.61)
	Removal %	91.88 (±0.2)	70.55 (±1.68)	49.66 (±3.89)
7	Uptake, mg/g	91.73 (±0.91)	67.87 (±2.33)	29.5 (±7.06)
	Removal %	88.21 (±0.88)	65.26 (±2.24)	28.37 (±6.79)

Table 5.7. Mercury removal by the modified chitosan Schiff base polymers at 200 mg/L initial Hg(II) concentration at dose 1g/L at three pH from 2-7

Initial Conc.	Parameters	Ch-imi	Ch-py	Ch-thio
2	Uptake, mg/g	169.69 (±4.48)	146.67 (±2.22)	146.1 (±0.96)
	Removal %	88.35 (±2.33)	76.27 (±1.16)	75.98 (±0.5)
4	Uptake, mg/g	189.67 (±1.76)	149.03 (±0.62)	163.4 (±0.08)
	Removal %	94.83 (±0.88)	74.52 (±0.31)	81.7 (±0.04)
7	Uptake, mg/g	172.53 (±2.38)	122.4 (±4.56)	43.93 (±11.18)
	Removal %	90.57 (±1.25)	64.25 (±2.39)	23.06 (±5.87)

5.3.9.2 Effect of initial concentration

The effect of initial Hg(II) concentration on uptake is studied using the data given in Table 5.5-5.7. Initial Hg(II) concentration was varied from 50 mg/L to 200 mg/L. The study showed the relationship between the Hg(II) concentration and available binding sites of the materials. It showed similar uptake of Hg(II) by all the three modified chitosan materials at low concentrations. With the increase in concentration, they started showing different uptake due to the completion of the available binding sites. All three showed >90% uptake at 50 mg/g Hg(II) concentration. With increasing concentration, removal decreased. Only Ch-imi showed >90% uptake throughout the pH range from 2-7. Hg(II) concentration variation was an important factor in exploring the Hg(II) uptake capacity of the modified chitosan Schiff base materials. Results showed the maximum uptake capacity of ~180 mg/g in the case of Ch-imi at 200 mg/L initial concentration.

5.3.9.3 Adsorption Kinetics

Adsorption kinetics of the Hg(II) uptake was examined with 50 mg/L of Hg(II) concentration, 1 g/L of material dose, and 1–300 minute time variance. The removal percentage showed >90% Hg(II) uptake by Ch-imi within 10 min. At the same time, Ch-py and Ch-thio showed Hg(II) uptake at min. of contact time. In the case of Ch-imi, 30 min. of contact time was sufficient enough to reach equilibrium for Hg(II) adsorption. The chitosan Schiff base materials-Hg(II) interactions were investigated by pseudo-first-order, pseudo-second-order, and Elovich kinetics model. The pseudo 1st order, pseudo 2nd order, and Elovich kinetics are as follows

$$q_t = q_e\,(1\text{-}e^{-k_1 t}) \qquad 5.9$$

$$q_t = \frac{k_2\, q_e^2\, t}{1 + k_2\, q_e\, t} \qquad 5.10$$

$$\frac{dq_t}{dt} = \alpha \exp^{-\beta q_t} \qquad 5.11$$

The parameters of various Kinetic models are given in Table 5.8, and the linear and non-linear fitting of the experimental results are shown in Figures 5.15 and 5.16b, respectively. Data fittings suggest Hg(II) adsorption by Ch-imi following pseudo-second-order kinetics, and Ch-py and Ch-thio follow Elovich kinetics. It confirms that the chemisorption was the rate-controlling steps in Hg(II) adsorption. As indicated above, the Elovich equation was the most suitable to describe Hg(II) adsorption by the Ch-py and Ch-thio. Surfaces of the modified chitosan materials are not similar everywhere. The degrees of Schiff base formation, acetylation, and free amine groups vary from one material to another. Therefore, it is very much likely to have different fittings of time-dependent experimental data by different polymers.

Time-dependent study at room temperature showed Hg(II) removal is almost complete within 60 mins (for Ch-imi, it is 10 mins). The data fits with either pseudo-second-order or Elovich rate plot, which usually means chemical adsorption. However, the experimental data were collected through shaking in an orbital shaker, aliquote collection, filtration and concentration measurements by AAS machine, and given the process finishes within minutes, describing the Kinetics by the three modified Schiff base polymer materials may not be that precise. What significant result obtained from the experiment was that Ch-imi shows very fast Hg(II) adsorption followed by Ch-py and Ch-thio (both comparable).

Table 5.8. Comparison of different kinetic models for Hg(II) adsorption

Polymer	**Fitting**	**First-order**			**Second-order**			**Elovich**		
		q_e	K_1	R^2	q_e	K_2	R^2	α	β	R^2
Ch-imi	Linear	3.56	$-3.5*10^{-5}$		49.37	0.03	0.99	$1.34*10^{6}$	0.35	0.57

	Non-linear	48.10	0.59	0.87	50.06	0.02	0.93	$1.57*10^{6}$	0.36	0.61
Ch-py	Linear									
	Non-linear	45.13	0.15	0.76	47.22	0.01	0.89	$1.38*10^{2}$	0.17	0.97
Ch-thio	Linear									
	Non-linear	43.80	1.06	0.47	45.50	0.03	0.82	$6.35*10^{5}$	0.37	0.90

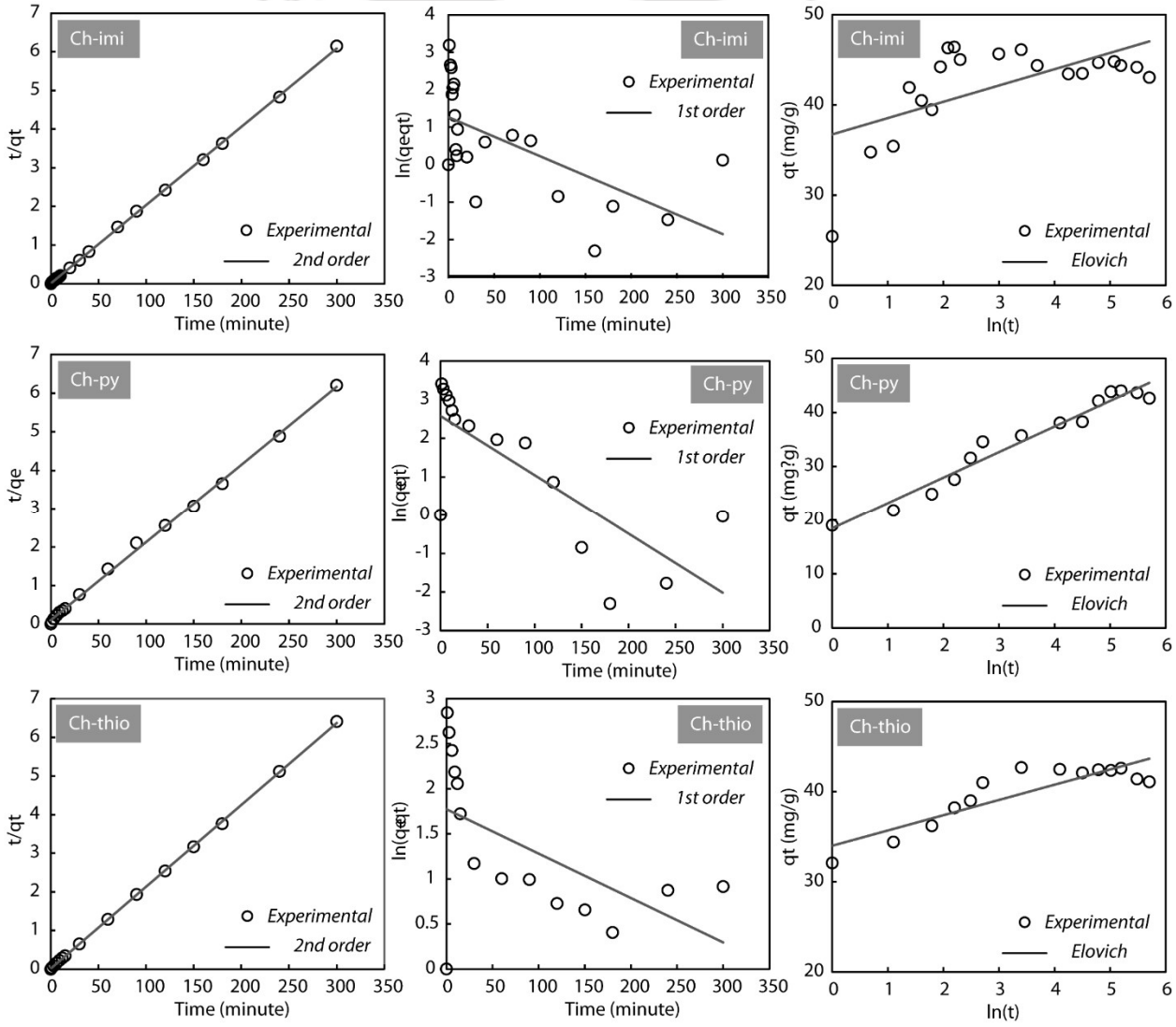

Figure 5.15. Linear fitting of the Hg(II) adsorption kinetics data of the chitosan polymers.

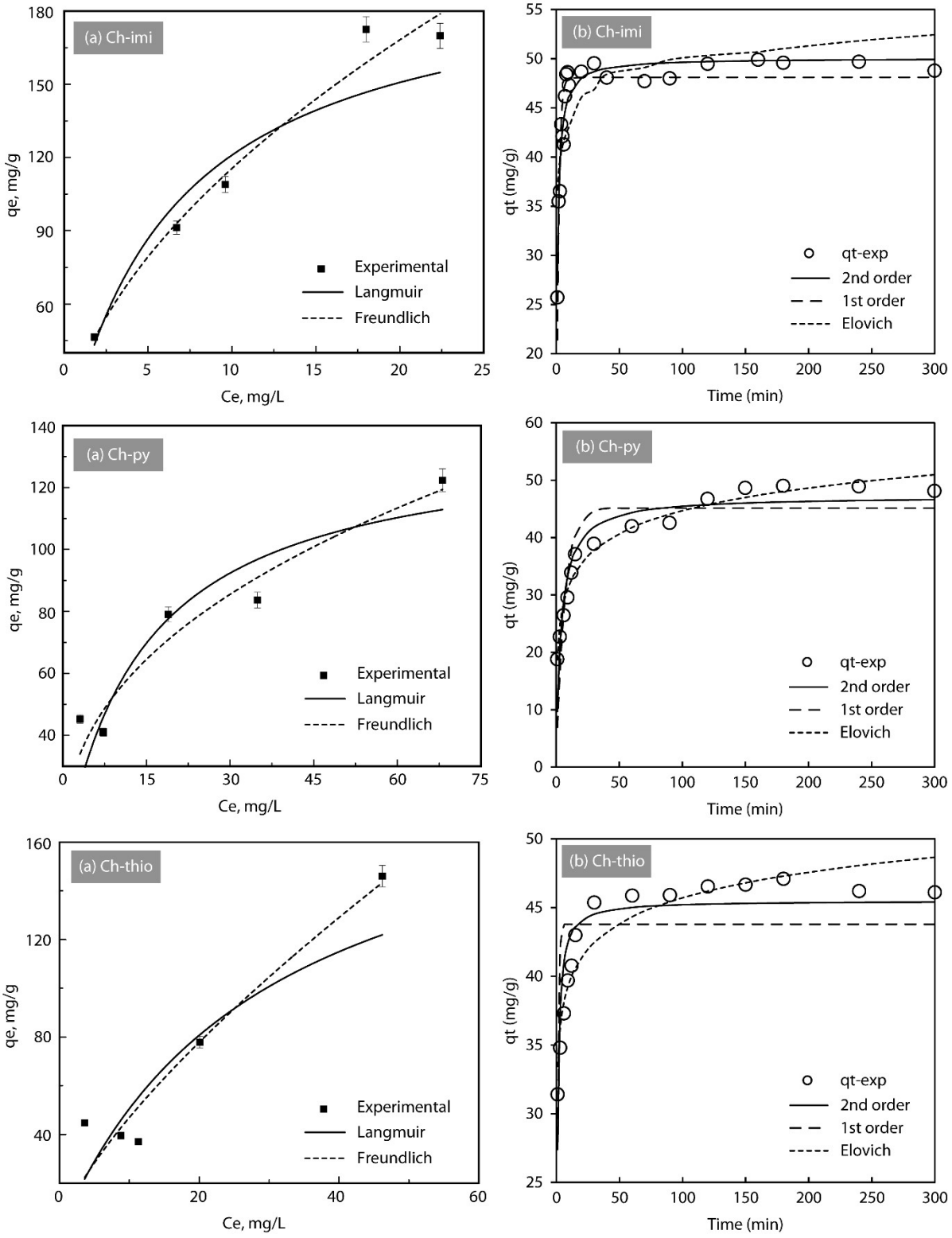

Figure 5.16. (a) Isotherm and (b) non-linear fittings of the kinetics data of Hg(II) removal by the chitosan polymers.

5.3.9.4. Adsorption Isotherm

Isotherms are essential for explaining the theoretical uptake capacity of different materials. Langmuir and Freundlich isotherms models were used to analyze the experimental data of Hg(II) uptake by the Schiff base materials.

The Langmuir isotherm is usually expressed as:

$$q=q_{max}\frac{K_L C_e}{1+K_L C_e} \qquad 5.12$$

Where Ce (mg/L) is the equilibrium concentration of Chromate, qe (mg/g) is the adsorption capacity at equilibrium, qmax (mg/g) is the monolayer adsorption capacity of the adsorbent, and KL (L/mg) is the affinity constant of adsorption in the Langmuir model.

Freundlich isotherm has the following general form,

$$q_e=K_f C_e^{\frac{1}{n}} \qquad 5.13$$

Here, Kf is the Freundlich capacity factor, and n is the index of heterogeneity.

Nonlinear regression was done to determine the isotherm parameters. The fitness of the isotherm model with the experimental data was verified using correlation coefficient (R2) and average relative error (ARE). The equation used to determine ARE is as follows,

$$ARE=\frac{100}{n}\sum_{i=0}^{n}\left[\frac{q_{eexp}-q_{ecal}}{q_{eexp}}\right] \qquad 5.14$$

Where qeexp and qecal are the experimental and calculated using isotherm chromium uptake values, respectively.

Table 5.9. Estimated isotherm parameters for adsorption of Hg(II) by the chitosan polymers

Polymers	Model	Model parameters		R^2	ARE (%)
Ch-imi	Langmuir	q_{max} (mg/g)	200.00	0.87	9.46
		K_L (L/mg)	0.15		
	Freundlich	K_f	35.50	0.96	1.19
		1/n	0.52		
Ch-py	Langmuir	q_{max} (mg/g)	136.80	0.82	2.82
		K_L (L/mg)	0.07		
	Freundlich	K_f	21.42	0.92	-1.94

Ch-thio	Langmuir	1/n	0.407	0.76	-17.04
		q_{max} (mg/g)	200.00		
		K_L (L/mg)	0.03		
	Freundlich	K_f	23.72	0.01	-21.19
		1/n	0.40		

Isotherms are beneficial for explaining the theoretical uptake capacity of different adsorptive materials. The fittings of the experimental results are given in Figure and Table. Comparison of the data obtained from the two isotherm models; it can be concluded that the Freundlich model was fitted better according to its higher R^2 value. It suggested that the adsorption of Hg(II) on the Chitosan Schiff base materials was a heterogeneous surface with multilayer adsorption. Although the difference in regression factor is too small that both the isotherm may actually work during the Hg(II) adsorption.

Our imidazole modified chitosan, Ch-imi, showed a high removal percentage, with a reasonably high uptake value, and fast removal kinetics compared to other materials listed in Table 5.10.

Table 5.10. Comparison of adsorption capacities with other known amine-based materials

Adsorbent	**Initial conc. (mg/L)**	**dose (g/L)**	**Time (h)**	**Removal (%)**	**Uptake (mg/g)**	**Ref.**
Chitosan-alginate nanoparticles (CANPs)	4	20	1.5	89	0.178	28
Thiourea functionalized chelating fiber	10	1	2	98~ (doubt)	11~(doubt)	29
Amide functionalized cellulose from sugarcane bagasse	250	1	24	71.2~	178~	30
Chitosan derivatives	100	1	24	79	79	31
Activated coke by thiol-functionalization	1	0.1	15	98~	9.8~	11
Chitosan coated magnetic nanoparticles	50	6	not given	84.5	7.04	32
Chitosan-poly(vinyl alcohol) hydrogel	-	-	-	-	585.9 (from isotherm)	33

Chitosan beads grafted with Polyacrylamide	500		60	-	322.6	34
Iodine/bromine/sulfuric acid modified chitosan	-	-	3	100	-	35
Chitosan/nanohydroxyapatite composite based scallop shells	180	1	-	-	~126	36
Ch-imi	100	1	10 min	90-95	~90-95	This work
Ch-imi	200	1	10 min	>90	~150-180	This work

5.3.9.5. Energy-dispersive X-ray analysis

EDAX analysis was performed of the material after Hg(II) adsorption. After the adsorption experiment at 50 mg/L initial concentration of Hg(II) at pH 4, solid materials were filtered, washed with distilled water, and dried well in a vacuum desiccator. The spectra are shown in Figure 5.17.

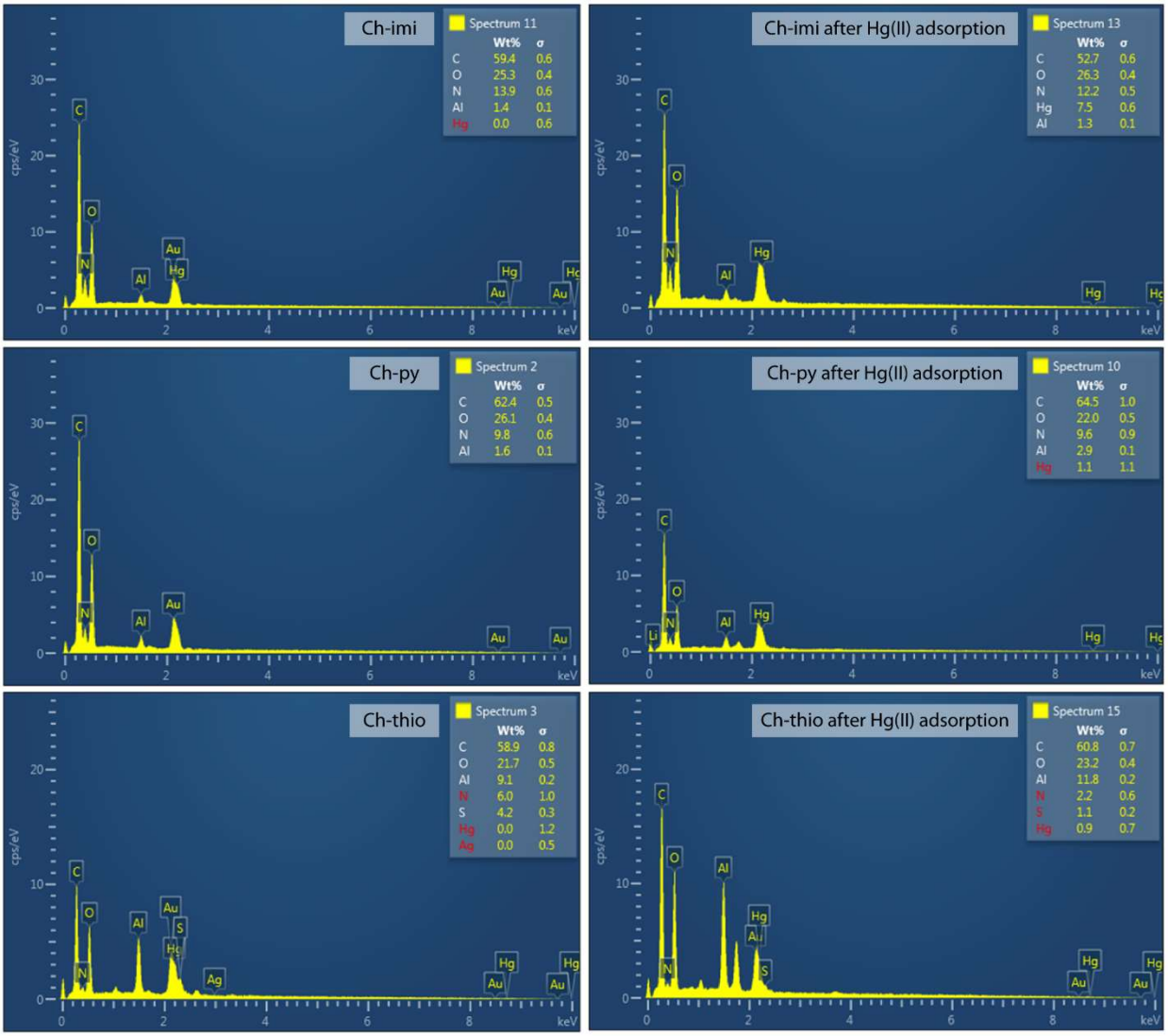

Figure 5.17. Energy-dispersive X-ray spectra of the modified chitosan materials before and after the Hg(II) adsorption.

EDAX studies showed the presence of Hg(II) on the material surface. The elemental percentage ratio of C:N:Hg came in accordance with the removal data. Ch-imi showed

maximum Hg(II) adsorption at pH 4, and its N content was also high. Therefore, its C:N:Hg ratio came higher compared to Ch-py, followed by Ch-thio. In chapter 4, we found L-thio ligand preferred Ag(I), though the EDAX spectra of the Ch-thio after Hg(II) adsorption did not show any peak related to Ag(I). This might be due to the presence of Ag(I) in very tiny quantities, which comes within the limiting range of EDAX. In comparison, ESI mass was sensitive enough to detect that. The presence of a peak related to Hg confirmed the adsorption of Hg(II) on the polymer surfaces.

5.3.9.6. Effect of other metal ions

Hg(II) ions are seldom present with other metal ions in industrial waste. Now adsorption performance depends on the ionic strength of a solution. Therefore, we have studied the effect of some metal ions: Zn^{2+}, Ca, Ni, Cu, Fe, Cd, and Pb on the Hg(II) adsorption capacity of Ch-imi. Since Ch-imi is the one that has showed maximum Hg(II) adsorption throughout a range of initial Hg(II) concentration and in a wide range of pH from 2-7 within 10 mins, the effect of other metal ions is thoroughly investigated on Ch-imi. In this study, Hg(II) adsorption experiment was performed with an initial Hg(II) concentration of 50 mg/L at pH 4 with 1 g/L dose of Ch-imi. The other metal ion concentrations were varied from 25-100 mg/L. The result is shown in Figure 5.18.

Hg(II) adsorption by Ch-imi remained unaffected in the presence of other metals ions except for Cu(II) when Cu(II) is present in high concentrations (0.4 mM). It is common for the imidazole donor ligands to form coordinate bonds easily with Cu(II). Therefore, a decrease in Hg(II) adsorption was observed. The study showed the high effectivity of imidazole modified chitosan in binding Hg(II) from the aqueous solution even when other metals ions are present.

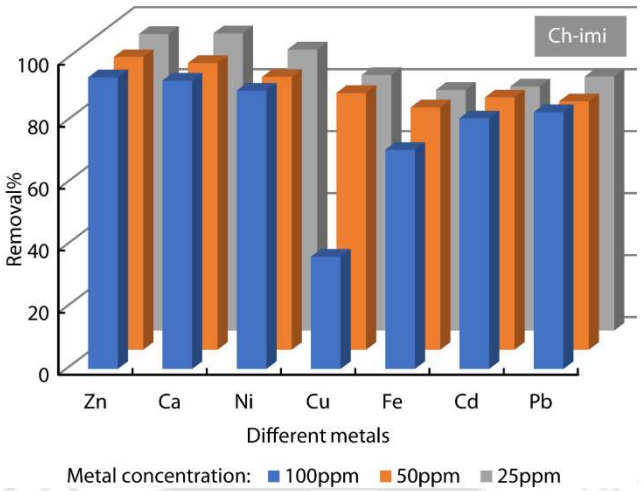

Figure 5.18. Effect of other metal ions on mercury(II) removal efficiency of Chi-imi at 50 mg/L concentration.

5.4. Conclusions

(i) This chapter has nicely demonstrated the fine modification of the amine group of the chitosan, a biopolymer, and controlling its effectivity toward Hg(II) adsorption. Functionalization of the chitosan amine with imidazole, pyridine, and thiophene group shows the Hg(II) complexation behavior changes drastically; imidazole modification is the best among the three. The Schiff base materials were synthesized in an acid-free solid-state, which converted the maximum amine groups into imine, and the separation of the Schiff base material was easy.

(ii) The maximum Hg(II) uptake from water obtained was more than 170 mg/g in a pH range from 2-7 by Ch-imi.

(iii) Kinetic study demonstrated that the chitosan polymer's Hg(II) removal mostly follows pseudo-second-order and the Elovich kinetic model. Fastest Hg(II) was shown by Ch-imi (with more than 90% removal within 10 mins).

(iv) Hg(II) removal by Ch-imi is hardly affected by the presence of other metal ions except for Cu(II) while present in very high concentrations (100 mg/L).

5.5. Bibliography

(1) Yardim, M. F.; Budinova, T.; Ekinci, E.; Petrov, N.; Razvigorova, M.; Minkova, V. Removal of Mercury (II) from Aqueous Solution by Activated Carbon Obtained from Furfural. Chemosphere 2003, 52 (5), 835–841. https://doi.org/https://doi.org/10.1016/S0045-6535(03)00267-4.

(2) Wang, Q.; Kim, D.; Dionysiou, D. D.; Sorial, G. A.; Timberlake, D. Sources and Remediation for Mercury Contamination in Aquatic Systems—a Literature Review. Environ. Pollut. 2004, 131 (2), 323–336. https://doi.org/https://doi.org/10.1016/j.envpol.2004.01.010.

(3) Xu, J.; Bravo, A. G.; Lagerkvist, A.; Bertilsson, S.; Sjöblom, R.; Kumpiene, J. Sources and Remediation Techniques for Mercury Contaminated Soil. Environ. Int. 2015, 74, 42–53. https://doi.org/https://doi.org/10.1016/j.envint.2014.09.007.

(4) Herrero, R.; Lodeiro, P.; Rey-Castro, C.; Vilariño, T.; Sastre de Vicente, M. E. Removal of Inorganic Mercury from Aqueous Solutions by Biomass of the Marine Macroalga Cystoseira Baccata. Water Res. 2005, 39 (14), 3199–3210. https://doi.org/https://doi.org/10.1016/j.watres.2005.05.041.

(5) Bernhoft, R. A. Mercury Toxicity and Treatment: A Review of the Literature. J. Environ. Public Health 2012, 2012, 460508. https://doi.org/10.1155/2012/460508.

(6) Hadi, P.; To, M.-H.; Hui, C.-W.; Lin, C. S. K.; McKay, G. Aqueous Mercury Adsorption by Activated Carbons. Water Res. 2015, 73, 37–55. https://doi.org/https://doi.org/10.1016/j.watres.2015.01.018.

(7) Skyllberg, U.; Bloom, P. R.; Qian, J.; Lin, C.-M.; Bleam, W. F. Complexation of Mercury(II) in Soil Organic Matter: EXAFS Evidence for Linear Two-Coordination with Reduced Sulfur Groups. Environ. Sci. Technol. 2006, 40 (13), 4174–4180. https://doi.org/10.1021/es0600577.

(8) Argüelles-Monal, W.; Peniche-Covas, C. Preparation and Characterization of a Mercaptan Derivative of Chitosan for the Removal of Mercury from Brines. Die Angew. Makromol. Chemie 1993, 207 (1), 1–8. https://doi.org/https://doi.org/10.1002/apmc.1993.052070101.

(9) Bhatt, R.; Kushwaha, S.; Bojja, S.; Padmaja, P. Chitosan-Thiobarbituric Acid: A Superadsorbent for Mercury. ACS Omega 2018, 3 (10), 13183–13194. https://doi.org/10.1021/acsomega.8b01837.

(10) Awad, F. S.; Abouzeid, K. M.; El-Maaty, W. M. A.; El-Wakil, A. M.; El-Shall, M. S. Efficient Removal of Heavy Metals from Polluted Water with High Selectivity for Mercury(II) by 2-Imino-4-Thiobiuret-Partially Reduced Graphene Oxide (IT-PRGO). ACS Appl. Mater. Interfaces 2017, 9 (39), 34230–34242. https://doi.org/10.1021/acsami.7b10021.

(11) Li, Z.; Wu, L.; Liu, H.; Lan, H.; Qu, J. Improvement of Aqueous Mercury Adsorption on Activated Coke by Thiol-Functionalization. Chem. Eng. J. 2013, 228, 925–934. https://doi.org/https://doi.org/10.1016/j.cej.2013.05.063.

(12) Heinze, T.; Petzold-Welcke, K.; van Dam, J. E. G. Polysaccharides: Molecular and Supramolecular Structures. Terminology BT - The European Polysaccharide Network of Excellence (EPNOE): Research Initiatives and Results; Navard, P., Ed.; Springer Vienna: Vienna, 2013; pp 23–64. https://doi.org/10.1007/978-3-7091-0421-7_3.

(13) Zargar, V.; Asghari, M.; Dashti, A. A Review on Chitin and Chitosan Polymers: Structure, Chemistry, Solubility, Derivatives, and Applications. ChemBioEng Rev. 2015, 2 (3), 204–226. https://doi.org/10.1002/cben.201400025.

(14) Bhatnagar, A.; Sillanpää, M. Applications of Chitin- and Chitosan-Derivatives for the Detoxification of Water and Wastewater - A Short Review. Advances in Colloid and Interface Science. Elsevier November 30, 2009, pp 26–38. https://doi.org/10.1016/j.cis.2009.09.003.

(15) Rinaudo, M. Chitin and Chitosan: Properties and Applications. Prog. Polym. Sci. 2006, 31 (7), 603–632. https://doi.org/https://doi.org/10.1016/j.progpolymsci.2006.06.001.

(16) Suginta, W.; Khunkaewla, P.; Schulte, A. Electrochemical Biosensor Applications of Polysaccharides Chitin and Chitosan. Chem. Rev. 2013, 113 (7), 5458–5479. https://doi.org/10.1021/cr300325r.

(17) Bhattacharya, S.; Ray, M. Chiral Resolution of 1-Phenylethylamine in Schiff Base Form within a Mixed Ligand Complex of Ni(II). Inorganica Chim. Acta 2020, 502 (December 2019), 119338. https://doi.org/10.1016/j.ica.2019.119338.

(18) Fleming, I.; Williams, D. Infrared and Raman Spectra BT - Spectroscopic Methods in Organic Chemistry; Fleming, I., Williams, D., Eds.; Springer International Publishing: Cham, 2019; pp 85–121. https://doi.org/10.1007/978-3-030-18252-6_3.

(19) Lavertu, M.; Xia, Z.; Serreqi, A. N.; Berrada, M.; Rodrigues, A.; Wang, D.; Buschmann, M. D.; Gupta, A. A Validated 1H NMR Method for the Determination of the Degree of Deacetylation of Chitosan. J. Pharm. Biomed. Anal. 2003, 32 (6), 1149–1158. https://doi.org/10.1016/S0731-7085(03)00155-9.

(20) Hirai, A.; Odani, H.; Nakajima, A. Determination of Degree of Deacetylation of Chitosan by 1 H NMR Spectroscopy. Polym. Bull. 1991, 26 (1), 87–94.

(21) Novoa-Carballal, R.; Fernandez-Megia, E.; Riguera, R. Dynamics of Chitosan by 1H NMR Relaxation. Biomacromolecules 2010, 11 (8), 2079–2086. https://doi.org/10.1021/bm100447f.

(22) Kumar, A.; Dubey, M.; Pandey, R.; Gupta, R. K.; Kumar, A.; Kalita, A. C.; Pandey, D. S. A Schiff Base and Its Copper(II) Complex as a Highly Selective Chemodosimeter for Mercury(II) Involving Preferential Hydrolysis of Aldimine over an Ester Group. Inorg. Chem. 2014, 53 (10), 4944–4955. https://doi.org/10.1021/ic403149b.

(23) Tekuri, V.; Sahoo, S. K.; Trivedi, D. R. Hg2+ Induced Hydrolysis of Thiazole Amine Based Schiff Base: Colorimetric and Fluorogenic Chemodosimeter for Hg2+ Ions in an Aqueous Medium. Spectrochim. Acta Part A Mol. Biomol. Spectrosc. 2019, 218, 19–26. https://doi.org/https://doi.org/10.1016/j.saa.2019.03.106.

(24) Neto, C. G. T.; Giacometti, J. A.; Job, A. E.; Ferreira, F. C.; Fonseca, J. L. C.; Pereira, M. R. Thermal Analysis of Chitosan Based Networks. Carbohydr. Polym. 2005, 62 (2), 97–103. https://doi.org/10.1016/j.carbpol.2005.02.022.

(25) Mucha, M.; Pawlak, A. Thermal Analysis of Chitosan and Its Blends. Thermochim. Acta 2005, 427 (1–2), 69–76. https://doi.org/10.1016/j.tca.2004.08.014.

(26) Hong, P. Z.; Li, S. D.; Ou, C. Y.; Li, C. P.; Yang, L.; Zhang, C. H. Thermogravimetric Analysis of Chitosan. J. Appl. Polym. Sci. 2007, 105 (2), 547–551. https://doi.org/10.1002/app.25920.

(27) Hahne, H. C. H.; Kroontje, W. The Simultaneous Effect of PH and Chloride Concentrations upon Mercury(II) as a Pollutant. Soil Sci. Soc. Am. J. 1973, 37 (6), 838–843. https://doi.org/https://doi.org/10.2136/sssaj1973.03615995003700060016x.

(28) Dubey, R.; Bajpai, J.; Bajpai, A. K. Chitosan-Alginate Nanoparticles (CANPs) as Potential Nanosorbent for Removal of Hg (II) Ions. Environ. Nanotechnology, Monit. Manag. 2016, 6, 32–44. https://doi.org/https://doi.org/10.1016/j.enmm.2016.06.008.

(29) Yao, X.; Wang, H.; Ma, Z.; Liu, M.; Zhao, X.; Jia, D. Adsorption of Hg(II) from Aqueous Solution Using Thiourea Functionalized Chelating Fiber. Chinese J. Chem. Eng. 2016, 24 (10), 1344–1352. https://doi.org/10.1016/j.cjche.2016.07.008.

(30) Sun, N.; Wen, X.; Yan, C. Adsorption of Mercury Ions from Wastewater Aqueous Solution by Amide Functionalized Cellulose from Sugarcane Bagasse. Int. J. Biol. Macromol. 2018, 108, 1199–1206. https://doi.org/10.1016/j.ijbiomac.2017.11.027.

(31) Kyzas, G. Z.; Bikiaris, D. N. Recent Modifications of Chitosan for Adsorption Applications: A Critical and Systematic Review. Mar. Drugs 2015, 13 (1), 312–337. https://doi.org/10.3390/md13010312.

(32) Nasirimoghaddam, S.; Zeinali, S.; Sabbaghi, S. Chitosan Coated Magnetic Nanoparticles as Nano-Adsorbent for Efficient Removal of Mercury Contents from Industrial Aqueous and Oily Samples. J. Ind. Eng. Chem. 2015, 27, 79–87. https://doi.org/10.1016/j.jiec.2014.12.020.

(33) Wang, X.; Deng, W.; Xie, Y.; Wang, C. Selective Removal of Mercury Ions Using a Chitosan–Poly(Vinyl Alcohol) Hydrogel Adsorbent with Three-Dimensional Network Structure. Chem. Eng. J. 2013, 228, 232–242. https://doi.org/https://doi.org/10.1016/j.cej.2013.04.104.

(34) Li, N.; Bai, R.; Liu, C. Enhanced and Selective Adsorption of Mercury Ions on Chitosan Beads Grafted with Polyacrylamide via Surface-Initiated Atom Transfer Radical Polymerization. Langmuir 2005, 21 (25), 11780–11787. https://doi.org/10.1021/la051551b.

(35) Zhang, A.; Xiang, J.; Sun, L.; Hu, S.; Li, P.; Shi, J.; Fu, P.; Su, S. Preparation, Characterization, and Application of Modified Chitosan Sorbents for Elemental Mercury Removal. Ind. Eng. Chem. Res. 2009, 48 (10), 4980–4989. https://doi.org/10.1021/ie9000629.

(36) Hassan, A. F.; Hrdina, R. Chitosan/Nanohydroxyapatite Composite Based Scallop Shells as an Efficient Adsorbent for Mercuric Ions: Static and Dynamic Adsorption Studies. Int. J. Biol. Macromol. 2018, 109, 507–516. https://doi.org/10.1016/j.ijbiomac.2017.12.094.

Findings of the thesis

The primary concern of my thesis work focused on study of amine-based polymers: synthesis, and modification of the amine functional groups in polymeric system, and application in heavy metal binding from aqueous solution. I basically worked with two polymers, aniline formaldehyde condensate and chitosan. In order to understand better binding of heavy metals with donor atoms, we have synthesized and thoroughly characterized some Hg(II) complexes and make the similar functionalization in polymeric system. The following major conclusions resulted from this study:

(i) Change in solvent ratio during synthesis drastically changed the surface property of AFC polymer. Synthesis in a polar solvent mixture (isopropanol: water as 1 : 3) increased the accessibility of the amine groups, which in turn increased the chromate adsorption capacity by ~30 times from the previously reported value.

(ii) Salt version of modified AFC remained active in terms of chromate removal for up to one year.

(iii) Along with chromate, the salt versions showed high Hg(II) adsorption. It also kept a scope for us to test these polymers to remove other heavy metals, indicating its broader application.

(iv) Complexation reaction of Hg(II) salt with thiophene, pyridine, and imidazole type Schiff base ligands indicated strong binding with imidazole type ligand. With thiophene ligand, hydrolysis of the ligand occurred, and we ended up with bis-complex of the starting amine compound.

(v) Synthesis of Schiff bases of chitosan and their thorough characterization. Imidazole functionalized chitosan showed the maximum Hg(II) removal among the three. Its Hg(II)

adsorption capacity was more than 170 mg/g throughout a pH range of 2 to 7 with more than 90% removal.

(vi) In designing a system effective for heavy metal removal, applying the principles first in a small molecular system, and then applying the same in a polymeric system, we get a clear understanding of the process is one of the significant findings that emerge from this thesis work.

Certain aspects of this work are suggested for future studies:

(i) The salt versions of the modified AFC can be used to remove other heavy metal ions or recover some oxyanions, e.g., MoO_4^{2-}, HVO_4^{2-}, WO_4^{2-} etc.

(ii) Further modification of the chitosan system with other ligands for other applications e.g., chiral ligands for chiral drug separation, catalysis etc. (Scheme 1.1).

List of Publications

1. **T. Dutta**, M. Ray, **Site orientation, accessibility, and surface hydrophobicity control on AFC polymer to increase hexavalent chromium removal performance**, *Chem. Eng. J.* 431 (2022) 133368. (https://doi.org/10.1016/j.cej.2021.133368)

2. **T.Dutta**, M.Ray, **Comparison of Hg^{2+}binding of small molecular ligand system vs. chitosan derived matrix: superiority of functionalization**, *manuscript submitted for publication.*

3. **T.Dutta**, M.Ray, **Long term storage capacity and multiple heavy metal binding efficiency of modified AFC**, *manuscript submitted for publication.*

4. C.R. Das, **T. Dutta**, M. Ray, **Effect of ligand and bridge substitution on chiral recognition of 1-phenylethylammonium cation by an anionic binuclear Ni (II) complex**, *Inorganica Chim. Acta.* 486 (2019) 367–376. (https://doi.org/10.1016/j.ica.2018.10.065)*

5. **T. Dutta**, C.R. Das, M. Ray, **Effect of ligand chirality and aromatic ring in the recognition of specific enantiomers of amino alcohols cation by a binuclear Ni(II) anion**, *manuscript submitted for publication.**

6. M. K Gupta, A. K. Chiranjivi, **T. Dutta**, V. K. Dubey, L. Rangan, **Synthesis and characterization of zinc derivatized 3, 5-dihydroxy 4′, 7-dimethoxyflavone and its anti leishmaniasis activity against Leishmania donovani**, *Biometals* (2022). Just accepted. (https://doi.org/10.1007/s10534-022-00364-x)*

* Content of these papers is not related to this thesis